Investigation of Human Centrosomes

- with a Special Focus

on the Function of Cep152 and Cep192 in Centriole Duplication

Inauguraldissertation

zur Erlangung der Würde eines Doktors der Philosophie

vorgelegt der

Philosophisch-Naturwissenschaftlichen Fakultät

der Universität Basel

von

Katharina Friederike Sonnen

aus Dortmund, Deutschland

Basel, 2012

Genehmigt von der Philosophisch-Naturwissenschaftlichen Fakultät

auf Antrag von

Prof. Erich A. Nigg

Prof. Peter Scheiffele

Dr. Zuzana Storchova

(Mitglieder des Dissertationskomitees)

Basel, den 24.04.2012

Prof. Martin Spiess

- Dekan -

This work is dedicated to my father

without whom I might have chosen a different path of life.

Table of Contents

1 Summary

Centrioles are symmetrical, barrel-shaped, microtubule-based structures, that serve as building platforms for the formation of centrosomes and cilia. In dividing cells, they recruit a matrix of proteins called pericentriolar material (PCM) to form the centrosome, the major microtubule-organizing centre in animal cells. Importantly, centrosomes form the poles of the bipolar mitotic spindle during cell division that ensures the equal segregation of chromosomes into the two emerging daughter cells, thereby preventing the occurrence of aneuploidy and tumorigenesis. In differentiating cells, centrioles also function as basal bodies for the formation of flagella and cilia. Mutations in several cilia-related proteins have been implicated in a set of diverse human diseases called ciliopathies. To ensure the proper segregation of centrioles during cell division, centriole duplication is tightly controlled and coordinated with the cell cycle. To date, several factors have been identified in human cells that are recruited in a consecutive fashion to nascent centrioles to template the outgrowth of one procentriole orthogonally to the pre-existing one during each cell cycle. In addition to structural components, these duplication factors include the kinase Plk4 (polo-like kinase 4), which is pivotal for the initiation of centriole duplication.

Here, we have taken two approaches to investigate centrosomes in more detail: first, the human centrosomal proteins Cep192 and Cep152 were functionally characterized; second, the localization of key centrosomal and centriolar components was analyzed using super-resolution three-dimensional structured illumination microscopy (3D-SIM).

1. Previously, Cep192 and Cep152 had been identified as novel centrosomal proteins in a proteomic screen. Homologues of Cep152 in flies and zebrafish had been implicated in PCM recruitment and centrosome duplication, but Cep152 had not been investigated in humans. Likewise, the worm homologue of Cep192 also functions in PCM recruitment and centrosome duplication. However, in humans its role in centriole duplication remained controversial.

   Here, we have established that Cep152 is dispensable, whereas Cep192 is essential for PCM recruitment in mitotic cells. This functional difference is further illustrated by their subcellular localization: During the cell cycle Cep152 remained confined around the proximal half of pre-existing centrioles. In contrast, Cep192 localized along

centriolar walls and proximal ends of both pre-existing centriole and growing procentriole in interphase and within the amorphous PCM cloud surrounding centrioles in mitosis. The stable centrosomal integration of Cep152 depended on Cep192, whereas Cep192 localized independently of Cep152.

Furthermore, both Cep152 and Cep192 were required for proper centriole duplication, thereby clarifying the controversy about the implication of Cep192 in this process. So far, it was not understood how the regulatory kinase Plk4 is recruited to nascent centrioles. Here, we show Cep192 and Cep152 to be essential for Plk4 recruitment, as only co-depletion of both proteins prevented recruitment of Plk4 to centrioles. Concomitantly, centriole duplication was only inhibited to a similar extent as in Plk4- or Sas-6-depleted cells, if both Cep152 and Cep192 were depleted. In agreement, we have identified and characterized interactions of Plk4 with the N termini of both Cep152 and Cep192. Finally, not only the recruitment of Plk4, but also of other duplication factors such as CPAP and Sas-6 was impaired in Cep152- and/ or Cep192-depleted cells. This places both Cep152 and Cep192 upstream of Plk4 and other known centriole duplication factors within the centriole duplication pathway.

We have also addressed the regulation of Cep152 and Cep192. Centrosomal levels of both proteins increased towards mitosis. Similarly, cytoplasmic Cep152 levels peaked when cells approached mitosis, whereas Cep192 levels were stable. We discuss initial results that hint at an involvement of Plk1, Plk4 and βTrCP in Cep152 degradation.

Hence, we show that both Cep152 and Cep192 function as centriole duplication factors. Both proteins exert a partly redundant function and their co-operation orchestrates Plk4 recruitment and thus canonical centriole duplication.

2. Using 3D-SIM we have analysed the spatial relationship of 18 centriole and PCM components of human centrosomes at different cell cycle stages.

   During mitosis, PCM proteins formed extended networks with interspersed γ-Tubulin. In interphase, most proteins were arranged at specific and defined distances from the walls of centrioles, resulting in ring-like staining. We have grouped proteins according to their measured ring diameters into three classes: inner, intermediate and outer PCM, respectively. Additionally, orientation of Cep152 with its C-terminus close to centriole

walls and its N-terminus facing outwards was visualised using site-specific antibodies against either terminus of the protein. At the distal end of centrioles, appendage proteins formed rings with several density masses, usually with a multiplicity below that expected from the 9-fold symmetry of centrioles. Although Cep164 remained centriolar throughout the cell cycle, the number of discernible density masses was clearly reduced during mitosis. At the proximal end, Sas-6 formed a dot at the site of daughter centriole formation, consistent with its role in cartwheel formation. Plk4 and STIL co-localized with Sas-6, but the bulk of the cartwheel protein Cep135 was associated with mother centrioles. Remarkably, Plk4 formed a dot on the surface of the mother centriole even before Sas-6 staining became detectable, indicating that Plk4 constitutes an early marker for the site of nascent centriole formation.

2 Introduction

After its discovery by Édouard van Beneden in 1876, the centrosome was named and characterized by Theodor Boveri in 1888 (Boveri, 1888). He was also the first to point at a potential correlation between centrosome amplification and malignant transformation and postulated a direct functional relationship (Boveri, 1914). However, only towards the end of the 20th century the significance of centrosomes was re-discovered and focussed research on centrosomes, including investigations of their function and regulation, were initiated.

2.1 Centrosome Structure

The centrosome is a small non-membranous organelle with a volume of approximately 1 µm³. It is usually found in close proximity to the nucleus. In G1 phase of the cell cycle the centrosome is composed of two centrioles surrounded by a protein matrix, the pericentriolar material (PCM, **Figure 1**) (Bornens, 2002; Rodrigues-Martins et al., 2007). The two

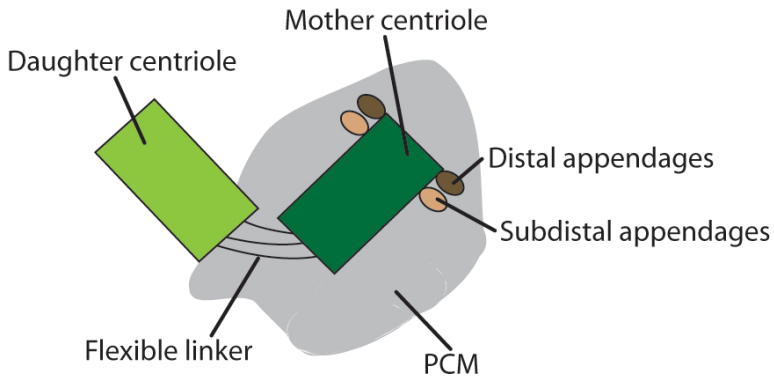

Figure 1 Centrosome structure. Centrosomes in G1 phase consist of two centrioles loosely connected by a physical linker. The two centrioles can be distinguished from each other by the presence of distal and subdistal appendages at the older mother centriole, whereas the younger daughter centriole lacks these structures. They are maturation factors that render the mother centriole competent to recruit pericentriolar material (PCM).

centrioles are symmetrical, barrel-shaped arrays of nine microtubule (MT) triplets. The centrioles of one centrosome differ from each other in the composition of their associated proteins. The parental, mature centriole has distal and subdistal appendages that the daughter centriole lacks (Pan and Snell, 2007). These appendages are implicated in the recruitment of

PCM, which is composed of proteins required for microtubule nucleation, notably constituents of the γ-tubulin ring complex (γTuRC), and various coiled-coil domain-containing proteins conferring stability to the protein matrix (Zheng et al., 1995; Bornens, 2002; Andersen et al., 2003).

2.2 Function of Centrosomes

In mammalian cells centrioles serve two distinct functions:

First, they can recruit a multitude of proteins to organize the PCM around the centriolar barrels (Bobinnec et al., 1998). PCM proteins constitute the basis for centrosomes to function as major microtubule-organizing centres by allowing the concentrated nucleation and anchoring of MTs (**Figure 2** A) (Bettencourt-Dias and Glover, 2007; Nigg and Raff, 2009; Bornens, 2012). In this way, they function in various cellular processes during interphase such as intracellular transport, motility and cell shape determination. As already detected at the end of the 19th century, centrosomes additionally contribute to spindle formation during mitosis, but they also regulate spindle positioning for asymmetric cell division and cytokinesis (Basto et al., 2006; Rodrigues-Martins et al., 2007). These processes are critical for the accurate segregation of the organism's genetic material during cell division. Given this crucial role of centrosomes in the formation of bipolar spindles, aberrant centrosome numbers can lead to the formation of monopolar or multipolar spindles resulting in aneuploid daughter cells. Interestingly, this is a common characteristic of most solid tumours analyzed to date (Nigg, 2002; Nigg, 2006), and this possible connection between centrosome number and carcinogenesis has already been emphasized at the beginning of the 20th century (Boveri, 1914).

Second, in differentiating cells centrioles serve as basal bodies for the formation of flagella and cilia, a process termed ciliogenesis (**Figure 2** B) (Fliegauf et al., 2007; Pearson et al., 2007). If motile, these organelles are essential for movement of the organisms themselves or of material along the extracellular space, such as mucus within the airway. If immotile, cilia function as sensory organs in which components of various signalling pathways (e.g. Wnt, Notch or Shh) are concentrated to integrate extracellular signals (Goetz and Anderson, 2010).

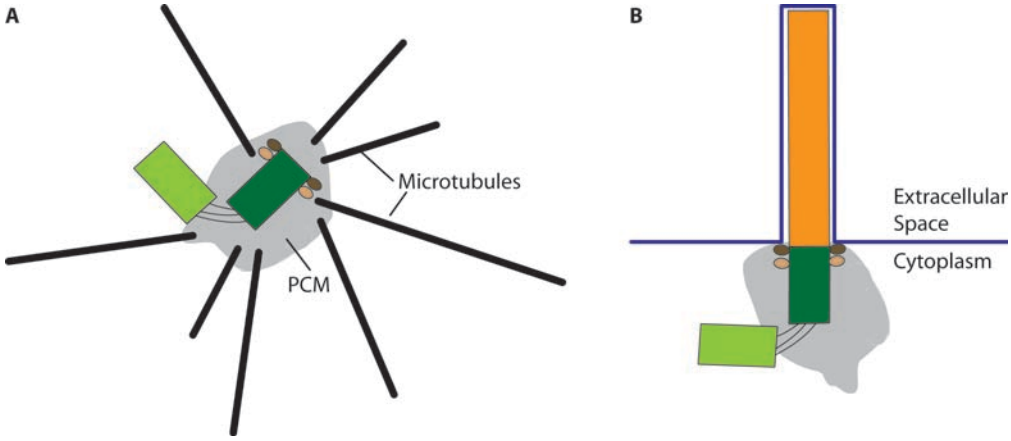

Figure 2 Centrioles are required for the local concentration of PCM proteins and cilium formation. A Pericentriolar material recruited to centrioles comprises γ-Tubulin ring complexes in addition to other proteins responsible for the nucleation and anchoring of microtubules emanating into the cytoplasm. **B** The mature mother centriole can attach to the plasma membrane and serve as basal body for ciliogenesis. (Daughter centriole: light green; mother centriole: dark green; PCM: gray; distal appendages: dark brown; subdistal appendages: light brown; ciliary axoneme: orange; plasma membrane: dark blue).

The requirement of centrioles for ciliogenesis is thought to be the predominant function and also the evolutionary determinant for the existence of centrioles. Recruitment of PCM and connection to the mitotic spindle apparatus is suggested to have evolved to allow the faithful segregation of centrioles into the emerging daughter cells during cell division (Pickett-Heaps, 1971; Debec et al., 2010). This is illustrated by the fact that organisms that never form cilia during their life cycle lack centrioles, such as higher plants.

Although direct genetic evidence for a role of centrosomes in carcinogenesis is only starting to emerge (Basto et al., 2008; Ganem et al., 2009), it is remarkable that mutations in several centrosomal proteins have recently been implicated in developmental diseases. For instance, mutations in CENPJ and Pericentrin cause microcephaly (Bond et al., 2005; Gul et al., 2006) and dwarfism, respectively (Griffith et al., 2007), demonstrating that centrosomes are critical for early development. Furthermore, mutations in several centrosomal proteins, that result in defective cilia, have been found to account for a diverse set of human diseases called ciliopathies, complex diseases that reflect ciliary dysfunction and are often characterized by polycystic kidneys, retinopathies and facio-digital developmental defects (Fliegauf et al., 2007).

2.3 Centrosome Biogenesis

Centriole biogenesis has been studied extensively by electron microscopy (Mizukami and Gall, 1966; Brinkley et al., 1967; Dippell, 1968; Sorokin, 1968; Anderson and Brenner, 1971; Kuriyama and Borisy, 1981; Vorobjev and Yu, 1982; Chretien et al., 1997). These studies have suggested the existence of two fundamentally distinct centriole assembly pathways: the centriole duplication cycle (centriolar pathway) and the *de novo* assembly of centrioles (acentriolar pathway). However, recent data indicate that the two pathways share common steps and that Plk4 controls both of them (Nigg, 2007; Rodrigues-Martins et al., 2007).

2.3.1 Centriole Duplication

To ensure the faithful segregation of centrioles during cell division, they are duplicated once in S phase and then subdivided equally into the two emerging daughter cells during M phase of the cell cycle. The order of events, by which the centrosome is duplicated during the cell cycle and then evenly distributed among the daughter cells, is referred to as the centrosome cycle. Its events are coordinated with the duplication and segregation of chromosomes, thereby ensuring the maintenance of euploidy.

2.3.1.1 Centrosome Cycle

The centrosome cycle is subdivided into four distinct phases: centriole duplication, centriole maturation, centrosome separation and centriole disengagement (**Figure 3**).

Similar to DNA replication, the duplication of centrioles begins at the onset of S phase when a procentriole (termed "daughter centriole") forms orthogonally to the proximal base of the pre-existing centriole (termed "parental" or "mother centriole") (Robbins et al., 1968;

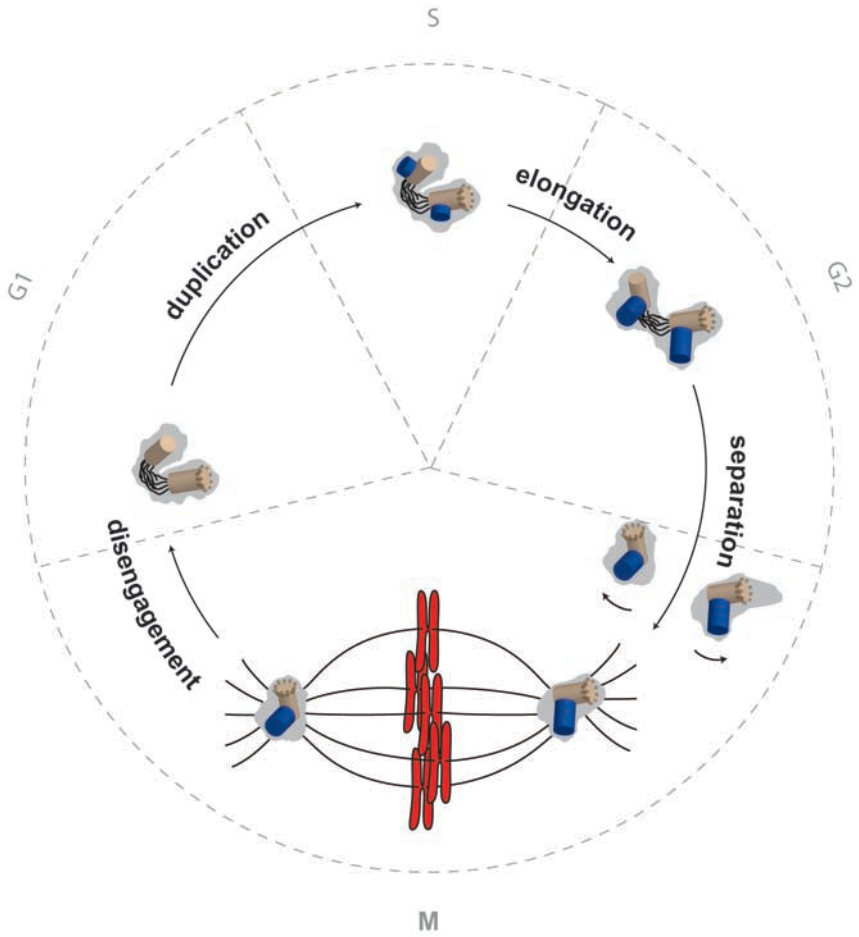

Figure 3 The centrosome cycle. Upon entry into S phase, the two centrioles of a G1 phase cell duplicate and then elongate during the following G2 phase. At mitotic onset, the centrosomes are separated to organize the bipolar mitotic spindle. At the mitotic exit, centriole disengagement of the previously tightly connected centrioles allows for another round of duplication. (Mother centrioles: gray; daughter centrioles: blue; chromosomes: red. Illustration adapted from J. Westendorf)

Kuriyama and Borisy, 1981; Vorobjev and Yu, 1982; Alvey, 1985; Kochanski and Borisy, 1990; Paintrand et al., 1992). During G2 phase the procentrioles continue to elongate. In addition, the former procentriole of the previous cycle matures by the addition of appendage proteins, which renders this centriole PCM-recruitment competent. This maturation is accompanied by the recruitment of further PCM proteins and thus an increase in MT nucleation activity (Palazzo et al., 2000). In late G2 phase the two centrosomes separate from

each other in response to the severing of a physical linker connecting the two parental centrioles, while the orthogonal association of mother and daughter centriole is maintained (Fry et al., 1998; Bahe et al., 2005). The separated centrosomes are then moved to opposite poles of the cell, where they organize the bipolar mitotic spindle (Blangy et al., 1995). During late M or early G1 phase centriole disengagement ensues when the parental and daughter centrioles finally lose their intimate, orthogonal connection, thereby completing the centrosome duplication cycle (Freed et al., 1999; Piel et al., 2000; Tsou and Stearns, 2006; Rodrigues-Martins et al., 2007).

After cell division each cell contains two centrioles, one being the mature mother centriole and one being the daughter centriole from the previous cell cycle. Subsequently, the centrosome cycle is either re-initiated or cells exit the cell cycle into quiescence and the mother centriole can serve as basal body for ciliogenesis at the plasma membrane.

2.3.1.2 Control of Centriole Duplication

Cells do not have a checkpoint to stop the cell cycle in the presence of multiple centrosomes (Sluder et al., 1997). Thus, for the maintenance of centrosome and centriole numbers during all subsequent cycles two conceptual rules have been postulated, namely *cell cycle control* and *copy number control* (Nigg, 2007; Nigg and Stearns, 2011).

- Cell cycle control signifies that centrioles duplicate only once during the cell cycle (Wong and Stearns, 2003; Tsou and Stearns, 2006). Using cell fusion assays, it was shown that centrosomes have an “intrinsic block” that prevents re-duplication within the same cell cycle (Wong and Stearns, 2003). Interestingly, centriole disengagement at the end of M phase has been suggested as the licensing step and prerequisite for another round of centriole duplication (Tsou and Stearns, 2006; Loncarek et al., 2008).

- Copy number control ensures that only one procentriole per centriole is formed. It is thought to be linked to the regulated initiation of centriole duplication in late G1 or early S phase (Bettencourt-Dias et al., 2005; Habedanck et al., 2005; Kleylein-Sohn et al., 2007). Only in recent years have proteins participating in centriole duplication been described. These proteins can be divided into centrosomal building blocks

(Kirkham et al., 2003; Dellatre et al., 2004; Kemp et al., 2004; Leidel et al., 2005) on the one hand and regulators on the other hand (Matsumoto et al., 1999; Meraldi et al., 1999; Tsou and Stearns, 2006). The centrosomal Polo-like kinase 4 (Plk4) has been identified as a centrosome-intrinsic component of a pathway regulating canonical centriole formation (Bettencourt-Dias et al., 2005; Habedanck et al., 2005).

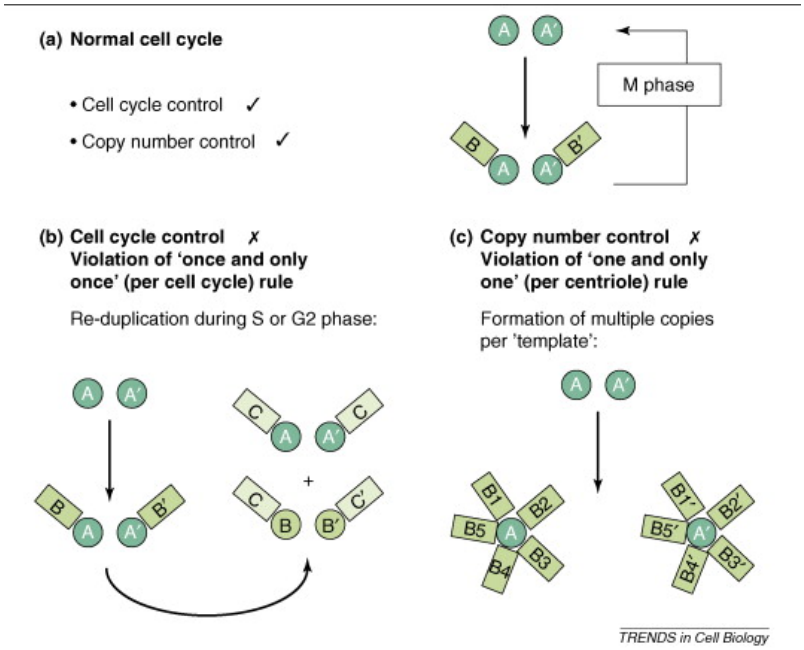

Figure 4 Centriole duplication is governed by cell cycle and copy number control. (**a**) Centriole duplication in a normal cell cycle gives rise to two daughter centrioles (B and B´) from two mother centrioles (A and A´). (**b**) Cell cycle control ensures that centriole duplication occurs only once per cell cycle. (**c**) Copy number control indicates that only one procentriole is formed per pre-existing centriole (adapted from Nigg, 2007).

2.3.1.3 Plk4 Controls the Number of Generated Daughter Centrioles

Plk4 is a member of the Polo-like kinase (Plk) family. Polo-like kinases are serine/ threonine kinases, which are essential regulators of mitotic and meiotic progression and are highly conserved in organisms ranging from yeast to humans (Barr et al., 2004; Bettencourt-Dias et al., 2005; Glover, 2005; Lee et al., 2005; Winkles and Alberts, 2005). In humans, the Plk family includes four members called Plk1, 2, 3, and 4. All members have an N-terminal

kinase domain (Barr et al., 2004; Dai, 2005; Lowery et al., 2005) and the defining C-terminal polo-box in common (Elia et al., 2003; Elia et al., 2003). In the case of Plk1 the polo-box domain consisting of two consecutive polo boxes can bind to phosphorylated motives of interaction partners having been phosphorylated by an upstream kinase (Elia et al., 2003). Thus, this constitutes an elegant mechanism of spatial and temporal control of Plk1 kinase activity. The structurally most divergent member of the Polo-like kinase family is Plk4. The kinase domain of Plk4 is followed by an extensive C-terminal region of more than 500 amino acids, including a single polo-box and a cryptic polo-box, a domain of unknown function that does not bind phosphorylated polo-box consensus binding sites (**Figure 5**). Conversely, the polo-box domain of other Plk family members consists of two polo-boxes (Fode et al., 1994).

Figure 5 Domain structure of Plk4. Schematic illustration of the domain composition of human Plk4 (dimensions drawn to scale, adapted from J. Westendorf).

Habedanck *et al.* (2005) established that Plk4 is recruited to the centrosome via its C-terminal region and remains associated with it throughout the cell cycle. The depletion of Plk4 prevents centriole duplication and causes the sequential loss of centrioles in successive cell divisions. Conversely, the overexpression of Plk4 overrides a copy number control mechanism and leads to centriole amplification by *bona fide* centriole overduplication (Bettencourt-Dias et al., 2005; Habedanck et al., 2005). In cells overexpressing Plk4 flower-like structures with 4 – 6 procentrioles as petals surrounding the parental centriole form nearly simultaneously and have been shown to be *bona fide* centrioles (Kleylein-Sohn et al., 2007). Following Plk4 induction centriolar building blocks are recruited consecutively to the centriole assembly site to allow procentriole outgrowth (Kleylein-Sohn et al., 2007).

Yet, how Plk4 regulates this recruitment cascade and how centriole duplication is limited to only one copy per existing centriole is currently not understood. Moreover, whereas events downstream of Plk4 are starting to be unravelled, factors upstream of Plk4 remain unknown to date.

2.3.2 *De novo* Centriole Biogenesis

In proliferating cells new centrioles normally form during the centrosome duplication cycle with parental centrioles as assembly platforms. However, it is well established that particular cell types, notably differentiated ciliated cells, produce large numbers of centrioles via an acentriolar assembly pathway and only to a limited extent via the templated centriole assembly (Dirksen, 1991; Dawe et al., 2007; Pearson et al., 2007). The acentriolar assembly pathway is termed "*de novo*", since pre-existing parental centrioles are not required.

Recent findings reveal that *de novo* centriole formation can be induced in both transformed and untransformed cells under certain conditions. In particular, *de novo* formation of centrioles occurred when resident centrioles had first been removed by laser ablation or microsurgery (La Terra et al., 2005). These studies indicate that the presence of a single resident centriole is sufficient to inhibit *de novo* formation (Marshall et al., 2001; La Terra et al., 2005).

The emerging consensus view is that *de novo* centriole biogenesis resembles the canonical centriole duplication cycle more closely than previously appreciated, but may be considerably slower (less efficient) and lack strict control over the number of centrioles produced. In other words, rather than being *bona fide* templates, pre-existing centrioles may act primarily as solid-state platforms to accelerate the assembly process (Khodjakov et al., 2002; La Terra et al., 2005; Rodrigues-Martins et al., 2007; Uetake et al., 2007). This implies that in normal proliferating cells the assembly of a procentriole in close proximity to a pre-existing centriole is kinetically favoured over *de novo* formation in the cytoplasm (Rodrigues-Martins et al., 2007).

2.4 Key Proteins Involved in Centrosome Biology

Centrosome-associated proteins can be subdivided into four groups based on their contribution to centrosome biology as well as their localization at centrioles: proteins involved in centriole duplication (1) and linkage of centrioles (2) in addition to appendage proteins (3) and those proteins that consititute the PCM (4). In the following sections I will briefly discuss the current knowledge of key members of each group.

2.4.1 Centriole Duplication Factors

In recent years, research on centriole duplication in various organisms has revealed a conserved mechanism, which can be characterized as an assembly cascade at the site of centriole formation. Here, both regulatory proteins and centriole building blocks mediate the consecutive outgrowth of a nascent procentriole (Carvalho-Santos et al., 2010).

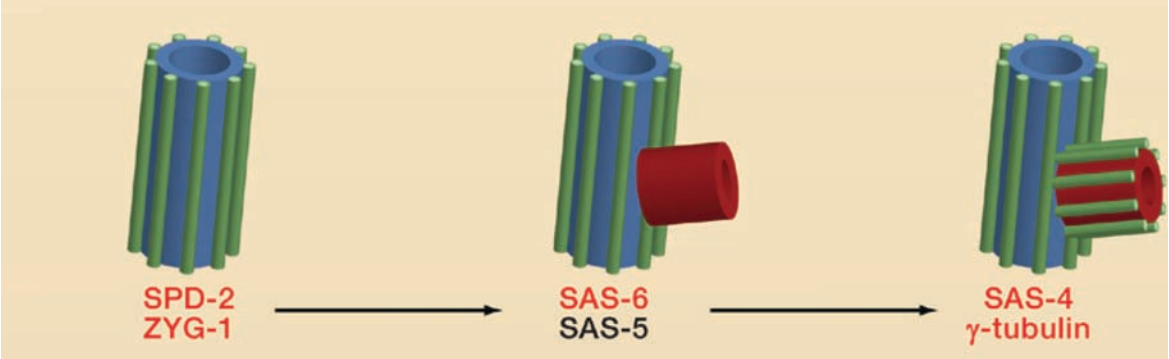

Figure 6 Centriole duplication in *C. elegans*. Spd-2 recruits the protein kinase Zyg-1, which then enables the recruitment of a complex of Sas-5 and Sas-6. After the formation of a central tube (red), centriolar microtubules (green) are assembled around it in a Sas-4-dependent way. Proteins highlighted in red have functional analogues in vertebrates (adapted from Nigg and Raff, 2009).

Pioneering work in *Caenorhabditis elegans* (*C. elegans*) has revealed a pathway involving the consecutive recruitment of specific proteins to the site of procentriole formation (**Figure 6**). Spd-2 is required for the recruitment of the kinase Zyg-1 (O'Connell et al., 2000; Kemp et al.,

2004; Pelletier et al., 2004), which in turn induces the recruitment of a complex consisting of Sas-6 and Sas-5, which finally mediate the recruitment of a protein called Sas-4 (Kirkham et al., 2003; Leidel and Gonczy, 2003; Leidel et al., 2005; Delattre et al., 2006; Pelletier et al., 2006). Sas-6 forms a central tube around which the MTs of the new centriole are nucleated in a Sas-4-dependent manner (Pelletier et al., 2006).

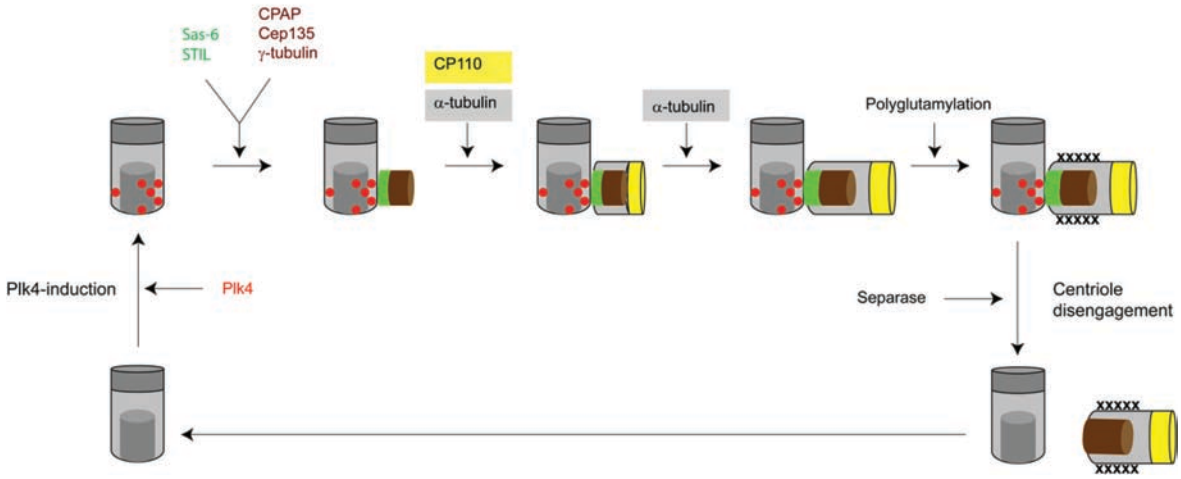

Figure 7 Centriole biogenesis in human cells. Similarly to *C. elegans*, procentriole formation initiates in S phase. After induction by Plk4 the proteins Sas-6, STIL, CPAP, Cep135 and γ-tubulin are recruited. Finally, the nascent centriole is elongated by addition of α/β-Tubulin dimers underneath a distal cap of CP110 (adapted from Kleylein-Sohn *et al.* (2007)).

In analogy, several centriole duplication factors have been identified in vertebrates. On the one hand, these factors are either homologous to *C. elegans* proteins or serve analogous functions: Sas-6 and CPAP (homologous to Sas-6 and Sas-4), Plk4 (which is analogous to Zyg-1) or STIL, the predicted homologue of Sas-5 and confirmed centriole duplication factor (Leidel et al., 2005; Cho et al., 2006; Kleylein-Sohn et al., 2007; Strnad et al., 2007; Kitagawa et al., 2011; Arquint et al., 2012; Vulprecht et al., 2012). On the other hand, a number of proteins essential for centriole duplication have evolved in other eukaryotes, which include for instance Cep135 or CP110 (Chen et al., 2002; Kleylein-Sohn et al., 2007). Initiation of human centriole duplication has been shown to require activity of the cell cycle kinase Cdk2 (Lacey et al., 1999; Matsumoto et al., 1999; Meraldi et al., 1999) in addition to the

centrosome-intrinsic activity of Plk4 (**Figure 7** and as discussed earlier in Section 2.3.1.3). Plk4 is thought to act by phosphorylating a still unknown substrate (Guderian et al., 2010). After recruitment of Sas-6 and STIL to pre-existing centrioles (Kleylein-Sohn et al., 2007; Strnad et al., 2007; Tang et al., 2011; Arquint et al., 2012) CPAP, Cep135, and γ-tubulin are recruited. Finally, CP110 is recruited and caps the distal end of the growing centriole (Kleylein-Sohn et al., 2007; Schmidt et al., 2009).

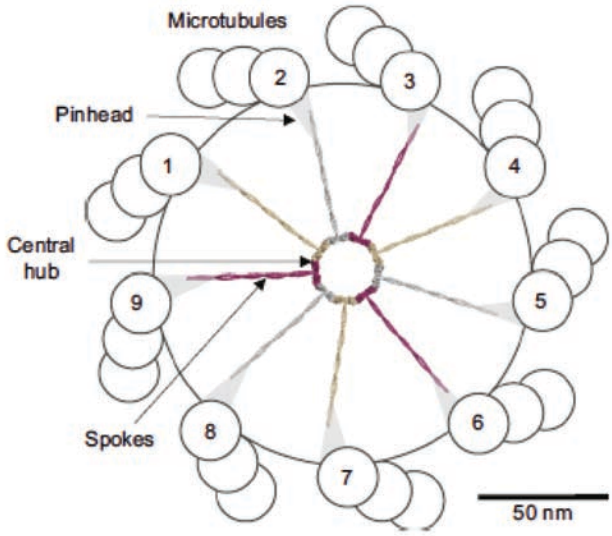

Figure 8 Structural model of the Sas-6-based cartwheel fitted into the centriole. EM studies have revealed that the centriolar cartwheel consists of a central hub, from which nine spokes emanate that connect to the centriolar microtubules via pinheads. Here, the structure model of the Sas-6 octadecamer is illustrated in the context of a centriolar barrel. It becomes apparent that the model conforms with the predicted dimensions of the cartwheel and that Sas-6 substantially contributes to the formation of the central hub, but also to the spokes (Kitagawa et al., 2011).

Interestingly, after initiation of centriole duplication a cartwheel-like structure with 9-fold symmetry is assembled on the pre-existing centriole (Gavin, 1984; Alvey, 1986). This cartwheel then serves as template for the outgrowth of a 9-fold symmetrical procentriole. In recent years, Bld10 and Bld12 have been identified as cartwheel proteins in *Tetrahymena* with Bld12 (homologous to Sas-6) lying at cartwheel hubs and Bld10 (homologous Cep135) at cartwheel spoke tips (Matsuura et al., 2004; Hiraki et al., 2007; Nakazawa et al., 2007). In agreement, solution of the Sas-6 structure by x-ray crystallography and electron microscopy

revealed that it self-assembles into octadecamers with 9-fold symmetry (**Figure 8**) (Kitagawa et al., 2011; van Breugel et al., 2011). Yet, whether and – if so – how Cep135 and Sas-5, the protein forming a complex with Sas-6 in *C. elegans*, contribute to cartwheel formation has not been understood sufficiently so far.

2.4.2 Linker Proteins

There are two types of linker structures connecting centrioles within one cell: the linker between mother and daughter centriole (1) and the linker between two mature mother centrioles (2) (for review see Nigg and Stearns (2011)).

First, the tight linker connecting mother and daughter centrioles is maintained during the cell cycle until centriole disengagement at mitotic exit (see Section for 2.3.1 details). As discussed earlier, the process of disengagement licenses the centrioles for another round of centriole duplication. Its nature has not been revealed yet, but both Plk1 and Separase have been implicated in its removal from centrioles (Tsou and Stearns, 2006; Tsou et al., 2009). A recent study has suggested that Cohesin might constitute the physical linker between mother and daughter centriole (Schockel et al., 2011). This would resemble the function of Cohesin in sister chromatid cohesion until anaphase of the cell cycle and thus constitute a molecular connection between the centrosome and chromosome duplication cycle (Tsou and Stearns, 2006; Nigg, 2007). Additionally, the cartwheel protein Sas-6 as well as STIL are concomitantly lost from centrioles during mitotic progression and have to be re-acquired before centriole duplication can commence in the following cell cycle (Strnad et al., 2007; Tang et al., 2011; Arquint et al., 2012).

Second, the loose linker connecting the two parental centrioles during interphase acts as a loose tether and consists of the filament-forming protein Rootletin (Bahe et al., 2005; Yang et al., 2006). At proximal ends of mother centrioles it interacts with C-Nap1 (Fry et al., 1998; Mayor et al., 2000), whose localization in turn has recently been shown to depend on the centrosomal protein Cep135 (Kim et al., 2008). Upon mitotic onset the linker is removed by phosphorylation of both C-Nap1 and Rootletin by the kinase Nek2, which subsequently leads to the dissociation of the linker proteins (Mayor et al., 2002; Bahe et al., 2005), which allows centrosome separation in late G2 phase and formation of a bipolar mitotic spindle.

2.4.3 Distal and Subdistal Appendages

Mature centrioles can be distinguished from immature daughter centrioles by the presence of distal and subdistal appendage proteins (Vorobjev and Yu, 1982; Paintrand et al., 1992). Those appendages can be seen as electron-dense material at the very end of the mother centriole by electron microscopy (**Figure 9**). To date, several proteins have been found to localize to either distal or subdistal appendages. Cep164, which mediates the binding of mother centrioles to the plasma membrane to allow the outgrowth of an axoneme during

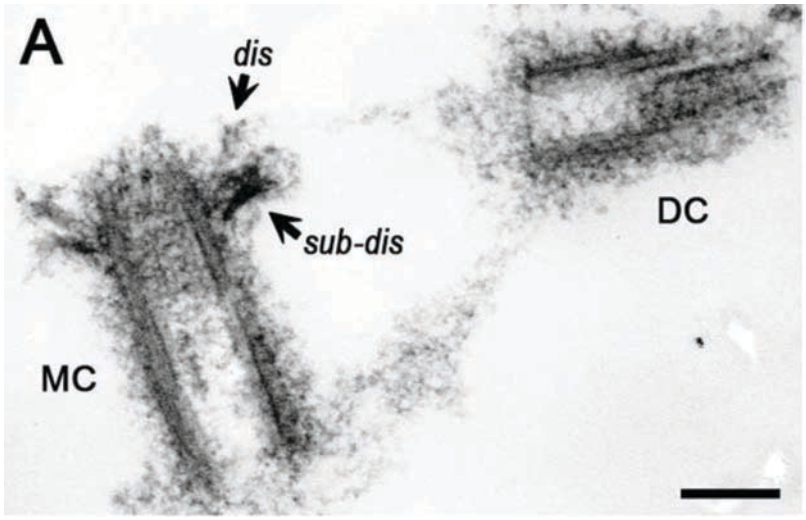

Figure 9 Mature centrioles are characterized by the presence of distal and subdistal appendages. An electron micrograph of a G1 centrosome reveals that the mother centriole (MC) harbours distal (dis) and subdistal (sub-dis) appendages, whereas the daughter centriole (DC) lacks them (scale bar 200 nm, adapted from Sillibourne *et al.* (2011)).

ciliogenesis, has been identified as a distal appendage protein (Graser et al., 2007). Only recently, Cep123, a protein of unknown function, has also been shown to reside at distal appendages (Sillibourne et al., 2011). In contrast, the proteins Ninein and Cep170 for instance specifically localize to subdistal appendages. Ninein, which is additionally found at proximal ends of mother centrioles, is implicated in PCM recruitment and anchorage of MTs that emanate into the cytoplasm during interphase (Mogensen et al., 2000; Ou et al., 2002). Thus, centriole maturation, i.e. the acquisition of appendage proteins, renders centrioles competent to both formation of cilia and recruitment of PCM proteins (Piel et al., 2000).

2.4.4 Pericentriolar Matrix

A main function of centrioles is the recruitment and spatial concentration of PCM proteins (Bobinnec et al., 1998). PCM proteins form a scaffold, within which γTuRCs are organized to nucleate the polymerization of microtubules for the formation of the cellular MT-based cytoskeleton (Moritz et al., 1995). In cells approaching mitosis centrosomal levels of PCM proteins strongly increase. These proteins are predicted to be organized in an amorphous arrangement surrounding centrioles (Dictenberg et al., 1998). The increase in centrosomal protein levels is accompanied by an increase in MT nucleation activity, which accounts for the high dynamics required for the formation of the mitotic spindle (**Figure 10**) (Luders and Stearns, 2007).

The key PCM component is the γTuRC. It consists of γ-Tubulin that is organized into a ring by the γ-Tubulin ring complex components (GCP) 2 – 6 and gets recruited to specific cellular localizations by GCP-WD/ NEDD1 (Moritz et al., 1995; Zheng et al., 1995; Murphy et al.,

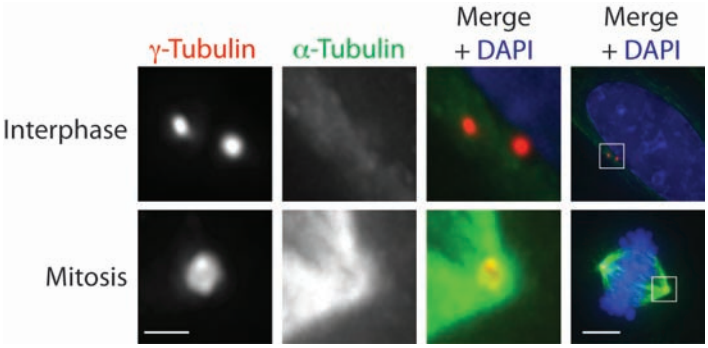

Figure 10 Centrosomal γ-Tubulin increase substantially upon mitotic onset to allow the formation of the mitotic spindle. U2OS cells were fixed and stained with the indicated antibodies (red: γ-Tubulin, green: α-Tubulin (MTs), blue: DAPI (DNA)).

2001; Luders et al., 2006). After nucleation, MTs can be released from γTuRCs and anchored within the PCM. Beside these functional components, several proteins have been identified to reside in the PCM and contribute to its stability and thus to the stable recruitment of γTuRCs and other MT-anchoring proteins. Those stabilizing factors include e.g. Pericentrin, Cep215 and Cep192 (Doxsey et al., 1994; Dictenberg et al., 1998; Gomez-Ferreria et al., 2007; Graser et al., 2007; Zhu et al., 2008). Notably, PCM-1, which localizes to so-called centriolar satellites, i.e. distinct spots around the distal end of centrioles, has also been implicated in this process.

2.5 Identification and Characterization of Novel Centrosomal Proteins

In 2003, Andersen *et al.* published a comprehensive study of the human centrosomal proteome. Applying the latest advancements in mass spectrometry available at that time, they identified various novel centrosomal proteins in addition to well-known ones. Back then, most of the novel proteins were uncharacterized. Following up on this screen, our laboratory has performed two RNA interference (RNAi) screens to determine the roles of several of these proteins at centrosomes: First, the depletion effect on the ability to form primary cilia was investigated, which revealed Cep164 as pivotal for this process (Graser et al., 2007). Second, a stable cell line, in which the overexpression of Plk4 could be induced, was employed to identify novel proteins involved in centriole duplication and to compile a recruitment pathway of the identified proteins (Kleylein-Sohn et al., 2007).

Two of the previously uncharacterized proteins are Cep152 and Cep192, which were of particular interest, even though they only showed a moderate effect on ciliogenesis and/ or centriole duplication in the aforementioned screens. This interest was based on their high sequence homology to proteins significant for proper centriole function in either *D. melanogaster* or *C. elegans*: Cep152 is the human homologue of the fly protein Asterless, which has been implicated in proper PCM recruitment and centriole duplication. In addition, Cep192 constitutes the human homologue of the worm protein Spd-2, which is required for the centrosomal recruitment of the regulatory kinase Zyg-1.

2.5.1 Cep152

Asterless, the fly homologue of Cep152, has been identified in a screen for mutants that result in male infertility (Bonaccorsi et al., 1998). In *asterless* mutants, the PCM proteins g-Tubulin and Centrosomin are not recruited to centrosomes, which prevents the formation of physiological MT asters. In 2007, the gene mutated in *asterless* was cloned and shown to constitute a pancentriolar and basal body protein (Varmark et al., 2007). Moreover, Asterless has also been found to be essential for cilia formation and centriole duplication in *Drosophila* and zebrafish (Blachon et al., 2008). Human Cep152 localizes to centrosomes upon overexpression and its depletion prevents proper formation of primary cilia and centriole duplication to a moderate extent (Andersen et al., 2003; Graser et al., 2007; Kleylein-Sohn et

al., 2007). Recently, mutations within the *cep152* gene have been detected in patients with primary microcephaly and Seckel syndrome (Guernsey et al., 2010; Kalay et al., 2010). The fact, that mutations in several centrosomal proteins have been linked to either of these diseases, hints at an essential, physiologically relevant function of Cep152 at human centrosomes as well.

2.5.2 Cep192

Homologues of Cep192 accomplish different functions in different organisms. Spd-2 has originally been characterized in *C. elegans* to be crucial for PCM recruitment and centriole duplication. As discussed earlier, it is required for the recruitment of the kinase Zyg-1 and thus all downstream centriole duplication factors (O'Connell et al., 2000; Kemp et al., 2004; Pelletier et al., 2004; Delattre et al., 2006). In contrast, dSpd-2 does not participate in centriole duplication in *D. melanogaster*, but is involved in recruitment of PCM to centrioles (Dix and Raff, 2007). Initial studies on the function of human Cep192 did not provide satisfactory conclusions on its function. Whereas both studies agreed on the involvement of Cep192 in γ-Tubulin recruitment to centrioles, they contradicted each other regarding the function of Cep192 in centriole duplication. On the one hand, Gomez-Ferreria *et al.* (2007) showed that Cep192 is dispensable for centriole duplication. On the other hand, Zhu *et al.* (2008) described Cep192 to be essential for this process. Noteworthy, although Spd-2 has been shown to mediate the recruitment of the regulatory kinase Zyg-1 to centrioles, the dependence of human Plk4 on Cep192 has not been addressed so far.

2.6 Three-Dimensional Structured Illumination Microscopy

In human cells, centriolar cylinders have approximate diameters of 150 – 200 nm and lengths of 400 – 450 nm (Paintrand et al., 1992; Bettencourt-Dias and Glover, 2007). To resolve centriolar and centrosomal substructures and the exact arrangement of several centriolar proteins with respect to each other, it is critical to employ high resolution imaging techniques. Immuno electron microscopy (immuno-EM) offers this possiblity. However, several novel super-resolution fluorescence microscopy techniques have recently been developed, which are

especially valuable for the visualization of structures as small as centrioles (e.g. “Stimulated Emission Depletion” (STED) or “three-dimensional structured illumination microscopy” (3D-SIM)). These techniques combine the advantages of fluorescence microscopy, such as simultaneous visualization of several proteins and simple preparation of specimens, with a high spatial resolution beyond the Abbe diffraction limit of light (Hell, 2007; Huang et al., 2010; Schermelleh et al., 2010; Toomre and Bewersdorf, 2010).

3D-SIM principally works by illuminating the object with multiple interfering laser lights followed by the mathematical processing of the detected interference information to reconstruct a high-resolution image. Application of 3D-SIM allows the simultaneous acquisition of z stacks for up to three different proteins at a spatial resolution of 130 nm in the x-y and 300 nm in the z-direction (Schermelleh et al., 2008; Baddeley et al., 2010). In contrast to other existing super-resolution techniques, 3D-SIM has the advantage that the axial resolution is also increased in addition to the lateral one (Willig et al., 2007; Schermelleh et al., 2010). Moreover, 3D-SIM is not limited to the detection of structures close to the sample surface, as it is the case for methods based on total internal reflection fluorescence (TIRF) microscopy (Reichert and Truskey, 1990). Thus, it allows the analysis of organelles up to several µm deep within fixed cells, such as centrosomes in late G2 or M phase of the cell cycle.

3 Aims of this Project

This project aimed at obtaining a deeper insight into the biology of mammalian centrosomes by, firstly, characterizing the centriolar protein Cep152 in detail and, secondly, by analyzing the subcellular localization of key centrosomal proteins at sub-Abbe resolution.

1. The function of centrosomes as microtubule-organizing centres in mammalian cells is well established and several proteins have been identified that are required to nucleate microtubules into the cytoplasm and to organize the PCM around centrioles. However, their inter-relations have not been understood to sufficient detail. Moreover, to ensure the faithful segregation of these organelles during cell division, they have to be duplicated once per cell cycle. Here, we have investigated and compared the functions of Cep152 and Cep192, proteins whose homologues have been implicated in both PCM recruitment and centriole duplication (Section 4). We particularly focussed on the centrosomal recruitment of the protein kinase Plk4, since its function has been investigated by loss- and gain-of-function analyses in detail, but its recruitment to centrioles and mode of action were not understood.

2. To unravel the function of centrosomal proteins it is pivotal to understand their localization at high resolution. Wide-field light microscopy has been used to determine the approximate localization of centrosomal proteins. However, the size of centrioles is in the range of the resolution limit of conventional light microscopy and they can thus not be sufficiently resolved. Additionally, electron microscopy revealed the localization of individual proteins within centrioles and centrosomes at high spatial resolution, but co-localization studies are difficult to perform by electron microscopy. Here, we applied structured illumination microscopy, a super-resolution technique, to investigate the localization of 18 centriolar as well as centrosomal proteins in U2OS and RPE-1 cells (Section 5).

4 Results I – Cep152 and Cep192 in Centrosome Function

Homologues of Cep152 and Cep192 are essential for PCM recruitment and/ or centriole duplication in *D. melanogaster* and *C. elegans*. However, the roles of human Cep152 and Cep192 were not understood sufficiently, when this project was started. To unravel the relevance of Cep152 and Cep192 in centrosome biology more precisely, their localization, their function and their cell cycle-specific expression have been investigated in detail. As homologues of both proteins accomplish similar functions in other organisms, we put particular emphasis on the comparison of the two proteins.

4.1 Sequence and Expression Analysis of Cep152 and Cep192

As a first approach to determine the functions of Cep152 and Cep192, we analysed their sequences to identify potential splice variants as well as predicted secondary and tertiary structures.

4.1.1 Cep152

4.1.1.1 Cep152 Splice Variants

Andersen *et al.* (2003) had identified Cep152 in a proteomic screen. They termed it "Cep152" based on the predicted molecular weight of the human mRNA clone KIAA0912. During the course of this study, five different isoforms could be found in various databases (NCBI, Ensembl and/ or Uniprot), which we termed Cep152-1 to Cep152-5 (**Figure 11**), some of which have been discontinued by Endsembl. These isoforms are generated by alternative splicing and primarily differ in the presence (isoforms 1 – 3) or absence (isoforms 4, 5) of an elongated C terminus.

Figure 11 Isoforms reported for human Cep152. Five potential Cep152 isoforms are generated by alternative splicing in human cells. These potential isoforms were named Cep152-1 to Cep152-5. Here, the isoforms together with their predicted lengths in base pairs (bp) and amino acids (AA) are illustrated schematically. NCBI reports different isoforms than Ensembl or Uniprot, whereby Ensembl has discontinued (discon.) two entries in 2010.

4.1.1.1.1 Generation of Cep152 Antibodies

Antibodies directed against Cep192 had already been available. But in order to investigate the localization and expression of Cep152 by IF microscopy or Western Blotting and to be able to perform immunoprecipitation experiments, polyclonal antibodies against Cep152 were raised in rabbits (**Figure 12**). To this end, two His-tagged Cep152 fragments were expressed in *E. coli* and used to immunize two rabbits each. One of these fragments spans the N-terminal 87 amino acids, which is common to all potentially expressed isoforms. The other fragment represents the C terminus of the long isoforms (i.e. amino acids 1434 – 1710 of isoform 1). This way, we intended to gain insight into the actual expression of the various isoforms. We termed the generated N-terminal antibodies Cep152-N 207 and Cep152-N 230 and the C-terminal ones Cep152-C 934 and Cep152-C 880.

After affinity purification with the antigens the obtained antibodies were tested for their specificity and efficacy in immunofluorescence (IF) microscopy, Western Blotting and immunoprecipitations (IPs). For IF the antibodies Cep152-N 207 and Cep152-C 934 were selected. Both antibodies stained the centrosome in U2OS and HeLa S3 cells and this staining was specifically lost, when Cep152 was depleted (**Figure 13** A and data not shown). Furthermore, both overexpressed Cep152-2 and Cep152-4 were detected by the N-terminal antibodies in Western Blot analysis, whereas the C-terminal antibodies only recognized the long isoform Cep152-2 (**Figure 13** B). Finally, we found Cep152-N 207 to

immunoprecipitate the overexpressed proteins Cep152-2, Cep152-2 lacking the C terminus and Cep152-4. In contrast, Cep152-C 934 could only immunoprecipitate full length Cep152-2 (**Figure 13** C).

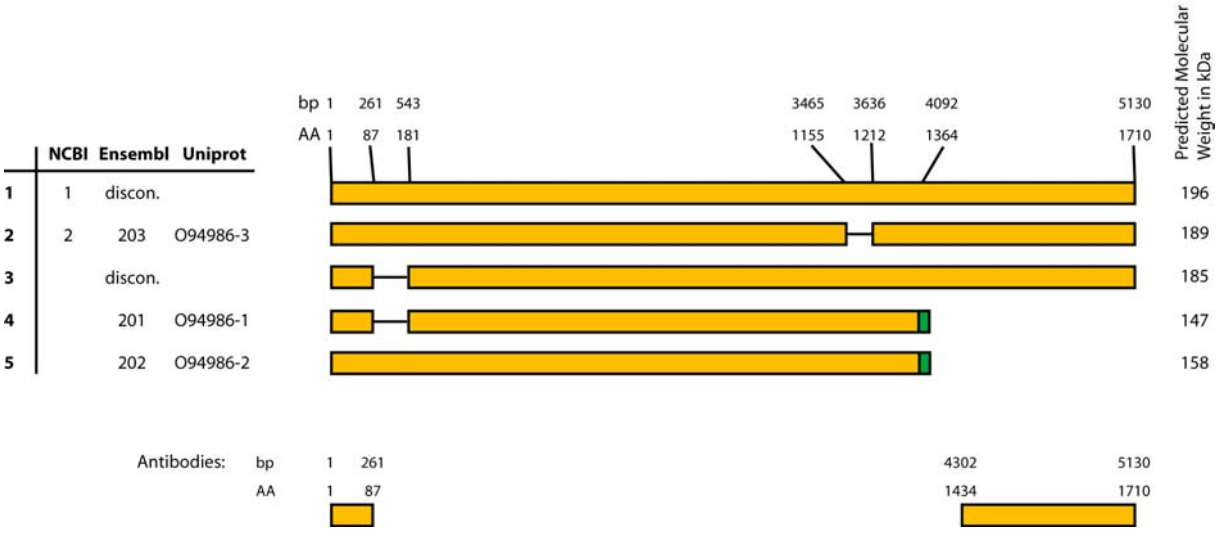

Figure 12 Cep152 antibodies targeting either the N or the C terminus were generated. His-tagged fragments of Cep152 spanning either the N-terminal amino acids 1 – 87 or the C-terminal amino acids 1434 – 1710 were used for the immunization of rabbits. The N-terminal antibody should recognize all Cep152, whereas the C-terminal one should only recognize the long isoforms.

Thus, the generated Cep152 antibodies are functional in immunostaining, Western Blotting and immunoprecipitation. Moreover, the N-terminal antibodies recognize all potential isoforms, whereas the C-terminal antibodies are specific for the long isoforms.

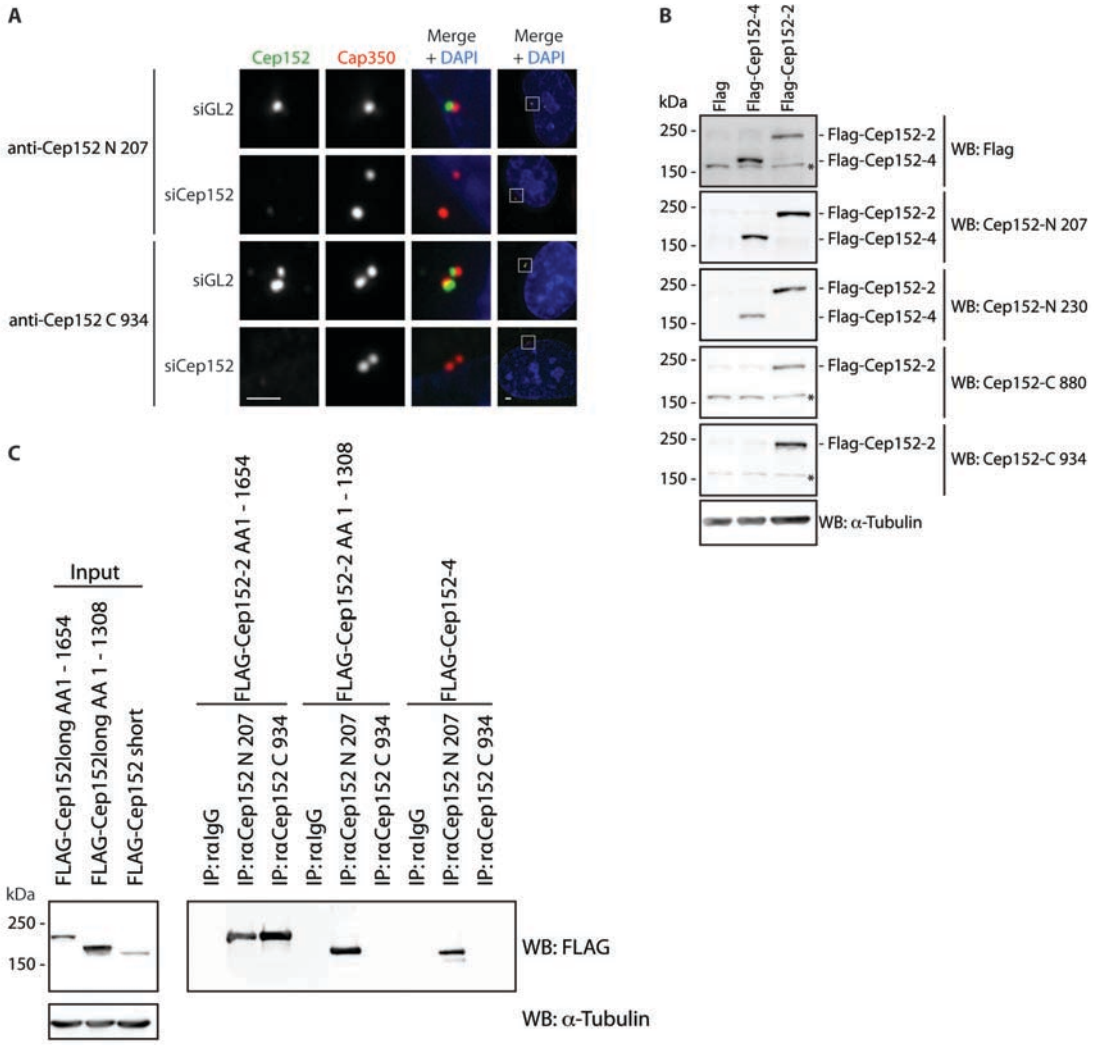

Figure 13 Generated Cep152 antibodies are functional in IF microscopy, Western Blotting and immunprecipitations. A U2OS cells were transfected with the indicated siRNA oligonucleotides for 48 h. After fixation the cells were stained with the indicated antibodies and analysed by IF microscopy (DAPI was used to stain DNA, scale bars represent 1 µm). **B** Either Flag vector control, Flag-Cep152-4 or Flag-Cep152-2 were overexpressed in U2OS cells for 48 h. After lysis the samples were analysed by Western Blotting using the indicated antibodies. Note that the N-terminal Cep152 antibodies detect both Cep152-4 and Cep152-2, whereas the C-terminal antibodies only detect the long isoform Cep152-2. Asteriks mark unspecific bands. **C** The indicated Flag constructs were overexpressed in HEK293T cells for 48 h. After lysis the samples were subjected to immunoprecipitation experiments using either IgG control, Cep152-N 207 or Cep152-C 934 antibodies. After elution the samples were analysed by Western Blotting using the indicated antibodies. Note that Cep152-N 207 can immunoprecipitate all constructs, whereas Cep152-C 934 can only immunoprecipitate full length Cep152-2 that contains the extended C terminus.

4.1.1.1.2 Expression of Cep152 Isoforms

Cep152 is possibly expressed in different isoforms (**Figure 11**), which can be subdivided into long isoforms (with an extended C terminus) or short isoforms (lacking the extended N terminus). RT-PCR using primers directed against the termini of either long or short isoform revealed expression of both long and short isoforms in all analysed cell types (**Figure 14** A). As different reverse primers with potentially differing PCR efficiencies were used to amplify either long or short isoforms, one cannot directly infer the relative abundance of these isoforms from the obtained results. Moreover, an antibody generated against the N terminus of Cep152 stained two bands, one just below 250 kDa and one above 150 kDa that were diminished upon depletion by RNAi (**Figure 14** B). Notably, both isoforms migrated at higher molecular weights than predicted from their sequences. This might be due to a partial SDS stability, which results in binding of less than expected SDS molecules and thus a slower migration in an electric field. In contrast to N-terminal antibodies, the C-terminal antibody only recognized the upper band (data not shown). Of both bands the lower band was much weaker, which implies that Cep152short is much less expressed than Cep152long.

Table 1 Full length Cep152 mRNA clones.

Accession	Description	Tissue Type	Corresponding Isoform
BX648822.1	Homo sapiens mRNA; cDNA DKFZp686C15165 (from clone DKFZp686C15165)	Human uterus endothel prim ary cell culture	Cep152-1
BC117182.1	Homo sapiens centrosomal protein 152kDa, mRNA (cDNA clone MGC:150791 IMAGE:40125733), complete cds	Lung and heart, PCR rescued clones	Cep152-2
AB020719.1	Homo sapiens KIAA0912 mRNA for KIAA0912 protein, partial cds	Brain	Cep152-4

These data indicate that at least one long and one short isoform of Cep152 are expressed in the human cell lines we use. When searching for isoform-specific EST and nucleotide sequences, we only identified three clones that could unequivocally be assigned to specific isoforms (**Table 1**), namely isoforms Cep152-1, Cep152-2 and Cep152-4. In mass spectrometry analysis of centrosomes purified from KE37 cells (Andersen et al., 2003), a peptide was detected spanning the sequence from exon 19 into exon 20: DSASQGTGQGDPGPAAGHHAQPLALQATEAEADK (with all isoforms containing exon 20 except for Cep152-2). This illustrates that exon 20 is indeed translated *in vivo*, either in long or short Cep152 isoforms. In addition, sequencing of cDNA amplified from a HeLa

cDNA library revealed the expression of Cep152-2. Thus, we decided to use Cep152-2 as long and Cep152-4 as short isoform for the experiments conducted later.

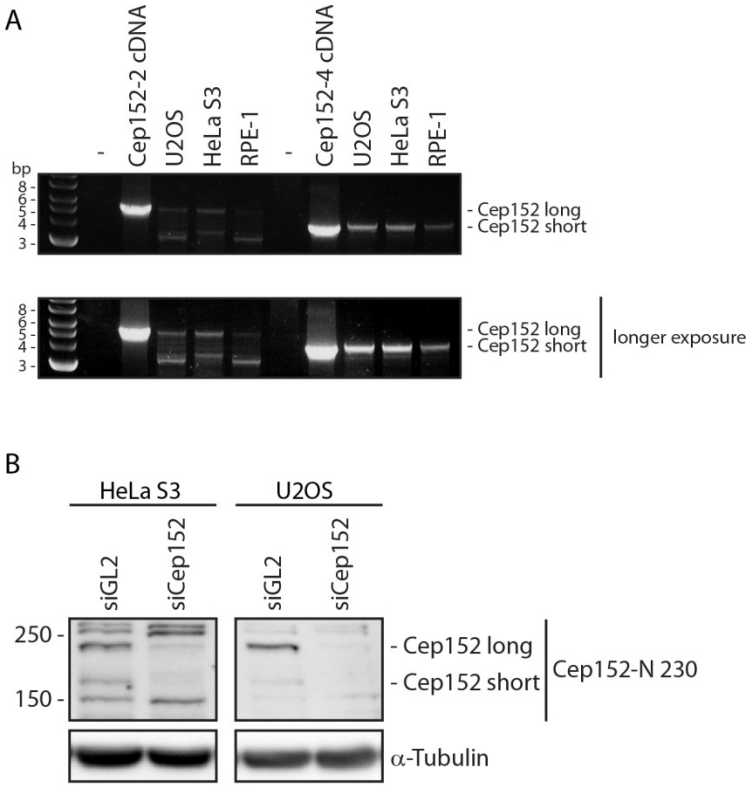

Figure 14 Long and short isoforms of Cep152 are expressed in human cell lines. A RNA was isolated from the indicated human cell lines and reverse transcribed using oligo dT primers. These cDNA libraries were taken as template for the amplification of Cep152 with primers either specific for the long or the short isoforms. Results were analysed by gel electrophoresis. **B** Cep152 was depleted from HeLa S3 and U2OS cells. After lysis the samples were analysed by immunoblotting using an antibody recognizing all potential isoforms. α-Tubulin was used as loading control.

4.1.1.2 Cep152 Structure Prediction

Having defined the sequences of Cep152 isoforms, we used the sequences of Cep152-2 and Cep152-4 as representatives for long and short isoforms, respectively, for basic structure predictions. We applied the software Psipred (http://bioinf.cs.ucl.ac.uk/psipred/) to predict the secondary structure. Both isoforms have a high frequency of predicted helical structures in the region approximately ranging from amino acids 200 to 1260 (data not shown). Moreover, the N terminus appears to be largely unstructured except for a helical region ranging from amino

acids 16 to 52 (**Figure 15**). Finally, the C terminus is predicted to be rather unstructured as well (data not shown).

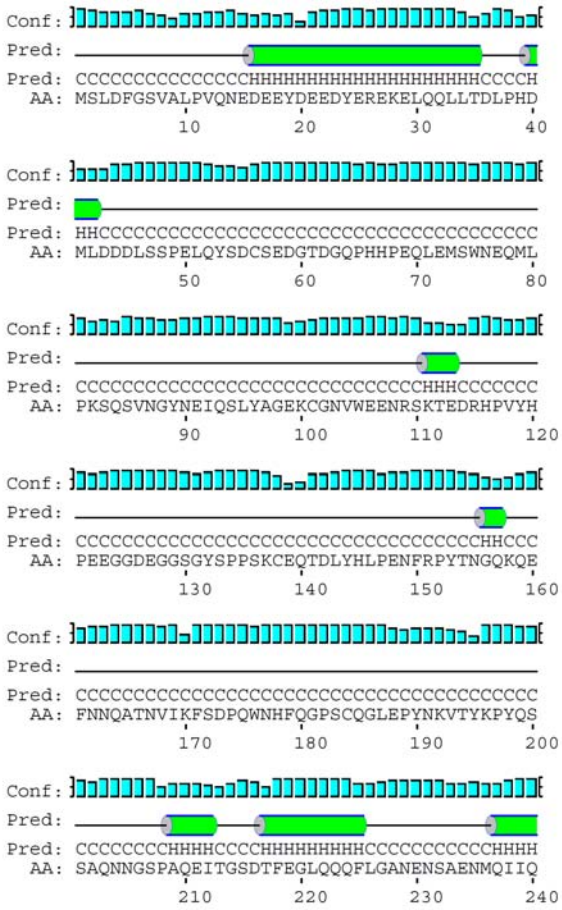

Figure 15 Secondary Structure Prediction using Psipred. The sequence of Cep152-2 was used for secondary structure prediction with Psipred. Here, the results for the N-terminal 240 amino acids are shown.

In addition to these secondary structure predictions we employed the software Coils (http://www.ch.embnet.org/software/COILS_form.html), since many centrosomal proteins are predicted to form coiled coils. Indeed, Cep152 has a high probability of forming coiled coils in the middle part of the protein, roughly ranging from amino acids 210 to 1400 (based on isoform 2) (**Figure 16**). These predictions nicely correlate with the results we obtained with Psipred, which predicted multiple α-helices for this region.

Taken together, human Cep152 potentially forms two types of isoforms, either with or without an extended C terminus. Both isoforms contain a long region, which is probably organized into coiled-coil structures, and an unorganized N terminus. The extended C terminus of the long isoforms is potentially disorganized as well. Apart from these coiled-coil regions no domains with predicted enzymatic activity were identified.

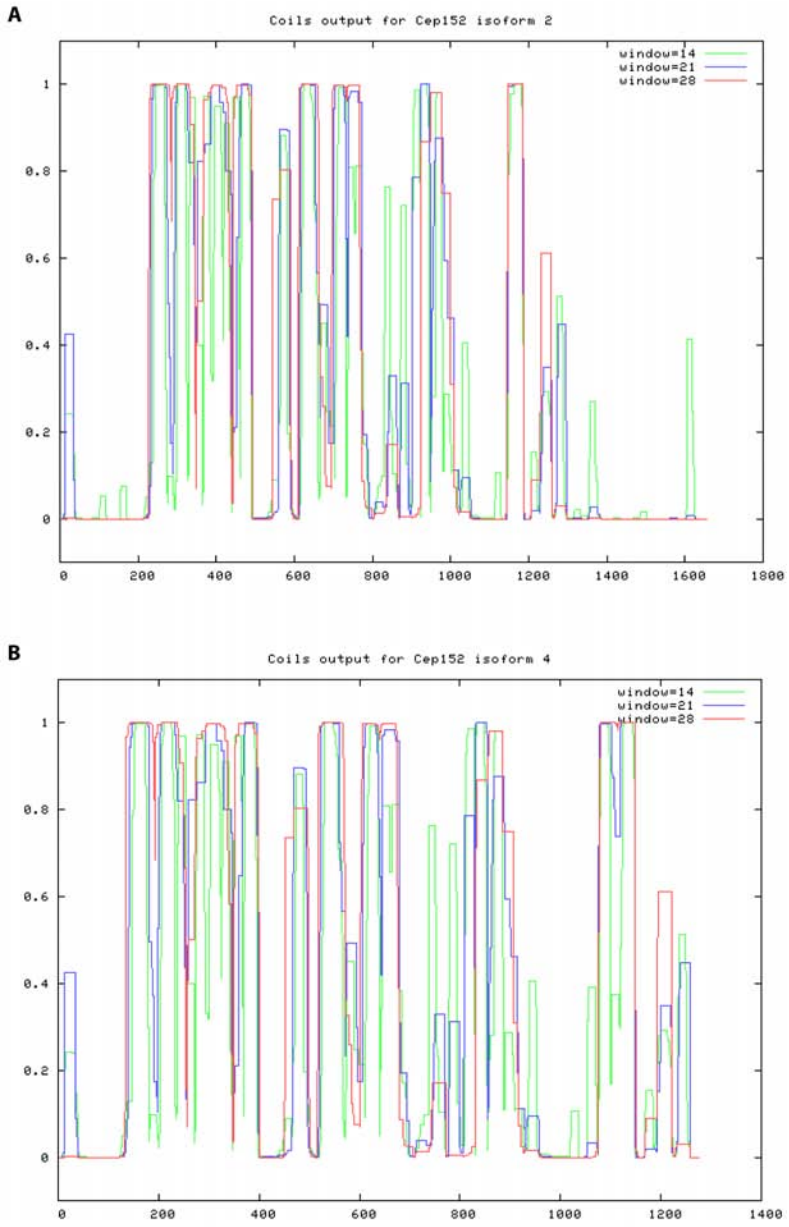

Figure 16 Several coiled-coil regions are predicted for Cep152. The primary sequences of Cep152 isoform 2 (**A**) and isoform 4 (**B**) were analysed using the Coils software (www.ch.embnet.org (Lupas et al., 1991)). Window indicates the number of residues with which the sequence was scanned. In both proteins four main regions (in Cep152-4 approximately AA 150 – 400, 450 – 700, 750 – 950 and 1050 – 1250) show a high probability of coiled coil regions. Note the single stretch of amino acids at the very N terminus with a higher probability of forming coiled coils.

4.1.2 Cep192

4.1.2.1 Cep192 Splice Variants and their Expression

In different databases five potential isoforms for Cep192 can be found, which we termed Cep192-1 to Cep192-5. Similar to Cep152, these isoforms are generated by alternative splicing and differ in the existence of extended N termini (**Figure 17**). By NCBI isoform 1 is by now annotated as reference sequence.

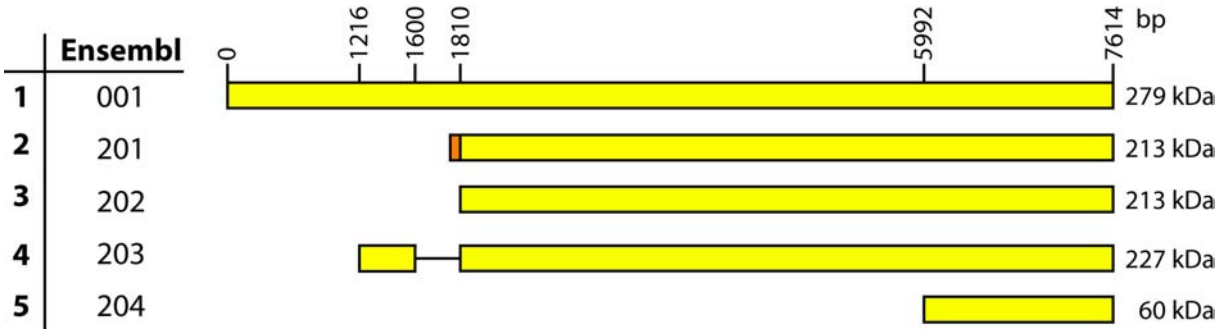

Figure 17 Five potential isoforms are reported for human Cep192. Five Cep192 isoforms generated by alternative splicing are potentially expressed in human cells. The differing colour represents a different translation start.

When Cep192 was depleted from HeLa S3 and U2OS cells and the samples were analysed by Western Blotting using an antibody directed against the C terminus of Cep192, only a prominent band above 250 kDa decreased compared to control depletions, even with long exposure times (**Figure 18** B). The molecular weight above 250 kDa corresponds to the longest of the possible isoforms, Cep192-1. Moreover, in U2OS cells another very weak band was diminished upon Cep192 depletion that ran in-between 250 kDa and the upper Cep192 band. This band might reflect the expression of one of the other Cep192 isoforms (2 – 4). To confirm the expression of the longest Cep192 isoform we generated cDNA libraries from HeLa S3, U2OS, HEK293T and RPE-1 cells, which were then used as template to amplify the N-terminal 3986 bp of Cep192-1 with sequence-specific primers. As positive control a plasmid containing Flag-Cep192-1 was used. In all cell lines a product was amplified at the expected size, which indicates that the longest isoform is expressed in all tested cell lines

(**Figure 18** C). The sequence of the product from U2OS cells was verified. When sequencing the additional amplified products we detected two sequences in which exon 12 or exon 12 and 13 were missing. These sequences correspond to the 5'-untranslated regions of isoforms 2 or isoform 4, respectively. Apart from that, we also consistently noticed that in U2OS samples more PCR products were produced.

Thus, as we detected one prominent band above 250 kDa by Western Blotting at least in HeLa S3 and U2OS cells, we concluded that mainly the first Cep192 isoform is expressed in the human cell lines we employ.

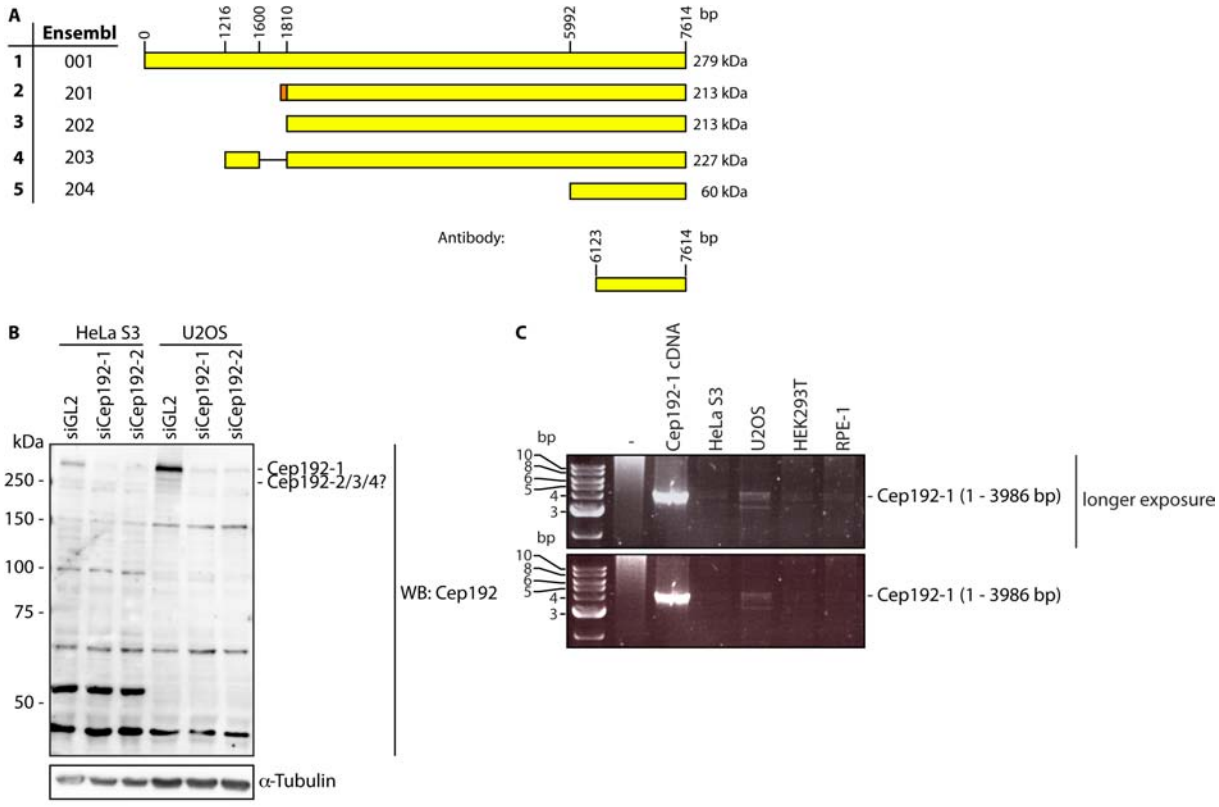

Figure 18 Mainly Cep192-1 is expressed in human cell lines. A The applied Cep192 antibody detects all potential isoforms. **B** HeLa S3 and U2OS cells were transfected with the indicated siRNA oligonucleotides for 72 h. After lysis the samples were analysed by Western Blotting. Note that a prominent band above 250 kDa is diminished upon Cep192 RNAi. A second weaker band just below is also diminished in U2OS cells. **C** RNA was isolated from the indicated cell lines and reverse transcribed using Poly-dT primers. These cDNA libraries were then used to amplify the N-terminal half of Cep192. As negative control no template was added, as positive control Flag-Cep192-1 plasmid was used.

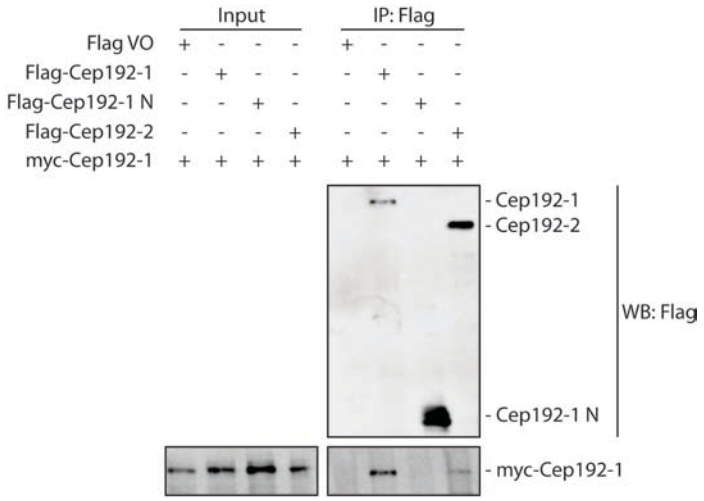

Figure 19 Cep192 can homodimerize. HEK293T cells were transfected with the indicated expression plasmids for 24 h (Cep192-1 N: amino acids 1 – 519). After lysis immunoprecipitations were performed using Flag antibodies and analysed by Western Blotting.

We cloned Cep192-1 by amplifying the N-terminal half of the cDNA from a U2OS cDNA library and cloned it into a previously published Cep192 construct corresponding to isoform Cep192-2 (Gomez-Ferreria et al., 2007) (see Materials and Methods for details). When we overexpressed either Flag-tagged Cep192-1, Cep192-1 AA 1 - 519 or Cep192-2 together with myc-tagged Cep192-1, only full length Cep192-1 or Cep192-2 interacted with Cep192-1 (**Figure 19**). This implies that Cep192 dimerizes and that the N terminus of Cep192-1 is neither necessary nor sufficient for this.

4.1.2.2 Cep192 Structure Prediction

In contrast to Cep152, structure predictions using the amino acid sequence of Cep192-1 revealed very few α-helical and β-sheet structures (using Psipred, data not shown) or coiled-coil regions (**Figure 20**).

Thus, human Cep192 potentially forms three types of isoforms, either with or without an extended N terminus or just the C-terminal region. The applied softwares for structure predictions do not reveal areas of defined structures. Furthermore, no domains with predicted enzymatic activity were identified.

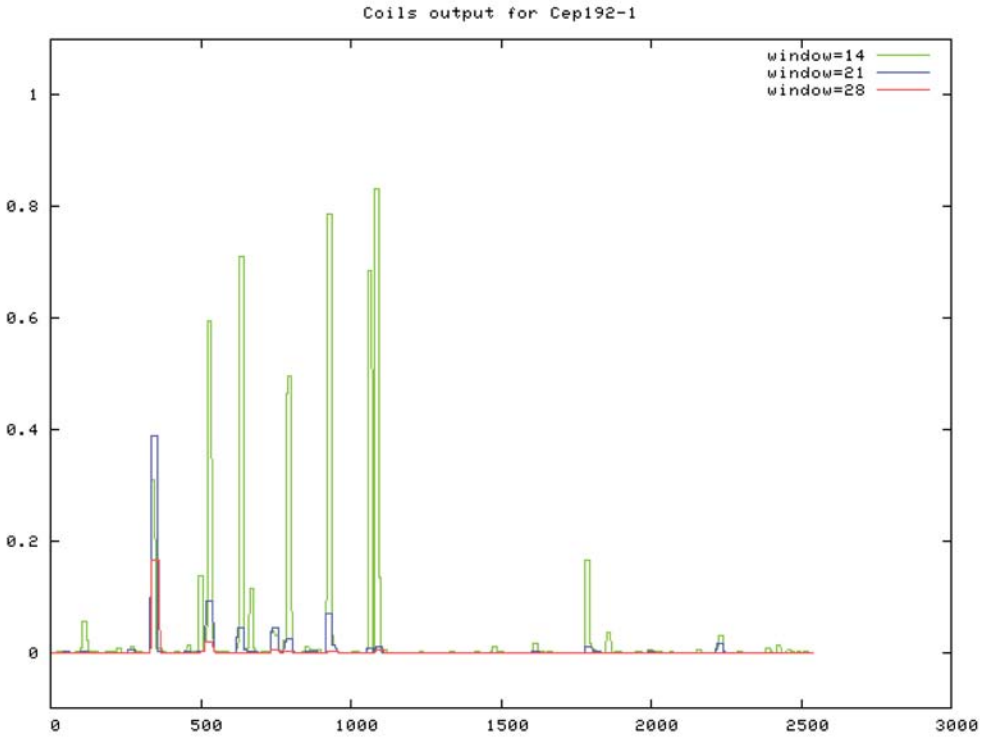

Figure 20 Few coiled-coil regions are predicted within the N-terminal half of Cep192-1. The amino acid sequence of Cep192-1 was analysed with the software Coils to predict coiled-coil regions. Window indicates the number of residues with which the sequence was scanned. Note that there is one region within the N terminus (AA 329 – 384) potentially forming coiled coils.

4.2 Localization of Cep152 and Cep192

Homologous proteins of both Cep152 and Cep192 function in PCM recruitment and/ or centriole duplication depending on the investigated organism. To understand the similarities and differences of Cep152 and Cep192 in humans, we initially examined their localization at high spatial resolution in different cell cycle stages.

4.2.1 Localization of Cep152

Andersen *et al.* (2003) identified Cep152 as a centrosomal protein in a proteomic screen and found overexpressed GFP-tagged Cep152 to indeed reside at centrosomes. We confirmed the centrosomal localization by IF microscopy. Furthermore, this localization was found to be

independent of microtubules attached to centrosomes, since depolymerization of microtubules by cold treatment did not disrupt Cep152 localization (data not shown). Here, we analyzed Cep152 localization in detail. We addressed the domain requirement for centrosomal recruitment on the one hand and the localization in sub-Abbe resolution on the other hand.

4.2.1.1 Localization of Cep152 at High Spatial Resolution

By widefield fluorescence microscopy we often observed a central hole within the Cep152-positive area, indicating that Cep152 might actually localize in a ring-like pattern (data not shown). Therefore, we employed immuno-EM and 3D-SIM to define the subcellular localization more precisely. For immuno-EM U2OS cells were stained with either the C-terminal or the N-terminal Cep152 antibody. For 3D-SIM cells were co-stained with C- as well as N-terminal Cep152 antibodies and an antibody against glutamylated tubulin. After depolymerisation of cytoplasmic microtubules by cold treatment the latter antibody stains both centrioles in G2 phase cells. With both microscopy methods Cep152 was detected as a ring surrounding the proximal half of the mother centriole, i.e. also at the interface between mother and growing daughter centriole. This did not depend on whether the N- or C-terminal antibody was employed (**Figure 21**).

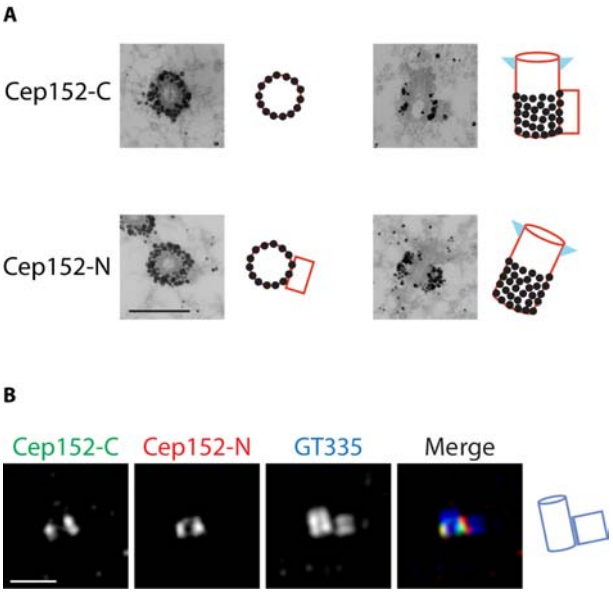

Figure 21 Cep152 localizes around the proximal half of mother centrioles. A U2OS cells were fixed and stained for immuno-EM. The cells were either stained with the C-terminal or the N-terminal Cep152 antibodies followed by nanogold-labelled secondary antibodies. **B** After fixation U2OS cells were stained with the indicated antibodies and analysed by 3D-SIM. Scale bars represent 1 µm. Centriole orientation is schematically illustrated.

Moreover, by immuno-EM Cep152 was detected at mother centrioles at different stages of centriole duplication, i.e. mother centrioles with and without visible daughter centrioles of different lengths (**Figure 22** A). We also found cells with two single disengaged centrioles, of which either only the appendage-bearing centriole or both centrioles were positive for Cep152 (**Figure 22** A), but we did never observe Cep152-negative centrioles that had already duplicated. In agreement with a recruitment of Cep152 before centriole duplication we obtained similar results by conventional IF microscopy (see below, **Figure 66**). This implies that Cep152 localizes around the mature centriole at different interphase stages. Similar results were obtained with 3D-SIM (data not shown). Additionally, we costained U2OS cells with antibodies against Cep152 and proteins localizing to the PCM. DAPI was used to visualize the DNA and CP110 antibodies to determine the number of centrioles per cell. This allowed us to determine the cell cycle stage and correlate it to the localization of Cep152 and the PCM protein γ-Tubulin. In G1 phase (only 2 centrioles per cell), S/G2 phase (4 centrioles) and in mitosis Cep152 remained localized as a distinct ring around mother centrioles. In contrast, γ-Tubulin was detected at both mother and daughter centrioles in S/G2 phase and in a wider web around centrioles in mitosis (**Figure 22** B). This is consistent with the previously

suggested amorphous composition of the PCM (Dictenberg et al., 1998). These results indicate that Cep152 is restricted to the centriolar walls independently of the cell cycle stage.

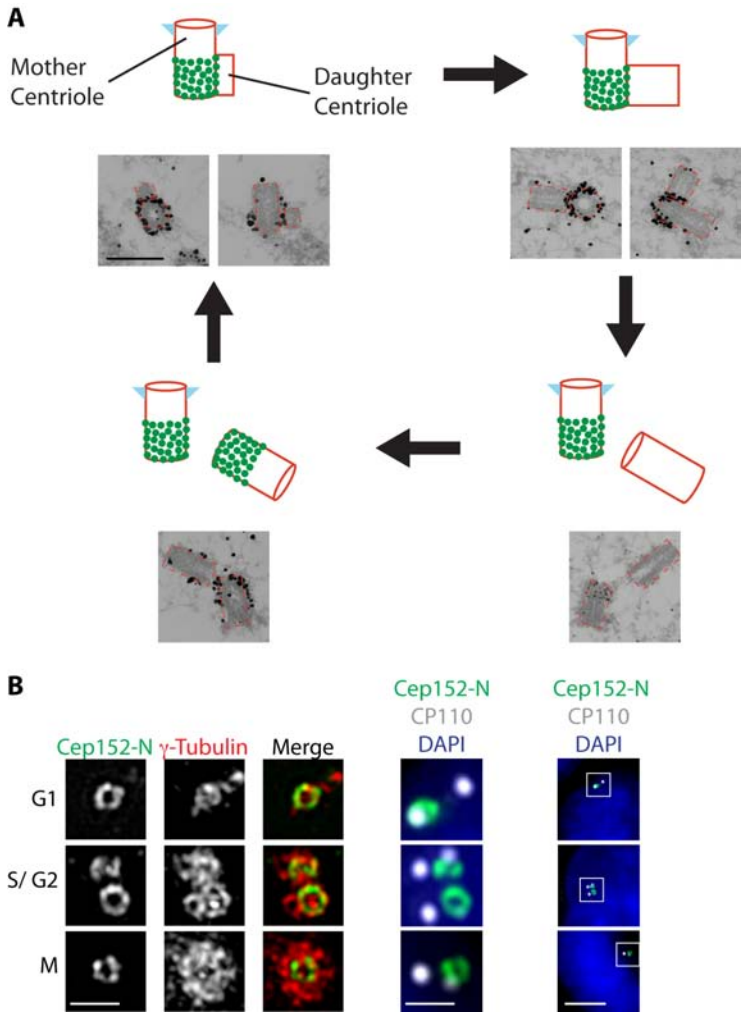

Figure 22 Cep152 localizes as a ring around the proximal end of the mother centriole throughout the cell cycle. A U2OS cells were fixed and stained with the C-terminal Cep152 antibody for immuno-EM. Scale bar represents 1 µm. **B** After fixation U2OS cells were stained with the indicated antibodies and the 488 and 594 channels were analysed by 3D-SIM. To visualize the cell cycle stage DNA was stained with DAPI and distal centriolar ends with CP110 antibodies, which were acquired using a conventional DV system. Scale bars represent 1 µm or 5 µm (overview images in the very right panel).

Taken together, Cep152 localizes around the proximal half of mother centrioles in both interphase and mitosis.

4.2.1.2 Central Coiled-Coil Domain of Cep152 is Required for Centrosomal Localization and Oligomerization

Based on the obtained structure predictions (Section 4.1.1.2) we generated deletion mutants of Cep152-2 to determine which part is required for centrosomal localization (**Figure 23**A): an N-terminal fragment covering amino acids 1 – 220, the middle coiled-coil region (amino acids 221 – 1308) and a C-terminal fragment covering amino acids 1309 – 1654. When we overexpressed these fragments in human cells, only the coiled-coil fragment localized to centrosomes (**Figure 23**B). We did not detect any centrosomal localization of the other fragments even in highly overexpressing cells.

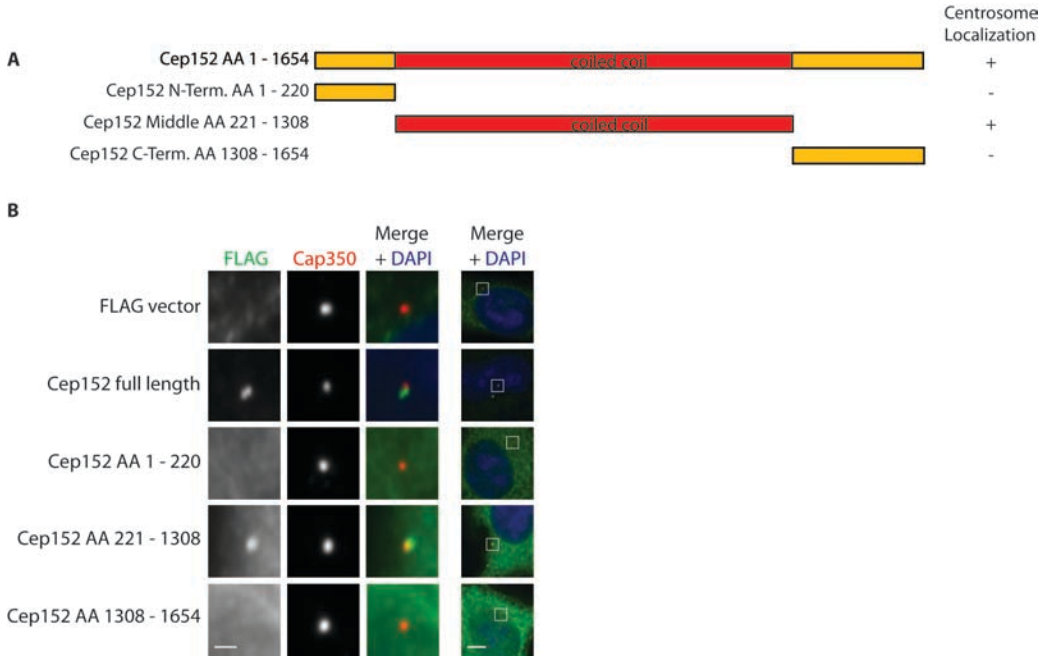

Figure 23 Central coiled-coil region of Cep152 is sufficient for centrosomal localization. A The indicated deletion mutants of Cep152-2 were generated. **B** U2OS cells were transfected with Flag-tagged expression constructs of these deletion mutants for 48 h. After fixation the cells were stained with the indicated antibodies. Scale bars represent 1 µm or 5 µm (overview in the right panel).

Furthermore, we tested whether Cep152 can dimerize or oligomerize by co-expressing Flag-tagged versions of Cep152 with myc-Cep152-2 and then performing immunoprecipitations. We found myc-Cep152-2 to be co-immunoprecipitated, whenever the Flag-tagged construct contained the central coiled-coil domain. This was also the case for the isoform Flag-Cep152-4. Thus, Cep152 can homodimerize and heterodimerize via its central coiled-coil region.

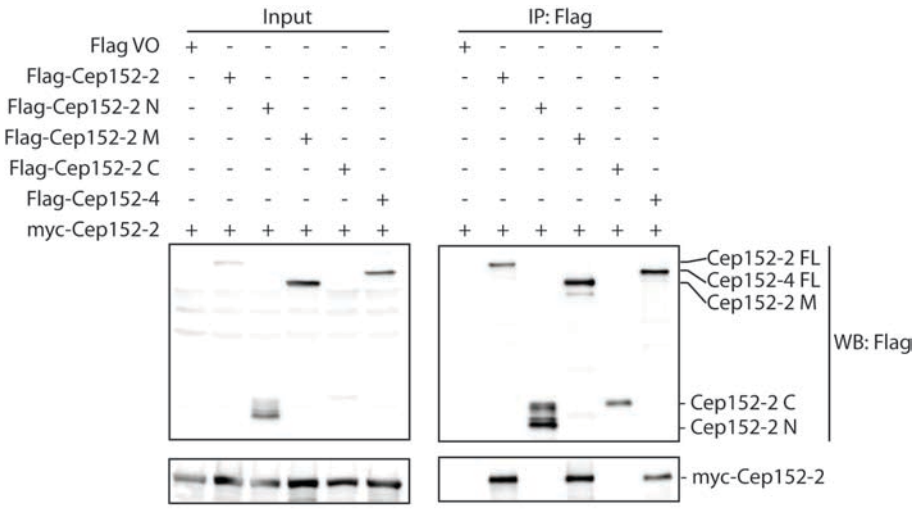

Figure 24 Cep152 oligomerizes via its central coiled-coil domain. HEK293T cells were transfected with the indicated expression plasmids for 24 h (Cep152-2 N: amino acids 1 – 220, Cep152-2 M: amino acids 221 – 1308, Cep152-2 C: amino acids 1308 – 1654). After lysis immunoprecipitations were performed using Flag antibodies and analysed by Western Blotting.

To rule out that the coiled-coil domain of Cep152 localizes to the centrosome by interacting with endogenous Cep152, we performed siRNA-rescue experiments. To this end, we intended to deplete the endogenous protein and then express the middle region of Cep152. As we could not obtain a UTR siRNA oligonucleotide, that efficiently depleted the protein, we generated oligoresistant expression constructs of Cep152 by inserting silent mutations wherever possible. To control the siRNA oligoresistance of the generated constructs, we stained cells simultaneously with an antibody against the tag of the overexpressed protein and with the N-terminal antibody Cep152-N to visualize endogenous Cep152 for IF microscopy. Even if endogenous Cep152 was not detected at centrosomes anymore, the ectopically expressed protein still localized to Cep135-positive centrosomes (**Figure 25**).

Thus, the central coiled-coil region of Cep152 is sufficient for homodimerization and for centrosomal localization.

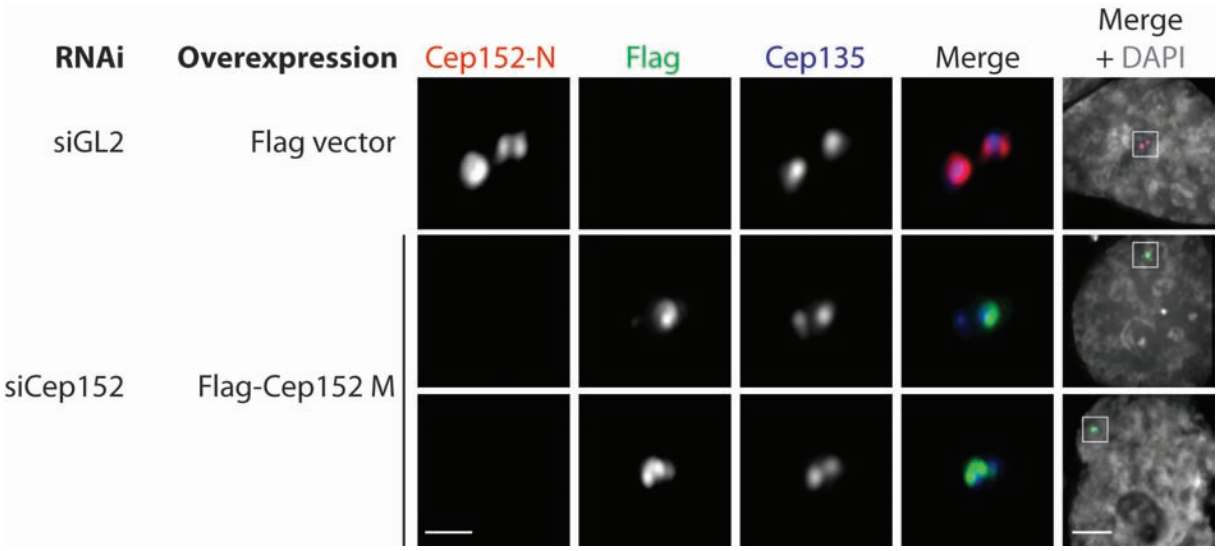

Figure 25 Cep152 M (AA 221 – 1308) localizes to centrosomes in the absence of endogenous Cep152. U2OS cells were transfected with the indicated siRNA oligonucleotides. After 24 h media was changed, 8 h later either Flag vector control or oligoresistant Flag-Cep152 M were overexpressed for 24 h. After fixation the cells were stained with the indicated antibodies. DAPI was used to visualize DNA. Scale bars represent 1 µm or 5 µm (overview images in the right panel).

4.2.2 Localization of Cep192

Previous studies had suggested that Cep192 localizes along centriolar walls in interphase. In addition, levels were increased in mitotic cells (Gomez-Ferreria et al., 2007; Zhu et al., 2008). However, due to low resolution of the images and low quality of the immuno-EM data, we investigated its localization in detail and compared it to the localization of Cep152.

4.2.2.1 Cep192 Localization Analyzed by Immuno-EM and Fluorescence Microscopy

By wide-field microscopy Cep192 was detected at centrosomes throughout the cell cycle. Similar to γ-Tubulin, the levels increased substantially towards mitosis, which is consistent with its role in PCM recruitment (**Figure 26** A). Moreover, we used both immuno-EM and 3D-SIM to determine the localization more precisely. Despite the existence of immuno-EM images of Cep192 in the literature (Zhu et al., 2008), we repeated the experiment to get images of higher quality. We found Cep192 to localize around mother and to a weaker extent around daughter centrioles in interphase with both methods employed (**Figure 26** B, C).

However, in mitotic cells Cep192 localized as an amorphous web surrounding the centrioles (**Figure 26** C), similarly to the PCM proteins NEDD1 and γ-Tubulin (see below, **Figure 79**).

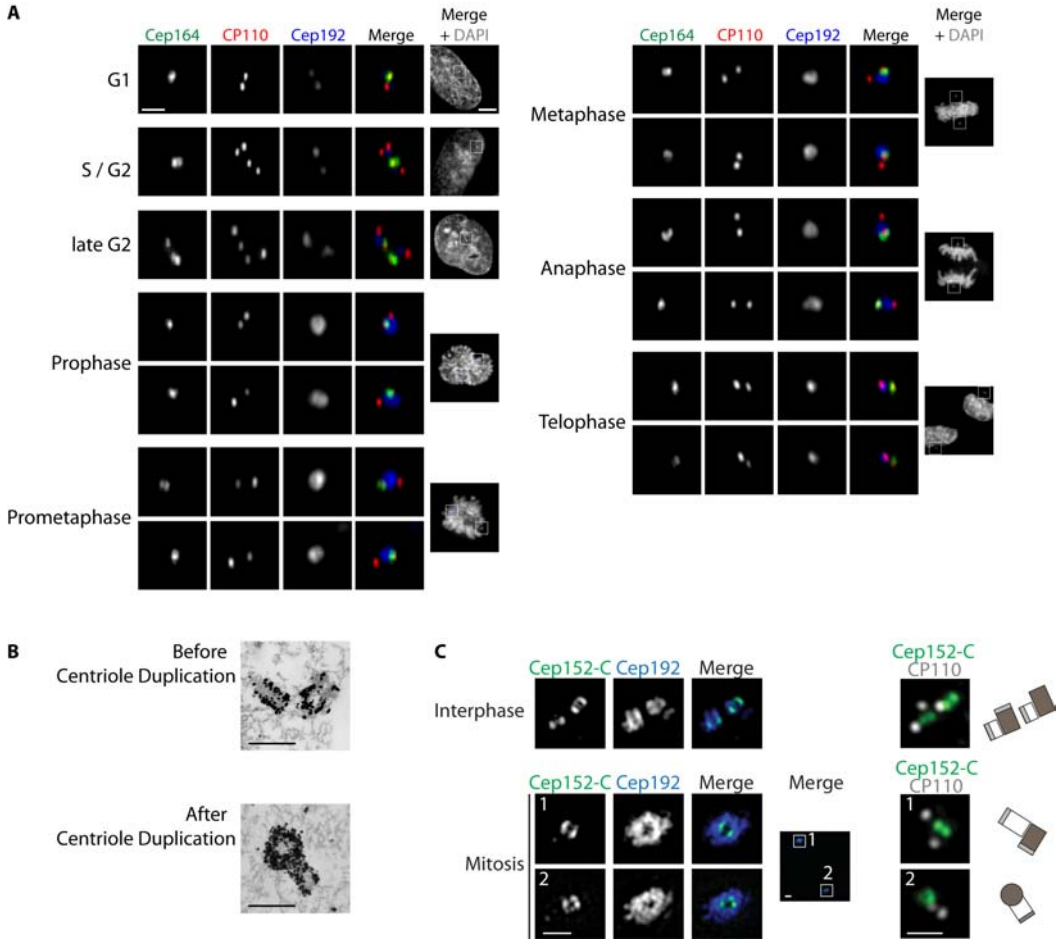

Figure 26 Cep192 localizes along mother and daughter centrioles in interphase and to the PCM in mitosis. A After fixation U2OS cells were stained with the indicated antibodies. DAPI was used to visualize DNA. Different cell cycle stages were identified based on the number of CP110 dots per cell as well as the shape of the DNA. Scale bars represent 1 µm and 5 µm (overview images in the right panels). **B** U2OS cells were fixed and stained for immuno-EM using a Cep192 primary antibody and nanogold-labelled secondary antibodies. Scale bars represent 1 µm. **C** U2OS cells were fixed and stained for 3D-SIM with the indicated antibodies. Interphase and mitotic cells were distinguished based on the distance between the centriole pairs. DV images of the Alexa 488 and Alexa 647 (gray) of the same cells were acquired to determine the orientation of the analysed centrioles (right panel). Scale bars represent 1 µm. (Figure A and B by E. Anselm)

4.2.2.2 Both Cep192-1 and Cep192-2 Localize to Centrioles in Interphase and the PCM in Mitosis

When overexpressing either Cep192-1 or Cep192-2 in U2OS cells, both isoforms localized to centrioles in interphase and also to the amorphous PCM in mitotic cells, which indicates that

the extended N terminus is not required for the mitotic PCM localization (**Figure 27**). Furthermore, when a construct containing the N-terminal 519 amino acids of Cep192-1 was overexpressed, no centrosomal localization was detected, which additionally implies that the N terminus is not sufficient for centrosomal localization (data not shown and **Figure 53**). The applied conventional widefield microscope does not allow to draw conclusions about a differential localization of the isoforms within interphase.

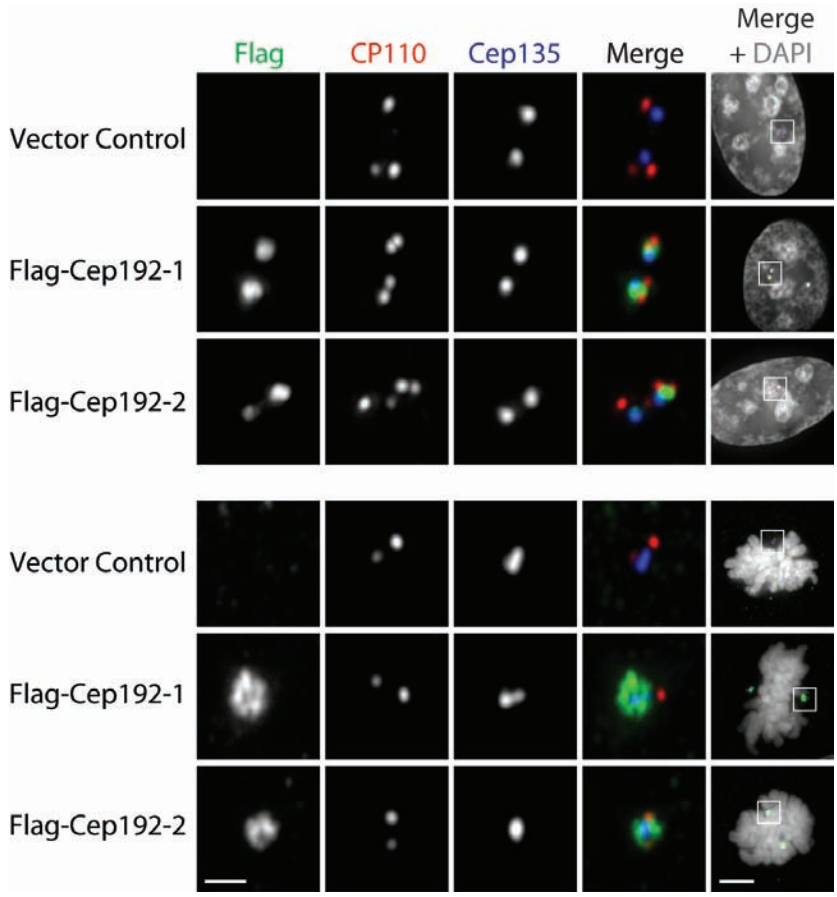

Figure 27 Both Cep192-1 and Cep192-2 localize to centrioles in interphase and to the amorphous PCM cloud in mitosis. U2OS cells were transfected with the indicated plasmids for 48 h. After fixation the cells were stained with the indicated antibodies and analyzed by immunofluorescence microscopy (Scale bar 1 µm or 5 µm (overview images), DAPI was used to visualize DNA).

4.3 Functional Interaction of Cep152 and Cep192

Despite their different localizations in mitotic cells, both Cep152 and Cep192 localize around centriolar walls in interphase. Whereas, Cep192 resides along both mother and daughter centrioles, Cep152 is confined to the proximal half of the mature centriole. Thus, we subsequently tested whether the localization of Cep152 depends on Cep192.

4.3.1 Stable Centrosomal Integration of Cep152 Depends on Cep192

To determine, whether Cep152 and Cep192 depend on each other, either Cep192 or Cep152 were depleted from human cells and the localization of the other one was checked. For IF microscopy, we employed antibodies that could detect all potential isoforms of either protein, i.e. a Cep152 antibody generated against the N terminus of the protein and a Cep192 antibody generated against the C terminus of the protein (Schmidt et al., 2009). To rule out any cell cycle effects, only cells in S phase, visualized by PCNA puncta within the nucleus, were considered. In Cep152-depleted cells centrosomal levels of Cep192 remained unchanged. However, if Cep192 was depleted, Cep152 was strongly reduced (**Figure 28**). This result was confirmed using another Cep192 siRNA oligonucleotide (data not shown).

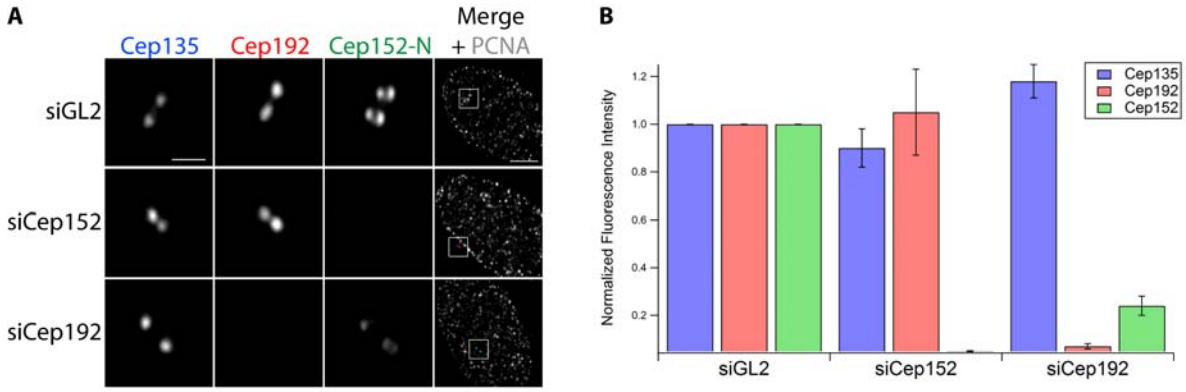

Figure 28 Cep152 is strongly reduced at centrosomes upon depletion of Cep192. U2OS cells were transfected with the indicated siRNA oligonucleotides for 72 h. After fixation the cells were stained with the indicated antibodies. PCNA was used to visualize S phase cells. In **A** representative images are shown. Scale bars represent 1 µm and 5 µm (overview images, right panel). In **B** the quantification of centrosomal Cep135, Cep192 and Cep152 levels is shown (three independent experiments, 10 cells each, error bars denote standard deviation). (Figure provided by E. Anselm)

As Cep192 localizes along both mother and daughter centrioles in interphase (**Figure 26**), reminiscent of other PCM proteins, we tested whether depletion of Pericentrin, another PCM protein, also impaired centriolar localization of Cep152. However, when we depleted Pericentrin, both Cep192 and Cep152 still localized to centrosomes. Similarly, depletion of either Cep192 or Cep152 did not interfere with Pericentrin localization (**Figure 29**).

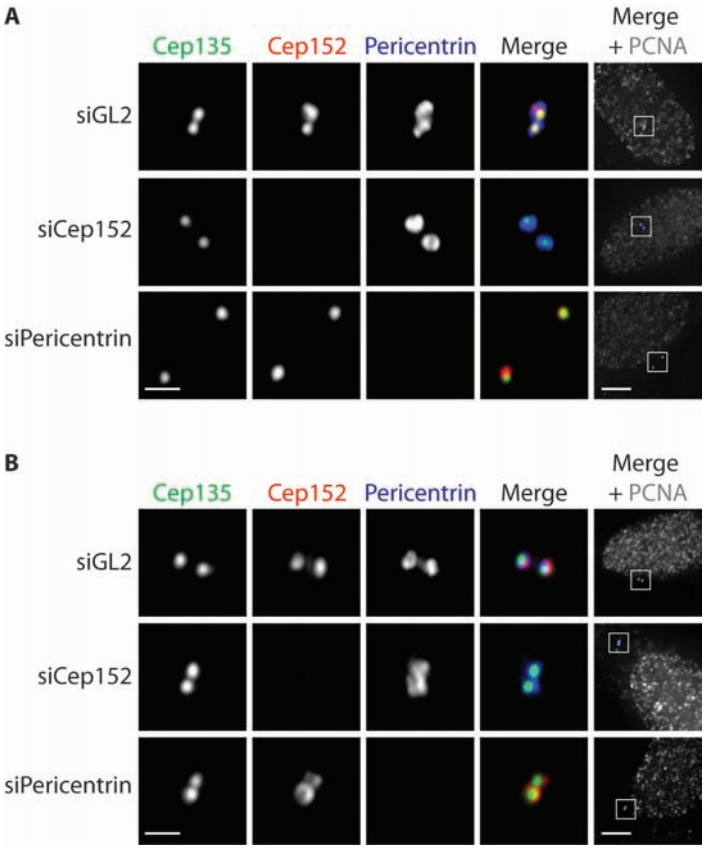

Figure 29 Pericentrin depletion does not interfere with the centrosomal localization of Cep192 or Cep152. U2OS cells were transfected with the indicated siRNA oligonucleotides for 72 h. After fixation the cells were stained with the indicated antibodies. The effect of Pericentrin depletion on Cep192 (**A**) and Cep152 (**B**) localization was examined. PCNA was used identify cells in S phase. Scale bars represent 1 µm or 5 µm (overview images, right panel).

Finally, we also checked the presence of the centrosomal proteins Cep63 and CPAP upon Cep192 depletion to support the observed reduction in Cep152 levels at centrosomes. It has been published previously that Cep152 is required for binding of Cep63 to centrioles (Sir et al., 2011). In addition, centrosomal CPAP localization is also dependent on Cep152 (Cizmecioglu et al., 2010; Dzhindzhev et al., 2010). Indeed, Cep63 and CPAP were barely

detectable in Cep192-depleted cells compared to GL2 control-depleted cells (**Figure 30** and data not shown).

Thus, Cep192 is required for the stable integration of Cep152 and potentially thereby also of Cep63 and CPAP into the centrosome.

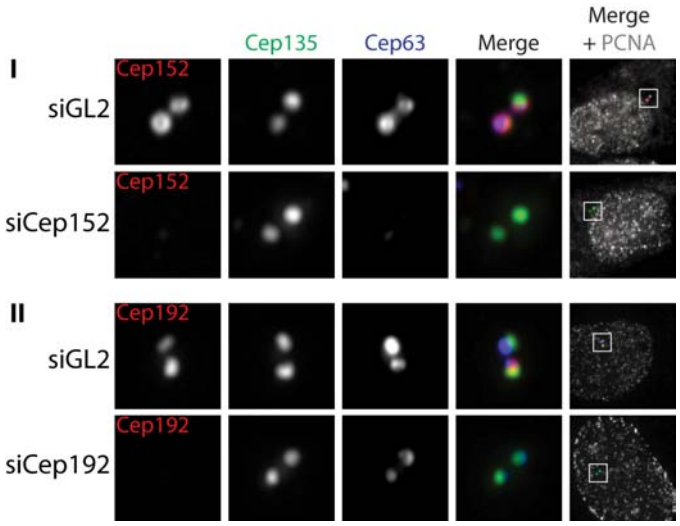

Figure 30 Cep192 depletion results in a reduction of Cep63 at centrosomes. U2OS cells were transfected with the indicated siRNA oligonucleotides for 72 h. After fixation the cells were stained with the indicated antibodies. PCNA was used identify cells in S phase. Scale bars represent 1 µm or 5 µm (overview images, right panel).

4.3.2 Interaction of Cep152 with Cep192

As Cep152 localization to centrosomes is dependent on Cep192, we next addressed the question whether both proteins also physically interact with each other. To this end, we co-expressed either Cep192-1 or Cep192-2 with Cep152 and performed co-immunoprecipitations (**Figure 31** A). In addition, we also investigated whether Cep192 interacts with Cep63, as Cep63 has been shown to reside in a common complex with Cep152 around mother centrioles. When we pulled on Cep192, we could indeed co-purify Cep152 with both Cep192 isoforms. In contrast, under similar conditions we only detected a weak unspecific interaction with Cep63. When we pulled on either Cep152, Cep63 or CPAP, Cep192 was only co-purified with Cep152 (**Figure 31** B). Finally, the central coiled-coil region of Cep152 was found to be required for the interaction with Cep192 (**Figure 31** C).

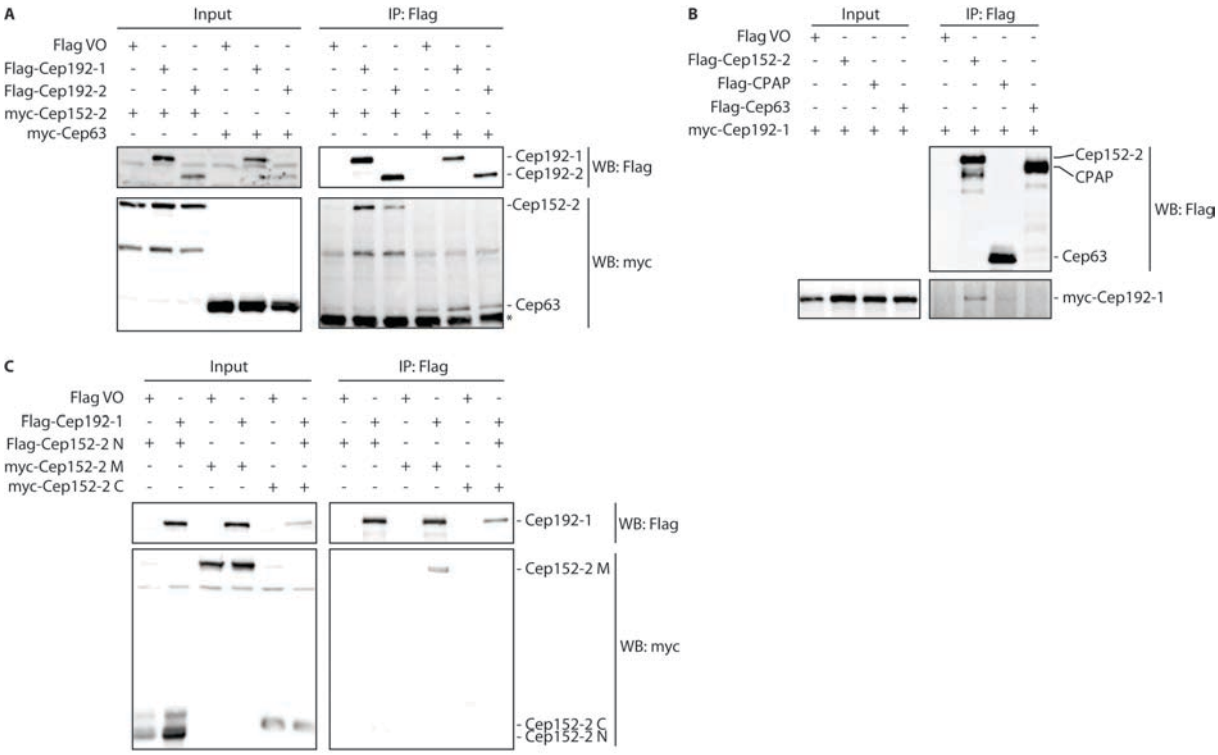

Figure 31 Overexpressed Cep152 and Cep192 interact with each other *in vivo*. A – C HEK293T cells were transfected with the indicated plasmids for 18 h. After lysis co-immunoprecipitations using Flag antibodies were performed and analyzed by Western Blotting (asterisks hint at IgG bands).

Yet, we were not able to detect an interaction on endogenous level, when either cytoplasmic Cep152 or Cep192 was immunoprecipitated (data not shown). In cells, Cep192 is more abundant than Cep152 (personal communication, M. Bauer) and – more importantly – localizes to the cytoplasm in addition to the centrosome, since centrosomal levels of Cep192 increase considerably upon mitotic onset (**Figure 26**), whereas cytoplasmic levels remain constant throughout the cell cycle. When releasing HeLa S3 cells from a double thymidine arrest, Cep192 levels were constant, even though an upshift of the Cep192 band was detected by Western Blot analysis (**Figure 32**). Therefore, we performed immunoprecipitation experiments after centrosome purification from KE37 cells. Western Blot analysis using the Cep192 antibody reproducibly revealed two bands above 250 kDa, which probably represent differing Cep192 isoforms. Interestingly, we detected an interaction of Cep152 with Cep192, if either protein was purified under these conditions (**Figure 33**). Whereas Cep192 was efficiently co-purified in Cep152 immunoprecipitations, very few Cep152 was co-purified in Cep192 immunoprecipitations. This might reflect the differing levels of Cep152 and Cep192

at centrosomes. Furthermore, we were not able to nicely detect Cep63 probably due to the low quality of the available antibody in Western Blotting. Finally, Cep135, another centriolar protein, was not co-purified in these immunoprecipitations.

Thus, Cep192 resides in a complex with Cep152 *in vivo*.

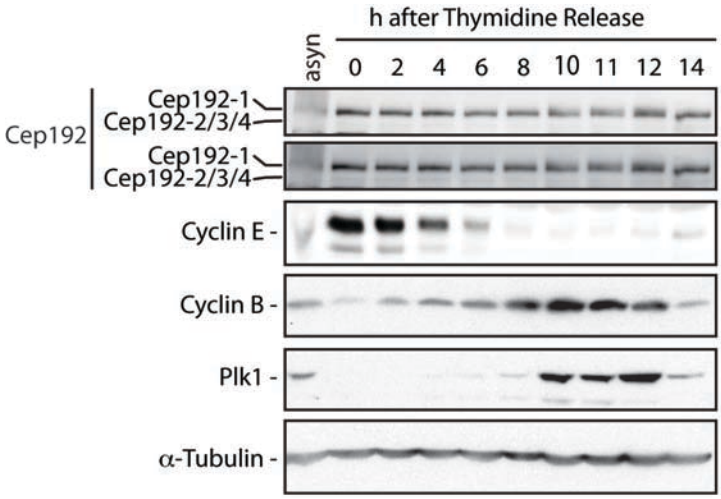

Figure 32 Cytoplasmic Cep192 levels do not vary during the cell cycle. HeLa S3 cells were released from a double thymidine arrest and samples taken every two hours. After lysis the samples were analyzed by Western Blotting using the indicated antibodies.

4.4 Function of Cep152 and Cep192 in PCM Recruitment and MT nucleation

Cep192 has been shown to be essential for PCM recruitment in human cells (Gomez-Ferreria et al., 2007; Zhu et al., 2008). However, the role of Cep152 in this process had not been addressed yet. In *D. melanogaster* Asterless, the Cep152 homologue, has been identified as a PCM-recruiting factor, that – if absent or mutated – results in the inability of centrosomes to form microtubule asters (Varmark et al., 2007). Therefore, we investigated whether Cep152 has a similar function in humans. To this end, we took three approaches: First, we performed immunoprecipitations analyzed by mass spectrometry to identify novel interaction partners of Cep152. Second, we depleted Cep152 and determined the amount of centrosomal γ-Tubulin.

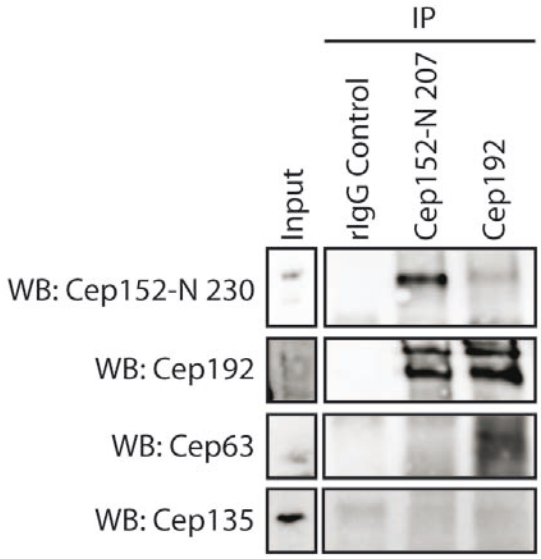

Figure 33 Cep192 interacts with Cep152 at centrosomes *in vivo*. Centrosomes were purified from KE37 cells. After addition of lysis buffer the lysate was used in immunoprecipitations using the indicated antibodies and analyzed by Western Blotting.

Finally, we analyzed the microtubule nucleation ability of centrosomes in Cep152-depleted cells.

4.4.1 The γTuRC as Novel Interaction Partner of Cep152

We performed immunoprecipitations of Cep152 using antibodies against endogenous Cep152. In a first attempt, Cep152 was immunoprecipitated using the C-terminal antibodies 880 and 934. Preimmune serum was used as negative control. The immunoprecipitates were separated by SDS gel electrophoresis and prominent bands were excised and analyzed by mass spectrometry (**Figure 34**). Cep152 was detected at the expected molecular weight of the long isoform. Interestingly, we also identified several components of the γTuRC in these samples among few other centrosomal proteins such as Cep290, PCM1 and Cep170 (see Appendix, **Table 3**).

In addition, Cep152 was immunoprecipitated with the antibodies Cep152-C 934 or Cep152-N 207, precipitated proteins were eluted and directly analyzed by mass spectrometry. In contrast to the negative control (rabbit IgG against dog) we detected several γTuRC components (GCPs), Plk1 and the regulatory PP2A subunit Aα among other proteins (see Appendix, **Table 4**). However, when the results were analyzed by label-free quantification, the detected

GCPs as well as all other potential interaction partners only constituted a minor component of the precipitate.

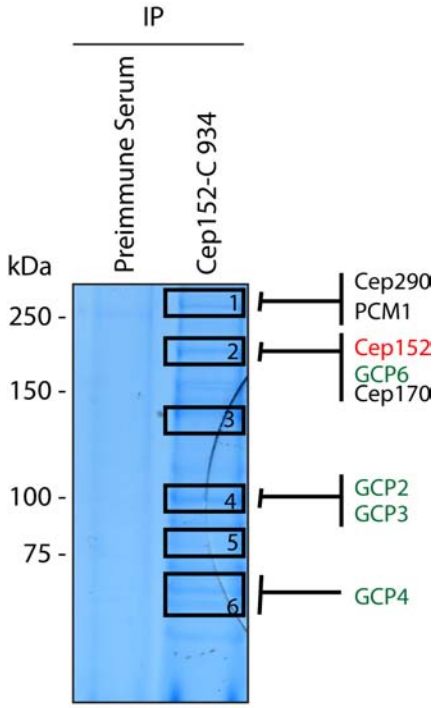

Figure 34 Several γTuRC components are identified in Cep152 immunoprecipitations. Lysates from HEK293T cells were prepared and used for immunoprecipitation experiments using either Cep152-C 934 or preimmune serum as control. The samples were analysed by SDS-PAGE. Distinct bands were excised from the gel and analyzed by mass spectrometry.

Since the fly homologue Asterless had been implicated in PCM recruitment, we tested nevertheless whether we could confirm the interaction with GCPs as well as other proteins by Western Blot analysis. Of all tested GCPs, GCP2 – 4 and GCP-WD/NEDD1 clearly interacted with Cep152. Contrary to that, C-Nap1 (a proximal centriolar protein) did not interact with Cep152. In addition, to rule out that γ-Tubulin is unspecifically pulled down in immunoprecipitations of centrosomal proteins, antibodies against the proximally localizing Cep135 was used as control. Indeed, we could co-immunoprecipitate γ-Tubulin with Cep152, but not with Cep135 or rabbit IgGs. Moreover, Cep135 was not immunoprecipitated by Cep152 antibodies. This suggests that the interaction is specific for Cep152. Finally, we released HeLa S3 cells from a double thymidine block and took samples every 3 hours. These samples were then used to perform endogenous immunoprecipitations, which were analyzed

by Western Blotting. The efficiency of the release was confirmed by the decrease in Cyclin E levels. Simultaneously, Cep152 levels increased slightly and decreased again. Importantly, we did not observe any cell cycle-specific changes in the interaction of Cep152 with γ-Tubulin. In contrast, more γ-Tubulin was co-precipitated when more Cep152 was present. These results also imply that the co-immunoprecipitation is indeed dependent on the presence of Cep152. Surprisingly, we also detected an interaction of γ-Tubulin with Cep135 in thymidine-arrested cells (0 h release).

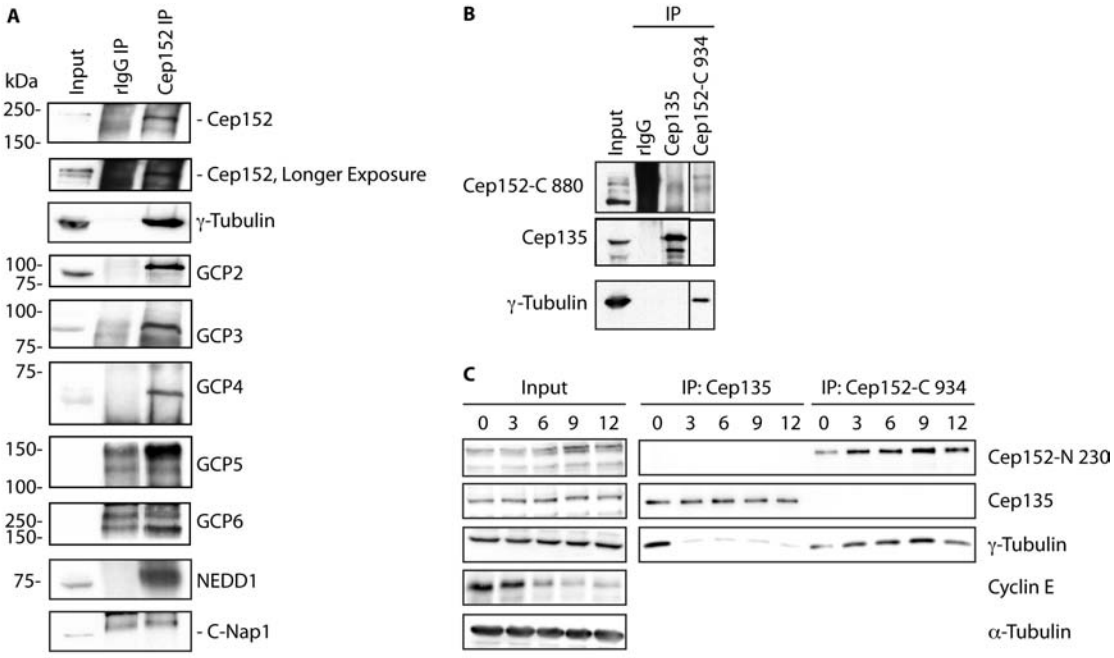

Figure 35 Cep152 interacts with several components of the γTuRC *in vivo*. A HEK293T cells were lysed and immunoprecipitations with either IgG control antibodies or Cep152-C 934 antibody were performed. Co-immunoprecipitated proteins were determined by Western Blotting with the indicated antibodies. **B** Immunoprecipitations from HEK293T lysates were performed using either IgG control, Cep135, Cep152-N 207 or Cep152-C 934 antibodies and analysed by Western Blotting. **C** HeLa S3 cells were released from a double thymidine block and samples taken every 3 hours. Immunoprecipitations were performed using either Cep135 or Cep152-C 934 antibodies and analysed by Western Blotting.

In order to identify a direct interaction partner of Cep152, immunoprecipitations after overexpression of any GCP in combination with Cep152-2 were performed. However, none of the GCPs identified by mass spectrometry (GCP1 – GCP6) was co-purified with Flag-Cep152-2. Of all known GCPs, NEDD1/ GCP-WD/ GCP7 is the most proximal one and represents the recruiting factor of the γTuRC (Luders et al., 2006). Even though NEDD1 had been identified in none of the immunoprecipitations analysed by mass spectrometry, we had

detected an interaction by Western Blot analysis. Thus, to test the hypothesis that Cep152 interacts via NEDD1 with the γTuRC, we co-expressed both proteins in human cells and performed co-immunoprecipitations. Indeed, myc-NEDD1 was co-purified, if we pulled on Cep152 (**Figure 36**). However, after *in vitro* translation an interaction by co-immunoprecipitation was never detected (data not shown).

Thus, Cep152 interacts with several components of the γTuRC *in vivo*.

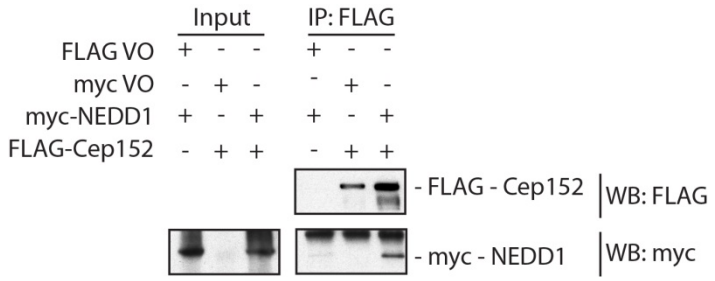

Figure 36 Cep152 interacts with NEDD1, if both proteins are co-expressed *in vivo*. HEK293T cells were transfected with the indicated plasmids for 24 h. After lysis co-immunoprecipitations using Flag antibodies were performed and analysed by Western Blotting.

4.4.2 Cep152 Depletion does not have a Detectable Effect on Centrosomal γ-Tubulin Recruitment or MT Nucleation

The interaction of Cep152 with the γTuRC prompted us to test, whether Cep152 participates in the recruitment of γTuRCs to centrosomes. Therefore, Cep152 or Cep192 as positive control were depleted for 72 h and centrosomal γ-Tubulin staining was analysed by IF microscopy. To ensure that we compared equal cell cycle stages, we stained the cells either with antibodies against PCNA to identify S phase cells or we stained the DNA with DAPI and then selected cells in prophase. Only if we depleted Cep192, γ -Tubulin levels were reduced – with a minor effect in interphase and a strong reduction in mitotic cells. However, if Cep152 was depleted, centrosomal levels of γ -Tubulin remained unchanged in both interphase and mitosis.

We additionally investigated whether the absence of Cep152 affects the ability of the centrosome to function as microtubule-organizing centre. To this end, we depleted Cep152,

GL2 as negative control and Cep192 as positive control. The cells – either in interphase or in mitosis – were then analyzed by a microtubule regrowth assay. In interphase microtubule asters emanating from centrosomes were detectable after 30 s of regrowth after cold treatment in GL2-depleted cells. Similarly, when either Cep152 or Cep192 were depleted, asters were also detectable after 30 s. This indicates that neither Cep192 nor Cep152 are required for MT nucleation in interphase (**Figure 38** A). However, in mitotic cells MT regrowth was clearly delayed, if Cep192 was depleted. But we still could not detect any differences between Cep152- and GL2-depleted cells (**Figure 38** B).

Thus, Cep152 is neither essential for MT nucleation in interphase nor in mitosis.

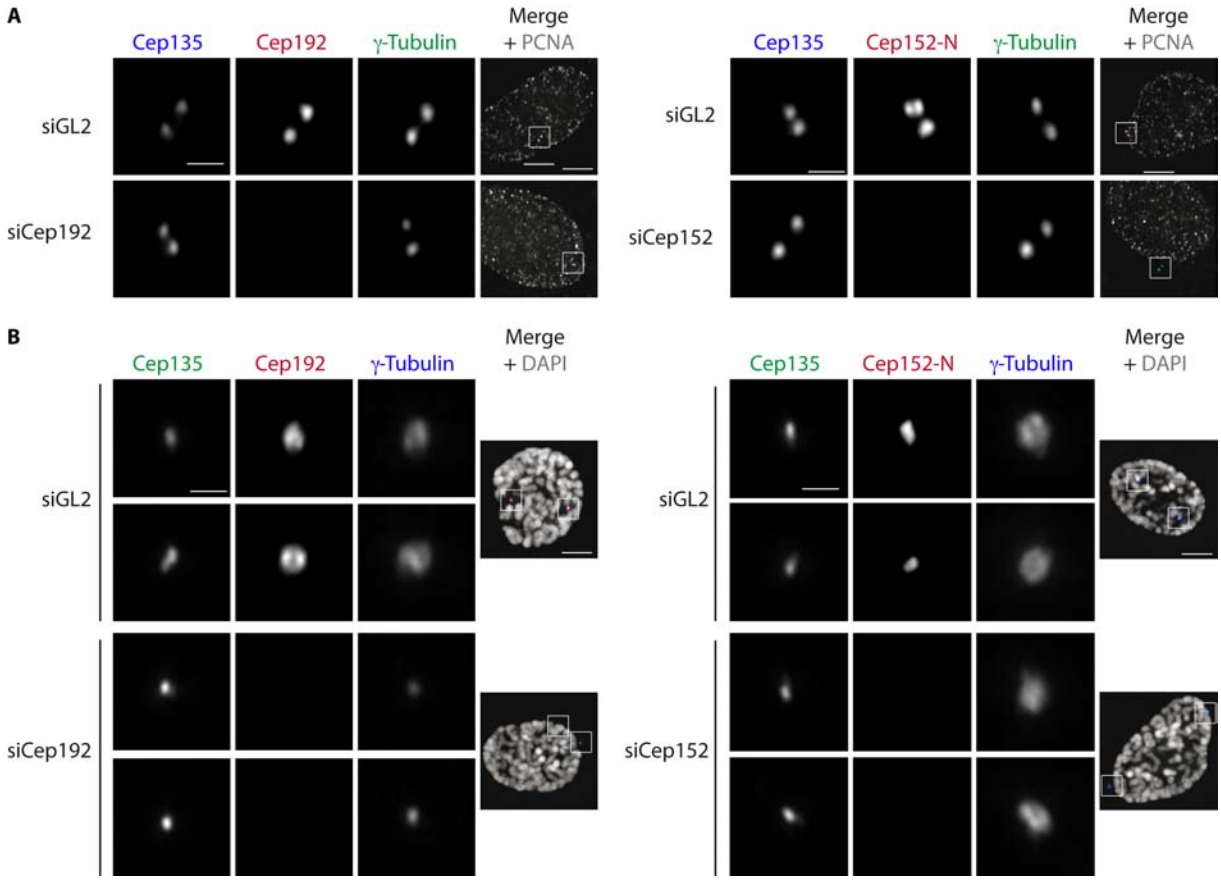

Figure 37 γ-Tubulin recruitment to centrosomes is not impaired in Cep152-depleted cells. U2OS cells were transfected with the indicated siRNA oligonucleotides for 72 h. After fixation the cells were stained with the indicated antibodies. Representative images are shown. **A** Cells in S phase were detected by a dot-like nuclear staining of PCNA. **B** Prophase cells were selected based on the DNA morphology labelled with DAPI. Scale bars represent 1 µm or 5 µm (overview images, right panels). (Figure by E. Anselm)

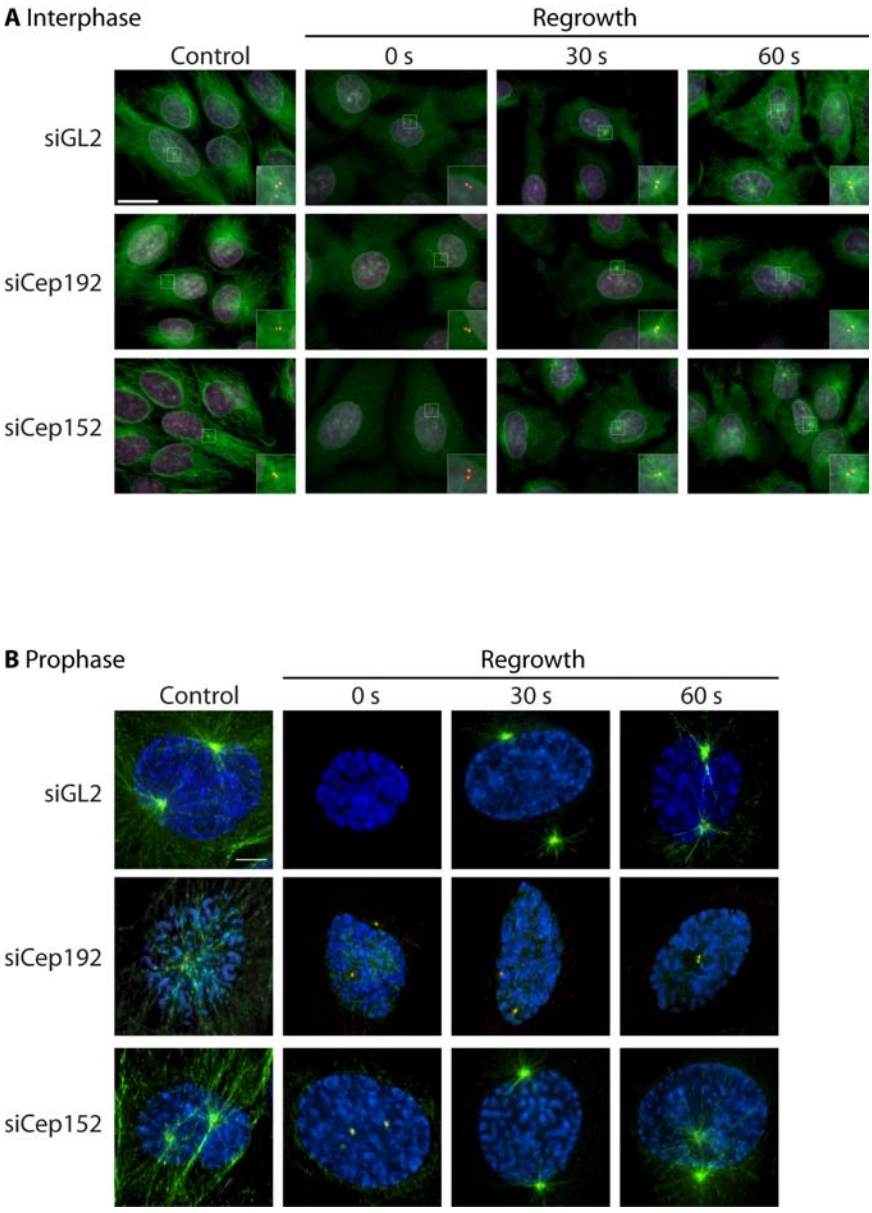

Figure 38 Cep152 depletion does not impair MT regrowth. U2OS cells were transfected with the indicated siRNA oligonucleotides. After 72 h microtubules were depolymerised on ice for 45 min. Cells were then incubated at 37°C, fixed at the indicated time-points and stained with antibodies against α-Tubulin (green) and Cep135 (red) and DAPI. Either cells in interphase (**A**, DAPI gray, scale bar 5 μm) or in prophase (**B**, DAPI blue, scale bar 1 μm) were analysed (Figure by E. Anselm).

4.5 Function of Cep152 and Cep192 in Centriole Duplication

Due to their localization surrounding mother centrioles where new daughter centrioles are formed, we investigated whether Cep152 and Cep192 are required for centriole duplication.

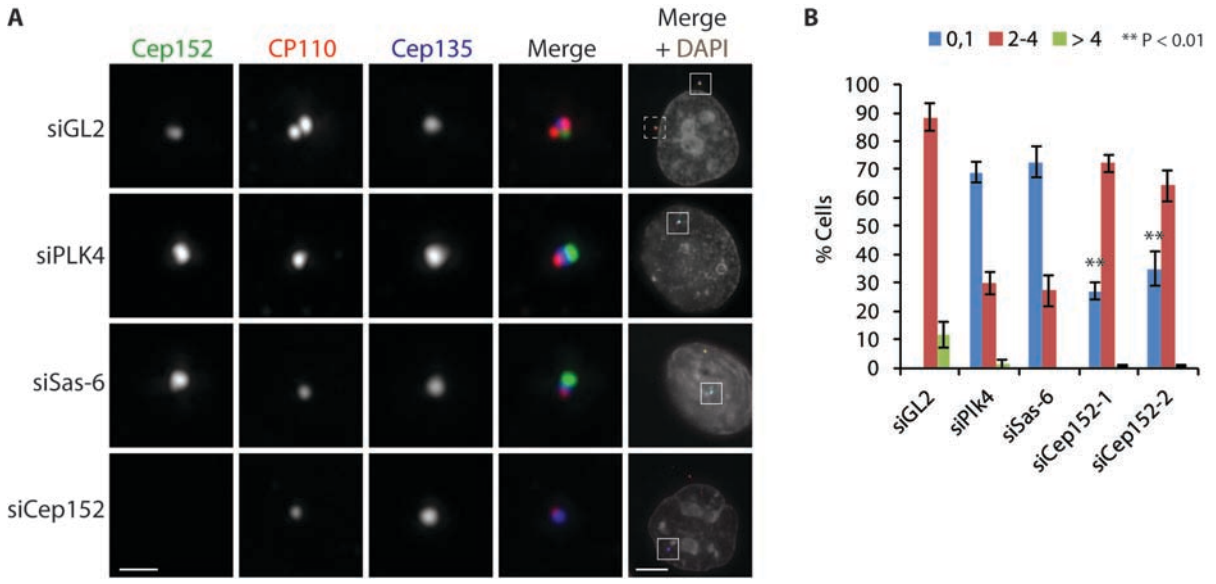

Figure 39 Cep152 depletion interferes with proper centriole duplication. U2OS cells were transfected with the indicated siRNA oligonucleotides for 72 h. After fixation the cells were stained with the indicated antibodies. DAPI was used to visualize DNA. In **A** representative images are shown. Scale bars represent 1 µm or 5 µm (overview images, right panel). In **B** the quantification of centriole numbers per cells is shown (three independent experiments, 100 cells each, error bars denote standard deviation).

4.5.1 Depletion of Cep152

To test whether Cep152 is involved in centriole duplication, we used two different Cep152 siRNA oligonucleotides to deplete the protein from U2OS cells and counted the number of centrioles per cell by IF microscopy. The distal centriolar protein CP110 was used as marker for centriole numbers. By flow cytometry we did not detect a cell cycle arrest (data not shown). Nevertheless, only cells with one or no centriole were considered to be duplication defective because centriole numbers normally vary between two and four centrioles during the cell cycle. As positive controls the regulatory kinase Plk4 and the centriole duplication factor Sas-6 were depleted. Indeed, we observed an effect on centriole duplication, when Cep152 was depleted, even though the effect was not as strong as with Plk4 depletion (**Figure 39**). Approximately 30 percent of cells did not have the expected amount of centrioles. In addition, the number of cells with overamplified centrioles was strongly decreased from about 10 % in GL2 control-depleted U2OS cells to 0 – 1 % in Cep152-depleted ones. This phenotype was confirmed in HeLa S3 cells (data not shown).

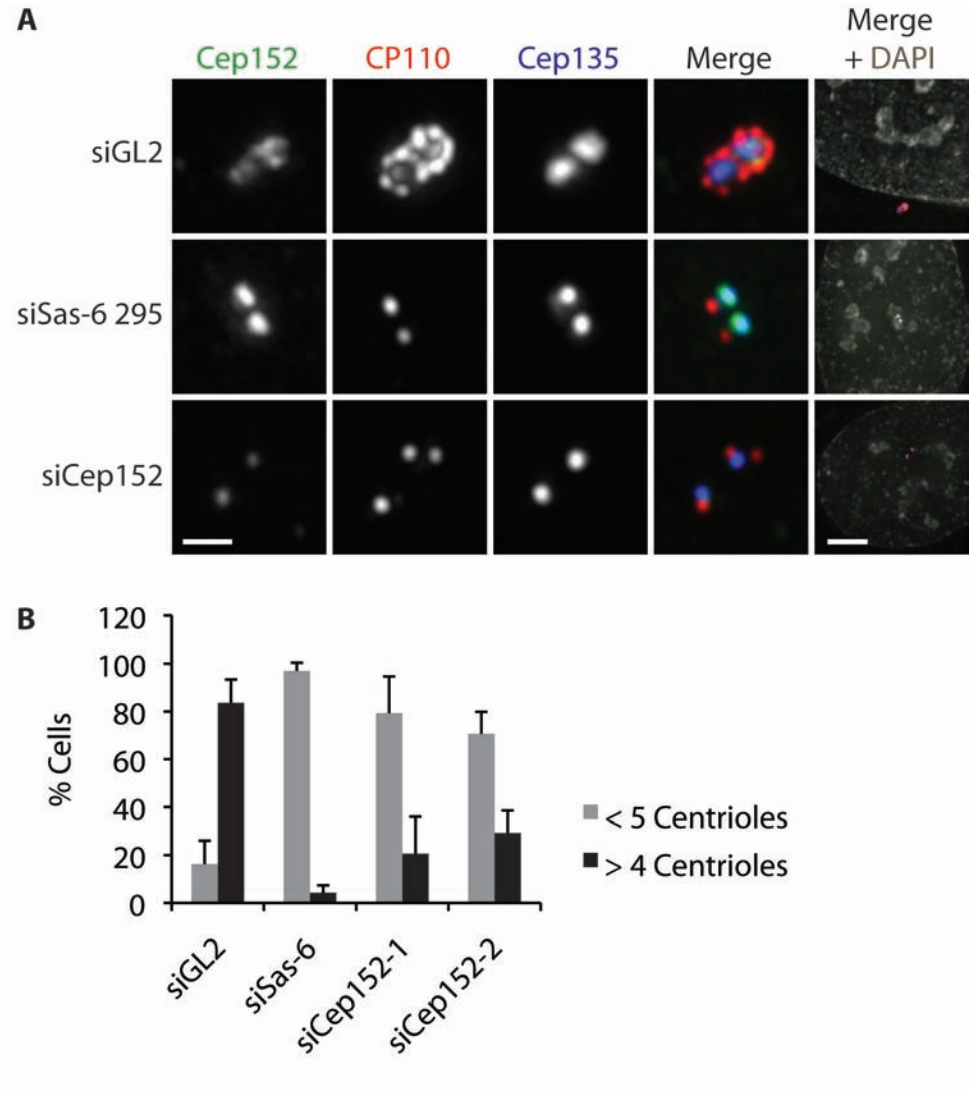

Figure 40 Cep152 depletion prevents Plk4-induced centriole over-duplication. U2OS:myc-Plk4 cells were transfected with the indicated siRNA oligonucleotides for 48 h, before cells were arrested in S phase and myc-Plk4 was induced for 16 h. After fixation the cells were stained with the indicated antibodies. DNA was visualized with DAPI. In **A** representative images are shown. Scale bars represent 1 µm or 5 µm (overview images, right panel). In **B** the quantification of centriole numbers per cells based on CP110 staining is shown (three independent experiments, 100 cells each, error bars denote standard deviation).

Furthermore, Cep152 was depleted from a U2OS cell line in which the overexpression of Plk4 can be induced by the addition of tetracycline (termed U2OS:myc-Plk4 cells). Upon Plk4 overexpression multiple daughter centrioles form around each mother centriole. This flower-like arrangement can nicely be visualized by IF microscopy using an antibody against a distal centriolar protein such as CP110. If Cep152 was depleted 32 h before S phase arrest and the induction of Plk4 for 16 h, overduplication of centrioles was inhibited (**Figure 40**). In Cep152-depleted cells only 20 – 30 % of cells contained overduplicated centrioles, whereas there were 82 % in the GL2 control-depleted cells.

4.5.1.1 Rescue of the Centriole Duplication Phenotype

Having shown that Cep152 depletion impairs centriole duplication, we sought to establish a rescue of the depletion phenotype. This would demonstrate that the observed effect was actually due to the depletion of Cep152 itself rather than an off-target effect on any other centriolar protein. To this end, full length constructs of Cep152 were generated that are resistant to the employed siRNA oligonucleotides. The oligoresistance was tested by depleting endogenous Cep152 and overexpressing the constructed Cep152 plasmids. By Western Blot analysis we found endogenous Cep152 to be efficiently depleted, whereas ectopic Cep152 was still expressed (**Figure 41**).

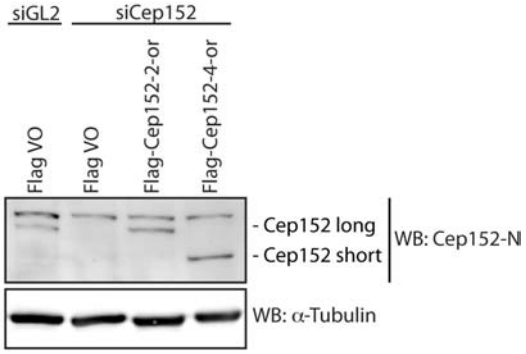

Figure 41 siRNA oligonucleotide-resistant Cep152 plasmids are expressed in Cep152 depletion background. U2OS cells treated as described in **Figure 42** A. The indicated siRNA oligonucleotides and overexpression constructs were used. After lysis the samples were analysed by Western Blotting.

As described earlier (**Figure 39**), Cep152 depletion had a significant, albeit rather low effect on centriole duplication in both normal U2OS and HeLa S3 cells. Based on these results, we decided to perform the centriole duplication rescue in U2OS:myc-Plk4 cells in which we induced the formation of "centriole flowers" by the induction of Plk4 overexpression. This set-up allowed a clearer read-out of the centriole duplication effect. Cells were treated as summarized in **Figure 42** A. After fixation, the number of centrioles per cell was counted by IF microscopy. Surprisingly, neither expression of Cep152-2 nor Cep152-4 rescued the depletion phenotype. However, upon co-expression of both isoforms, centriole duplication was rescued (**Figure 42**).

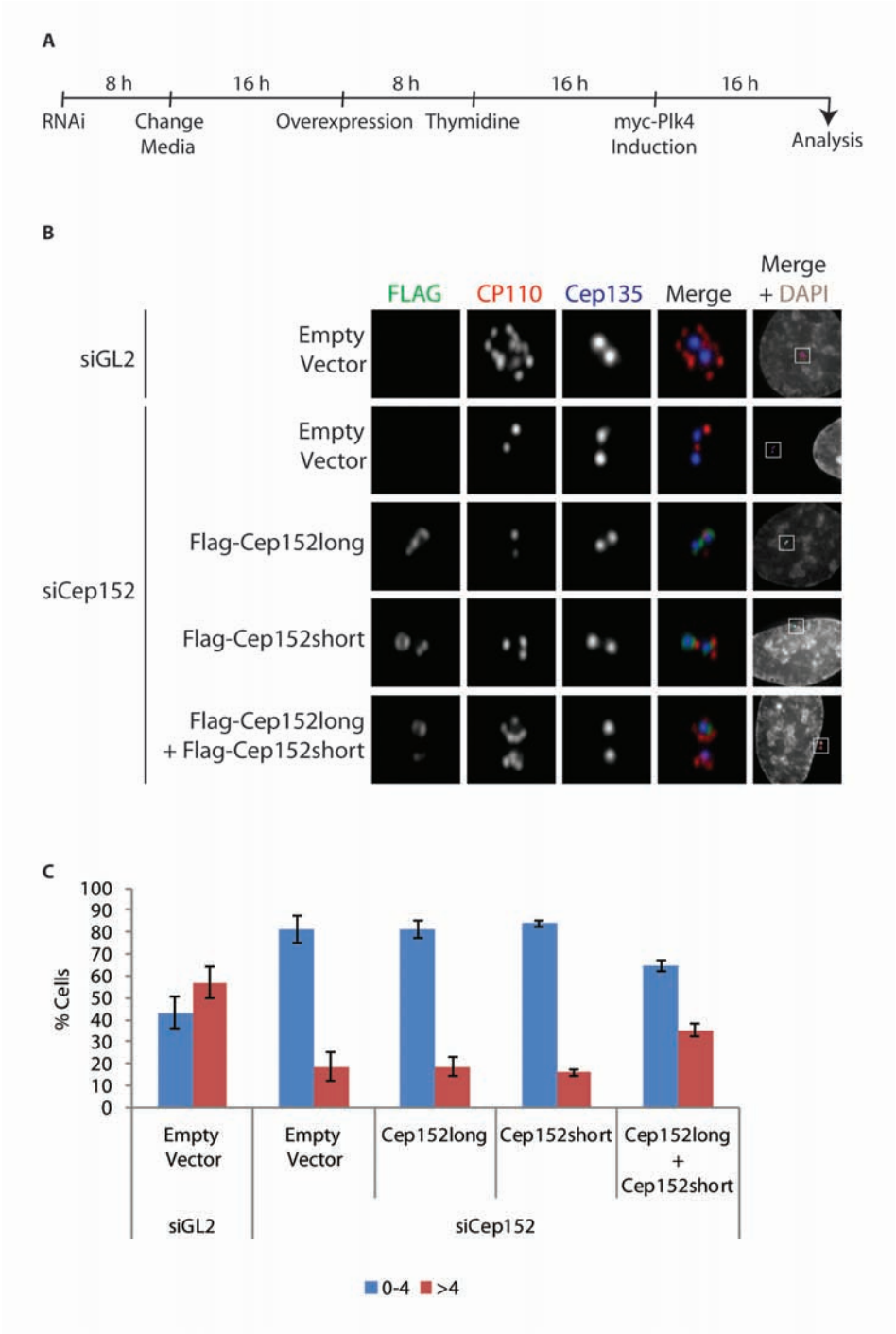

Figure 42 Centriole duplication can be rescued by co-expression of Cep152-2 and Cep152-4. U2OS:myc-Plk4 cells were treated as described in **A**. After fixation cells were stained with the indicated antibodies to count centriolar numbers per cell. Representative images are shown in **B** (scale bars represent 1 µm or 5 µm (overview images, right panel) and the quantification is shown in **C** (3 independent experiments, 100 cells each, error bars denote standard error).

These results suggest that the observed centriole duplication phenotype is specific for a depletion of Cep152 rather than an off-target effect. In addition, they imply that both Cep152-2 and Cep152-4 are required for proper centriole duplication.

4.5.2 Depletion of Cep192

In the literature two controversial studies on the involvement of Cep192 in centriole duplication are available (Gomez-Ferreria et al., 2007; Zhu et al., 2008). Here, we re-investigated the function of Cep192 by depleting the protein from U2OS cells for 72 h and determining the number of centrioles per cell (**Figure 43**). Indeed, centriole duplication was impaired compared to control-depleted cells. Interestingly, the duplication phenotype was not as strong as in Plk4-depleted cells, but was comparable to the one observed in Cep152-depleted cells. Similar results were obtained using HeLa S3 cells (data not shown).

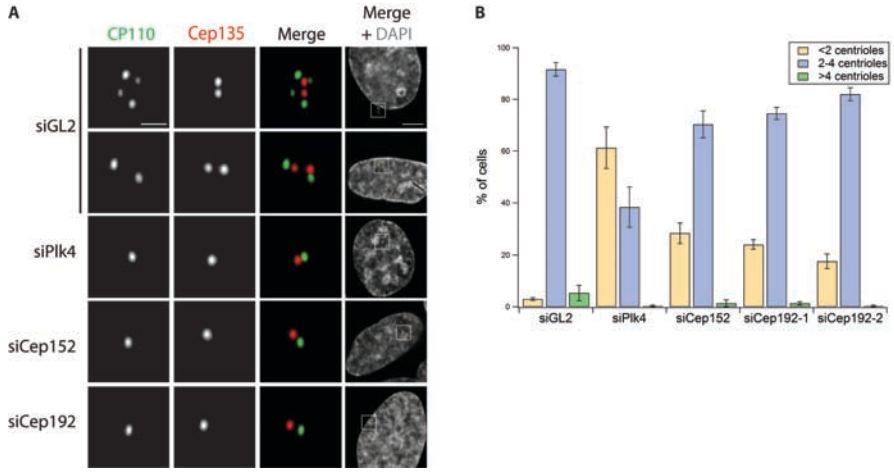

Figure 43 Cep192 depletion interferes with proper centriole duplication. U2OS cells were transfected with the indicated siRNA oligonucleotides for 72 h. After fixation the cells were stained with the indicated antibodies. DAPI was used to visualize DNA. In **A** representative images are shown. Scale bars represent 1 µm or 5 µm (overview images, right panel). In **B** the quantification of centriole numbers per cells is shown (three independent experiments, 100 cells each, error bars denote standard deviation). Figure by E. Anselm.

Thus, we can confirm the centriole duplication defect reported for Cep192 depletion by Zhu et al. (2008).

4.5.3 Recruitment of Plk4 to Centrosomes

Our laboratory has published previously that the kinase Plk4 is an early determinant of this pathway. Plk4 levels define the amount of duplication factors localizing around mother centrioles and thus the number of daughter centrioles forming around each pre-existing centriole (Bettencourt-Dias et al., 2005; Habedanck et al., 2005; Kleylein-Sohn et al., 2007). However, proteins lying upstream of Plk4 or the recruiting factor of Plk4 to centrioles itself were completely unknown at the time this project was initiated. As Cep152 localizes around the proximal half of mother centrioles and not only in-between mother and emerging daughter centriole such as the duplication factor Sas-6 (Kleylein-Sohn et al., 2007; Strnad et al., 2007), we hypothesized that it might actually participate early in the centriole duplication recruitment pathway. In contrast to Cep152, Cep192 localizes along the whole centriolar walls of both mother and daughter centrioles, i.e. also to centriolar regions where Plk4 is never found, even when overexpressed. Therefore, we initially investigated the involvement of Cep152 in the recruitment of Plk4.

4.5.3.1 Functional Relationship between Cep152 and Plk4

4.5.3.1.1 Interaction of Cep152 with Plk4

To understand whether Cep152 might be required for Plk4 recruitment, we checked a potential interaction between Plk4 and Cep152. Indeed, if Flag-Cep152-2 or Cep152-4 were co-expressed with either CP110 or Plk4 in HEK293T cells, only Plk4 was co-purified in immunoprecipitation experiments, but not CP110. The interaction between Cep152 and Plk4 in co-immunoprecipitations was detected regardless of the bait protein (**Figure 44** A). During the course of this study a Plk4 antibody was published that is functional in Western Blotting (Cizmecioglu et al., 2010). The authors also reported an interaction of Cep152 and Plk4 at endogenous levels. Here, we confirmed the interaction by immunoprecipitation of endogenous Cep152 (**Figure 44** B). In addition, the interaction was abolished when Cep152 was depleted, confirming that the interaction was specific (**Figure 44** C). Moreover, we overexpressed either CP110 or Plk4 in HEK293T and analyzed co-purification of endogenous Cep152 by Western Blotting. Only if Plk4 was immunprecipitated, Cep152long and

Cep152short were co-purified (**Figure 44** D). Finally, an interaction was also detected when Cep152 and Plk4 were translated *in vitro* (**Figure 44** E).

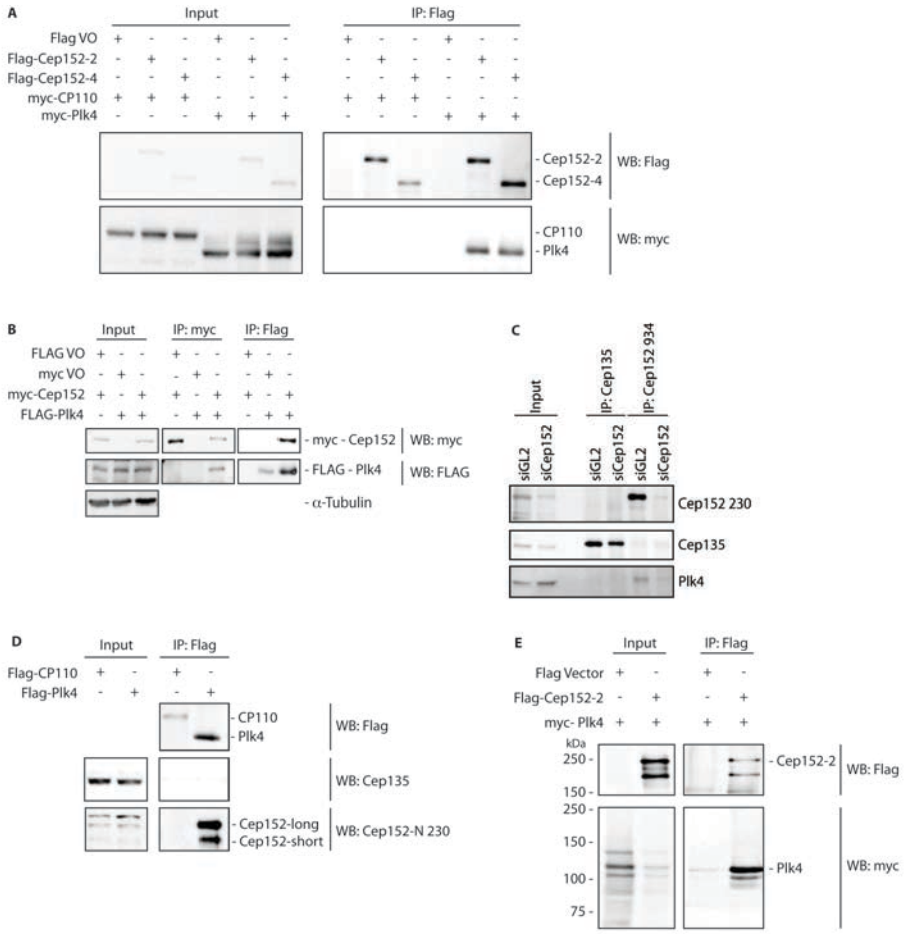

Figure 44 Plk4 interacts with Cep152long and Cep152short *in vivo*. A, B HEK293T cells were transfected with the indicated plasmids for 24 h. After lysis the samples were subjected to immunoprecipitation experiments and analyzed by Western Blotting. **C** HeLa S3 cells were arrested with a double thymidine block and transfected with the indicated siRNA oligonucleotides for 36 h. After a release for 9 h cell lysates were prepared. Immunoprecipitations of these HeLa S3 cell lysates were performed using either Cep135 or Cep152-C 934 antibodies. After elution the samples were analyzed by Western Blotting. **D** HEK293T cells were transfected with the indicated plasmids for 24 h. After lysis immunoprecipitations using Flag antibodies were performed and co-purified proteins were detected by Western Blot analysis. **E** The indicated proteins were co-expressed by *in vitro* translation. Afterwards, co-immunoprecipitaion experiments were performed using Flag antibodies. Eluates were analyzed by Western Blotting.

Next, we mapped the region required for this interaction on each protein. We co-expressed various deletion mutants of one protein with the full length form of the other one and performed co-immunoprecipitation experiments. We used the Cep152 fragments described

earlier in this study (Section 4.2.1.2) and detected an interaction of Plk4 with both full length and the N-terminal 220 amino acids of Cep152 (**Figure 45** A). These amino acids represent the potentially unfolded region N terminally to the central coiled-coil domain. Interestingly, there is a conserved SSP site at amino acids 47 to 49. Phosphorylated SSP sites are known binding sites for polo boxes. With regard to the presence of a polo box in the sequence of Plk4, it is tempting to speculate that interaction of Cep152 with Plk4 is dependent on phosphorylation of this site. But mutating this site to AAP did not abolish the interaction with Plk4 (**Figure 45** B). Additionally, there is a stretch of amino acids predicted to form an alpha helix within the N terminus of Cep152 (**Figure 15**), which might be required for the interaction with Plk4. Indeed, if these N-terminal 45 amino acids were deleted, the interaction with Plk4 was abolished (**Figure 45** C). This result also indicates that the SSP mutant of Cep152 does not interact with Plk4 via homodimerization with endogenous Cep152, as deleting the N-terminal 45 amino acids did interfere with the interaction of Cep152 with Plk4 despite the presence of the central coiled-coil region and the resulting dimerization with endogenous Cep152.

Thus, Cep152 interacts with Plk4 via its N terminus and the very N-terminal alpha helix is necessary for this interaction.

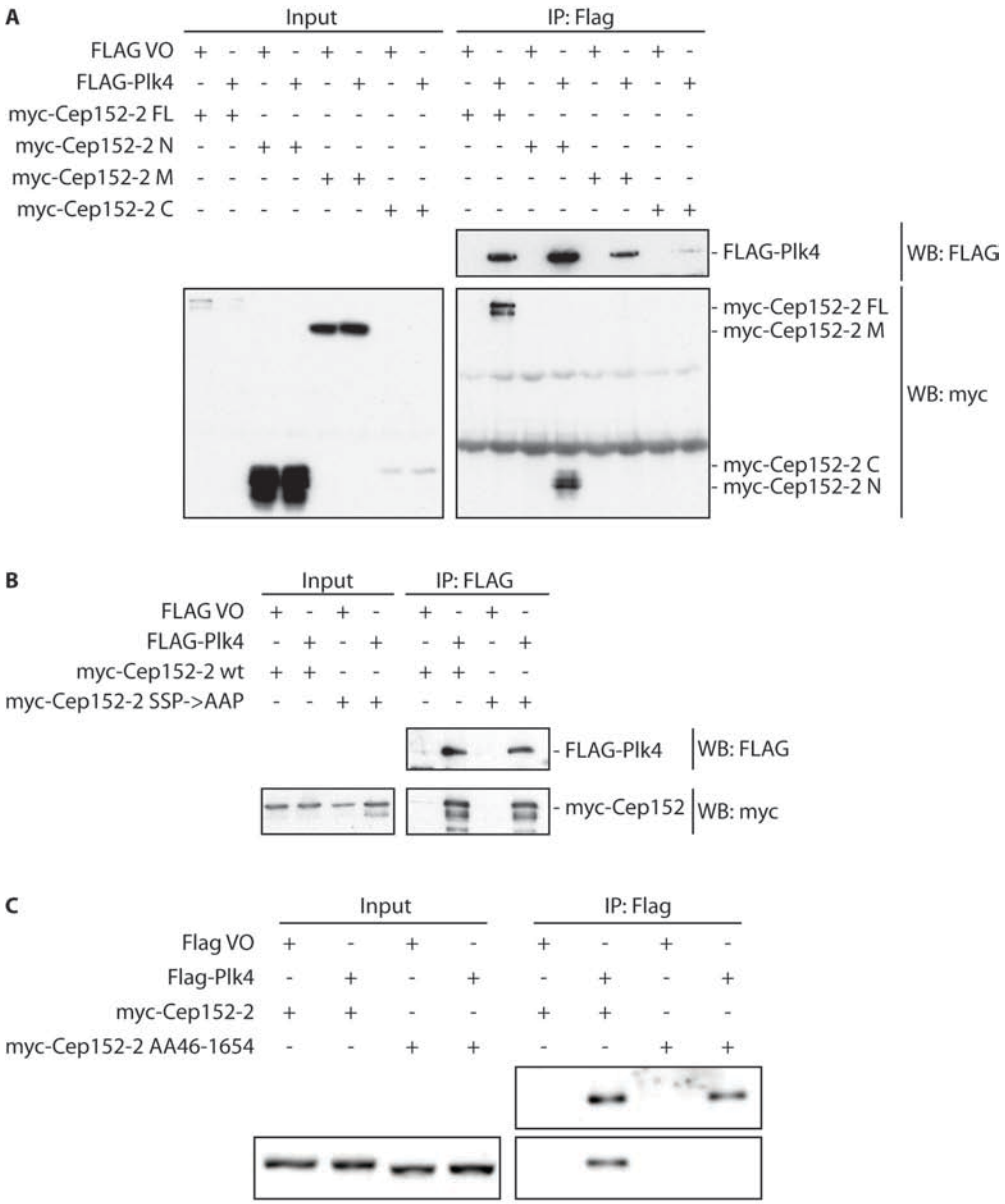

Figure 45 Plk4 interacts with the N terminus of Cep152. **A – C** HEK293T cells were transfected with the indicated plasmids for 24 h. After lysis co-immunoprecipitations were performed using Flag antibodies and eluates were analyzed by Western Blotting. (**A**: Cep152-2 N: amino acids 1 – 220, Cep152-2 M: amino acids 221 – 1308, Cep152-2 C: amino acids 1308 – 1654)

Moreover, we mapped the interaction site of Cep152 on Plk4. By co-expressing different fragments of Plk4 with full length Cep152 we identified amino acids 265 – 887 to be essential for this interaction (**Figure 46**). This part corresponds to the middle linker and the cryptic polo box.

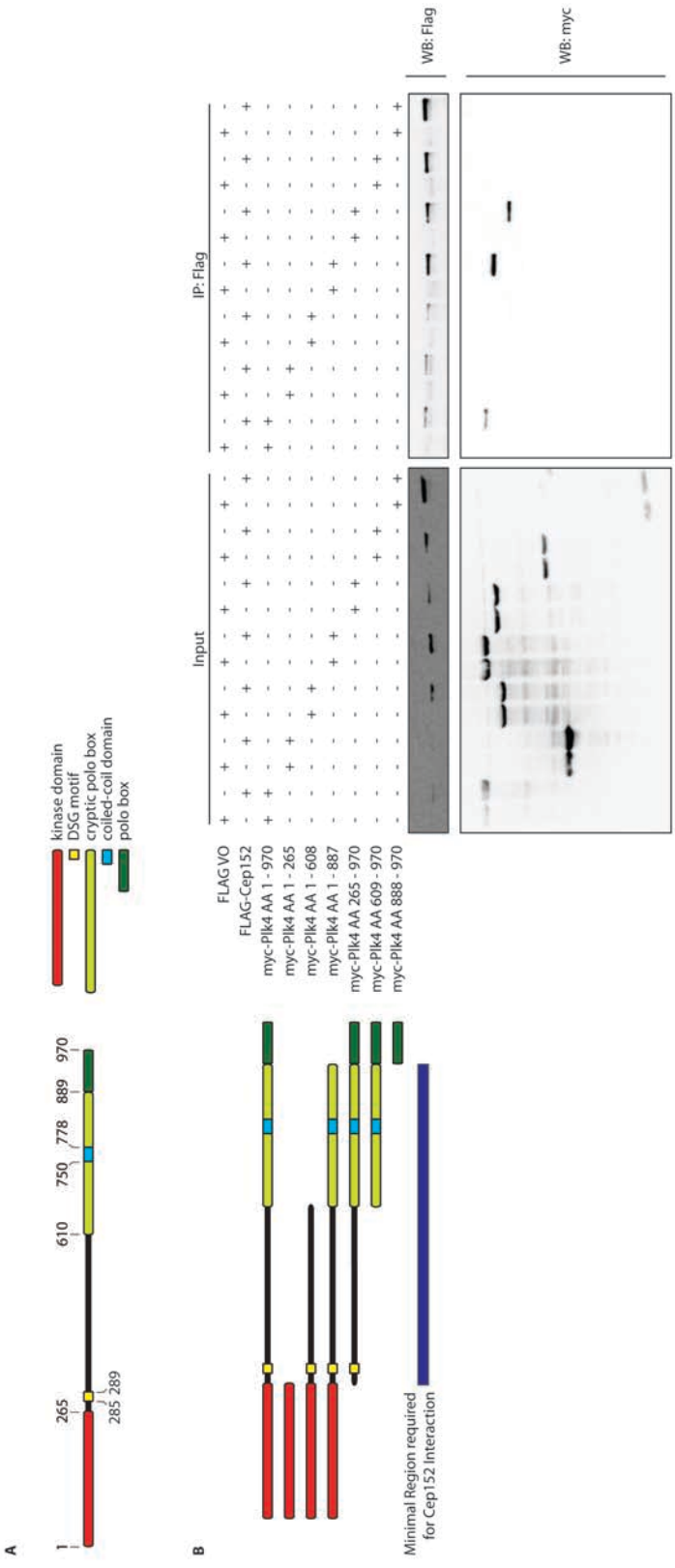

Figure 46 Amino acids 265 – 887 of Plk4 are necessary for the interaction with Cep152. A Schematic domain structure of Plk4 (Figure by J. Westendorf). **B** HEK293T cells were transfected with the indicated plasmids for 24 h. After lysis the samples were subjected to co-immunoprecipitation experiments using Flag antibodies. After elution the results were analysed by Western Blotting.

4.5.3.1.2 Centrosomal Recruitment of Plk4 is not Impaired upon Cep152 Depletion

Having determined an interaction of Cep152 with Plk4 we then investigated whether Cep152 might be the long-sought recruiting factor of Plk4. Therefore, Cep152 was depleted from U2OS cells and the centrosomal localization of Plk4 was analysed in S phase cells. However, Plk4 was not lost from centrosomes upon Cep152 depletion. In contrast, Plk4 levels even appeared to be slightly increased and Plk4 was occasionally not restricted to one confined dot anymore (**Figure 47**). Moreover, we depleted Cep152 prior to the induction of myc-Plk4 overexpression in U2OS:myc-Plk4 cells and investigated the recruitment of induced myc-Plk4. Whereas Sas-6, glutamylated Tubulin, Cap350, Cep192 and CPAP were reduced – presumably due to the lack of additional daughter centrioles, myc-Plk4, NEDD1 and γ-Tubulin remained unchanged (data not shown).

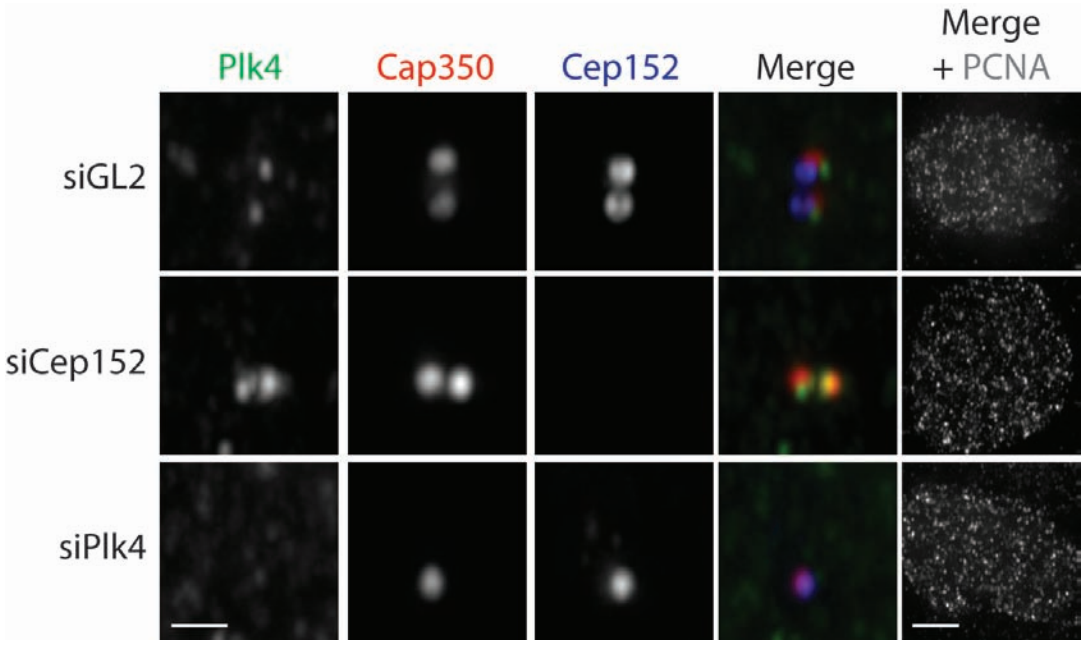

Figure 47 Cep152 depletion does not lead to loss of Plk4 from centrosomes. U2OS cells were transfected with the indicated siRNA oligonucleotides for 48 h. After fixation the cells were stained with the indicated antibodies for IF microscopy. PCNA was used to visualize cells in S phase. Scale bars represent 1 µm or 5 µm (overview image, right panel).

4.5.3.2 Search for a Plk4-Recruiting Factor

Since Cep152 depletion did not result in a loss of Plk4 from centrosomes, we reasoned that another centriolar protein must serve this function in human cells. We hypothesized that a

potential recruiting factor has to interact with Plk4 and to reside upstream of Plk4 in the centriole duplication pathway. Kleylein-Sohn *et al.* have shown previously that centrosomal levels of centriole duplication factors such as Sas-6, CP110 or Cep135 depend on Plk4 amounts, so that these proteins are unlikely to function upstream of Plk4 (2007). Thus, we checked the interaction of Plk4 with other proteins that localize around the mother centriole independently of Plk4 levels (Cep152, Cep63 or CPAP). However, we did not find Cep63 or CPAP to interact with Plk4 in co-immunoprecipitation experiments (**Figure 48**). In addition, single depletion of either Cep63 or CPAP did not lead to a complete loss of Plk4 from centrosomes (data not shown).

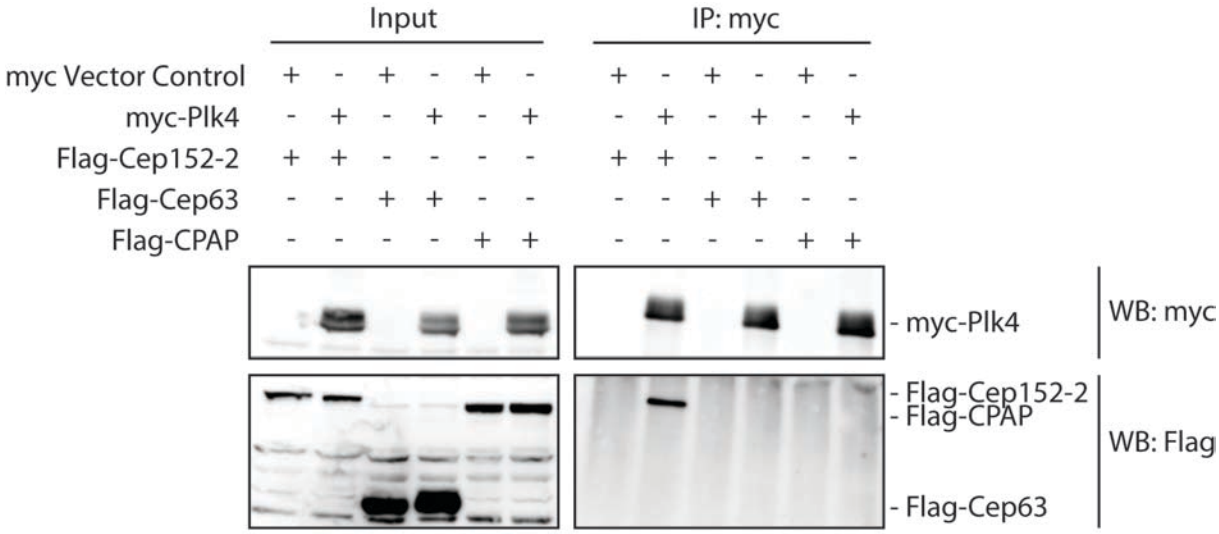

Figure 48 Plk4 does not interact with Cep63 or CPAP. HEK293T cells were transfected with the indicated plasmids for 24 h. After lysis co-immunoprecipitaion experiments were performed using myc antibodies. The eluates were then analysed by Western Blotting.

4.5.3.3 Cep152 and Cep192 Co-Operate in the Recruitment of Plk4

In *C. elegans* the localization of the kinase Zyg-1, which plays an analogous role as Plk4 in humans, is dependent on the protein Spd-2 (Delattre et al., 2006). Interestingly, the function of its human homologue Cep192 in centrosomal Plk4 recruitment has never been addressed so far. Due to its localization along the whole centriolar wall Cep192 also localizes in-between

mother and daughter centrioles. This renders it to be possibly involved in Plk4 recruitment – just like its *C. elegans* homologue.

4.5.3.3.1 Only Co-Depletion of Cep152 and Cep192 Prevents Centrosomal Plk4 Recruitment

When Cep192 was depleted from U2OS cells for 72 h, Plk4 recruitment was indeed impaired, even though low levels of Plk4 were still detectable (**Figure 49**). Next, we asked whether Cep192 and Cep152 might have a synergistic and partly redundant function in the recruitment of Plk4, since we had characterized a strong interaction between Cep152 and Plk4 earlier. Thus, both proteins were also co-depleted in the same experimental set-up. As we had to stain cells for Plk4, DAPI (to identify cells in interphase) and a centrosomal marker and, additionally, Cep152 depletion was generally more efficient than Cep192 depletion, we chose co-depleted cells based solely on Cep192 staining. As mentioned before, Plk4 levels were slightly increased upon depletion of Cep152. However, if Cep192 was depleted, centrosomal Plk4 levels were strongly reduced. Interestingly, only co-depletion of Cep192 and Cep152 resulted in a similar reduction of centrosomal Plk4, as we observed when Plk4 itself was depleted by RNAi. In contrast, depletion of the PCM protein Pericentrin did not impair centriolar Plk4 recruitment (data not shown).

To rule out any effect on cytoplasmic Plk4 levels by either regulated degradation or an RNAi off-target effect, we also checked cytoplasmic levels by Western Blot analysis. However, Plk4 levels were not reduced upon depletion or co-depletion of those proteins. In contrast, Plk4 levels were even increased considerably, if Cep152 was depleted (**Figure 50**). This effect was further enhanced upon co-depletion of Cep152 and Cep192. Similar results were obtained using HeLa S3 cells (**Figure 58**). However, it implies that depletion of Cep152 and/or Cep192 does not result in a decrease in cytoplasmic Plk4 levels.

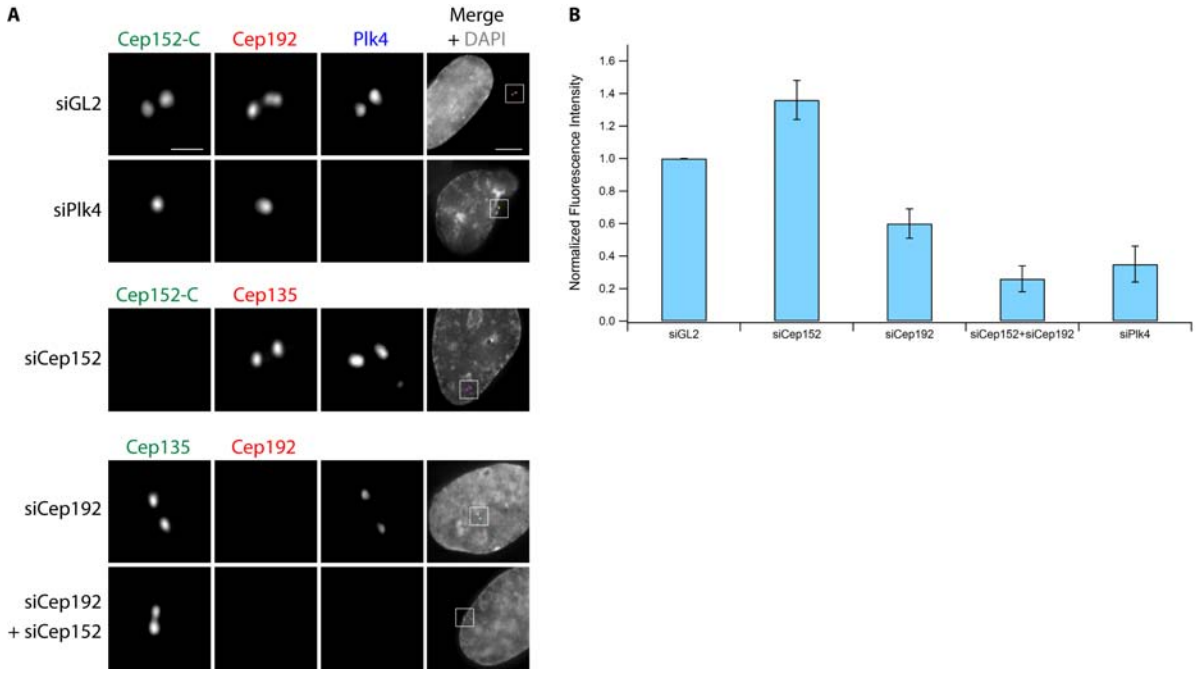

Figure 49 Co-depletion of Cep152 and Cep192 results in a loss of Plk4 from centrosomes similar to Plk4 depletion. U2OS cells were transfected with the indicated siRNA oligonucleotides for 72 h. After fixation the cells were stained with the indicated antibodies. In **A** representative images are shown. Scale bars represent 1 µm or 5 µm (overview images, right panel). In **B** the quantification of centrosomal Plk4 levels is shown (3 independent experiments, 10 – 15 cells each, error bars denote standard deviation). (Experiment was performed by E. Anselm)

Furthermore, we confirmed the observed effect on Plk4 recruitment in the U2OS:myc-Plk4 cell line, in which the overexpression of Plk4 can be induced (described earlier, Section 4.5.1). We took advantage of the Plk4 inducability by first depleting the tested proteins for 48 h and then inducing Plk4 for 16 h. This allowed the specific analysis of the centrosomal recruitment of newly formed Plk4. Because of level differences in induced Plk4 in individual cells, we only took cells into account in which myc-Plk4 was also detectable within the cytoplasm. Also in this case Plk4 was only strongly reduced compared to GL2 control-depleted cells or even completely lost, if both Cep152 and Cep192 were co-depleted (**Figure 51**).

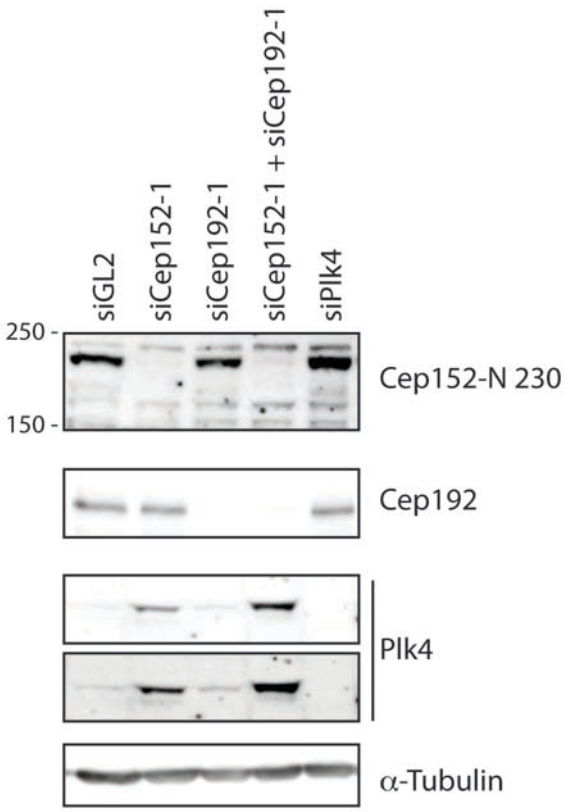

Figure 50 Depletion of Cep152 and/ or Cep192 does not lead to a reduction in cytoplasmic Plk4 levels. U2OS cells were depleted with the indicated siRNA oligonucleotides for 72 h. After lysis the samples were analyzed by Western Blotting using the indicated antibodies.

Thus, Cep192 is required for proper centrosomal Plk4 recruitment, whereas Cep152 is dispensable, unless Cep192 is depleted in addition. This suggests that Cep152 and Cep192 co-operate in Plk4 recruitment in human cells.

4.5.3.3.2 Interaction of Cep192 with Plk4

Having shown that Cep192 depletion impairs Plk4 recruitment and only double depletion of Cep192 and Cep152 leads to a complete loss of Plk4 from centrioles, a potential interaction of Plk4 with Cep192 was investigated. Similarly to Cep152, in co-immunoprecipitation experiments Plk4 indeed interacted with Cep192-1, if both proteins were overexpressed (**Figure 52**). In contrast, under the same conditions Cep63 or CPAP did not show an interaction with Plk4. However, an interaction between Cep192 and Plk4 was never detected on endogenous level (data not shown), which might result from the differing expression levels

of Cep192 and Plk4. Moreover, we did not detect an interaction, if Cep192 and Plk4 were translated *in vitro* (data not shown).

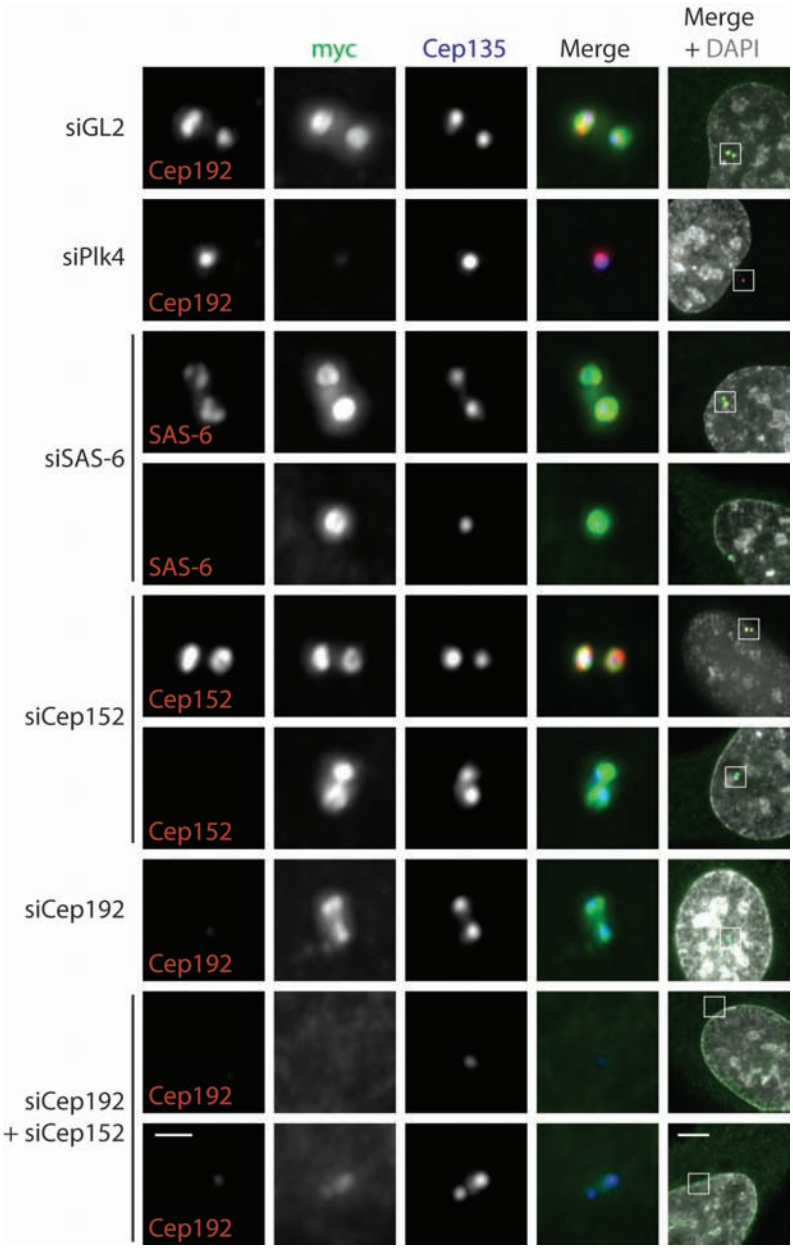

Figure 51 Co-depletion of Cep152 and Cep192 prevents the recruitment of induced myc-Plk4 to centrosomes. U2OS:myc-Plk4 cells were transfected with the indicated siRNA oligonucleotides for 48 h and then myc-Plk4 expression was induced for 16 h. After fixation the cells were stained with the indicated antibodies for IF microscopy. DNA was stained with DAPI. For Sas-6 and Cep152 depletion non-depleted cells are shown to illustrate antibody specificity. Scale bars represent 1 µm or 5 µm (overview images, right panel).

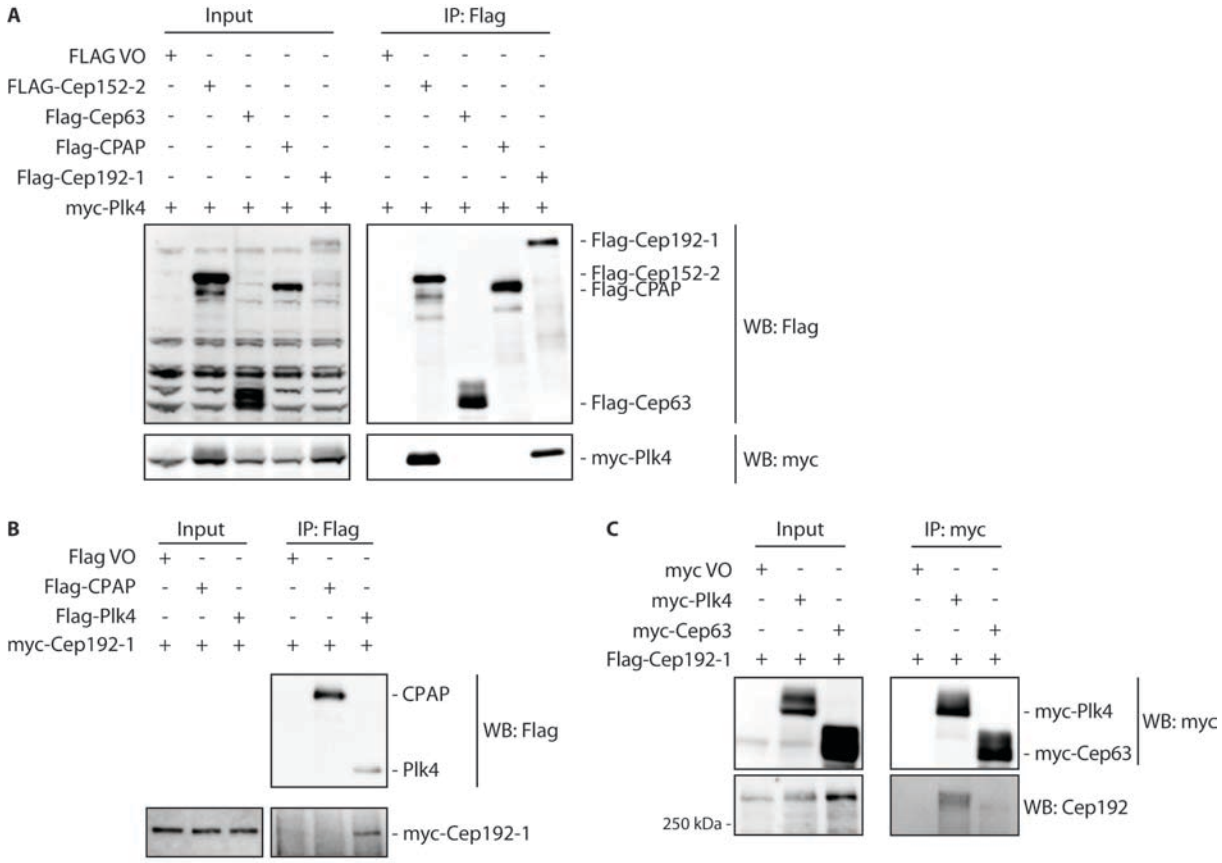

Figure 52 Cep192 interacts with Plk4. HEK293T cells were transfected with the indicated plasmids. Co-immunoprecipitations using Flag antibodies (**A, B**) or myc antibodies (**C**) were performed and analysed by Western Blotting using the indicated antibodies.

Moreover, Plk4 specifically interacted with the N terminus of Cep192 (**Figure 53** A). Plk4 was not immunoprecipitated with isoform Cep192-2 lacking the N-terminal 603 amino acids of isoform 1, whereas we detected an interaction, if the N terminus of Cep192 was co-expressed with Plk4. This indicates that full length Cep192-1 is capable of this interaction, but not the other Cep192 isoforms. Accordingly, overexpression of the N terminus in U2OS cells, which did not localize to centrosomes, had a dominant-negative effect and completely prevented the centrosomal recruitment of Plk4 (**Figure 53** B). Conversely, overexpression of Cep192-1 or Cep192-2, both localizing to centrosomes, only occasionally abolished centriolar Plk4 recruitment, presumably by sequestration of Plk4 in the cytoplasm.

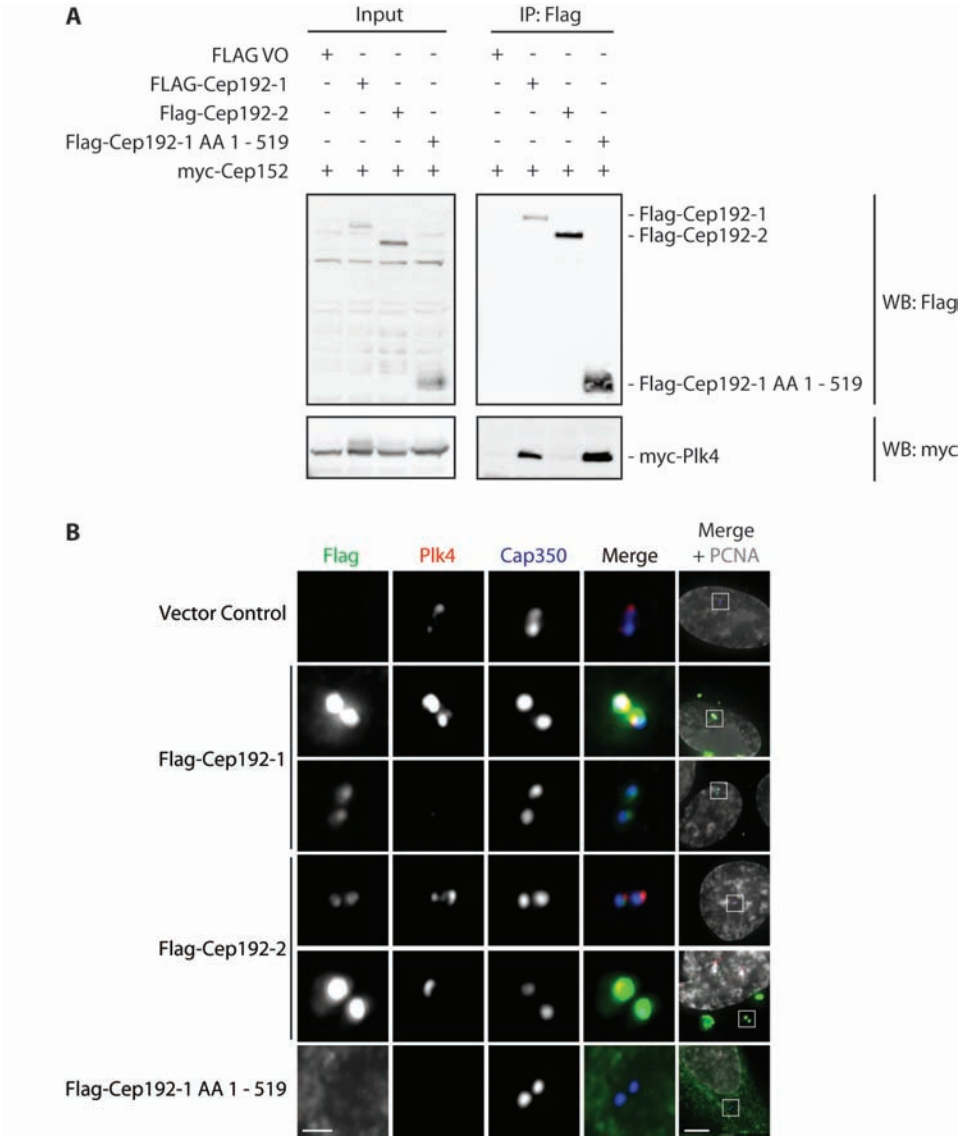

Figure 53 The N terminus of Cep192 interacts with Plk4. A HEK293T cells were transfected with the indicated plasmids. After lysis co-immunoprecipitations were performed and analyzed by Western Blotting. **B** U2OS cells were transfected with the indicated constructs. After fixation the cells were stained with antibodies against Flag, Plk4 and Cap350, DNA was stained with DAPI (Scale bars indicate 1 µm and 5 µm (overview images)).

When analyzing the sequence of Cep192-1 with Coils, we had found one potential coiled-coil region within the N-terminal part (**Figure 20**). As the binding region of Cep152 contains a similar stretch that is required for Plk4 interaction, we hypothesized that the same might be true for Cep192. However, deleting these amino acids did not abolish interaction of the N terminus of Cep192 with Plk4 (**Figure 54**).

Thus, Plk4 interacts with the N terminus of Cep192-1 *in vivo*.

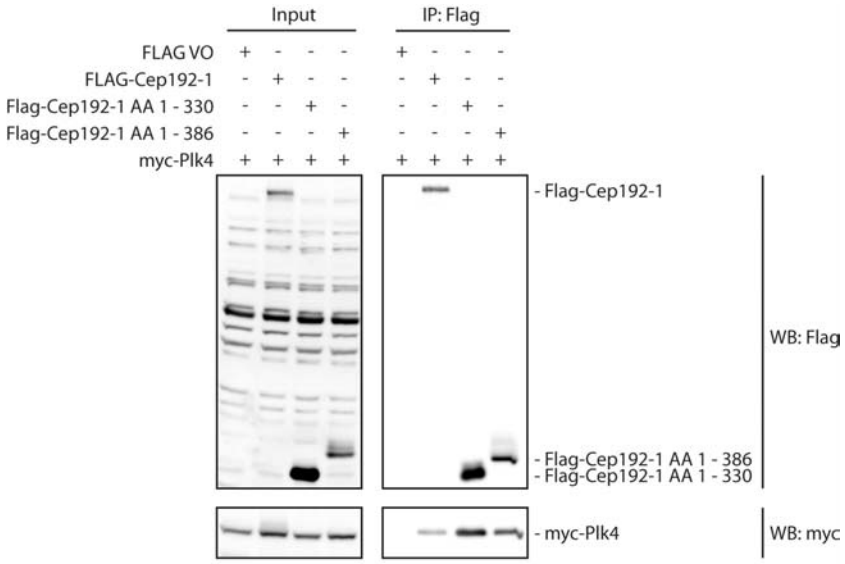

Figure 54 Amino Acids 1 – 330 of Cep192-1 are sufficient to interact with Plk4. HEK293T cells were transfected with the indicated plasmids for 18 h. After lysis the samples were analysed by co-immunoprecipitations using Flag antibodies followed by Western Blotting.

4.5.4 Cep152 and Cep192 Co-Operate in Centriole Duplication

In centriole duplication assays neither Cep152 nor Cep192 depletion led to a centriole duplication defect as strong as Sas-6 or Plk4 depletion (Sections 4.5.1 and 4.5.2). As we had already observed that Cep152 and Cep192 co-operate in Plk4 recruitment, we tested whether Cep192 and Cep152 might also have a synergistic or partly redundant function in centriole duplication. To this end, we co-depleted both proteins and then determined the number of centrioles per cell by IF microscopy. Indeed, co-depletion led to a significant increase in the number of cells with no or only one centriole (**Figure 55**).

Moreover, co-depletion of both Cep152 and Cep192 also affected centriole overduplication in U2OS cells, in which myc-Plk4 expression was induced for 16 h after 48 h of incubation with siRNA oligonucleotides (**Figure 56**). We distinguished between cells with (>4 centrioles) or without (<5 centrioles) overduplicated centrioles. Single depletion of Cep192 resulted in a centriole duplication defect similar to the one observed with Cep152 depletion. However, the

extent of the depletion effect of either protein was not as strong as the one of Sas-6. But if both Cep152 and Cep192 were co-depleted, centriole duplication was severely suppressed.

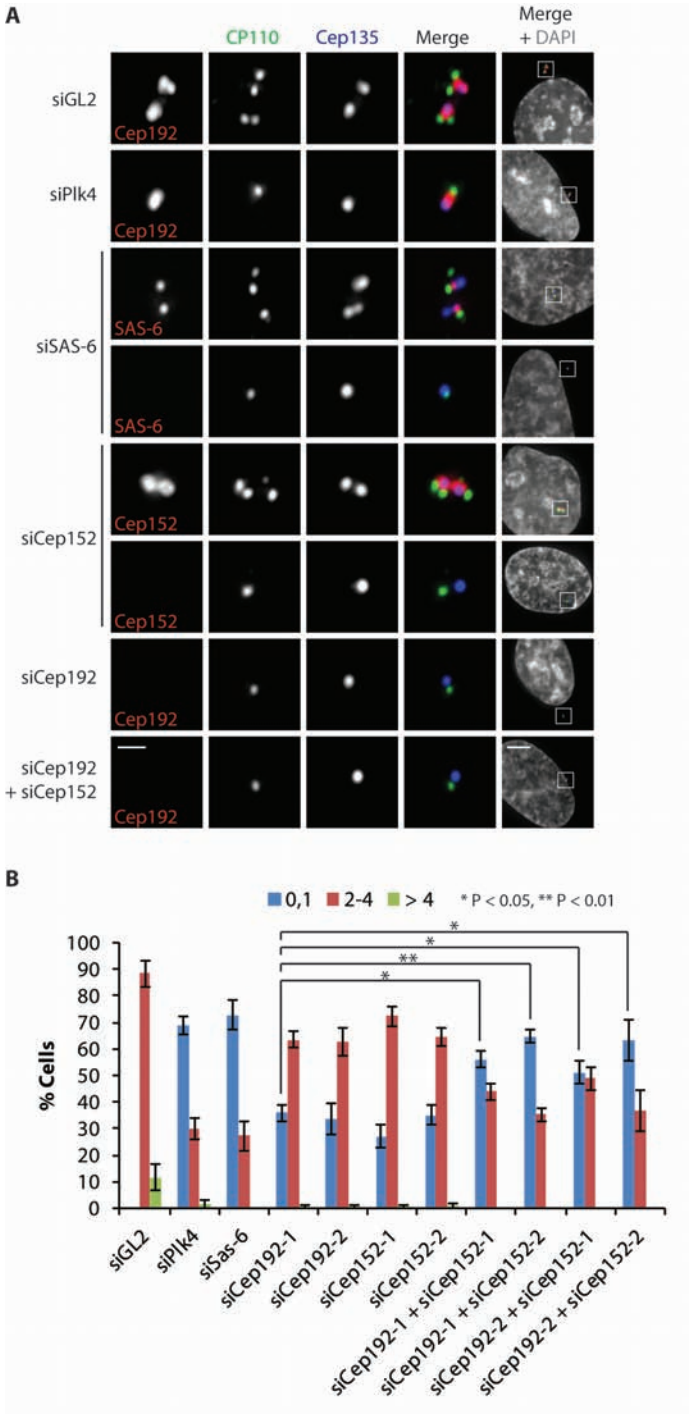

Figure 55 Co-depletion of Cep152 and Cep192 results in a similar centriole duplication defect as Sas-6 or Plk4 depletion. U2OS were transfected with the indicated siRNA oligonucleotides for 72 h. After fixation the cells were stained with the indicated antibodies and the number of centrioles was determined by IF microscopy. Representative images are shown in **A** (scale bars represent 1 µm or 5 µm (overview images, right panel). For Sas-6 and Cep152 depletion non-depleted cells are shown to illustrate antibody specificity. The quantification is shown in **B** (three independent experiments, 100 cells each, error bars denote standard deviation).

Taken together, Cep152 and Cep192 co-operate in both Plk4 recruitment and centriole duplication.

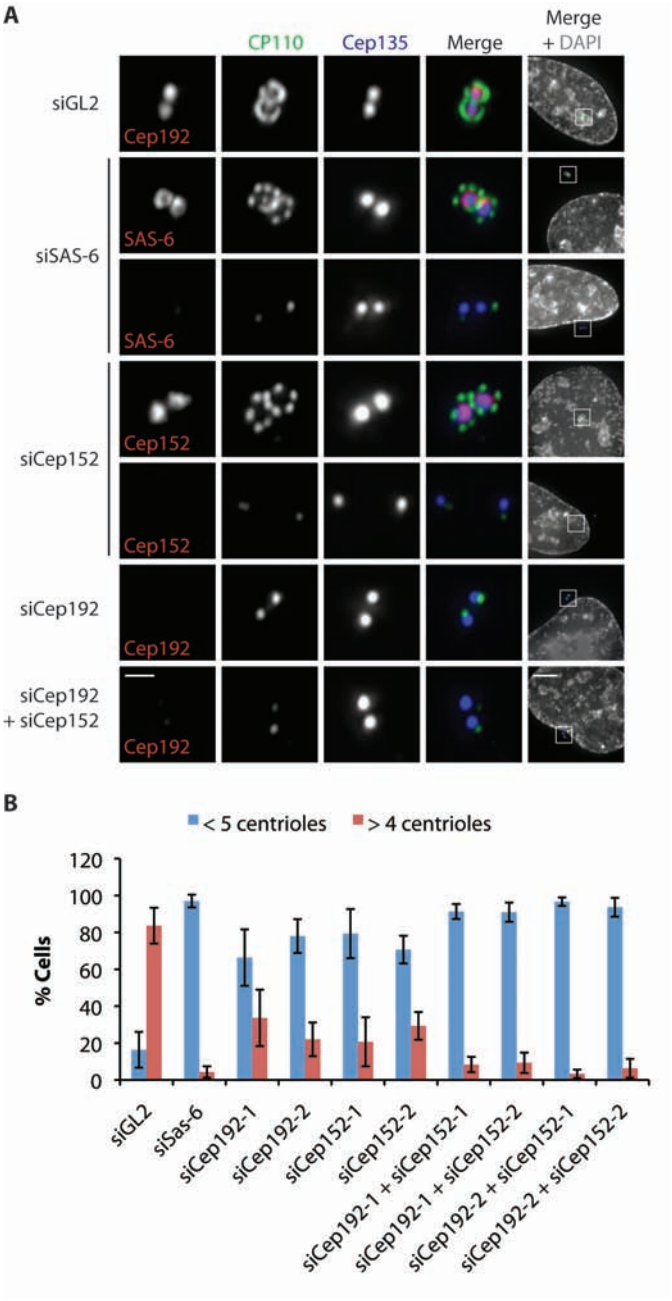

Figure 56 Co-depletion of Cep152 and Cep192 results in a similar centriole duplication defect after myc-Plk4 overexpression as Sas-6 depletion. U2OS:myc-Plk4 cells were transfected with the indicated siRNA oligonucleotides for 48 h before arrest in S phase and the induction of myc-Plk4 overexpression for 16 h. After fixation the cells were stained with the indicated antibodies and the number of centrioles was determined by IF microscopy. Representative images are shown in **A**. For Sas-6 and Cep152 depletion non-depleted cells are shown to illustrate antibody specificity. Scale bars represent 1 µm or 5 µm (overview images, right panel). The quantification is shown in **B** (three independent experiments, 100 cells each, error bars denote standard deviation).

4.5.4.1 Effect of Cep152 and Cep192 on Other Centriole Duplication Factors

To unravel the mechanism further of how Cep152 and Cep192 participate in centriole duplication, we took two approaches: First, the recruitment of components of the centriole duplication pathway in Cep152- and Cep192-depleted cells was analyzed. Second, we sought to identify novel Cep152 and Cep192 interaction partners that are known to be involved in centriole duplication.

4.5.4.1.1 Dependence of Centrosomal Localization of Known Centriole Duplication Factors on Cep152 and Cep192

We have dealt with the recruitment of CPAP and Cep63 to centrioles earlier (Section 4.3.1), both of which depend on Cep152 and Cep192. For several other known centriole duplication factors proteins lying upstream of those within the duplication recruitment pathway have been identified. For instance STIL localization has been shown to depend on Sas-6 (Tang et al., 2011; Arquint et al., 2012; Vulprecht et al., 2012). However, it is not known how Sas-6 and Cep135 are recruited to centrioles. As will be discussed later, Cep135 only becomes visible at emerging daughter centrioles from late G2 phase on (Section 5.3). Thus, the potential pool that might be required for centriole duplication is difficult to investigate. Localization of the mother-specific pool of Cep135 was independent of Cep192 or Cep152 (see e.g. **Figure 55** and **Figure 56**). In contrast, Sas-6 as cartwheel protein is recruited to mother centrioles already in G1 phase and is then required for the recruitment of STIL. Hence, we analyzed the dependence of Sas-6 on Cep152 and Cep192 in U2OS cells. However, single depletion of either Cep152 or Cep192 did not result in a loss of Sas-6 from centrioles (**Figure 57**), even though we often observed unequal Sas-6 staining of both centrosomes present within a Cep192-depleted cell. As control we confirmed that cytoplasmic levels of various proximal proteins remained unchanged upon Cep152 and/ or Cep192 depletion (**Figure 58**).

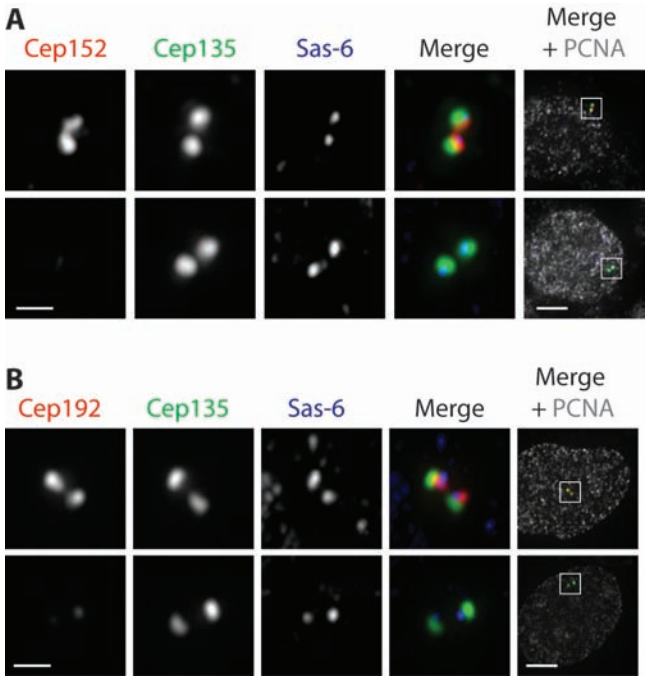

Figure 57 Depletion of either Cep152 or Cep192 does not result in the loss of Sas-6 from centrioles. U2OS cells were transfected with either Cep152 (**A**) or Cep192 (**B**) siRNA oligonucleotides for 72 h. After fixation the cells were stained with the indicated antibodies to visualize centrosomal Sas-6. PCNA was used to identify cells in S phase. Scale bars represent 1 µm or 5 µm (overview images, right panels).

Next, we hypothesized that only double depletion of Cep152 and Cep192 might prevent centriolar recruitment of Sas-6 – similarly to the effect of double depletion on Plk4 localization. Therefore, we co-depleted Cep152 and Cep192 from U2OS cells and investigated the localization of Sas-6 in S phase cells by IF microscopy (**Figure 59**). However, also in depleted cells Sas-6 was mostly detectable; even if only one centrosome per cell was left, it was mostly Sas-6 positive. But we often noticed a striking difference of Sas-6 localization between the two centrosomes within a cell. This phenotype was increased and sometimes resulted in the complete absence of Sas-6 from one centriole and normal Sas-6 levels at the other one, if both Cep152 and Cep192 were co-depleted. We confirmed that the Sas-6-positive centriole reproducibly represented the more mature, appendage-bearing mother centriole by co-staining cells for the appendage protein Ninein (data not shown). This suggests that Cep192 (and Cep152) might be required for the recruitment of Sas-6 of newly duplication-competent centrioles.

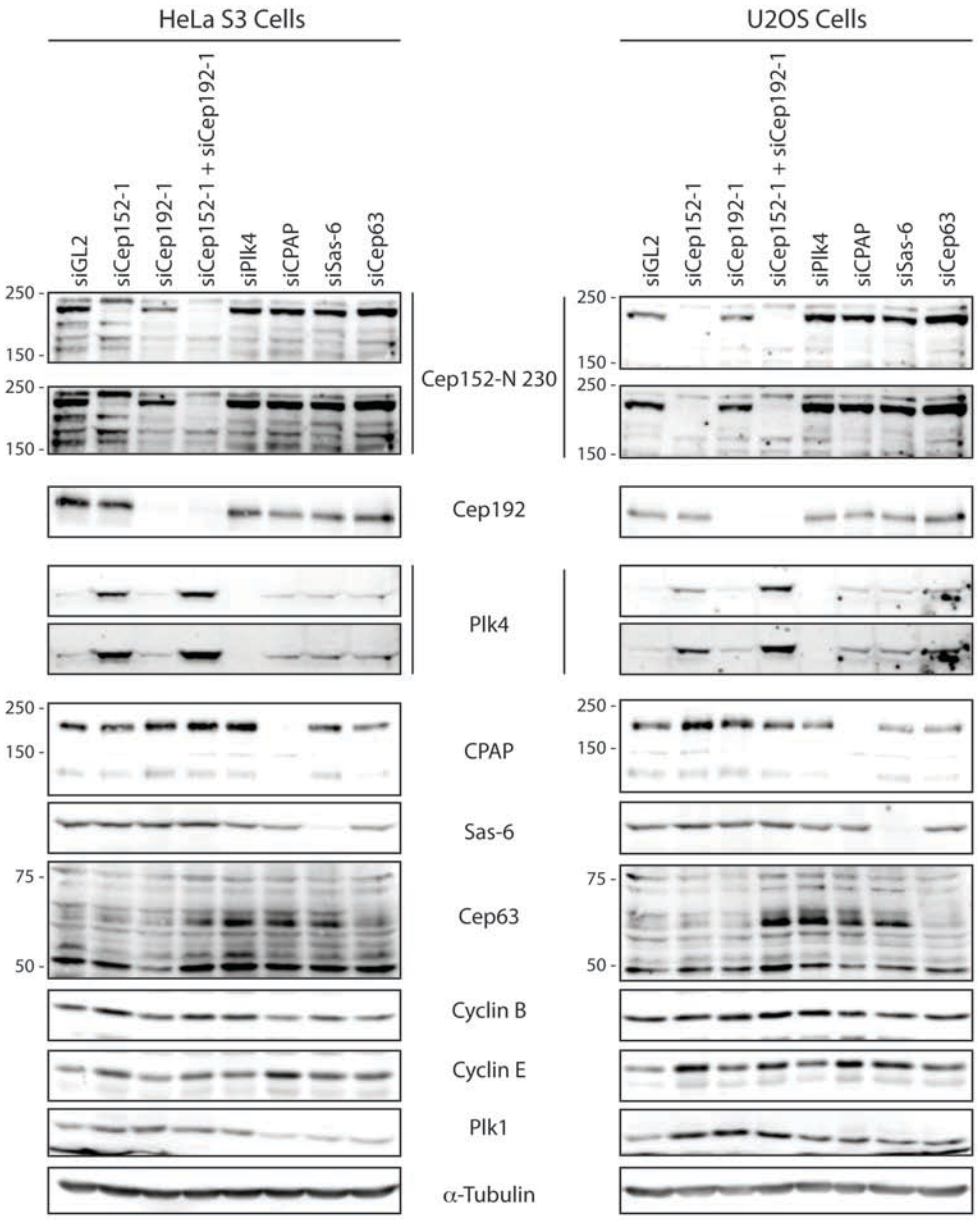

Figure 58 Cep152 and/ or Cep192 depletion do not affect cytoplasmic levels of other proximal centriole duplication factors. HeLa S3 and U2OS were transfected with the indicated siRNA oligonucleotides for 72 h. After lysis the samples were analyzed by Western Blotting using the indicated antibodies. As loading control α-Tubulin was used in addition to the cell cycle markers Cyclin B, Cyclin E and Plk1.

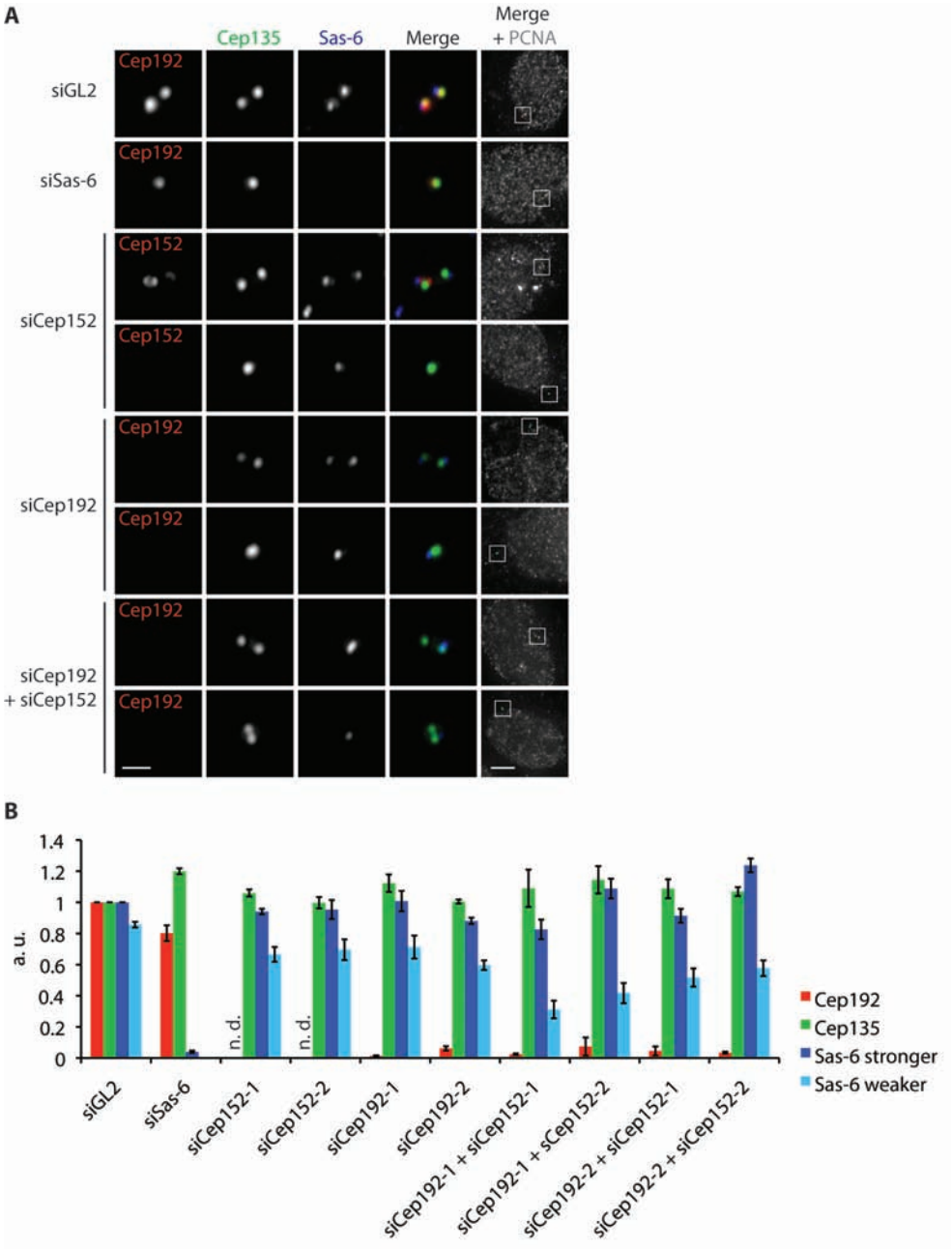

Figure 59 Co-depletion of Cep152 and Cep192 impairs centriolar recruitment of Sas-6. U2OS cells were transfected with the indicated siRNA oligonucleotides for 72 h. After fixation the cells were stained with antibodies against either Cep152 or Cep192 in addition to Cep135, Sas-6 and PCNA and analyzed by widefield microscopy. Representative images are depicted in **A**. Scale bars represent 1 µm or 5 µm in the overview images. Quantification of centrosomal Cep192, Cep135 and Sas-6 levels are shown in **B** (three independent experiments, 10 cells each, error bars denote standard error). Cep192 levels were not quantified in Cep152-depleted cells (n. d.).

This reduction in Sas-6 levels could potentially be explained by an alteration of either Plk1 or Plk4 at centrosomes. With regard to Plk1, it has been suggested previously that phosphorylation of an unknown substrate by Plk1 in mitosis renders the previous daughter

centriole duplication-competent in the following cell cycle (Wang et al., 2011). As marker for duplication competence Sas-6 had been used. Thus, we addressed the question whether impaired Plk1 recruitment could account for the observed effect on Sas-6 recruitment. Yet, Plk1 was only detectably reduced when formation of the extended PCM cloud in mitosis was prevented by depletion of either Cep192 or Pericentrin, but not upon Cep152 depletion (data not shown). Additionally, Pericentrin depletion, which also prevents centrosomal accumulation of Plk1 in mitosis, did not impair Sas-6 recruitment (**Figure 60**). This indicates that the centrosomal accumulation of Plk1 within the PCM upon mitotic onset cannot account for Sas-6 recruitment in the following cell cycle.

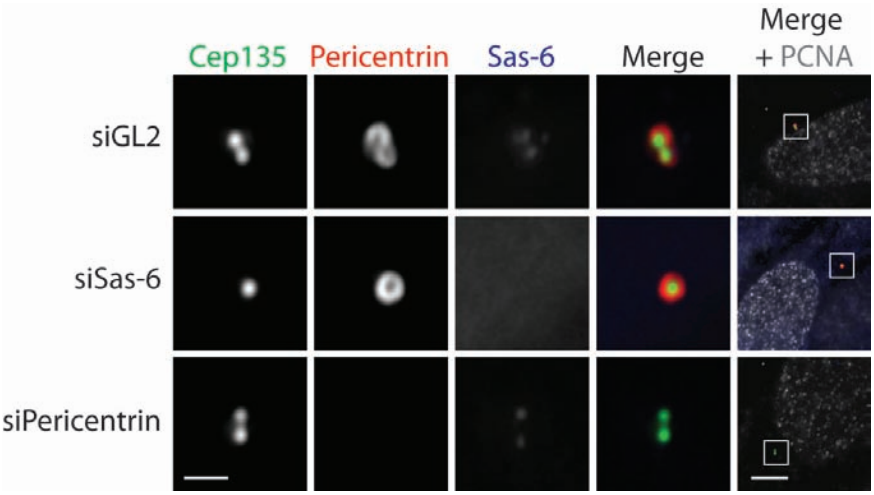

Figure 60 Pericentrin depletion does not impair centriolar Sas-6 recruitment. U2OS cells were transfected with the indicated siRNA oligonucleotides for 72 h. After fixation the cells were stained with the indicated antibodies and analyzed by IF microscopy (scale bar 1 µm or 5 µm (overview images), PCNA antibodies were used to visualize cells in S phase).

In Plk4-depleted cells, Sas-6 was mostly not detectable at centrosomes. However, when we especially examined Plk4-depleted cells in which two centrosomes were still present, we occasionally observed very low Sas-6 levels at one of the centrosomes (**Figure 61**). Even though centrosomal Sas-6 were reduced to a higher extent in Plk4-depleted than in Cep152/ Cep192-depleted cells, it is still possible that Cep152/Cep192-depletion interferes with Sas-6 recruitment indirectly via Plk4. This is particularly the case, as Plk4 depletion is more efficient than Cep152 or Cep192 depletion and thus leads to a faster reduction of centrosomal Plk4 levels.

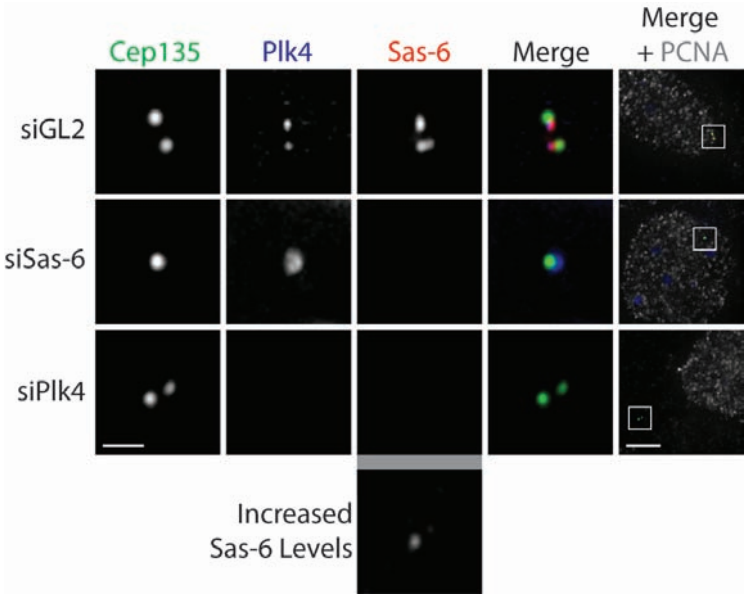

Figure 61 Plk4 depletion prevents centriolar Sas-6 recruitment. U2OS cells were transfected with the indicated siRNA oligonucleotides for 72 h. After fixation the cells were stained with the indicated antibodies and analyzed by IF microscopy. (scale bar 1 µm or 5 µm (overview images), PCNA antibodies were used to visualize cells in S phase). The Sas-6 signal in the Plk4-depleted cell was post-acquisitionally increased to visualize residual Sas-6 (Bottom panel: Increased Sas-6 Levels).

4.5.4.1.2 Interaction of Cep152 and Cep192 with Centriole Duplication Factors

While this work was in progress, two groups published the interaction of Cep152 with the centriole duplication factor CPAP (Cizmecioglu et al., 2010; Dzhindzhev et al., 2010). They suggested that both proteins interact directly with each other and that Cep152 is required for the recruitment of CPAP to centrosomes in human cells. When we performed immunoprecipitations of endogenous Cep152 with either the C-terminal or the N-terminal antibody, we did not detect any other centriole duplication factor in the immunoprecipitates (data not shown). Moreover, when we co-expressed Cep152 with various duplication factors followed by co-immunoprecipitations, we only detected an interaction with CPAP, but not with either CP110, Sas-6, STIL or Cep135 (**Figure 62** A and data not shown). The interaction between Cep152 and CPAP was reproducibly weaker than the one with Plk4 (**Figure 62** A and B).

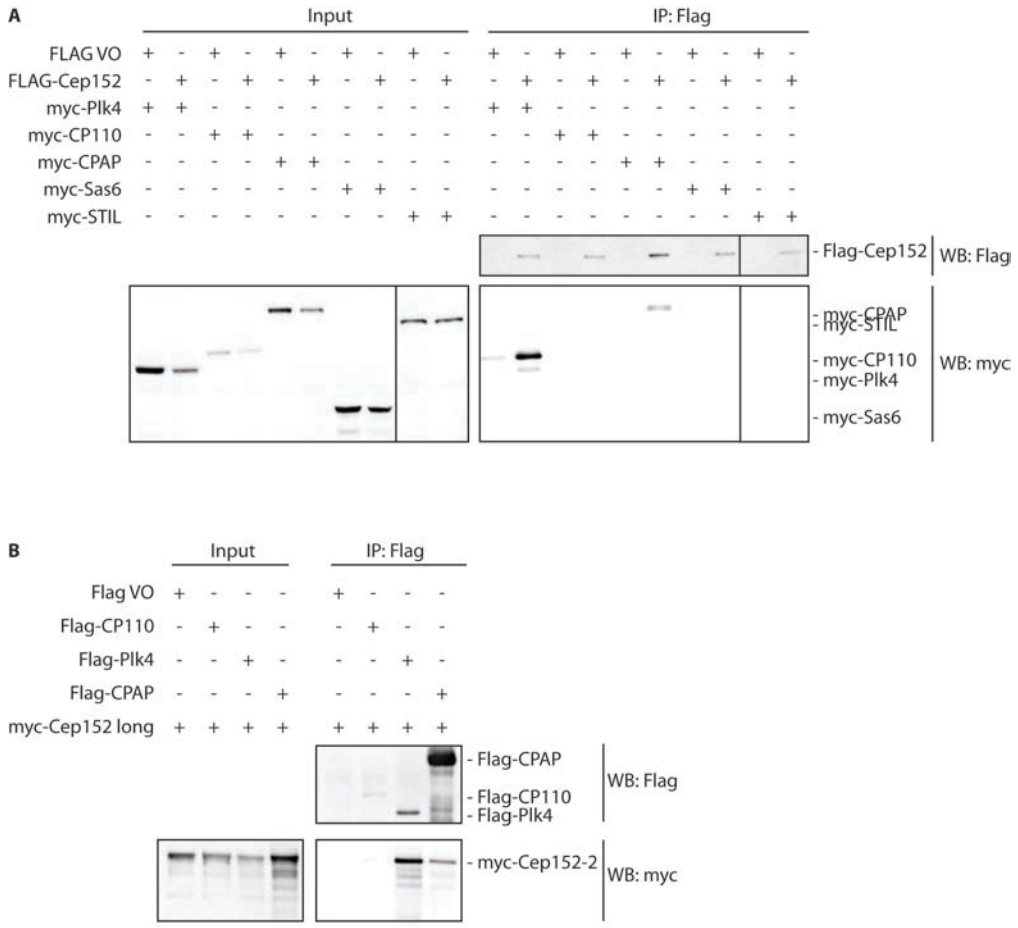

Figure 62 In co-immunoprecipitation experiments Cep152 interacts with Plk4 and CPAP, but not with CP110, Sas-6 or STIL. A HEK293T cells were transfected with the indicated plasmids for 24 h. After lysis co-immunoprecipitations were performed using Flag antibodies and analyzed by Western Blotting using the indicated antibodies. **B** The indicated proteins were *in vitro* translated. Then immunoprecipitations were performed using Flag antibodies and analyzed by Western Blotting.

In addition, immunoprecipitations of endogenous Cep192 did not reveal any interaction with either Cep152, Cep63, Cep135, Plk4 or CPAP. However, if Cep192 was co-expressed with either of those proteins, a very weak interaction with the predicted cartwheel proteins Sas-6, STIL and Cep135 was reproducibly detected, even though the detected bands were much weaker than the one of Plk4 (**Figure 63** A). However, the expression levels of STIL and Cep135 co-expressed with Cep192 were consistently higher than those co-expressed with empty vector. Thus, to rule out that the co-purified proteins bind unspecifically, we also pulled on those proteins and tried to co-purify Cep192. However, we could not reproduce the interaction in this manner (**Figure 63** B).

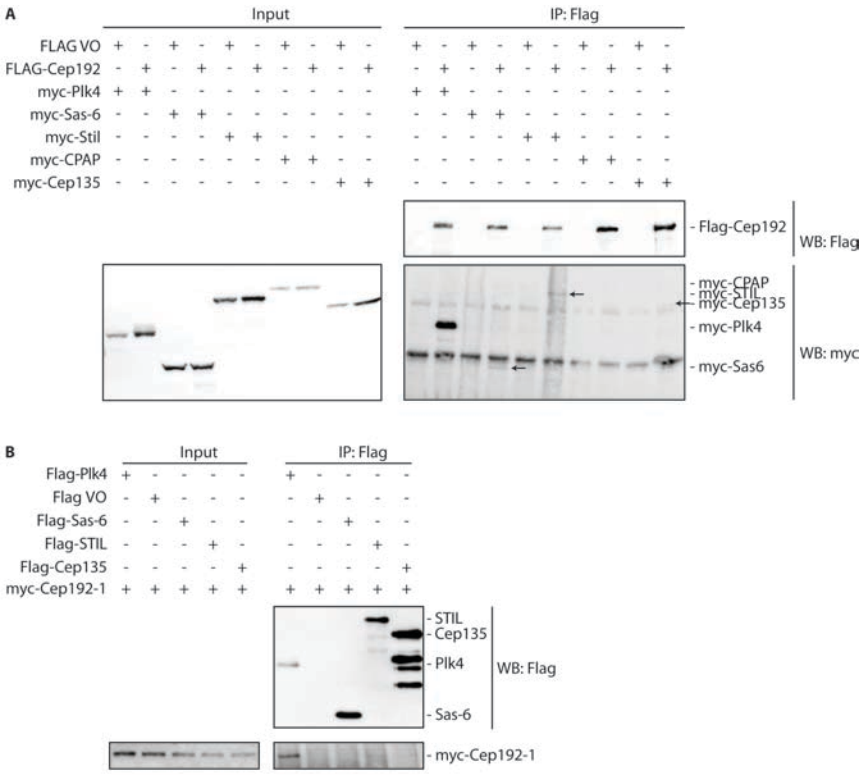

Figure 63 In co-immunoprecipitation experiments Cep192 interacts with Plk4 and weakly with Sas-6, STIL and Cep135. A, B HEK293T cells were transfected with the indicated plasmids for 24 h. After lysis co-immunoprecipitations were performed using Flag antibodies and analyzed by Western Blotting using the indicated antibodies. Arrows indicate weak bands for Sas-6, STIL and Cep135.

Thus, among other known centriole duplication factors in addition to Plk4 we only detected an interaction of Cep152 with CPAP and a very weak one – if at all – of Cep192 with Sas-6, STIL and Cep135.

4.5.5 Phosphorylation of Cep152 by Plk4

Plk4 is a Ser/Thr kinase whose enzymatic activity is required for centriole duplication (Habedanck et al., 2005; Guderian et al., 2010). However, to date, very few proteins have been identified as physiological Plk4 substrate, such as Plk4 itself and GCP6 (Carvalho-Santos et al., 2010; Guderian et al., 2010; Holland et al., 2010; Sillibourne et al., 2010; Bahtz et al., 2012). Due to the detected interaction of Plk4 with Cep152, we also tested whether Cep152 is phosphorylated by Plk4.

4.5.5.1 Cep152 is an *in vitro* Substrate of Plk4

To investigate a potential phosphorylation of Cep152 by Plk4, we purified recombinant GST-Cep152-2 and GST-Cep152-4 from *E. coli* and used those as substrate for *in vitro* kinase assays. We used a fragment of Plk4 consisting of amino acids 1 – 430 (recombinant kinase domain) as active kinase (Guderian et al., 2010). Interestingly, GST-Cep152-2 appeared to be more strongly phosphorylated than GST-Cep152-4. This was eminent because of the stronger autoradiography and an upshift that was only observed, if GST-Cep152-2 was phosphorylated by Plk4 (**Figure 78**).

4.5.5.2 Identification of Plk4 Phosphorylation Sites on Cep152

After having observed that Cep152 is phosphorylated by Plk4 *in vitro*, we next checked for a phosphorylation by Plk4 *in vivo* and attempted to identify phosphorylation sites. If Plk4 overexpression was induced in U2OS cells, an upshift of Cep152 by gel electrophoresis was detected (personal communication, L. Cajanek), which implies that Cep152 might be an *in vivo* substrate of Plk4. Moreover, we used Cep152 purified from HEK293T cells as substrate in an *in vitro* kinase assay. Initially, we confirmed that the purified Cep152 was indeed phosphorylated by Plk4. To this end, we analyzed the samples by autoradiography after gel electrophoresis and Western Blotting (**Figure 64**). The samples were then analyzed by mass spectrometry and potential Plk4 phosphorylation sites were determined by label-free quantification (kindly assisted by M. Bauer and A. Schmidt). The advantage of using Cep152 purified from human cells is that we were able to identify phosphorylation sites that were increased due to the performed kinase assay, but were already present *in vivo*, in addition to new phosphorylation sites.

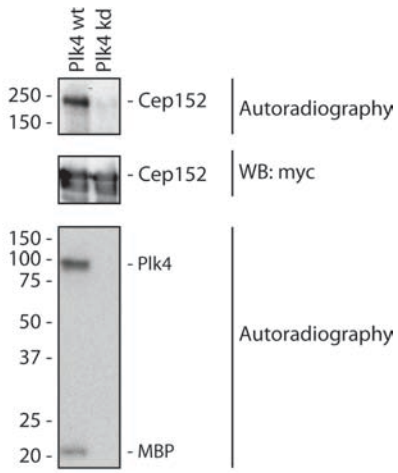

Figure 64 Plk4 phosphorylates Cep152 purified from human cells. Myc-Cep152-2 was expressed in HEK293T cells for 24 h. After purification myc-Cep152-2 was used as substrate for an in vitro kinase assay using recombinant Plk4 (AA 1 – 430). The samples were separated by SDS-PAGE and analysed by Western Blotting and autoradiography.

After the kinase assays Cep152 was eluted and Cep152 phosphosites present in Plk4 kinase dead and Plk4 wildtype samples identified. When analyzing the obtained results, logarithmic ratios of each peptide with Plk4 wt divided by Plk4 kd were calculated, i.e. numbers above 0 indicate an increased detection of that particular peptide in the kinase assay compared to control. In addition, logarithmic ratios of the phosphopeptides were compared with those of the unphosphorylated peptides and only phosphosites were taken into account, of which ratio(phospho) > ratio(non-phospho). This was used as internal control to avoid false positive results, in which both the phosphorylated and the unphosphorylated peptide were detected in an elevated amount. Using these algorithms, only three phosphosites were found that were considerably upregulated in the Plk4 wildtype kinase assay (serine 1533, threonine 1542 and threonine 1621, **Figure 65** A). However, one of those was not conserved at all, whereas the other two were at least partly conserved in mammalians (**Figure 65** B). Further experiments are required to verify the in vivo phosphorylation of these sites and to determine their significance in centriole duplication.

A

Residue	Peptide Sequence	Charge	Po4	Score	t-test	Log ratio, WT (Median)/ KD (Median)
S1533	EASFVHGRPQGTLEIPSESVK	3	yes	24.31	0.035125538	1.126101641
	EASFVHGRPQGTLEIPSESVK	3	no	29.49	0.751792657	-0.005857642
T1542	PQGTLEIPSESVK	2	yes	54.34	0.026445587	0.630791251
	PQGTLEIPSESVK	2	no	68.19	0.041265925	0.346751833
T1621	LSSTLPSSVCQQPSR	2	yes	61.06	0.000462855	0.39023619
	LSSTLPSSVCQQPSR	3	no	55.64	0.667009774	0.021750465
	LSSTLPSSVCQQPSR	2	no	80.72	0.467790666	-0.121637983

B

Figure 65 Potential Plk4 phosphosites identified on Cep152 by mass spectrometry. A myc-Cep152-2 was purified from HEK293T cells and used as substrate in kinase assays with either Plk4 wildtype or kinase dead (amino acids 1 – 430). After elution the samples were analyzed by mass spectrometry. Only three phosphosites were identified to be upregulated in the kinase assay compared to control. The score reflects the confidence and t-test the significance of the detected peptides. **B** The indicated Cep152 homologues were aligned using ClustalW2 and illustrated with espript. For human Cep152 isoform Cep152-2 was used. Note that two different sequences for Cep152 of *rattus norvegicus* were included, only one harbouring an extended C terminus. Boxed areas highlight the identified phosphosites.

4.6 Regulation of Cep152

As mentioned earlier, cytoplasmic levels of Cep192 are stable (**Figure 32**), whereas centrosomal levels increase upon mitotic onset (**Figure 26**). This increase has been attributed to the kinase activity of Plk, when cells approach mitosis (Haren et al., 2009; Santamaria et al., 2011). Therefore, we concentrated on a potential regulation of Cep152 levels, since that had not been addressed so far. When investigating IF images of Cep152 we noticed cell cycle-specific centrosomal level changes of Cep152. This prompted us to analyze both cytoplasmic and centrosomal levels in more detail.

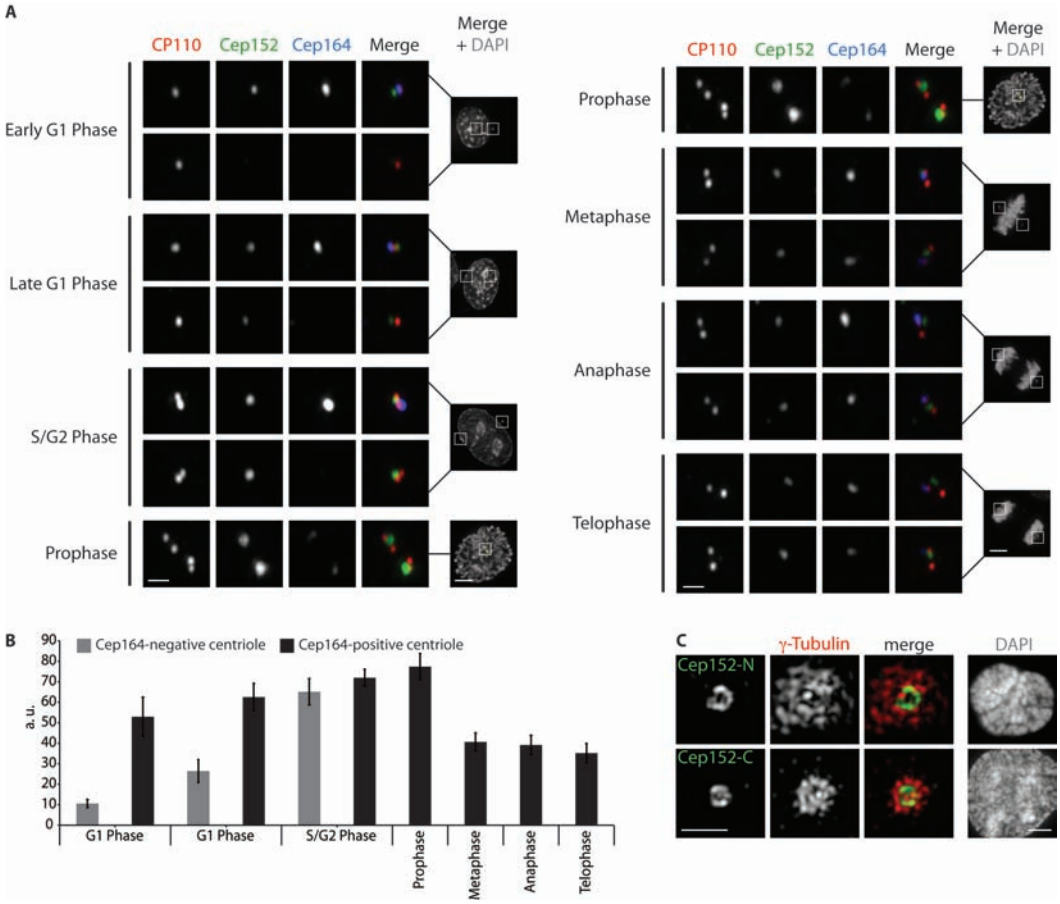

Figure 66 Centrosomal Cep152 levels peak in prophase. A,B U2OS cells were fixed and stained with the indicated antibodies for IF microscopy. For Cep152 antibody Cep152-C 934 was used. DNA was stained with DAPI. In **A** representative images are shown (scale bars represent 1 µm or 5 µm (overview images, right panels). In **B** quantification of centrosomal Cep152 fluorescence intensities is depicted. Centriole pairs were differentiated depending on the presence of Cep164 staining. Error bars denote standard deviation. **C** Prophase cells stained with the indicated antibodies were imaged by 3D-SIM. DNA was stained with DAPI and visualized using a DV system. Scale bars represent 1 µm or 5 µm (DV images).

4.6.1 Centrosomal Cep152 Levels Peak in Prophase

To determine centrosomal Cep152 levels at different cell cycle stages, we stained U2OS cells with either Cep152-C 934 or Cep152-N 207 in combination with antibodies against CP110 and Cep164 and DAPI. CP110 allowed us to define the number of centrioles per cell, i.e. the state either before or after centriole duplication. With DAPI we were able to differentiate interphase from different mitotic stages depending on the constitution of nuclear DNA. Finally, we co-stained cells with Cep164, a distal appendage protein that is recruited to

mother centrioles upon maturation. Both Cep152 antibodies gave similar results. During the whole cell cycle Cep152 is confined to one distinct position within a centriole pair close to Cep164. Only after centriole disengagement upon mitotic exit, but before centriole duplication visualized by CP110 staining at daughter centrioles, Cep152 becomes detectable at the previous daughter centriole. Moreover, Cep152 levels increased until prophase and then rapidly dropped during mitosis, even though it was never completely lost. As shown earlier, Cep152 remains confined to centriolar walls, when cells approach mitosis (**Figure 22**). Analysis of cells particularly in prophase by 3D-SIM revealed that Cep152 was still restricted to the proximity of the centriolar walls even in this cell cycle stage (**Figure 66** C).

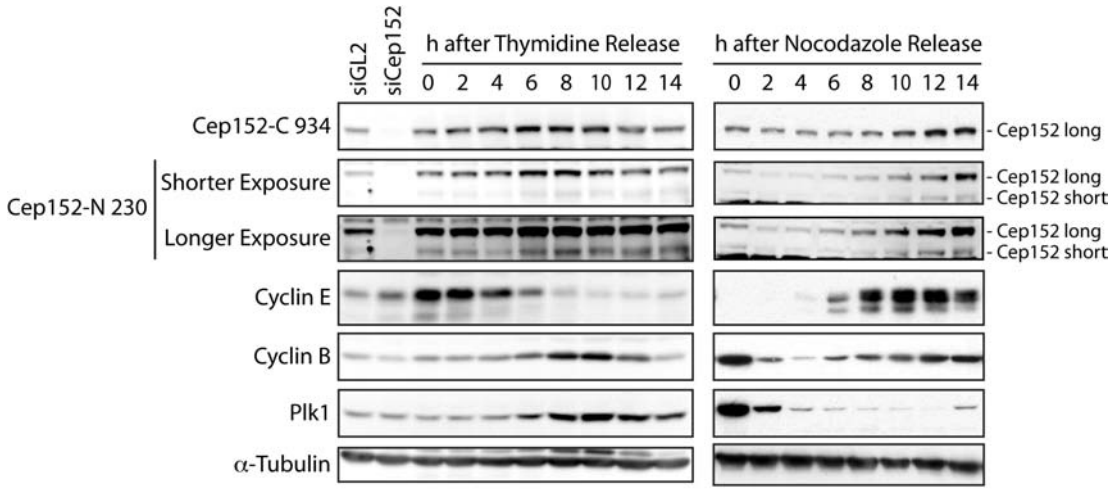

Figure 67 Cytoplasmic Cep152 levels peak in late G2 phase. HeLa S3 cells were either released from a double thymidine or from a nocodazole arrest. Samples were taken at the indicated time-points after release and analyzed by Western Blotting using the indicated antibodies. Asynchronously growing GL2 control- or Cep152-depleted cells were analyzed as control.

4.6.2 Changes in Protein Levels

Centrosomal levels of Cep152 might fluctuate solely by regulation via post-translational modifications or by regulated expression and degradation. To understand whether expression and degradation is also involved, we switched to HeLa S3 cells, as they are more efficiently released from cell cycle arrests than U2OS cells. HeLa S3 cells were either released from double thymidine block or from nocodazol arrest. The expression was then analyzed by Western Blotting using Cep152 antibodies as well as specific cell cycle markers to determine

the cell cycle stage (**Figure 67**). Upon release from S phase levels of both long and short Cep152 isoforms increased until late G2 phase and then decreased again. This decrease was concomitant with an increase in Cyclin B as well as Plk1 levels. Accordingly, upon release from mitotic arrest Cep152 levels increased during interphase.

4.6.3 Significance of Cep152 Regulation

We have demonstrated earlier that diminished Cep152 levels impair faithful centriole duplication. In contrast, the effect of elevated Cep152 levels on centriole duplication was still unknown. To test whether Cep152 has to be tightly regulated, Cep152 was ectopically overexpressed in U2OS cells and the number of centrioles per cell was determined based on CP110 staining. Several proteins induce centriole over-duplication if overexpressed, such as Plk4, Sas-6 or STIL (Bettencourt-Dias et al., 2005; Habedanck et al., 2005; Strnad et al., 2007; Kitagawa et al., 2011; Tang et al., 2011; Arquint et al., 2012; Vulprecht et al., 2012). However, the overexpression of both Cep152-2 and Cep152-4 led to a slight increase of cells with no or only one centriole (**Figure 68** A). Similar results were obtained when co-expressing Cep152-2 and Cep152-4 (data not shown). It is possible that no centriole overduplication was induced, similar to e.g. Plk4 or STIL overexpression, because other centriole duplication factors are limiting despite the presence of excess Cep152. A possible explanation for the negative effect on centriole duplication could be the sequestration of essential centriole duplication factors away from centrioles, such as its interaction partner Plk4. Indeed, centrosomal Plk4 levels were reduced compared to control cells (**Figure 68** B). To rule out an effect of Cep152 on the stability of Plk4, we confirmed that overexpression of Cep152 in asynchronously growing cells did not change cellular Plk4 levels by Western Blotting (**Figure 68** C).

Thus, cellular Cep152 levels have to be tightly regulated to allow proper centriole duplication to occur.

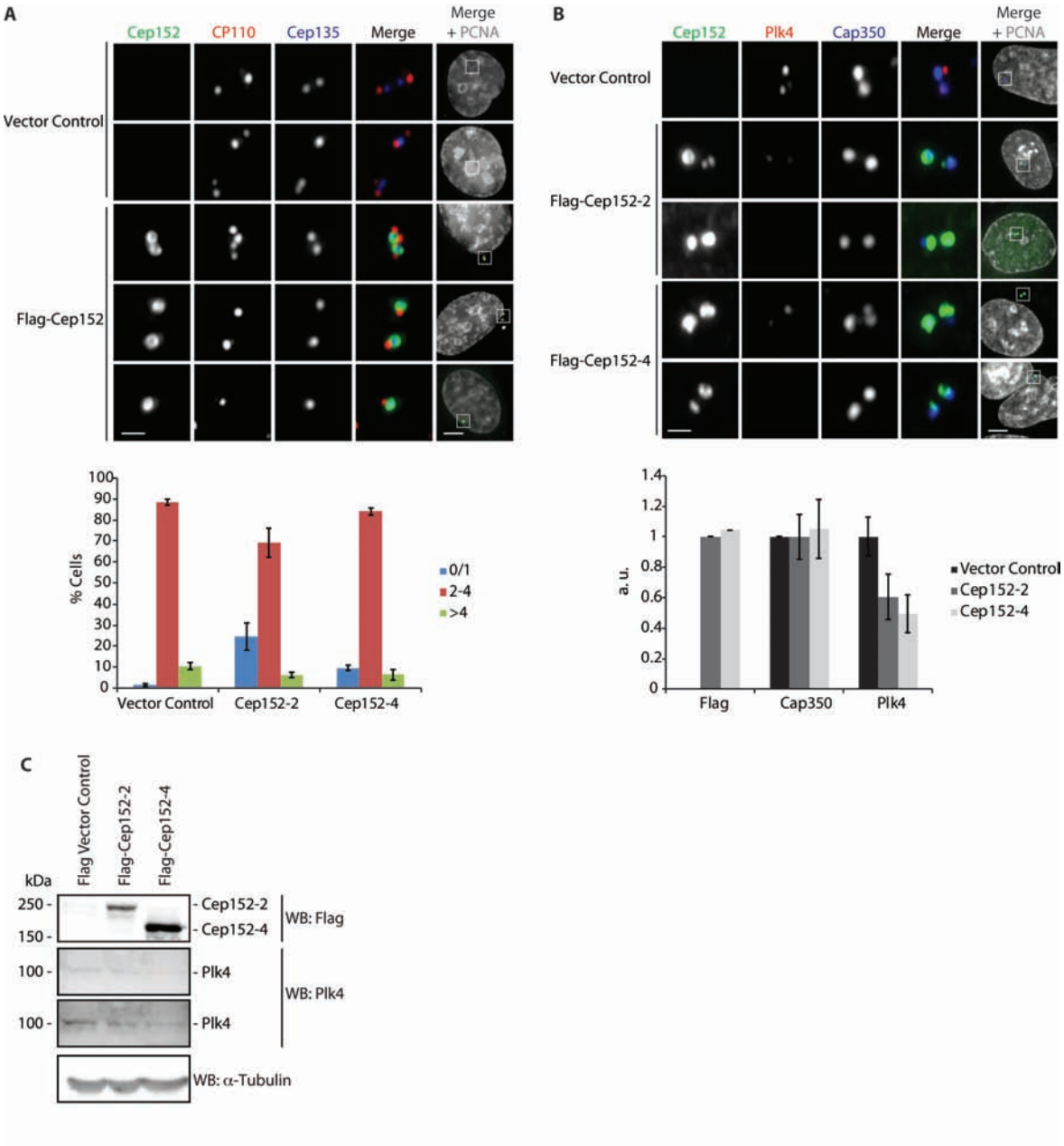

Figure 68 Cep152 overexpression interferes with faithful centriole duplication. U2OS cells were transfected with either Flag vector control, Flag-Cep152-2 or Flag-Cep152-4 for 48 h. **A** After fixation cells were stained with antibodies against Flag, CP110 and Cep135 and DNA was visualized with DAPI. In the upper panel representative images are shown (scale bars represent 1 µm or 5 µm (overview images, right panel). In the lower panel the quantification of centriole numbers per cell is shown (three independent experiments, 100 cells each, error bars denote standard deviation). **B** After fixation the cells were stained with the indicated antibodies for immunofluorescence microscopy. In the upper panel representative images are shown (scale bars represent 1 µm or 5 µ m (overview images, right panel)). In the lower panel quantification of centrosomal fluorescence intensities of overexpressed protein, Cap350 and Plk4 is shown (three independent experiments, 15 cells each, error bars denote standard deviation). **C** The cells were lysed and the samples analyzed by Western Blotting using the indicated antibodies.

4.6.4 Mechanistic Insights into the Regulation of Cep152

To unravel the mechanism of how Cep152 is regulated in human cells, we first searched its sequence for conserved sites that might account for the regulation. Afterwards, we tested whether the identified proteins were indeed involved in the regulation.

4.6.4.1 Identification of Potential Regulatory Sites

Sequence analysis of Cep152 did not reveal any regulatory sites such as KEN or D boxes, which are known binding sites for the E3 ubiquitin ligase complex APC/C. But we identified a conserved DSGXXS motif within the C terminus of the long isoforms of Cep152 (amino acids 1643 – 1648 of isoform 2) in addition to the conserved SSP site within the N terminus (amino acids 47 - 49). If phosphorylated at both serines, DSG motives provide a docking site for the F box protein βTrCP (Guardavaccaro et al., 2003; Jin et al., 2003; Watanabe et al., 2004; Nakayama and Nakayama, 2005). F box proteins are components of SCF E3 ligases (**S**kp, **C**ullin, **F**-box), a diverse family of ubiquitin ligases whose specificity is determined by the attached F box proteins. SSP sites on the other hand are – once phosphorylated at the second serine – binding sites for polo box-containing proteins such as polo-like kinase 1 (Plk1) (Cheng et al., 2003; Elia et al., 2003). These sequence conservations might hint at a role of βTrCP and Plk1 in the regulation of Cep152.

4.6.4.2 Involvement of βTrCP and the Kinases Plk1 and Plk4 in Cep152 Regulation

To test whether the identified sequences were essential for the degradation of Cep152, we firstly analysed the effect of depletion or inhibition of the implicated proteins on Cep152 levels. Secondly, the effect of mutating these sites on Cep152 stability was assessed. Thirdly, we investigated the interaction of the potentially regulating proteins with Cep152 and, finally, phosphorylation of Cep152 by other mitotic kinases was checked.

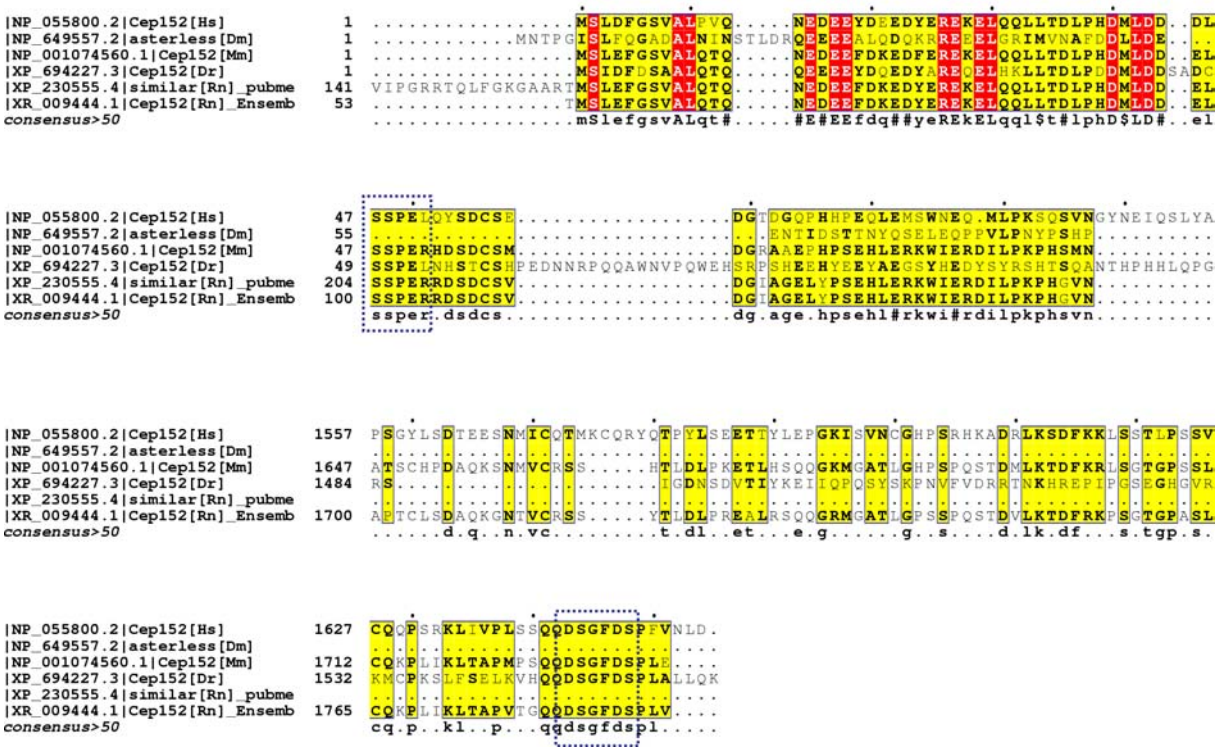

Figure 69 Conservation of sites potentially involved in Cep152 regulation. The indicated Cep152 homologues were aligned using ClustalW2 and illustrated with espript. For human Cep152 isoform Cep152-2 was used. Note that two different sequences for Cep152 of *rattus norvegicus* were included, only one harbouring an extended C terminus. Boxed areas highlight the conserved SSP site and DSG motif.

4.6.4.2.1 Interference with βTrCP, Plk1 and Plk4 Increases Cep152 Levels

If Plk1 and βTrCP were indeed involved in the degradation of Cep152, then their depletion should result in increased Cep152 levels. As control Plk4 was also depleted, to rule out that βTrCP depletion might affect Cep152 levels by increasing Plk4 levels, since it is a known βTrCP substrate (Cunha-Ferreira et al., 2009; Guderian et al., 2010; Holland et al., 2010; Sillibourne et al., 2010). However, when we depleted either of those proteins by RNAi in asynchronous HeLa S3 cells for 48 h, we did not detect changes in Cep152 levels (data not shown). Thus, we arrested cells in prometaphase by addition of nocodazol or monastrol for 20 h after transfection of cells with siRNA oligonucleotides, i.e. in the cell cycle stage, when Cep152 should have been degraded. Indeed, Cep152 levels were increased compared to control-depleted cells under these conditions (**Figure 70** and data not shown). Surprisingly, Cep152 levels were also elevated in Plk4-depleted cells. Due to the low quality of the applied antibodies we were not able to reproducibly detect the short isoforms in the performed

experiments. In addition to cytoplasmic levels, centrosomal Cep152 levels were also increased about 1.5 – 2-fold, if either Plk4, Plk1 or βTrCP were depleted (**Figure 70** B, C).

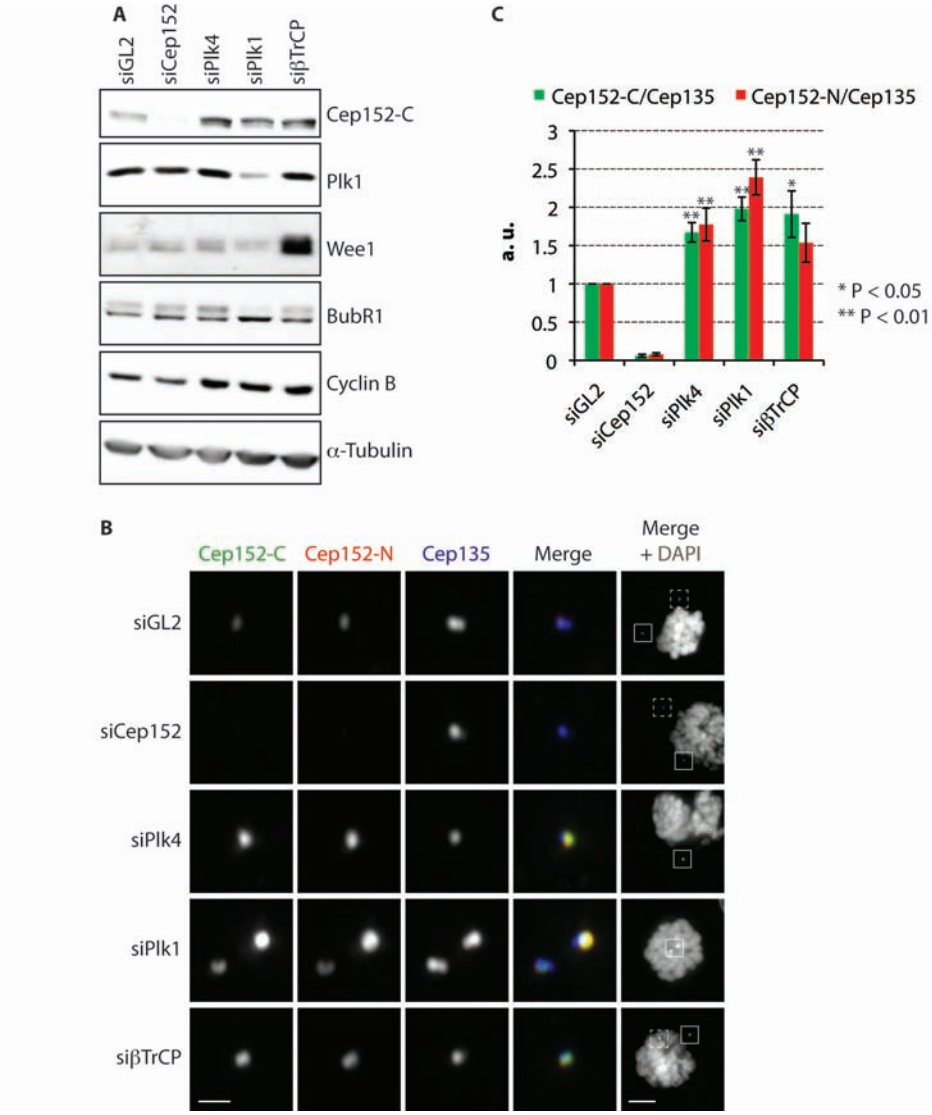

Figure 70 Depletion of βTrCP, Plk1 or Plk4 increases Cep152 levels in prometaphase. HeLa S3 cells were transfected with the indicated siRNA oligonucleotides for 48 h. The cells were then arrested in prometaphase by the addition of nocodazole. **A** After lysis the samples were analysed by Western Blotting using the indicated antibodies. **B,C** After treatment the cells were fixed and stained with the indicated antibodies for IF microscopy. In **B** representative images are depicted. Scale bars denote 1 µm or 5 µm (overview images, right panel). Boxed areas illustrate the magnified region, dashed boxes hint at the other centriole pair within the cell. In **C** the quantification of centrosomal Cep152 levels is shown. The levels were normalized by division by centrosomal Cep135 fluorescence intensity (three independent experiments, error bars denote standard deviation, student's t-test was calculated).

In addition to depletion of Plk1, we also inhibited Plk1 with the small molecule inhibitor TAL (Santamaria et al., 2007). By inhibition of Plk1 cells arrest in prometaphase with monopolar spindles, which is why we used monastrol, an Eg5 small molecule inhibitor, as control to induce a similar cell cycle arrest. Consistent with Plk1 depletion, its inhibition also resulted in an increase in both centrosomal and cytoplasmic Cep152 levels compared to monastrol-treated cells (**Figure 71**).

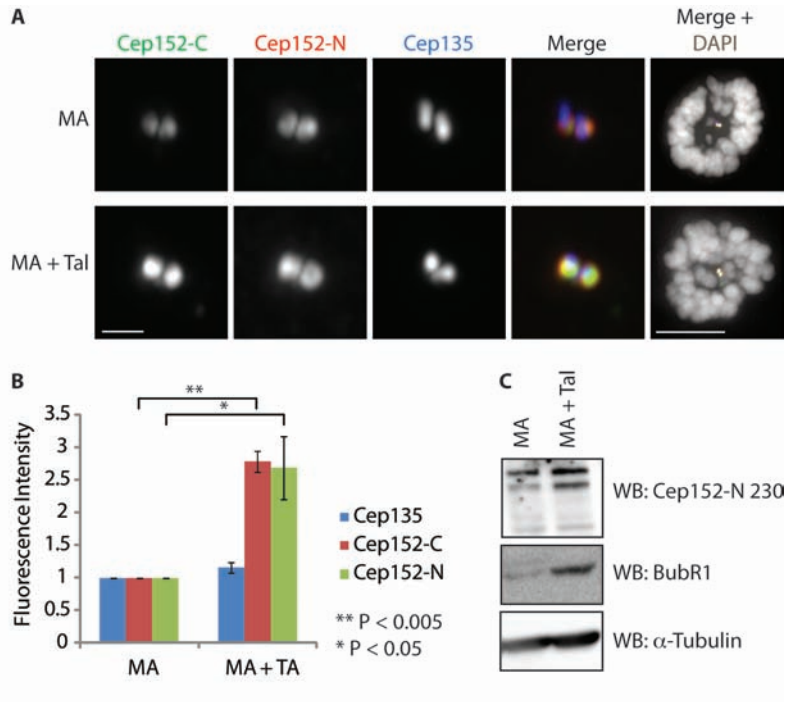

Figure 71 Cep152 levels are increased in Plk1-inhibited prometaphase cells. HeLa S3 cells were inhibited with either monastrol or monastrol + TAL for 20 h. **A, B** After drug treatment the cells were fixed and stained with the indicated antibodies. DNA was stained with DAPI. In **A** representative images are shown. Scale bars represent 1 µm and 5 µm (overview images, right panel). In **B** quantification of three independent experiments is shown (15 cells each, error bars denote standard deviation). **C** After drug treatment the cells were lysed and analyzed by Western Blotting using the indicated antibodies.

Surprisingly, we had found Cep152 levels to be increased, if Plk4 was depleted. To confirm an involvement of Plk4 in Cep152 regulation we overexpressed Plk4 and then checked for cytoplasmic and centrosomal Cep152. To this end, myc-Plk4 was induced in U2OS:myc-Plk4 cells for 72 h either in cycling or in S phase-arrested cells (**Figure 72**). Cep152 levels were in fact decreased, if Plk4 was overexpressed over an extended period of time in cycling cells. In contrast, Cep152 remained unchanged, if cells were arrested in S phase.

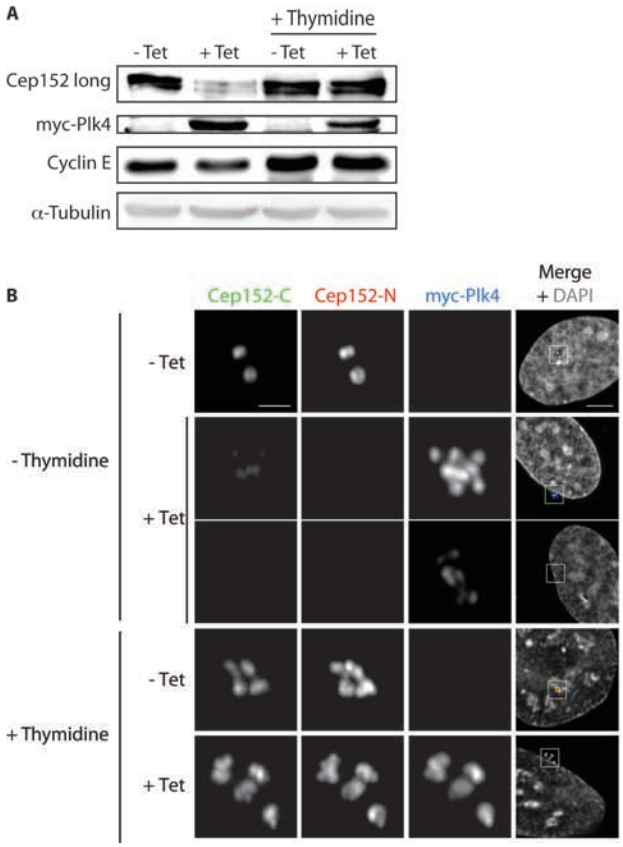

Figure 72 Plk4 overexpression in cycling cells results in the drop of Cep152 levels. U2OS:myc-Plk4 cells were either left untreated or arrested in S phase with thymidine. Concomitantly, myc-Plk4 expression was induced by the addition of tetracycline (Tet). After 72 h the samples were analyzed. After drug treatment the cells were lysed and analyzed by Western Blotting with the indicated antibodies (**A**) or the cells were fixed and stained with the indicated antibodies for IF microscopy (Scale bars represent either 1 µm or 5 µm (overview images right panel, **B**). (Figure by E. Anselm)

4.6.4.2.2 Mutating the SSP or the DSG Motifs of Cep152 only has a Minor Effect on its Stability

After having established that changes in either βTrCP, Plk1 or Plk4 levels affect Cep152 levels, we then set out to understand whether these proteins directly act on Cep152. To this end, we initially sought to unravel whether phosphorylation of the conserved DSG motif within the C terminus of Cep152 is essential for the interaction with βTrCP. Both serines within the DSG motif were mutated to alanine (mutant construct termed Cep152-2 DSGA), which should prevent the interaction with βTrCP and thus the degradation of Cep152. When

we overexpressed this mutant in U2OS cells, we detected a similar effect on centriole duplication and centrosomal localization of Plk4 in both quality and quantity as observed when overexpressing Cep152-2 wildtype (**Figure 68** and data not shown). In a cycloheximide (CHX) assay, in which translation is inhibited to detect the degradation of already present protein, both wildtype and DSG mutant Cep152-2 were stable for 8 h of treatment, whereas Cep152-4 was rapidly degraded (**Figure 73** A). As endogenous Plk4 is very low abundant (M. Bauer, personal communication) and might be the limiting factor, if Cep152 is overexpressed, we co-expressed Plk4 in an attempt to force Cep152-2 to be degraded. However, Plk4 overexpression did not induce the degradation of Cep152-2 in CHX assays either (**Figure 73** B). The sequences of Cep152-2 and Cep152-4 were then compared to find out why Cep152-4 is rapidly degraded, whereas Cep152-2 is relatively stable under these conditions. But we neither identified any additional regulatory sites nor any sequences that affect general protein stability such as PEST domains (Rogers et al., 1986) within exon 20 that is unique to Cep152-4 (**Figure 11**). Therefore, we hypothesized that lack of the extended C terminus might render the short isoform more unstable and thus susceptible to unregulated protein degradation. Moreover, we hypothesized that dimerization of short with long isoforms might stabilize the short ones. This would also explain the cell cycle-specific changes in protein levels of the short isoform simultaneously with the long isoforms despite the lack of a DSG motif. To test this, a CHX assay was performed, in which Cep152-2 and/or Cep152-4 were co-expressed and the protein degradation was checked by Western Blot analysis. To exclude the possibility that Cep152-4 is stabilized by co-expression of any centriolar protein, we co-expressed either isoform with CPAP or both isoforms together. Indeed, we observed a slight stabilization of Cep152-4 when co-expressed with Cep152-2 (**Figure 73** C).

It is possible that no degradation of Cep152-2 was observed in CHX assays, because cell cycle progression might be essential for efficient degradation. To account for this possibility, HeLa S3 cells were transfected with either wildtype or mutant Cep152 and then released from a thymidine arrest. In addition to the DSG mutant, we mutated the second serine of the SSP site within the N terminus of Cep152 to alanine (SAP, termed SSPA), which should prevent the interaction of Cep152 with Plk1 and thus a Plk1-dependent degradation. When we overexpressed these mutants in HeLa S3 cells and released them from a thymidine arrest, we detected a slight stabilization of the mutant proteins compared to wildtype Cep152-2 (**Figure 74**).

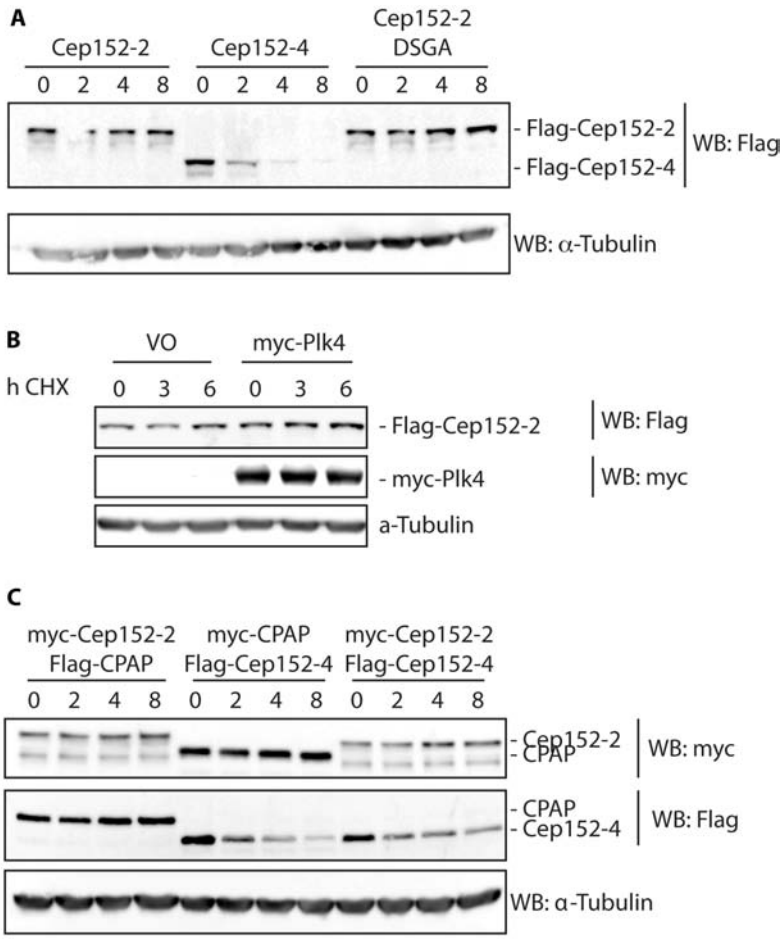

Figure 73 Cep152-2 is stable in CHX assays, whereas Cep152-4 is rapidly degraded. HEK293T cells were transfected for 24 h. Cycloheximide was then added to the cells. Samples were taken at the indicated time-points and analyzed by Western Blotting using the indicated antibodies. **A** Cells were transfected Flag-tagged constructs of Cep152-2, Cep152-4 or Cep152-2 DSG->A mutant. **B** Cells were co-transfected with Flag-Cep152-2 in addition to either myc vector control or myc-Plk4. **C** Cells were co-transfected with the indicated myc- and Flag-tagged constructs.

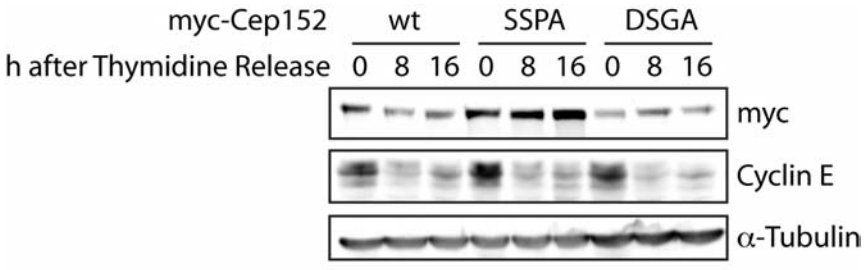

Figure 74 SSP and DSG mutant Cep152 are slightly stabilized, if released from thymidine. HeLa S3 cells were transfected with the indicated Cep152-2 constructs for 24 h. The cells were then arrested with thymidine and released. At the indicated time-points samples were taken and analyzed by Western Blotting using the indicated antibodies. Cyclin E was used to confirm the efficiency of the thymidine release.

4.6.4.2.3 Investigating the Interaction of Cep152 with βTrCP, Plk1 and Plk4

If βTrCP regulates the degradation of Cep152, it should interact with Cep152 and this interaction should depend on phosphorylation of a DSG motif. In co-immunoprecipitation experiments Cep152-2 interacted with βTrCP. However, Cep152 in which the serines of the conserved DSG motif were mutated to alanine still interacted with βTrCP (**Figure 75** A). When pulling on Cep152, βTrCP was found to bind unspecifically to beads (data not shown), which did not allow us to draw conclusions from these experiments. Moreover, Cep152 was not destabilized, if βTrCP was overexpressed. Surprisingly, Cep152 lacking the C terminus and thus the DSG motif also showed an interaction. Next, we hypothesized that the observed interaction might be non-specific and that actually endogenous Plk4 might be limiting in this experimental set-up, if it is indeed the phosphorylating kinase upstream of βTrCP. To rule out this possibility, we additionally expressed wildtype or kinase dead Plk4, in which its DSG motif was mutated so that it was not able to interact with βTrCP itself (**Figure 75** B). But also under these conditions there were no binding differences of Cep152 wt and Cep152 DSGA with βTrCP. Therefore, we searched for other potential interaction sites of βTrCP that should consist of the following degenerated amino acid sequence: (DEST)(DEST)GX_{1+n}(DEST). Using this sequence there is only one additional potential "DSG" motif present within the N terminus of Cep152 (**Figure 75** C). But neither single mutation of this site nor double mutation of both "DSG" motives prevented the interaction with βTrCP. Finally, we co-expressed βTrCP with different fragments of Cep152 and found the central coiled-coil domain to interact with βTrCP as well (**Figure 75** D). These data indicate that the observed interaction might be unspecific.

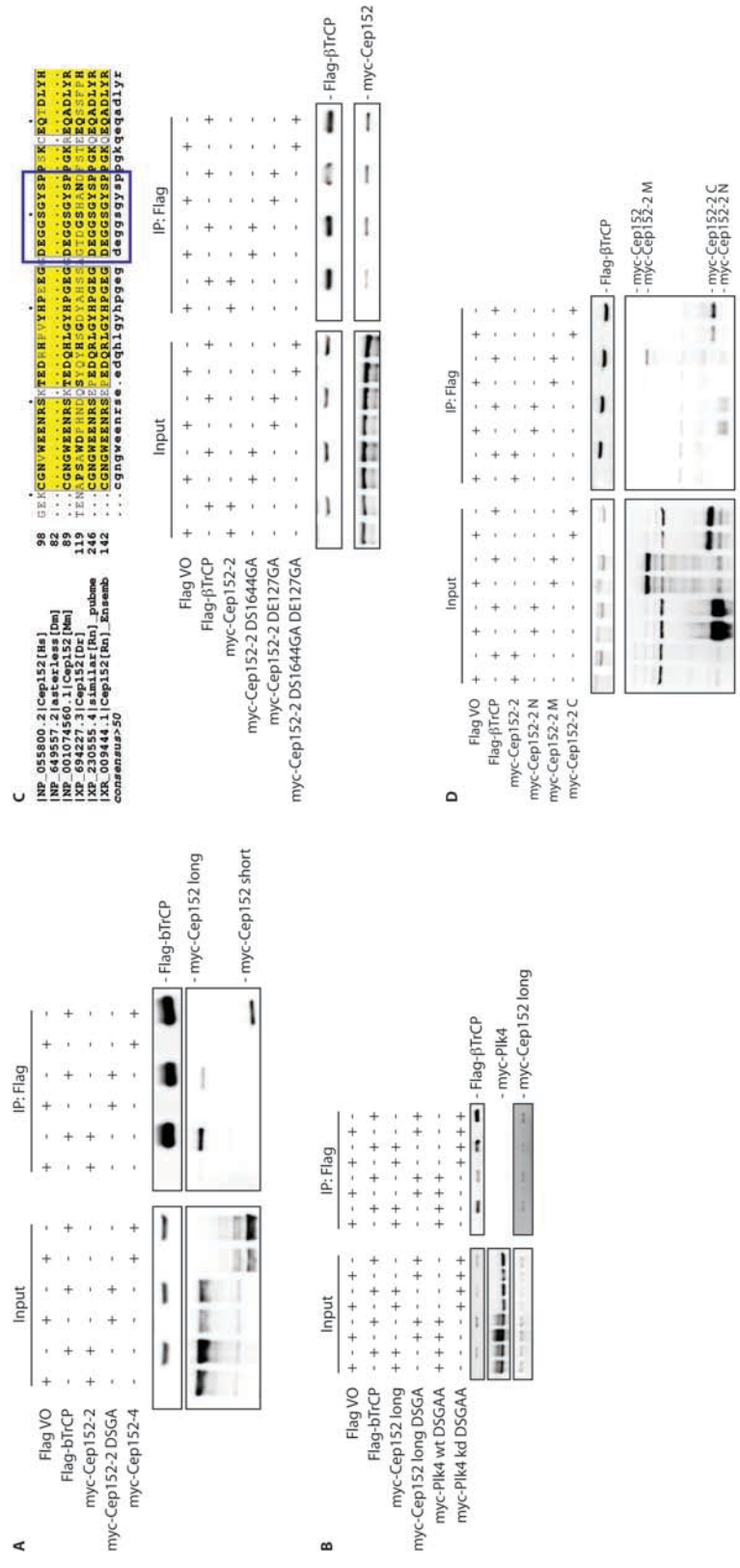

Figure 75 Interaction of βTrCP with Cep152 is not abolished, if the DSG motives of Cep152 are mutated. **A, B, D** HEK293T cells were transfected with indicated plasmids for 24 h. After lysis co-immunoprecipitation experiments were performed using Flag antibodies. After elution the samples were analyzed by Western Blotting using the indicated antibodies. **C** Search for additional potential binding sites for βTrCP revealed the sequence DEGGS within the N terminus of Cep152, that is partially conserved. Mutation of this site did not prevent interaction with βTrCP either (**D**).

Next, a possible involvement of Plk4 and Plk1 in Cep152 regulation was investigated further. If Plk4 regulates the degradation of Cep152 in late G2 phase, Plk4 levels might also peak at this cell cycle stage. In the literature conflicting data are available on the changes of Plk4 levels during the cell cycle. Therefore, we decided to determine centrosomal as well as cytoplasmic levels during the cell cycle. As Plk4 staining is clearer in U2OS cells, this cell line was used to determine centrosomal levels by IF microscopy. From G1 phase on Plk4 levels increased strongly towards mitosis, were highest in prophase and then decreased again until telophase (**Figure 76** A). Apart from that, cytoplasmic Plk4 levels were analyzed in HeLa S3 cells, in which the release from thymidine is more efficient. Upon release from S phase Plk4 levels increased in late G2 phase and peaked in M phase similarly to Plk1 (**Figure 76** B). Importantly, Cep152 peaked after 6 – 8 h of release, whereas Plk4, Plk1 and Cyclin B peaked only after 8 – 10 h.

Moreover, we examined the interaction of Cep152 with Plk1 further. As shown earlier, Plk1 had been found in several of the performed endogenous immunoprecipitations analyzed by mass spectrometry (Section 4.4.1). To confirm this interaction and to determine, when both proteins interact with each other, we released HeLa S3 cells from a thymidine arrest, took samples every 3 h and then performed immunoprecipitation experiments with either the antibody Cep152-C 934 or Cep135 as control (**Figure 77** A). Upon release from S phase Cep152 and Plk1 levels increased, whereas Cyclin E levels decreased. When Cep152 was immunoprecipitated, levels of co-purified Plk1 as well as Plk4 increased coincidentally with the increase of Cep152. Potentially, the increase in Plk4 levels after release from Thymidine arrest was not detected in the input samples due to the low quality of the antibody. Cep135 was neither co-purified nor did Cep135 immunoprecipitation result in a similar increase in co-purified Plk1 and Plk4. However, Plk1 weakly interacted with Cep135 in S phase-arrested cells. Moreover, we arrested HeLa S3 cells either in S phase or in G2 phase by treatment with thymidine or the CDK1 inhibitor RO3306, respectively. After lysis, we performed immunoprecipitation experiments with the Cep152 antibodies Cep152-N 207 and Cep152-C 934 (**Figure 77** B). As expected, the N-terminal antibody purified both long and short Cep152 isoforms, whereas the C-terminal antibody bound Cep152long. Cep152 levels decreased in RO-treated compared to thymidine-treated cells. Furthermore, we detected an interaction of Cep152 with Plk1, if Cep152 was precipitated with the C-terminal antibody. Presumably, the N-terminal antibody does not allow binding of Plk1 because of steric hindrance. In RO-

arrested cells more Plk1 was co-purified than in S phase-arrested cells. Hence, endogenous Plk4 and Plk1 interact with Cep152 and the interaction increases after release from S phase.

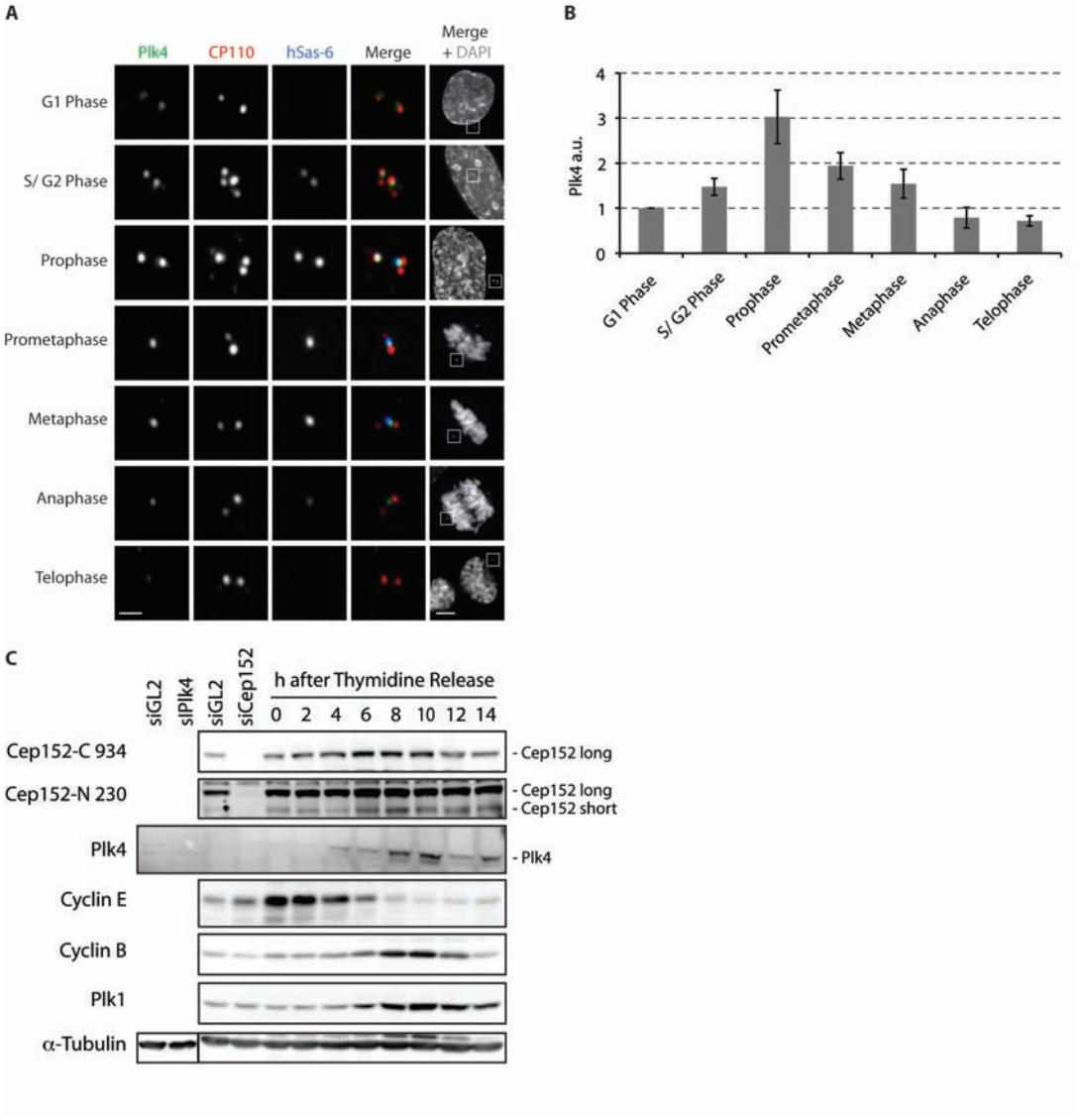

Figure 76 Plk4 levels peak in M phase. A, B U2OS cells were fixed and stained with the indicated antibodies. In **A** representative images are shown. Scale bars represent 1 µm or 5 µm (overview images, right panel). DNA was stained with DAPI. In **B** the quantification from three independent experiments is depicted (10 cells each, error bars denote standard deviation). C HeLa S3 cells were released from a double thymidine arrest. Samples were taken at the indicated time-points after release and analyzed by Western Blotting using the indicated antibodies. Asynchronously growing GL2 control-, Plk4- or Cep152-depleted cells were analyzed as control.

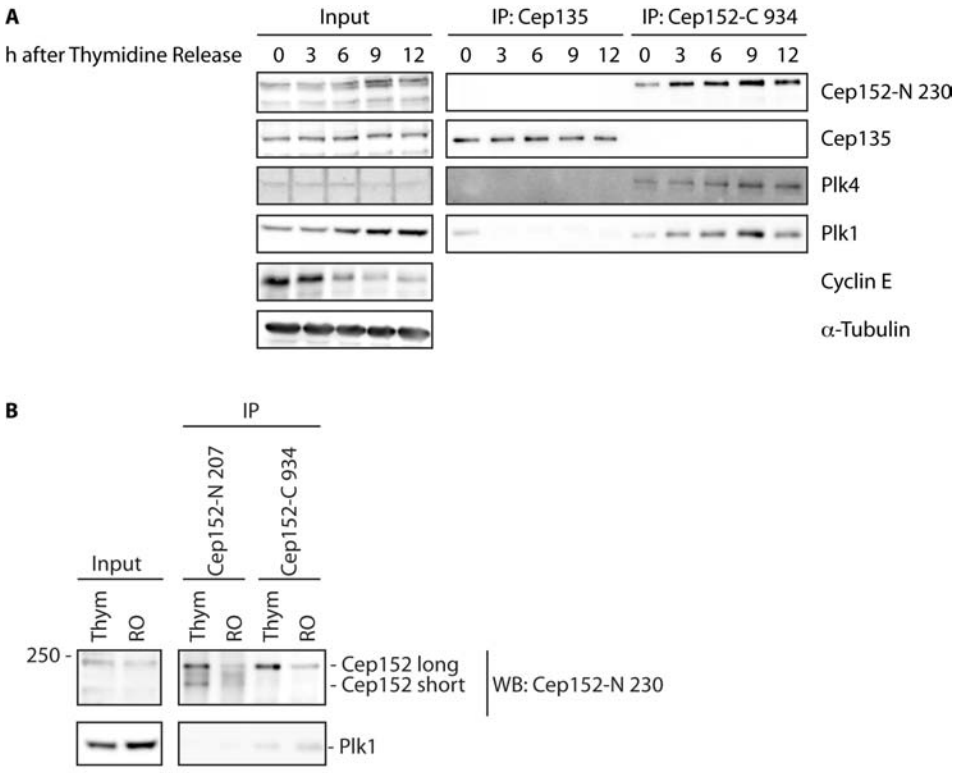

Figure 77 After release from S phase levels of Plk1 and Plk4 co-purified with Cep152 increase. A HeLa S3 cells were released from a double thymidine arrest and samples were taken at the indicated time-points. Then immunoprecipitations using the indicated antibodies were performed and analyzed by Western Blotting using the indicated antibodies. **B** HeLa S3 cells were either arrested in S phase with thymidine or in G2 phase with RO3306 (RO). Immunoprecipitations were performed using the indicated antibodies and analyzed by Western Blotting using the indicated antibodies.

4.6.4.2.4 Phosphorylation of Cep152 by Other Cell Cycle-Relevant Kinases

If Plk4 and/ or Plk1 are directly involved in the degradation of Cep152, a phosphorylation of Cep152 by these kinases would be expected. As described earlier, Plk4 indeed phosphorylated Cep152 using only the kinase domain of Plk4 as active enzyme (Section 4.5.5). In contrast, Plk1 did not phosphorylate Cep152 in *in vitro* kinase assays (data not shown). However, for various Plk1 substrates it has been shown that prephosphorylation of the Plk1 binding site is required to allow a consecutive phosphorylation by Plk1. Upstream kinases that are active in interphase or late G2 phase and have been described to function at centrosomes are CDKs and Aurora A among others in addition to Plk4 and Plk1. Indeed, CDK2 and Aurora A did phosphorylate Cep152 – either purified from bacteria or from HEK293T cells – in *in vitro* kinase assays (**Figure 78** and data not shown), albeit not as strongly as Plk4.

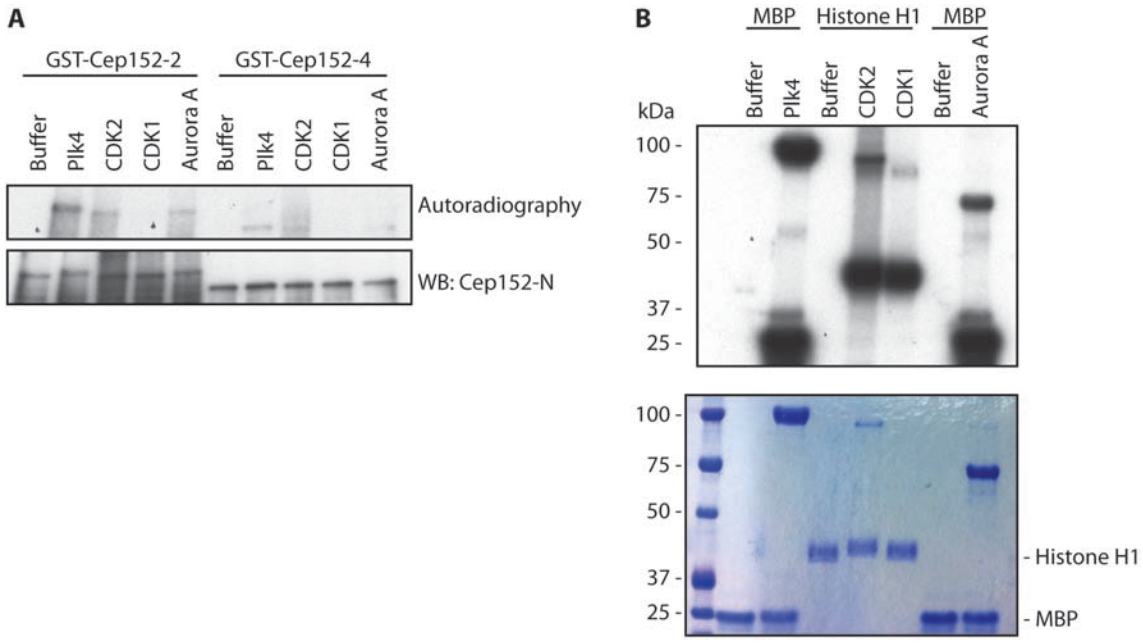

Figure 78 Cep152 is an *in vitro* substrate of Plk4, CDK2 and Aurora A. A Recombinant GST-Cep152-2 and GST-Cep152-4 were used as substrate in *in vitro* kinase assays. As negative control only buffer was used. Results were analysed by SDS PAGE followed by autoradiography and Western Blotting using the antibody Cep152-N 230. **B** Control kinase assays were performed using MBP as substrate for both Plk4 and Aurora A and Histone H1 for CDK1 and CDK2. Afterwards, samples were analysed by SDS PAGE followed by autoradiography.

Hence, CDK, Aurora A or Plk4 might account for the priming phosphorylation required for binding of Plk1 to Cep152.

5 Results II – Analysis of the Centrosome in Super Resolution

To determine the architecture of human centrosomes at high resolution, we applied the super-resolution technique 3D-SIM. Initially, we focused on proteins that were expected to undergo cell cycle-dependent changes in amount and disposition, providing an excellent opportunity to validate the applicability of 3D-SIM for our specimen. Subsequently, we extended our studies to multiple aspects of centrosome organization, including the relationship between centrioles and PCM, the arragement of appendages and the biogenesis of centrioles.

5.1 Pericentriolar Material

In cycling cells centrosomes function as MTOCs by concentrating γTuRCs in their PCM, which nucleate and anchor microtubules (Doxsey et al., 2005; Luders and Stearns, 2007). At the onset of mitosis their MT nucleation activity is increased by recruiting additional PCM components. Pioneering work on the structure of the PCM has revealed an amorphous arrangement of Pericentrin and γ-Tubulin around centrioles (Dictenberg et al., 1998). Here, we examined the disposition of γ-Tubulin, its recruiting factor NEDD1 (Luders et al., 2006) and other structural PCM proteins in U2OS cells during interphase and early mitosis. In these experiments as in all subsequent ones, widefield microscopy was used to select centrosomes for analysis and, where appropriate, cartoons are drawn to illustrate the orientation of centrioles (**Figure 79**, right-hand panels).

In interphase cells, both γ-Tubulin and NEDD1 localized in ring-like patterns around the mother and to a lesser extent to the daughter centriole (**Figure 79**, upper panel). Interestingly, both proteins were also detected as dots at the center of the ring surrounding the mother centriole, suggesting that these proteins also localize within the lumen of at least the mother centriole. When U2OS cells approached mitosis, indicated by centrosome separation (**Figure 79**, lower panel), γ-Tubulin and NEDD1 showed a much broader distribution and both proteins formed web-like arrays. These arrays showed a considerable degree of overlap (marked by arrows). This is consistent with the expected close proximity of γ-Tubulin and NEDD1, even though co-localization was not complete.

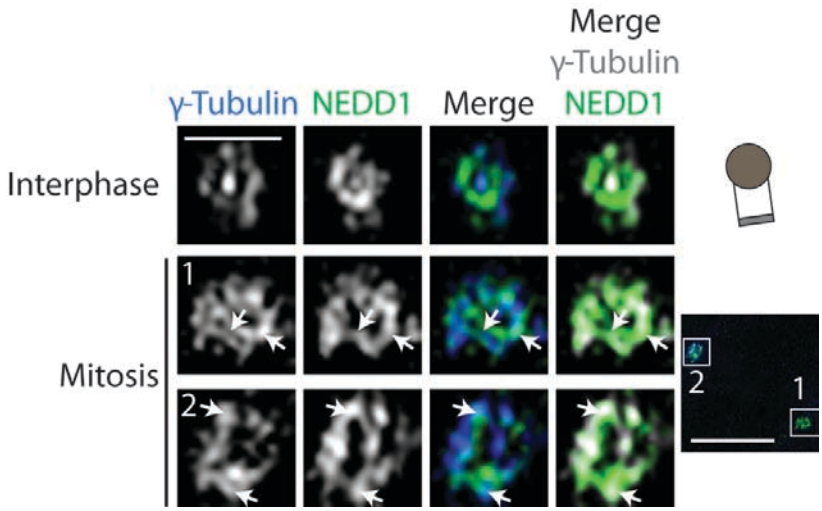

Figure 79 NEDD1 and γ-Tubulin localize similarly to each other in interphase and mitosis. U2OS cells were fixed, stained with the indicated antibodies and analyzed by 3D-SIM. The localizations of NEDD1 and γ-Tubulin were compared with each other in interphase (upper panel) and mitotic cells (after centrosome separation, lower panel). Arrows point at places of overlap. Scale bar represents 0.5 µm.

Localization of γTuRC Proteins Relative to Other PCM Proteins

We then correlated the localization of γ-Tubulin with three prominent PCM proteins, namely Pericentrin, Cep215 and Cep192. All of the three proteins showed the peripheral-ring staining surrounding mother centrioles, but not the central location within it (**Figure 80**, left panels). In agreement with the expansion of the PCM towards mitosis, Pericentrin, Cep215 and Cep192 also formed extended networks (**Figure 80**, right panels). Notably, γ-Tubulin staining did not show extensive co-localization with any of the three PCM proteins. In contrast, we rather detected areas of mutual exclusiveness between the examined proteins (arrowheads).

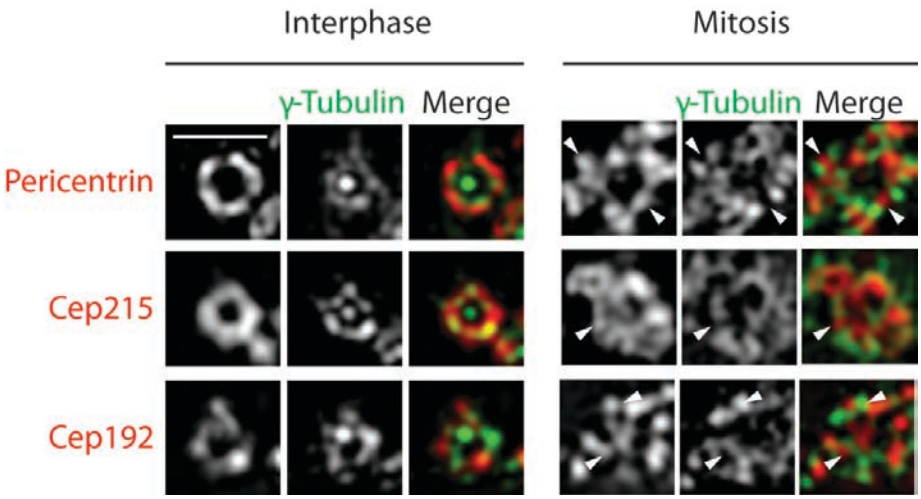

Figure 80 Pericentrin, Cep215 and Cep192 localizations do not overlap with γ-Tubulin localization. U2OS cells were fixed, stained with the indicated antibodies and analyzed by 3D-SIM. The localization of pericentrin, Cep215 and Cep192 was compared to γ-Tubulin in interphase (left panel) and mitotic cells (right panel). Arrowheads point at places of alternating dipositions. Scale bar represents 0.5 µm.

5.1.1 PCM Proteins are Specifically Organized Around Centrioles in Interphase

Having confirmed the utility of 3D-SIM for the investigation of centrosome architecture, we proceeded by examining the localization of 18 centriolar and centrosomal proteins to interphase centrosomes. Principally, the analyzed proteins revealed two distinct localization patterns in top-views of centrioles: either dot- or ring-like patterns or a combination of the two (**Figure 81** A). Among all proteins analyzed in this study, only four showed compact dots with a diameter of 80 – 100 nm rather than ring-like arrangements, notably Centrin, Sas-6, STIL and Plk4. Conversely, γ-Tubulin, NEDD1 and CPAP revealed both central dot and ring localizations (**Figure 79** A, **Figure 81** A). All other proteins localized in a ring-like pattern around centrioles.

To determine the ring diameters of the examined proteins, we measured distances between opposing intensity maxima (**Figure 81** B and Appendix **Table 5**). We neither took absolute intensity values nor peak widths into account, as these depend on antibody quality and acquisition conditions. Regarding the size of IgG antibodies of about 8 nm the labeling technique can account for maximally 32 nm in diameter. As reference for the width of the centriolar cylinder, glutamylated Tubulin was stained with the antibody GT335 (Wolff et al.,

1992; Bobinnec et al., 1998). This approach revealed a ring with a diameter of approx. 170 nm (**Figure 81** A, B), which is consistent with an earlier study describing the structure of centrioles by electron microscopy (Paintrand et al., 1992) and underlines the accuracy of the method employed in the present study. Interestingly, Cep135 and CP110 were arranged as rings of very similar sizes at the proximal or distal centriolar end, respectively (**Figure 81** B, C).

All other proteins examined formed larger rings around centrioles. Based on the measured diameters, these proteins were subdivided into three groups: inner, intermediate and outer PCM (**Figure 81** B and **Table 5**). According to this classification, NEDD1 belongs to the inner category, but γ-Tubulin to the intermediate one. Considering that NEDD1 and γ-Tubulin localize at proximal and distal end of γTuRCs, respectively, with γ-Tubulin in direct contact to minus ends of MTs, the obtained results indicate that reveal the orientation of γTuRCs from the inner to the intermediate PCM.

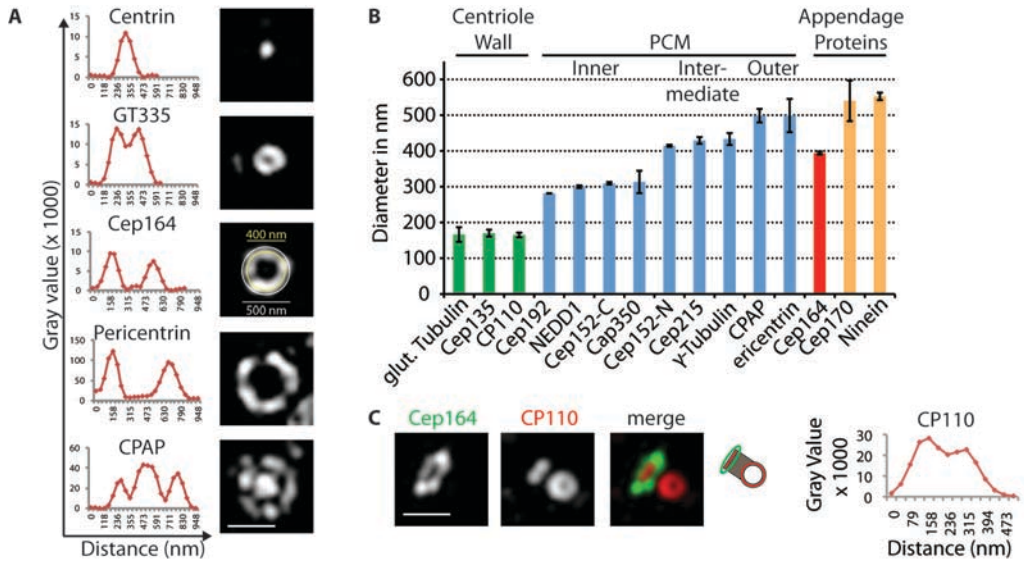

Figure 81 Several centrosomal proteins localize in a ring-like pattern around centrioles. U2OS cells were fixed, stained and analyzed by 3D-SIM. **A** Exemplary images of proteins localizing in a dot-, ring- or ring/dot-like pattern to centrioles are shown in the right panel (scale bar 0.5 µm) and density plots of cross-sections are shown in the left panel. Measurement of distances between opposing intensity maxima are summarized in **B**. Based on their localization the proteins were subdivided into 3 categories: centriole wall, PCM and appendage proteins. **C** CP110 also localizes as a ring at distal ends of centrioles. In the left panel representative images and in the right panel a density plot of a CP110 ring in cross-section are depicted.

Whenever staining was detected at both mother and growing daughter centriole (Cep192, NEDD1, Cap350 and γ-tubulin), the ring around daughter centrioles was invariably smaller than the one around mother centrioles (**Table 5**).

5.1.2 Investigation of Protein Orientation by SIM

When interpreting the obtained results, it is important to bear in mind that large proteins might span considerable distances. The high resolution of 3D-SIM offers the interesting opportunity to resolve protein orientations by using antibodies directed against specific domains. To illustrate this possibility, we visualized the orientations of Cep152 with the antibodies Cep152-N and Cep152-C. Consistently, Cep152-C stained a smaller ring than the Cep152-N (Cep152-C: 309.6 +- 3.5 nm, Cep152-N: 414.4 +- 2.5 nm; **Figure 82** and **Table 5**). This implies that Cep152 spans the PCM from the inner to the intermediate region with the C terminus closer to the centriolar wall and the N terminus facing outwards – potentially in an extended rod-like shape.

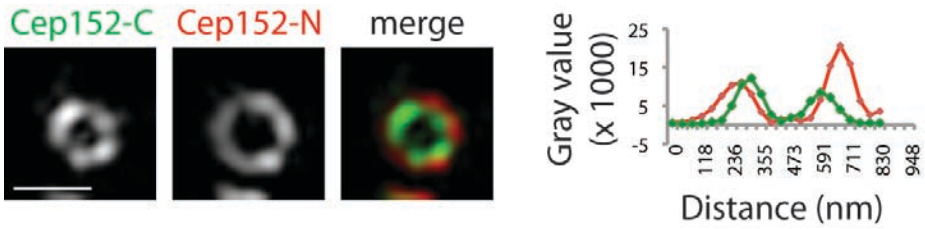

Figure 82 Cep152-N stains a wider ring than Cep152-C. U2OS cells were fixed, stained with the indicated antibodies and analyzed by 3D-SIM. In the left panel representative images are shown (scale bar 0.5 µm). In the right panel density plots of ring cross-sections of each channel are depicted.

5.2 Appendage Proteins

The rings with the largest diameters (approx. 550 nm) were seen when staining centrosomes with antibodies against the subdistal appendage proteins Ninein (Mogensen et al., 2000) and Cep170 (Guarguaglini et al., 2005) (**Figure 81** B, **Figure 83** top view, **Table 5**). In contrast,

antibodies against the distal appendage protein Cep164 stained rings of about 400 nm (**Figure 81** A, B, **Figure 83** top view, **Table 5**). In sideview, Ninein and Cep170 localized to very similar positions but slightly more proximally than the distal appendage protein Cep164 (**Figure 83** side view). Our measurements are in good agreement with previous estimates of appendage sizes, as determined by electron microscopy (Paintrand et al., 1992) and other super-resolution microscopy techniques, notably photoactivated localization microscopy (PALM) and stochastic optical reconstruction microscopy (STORM) (Sillibourne et al., 2011). Minor differences in the reported estimates can be explained by differences in data representation. In particular, Sillibourne et al. (2011) took the outer diameter into account, whereas we measured the distance between intensity maxima (**Figure 81** A, panel Cep164).

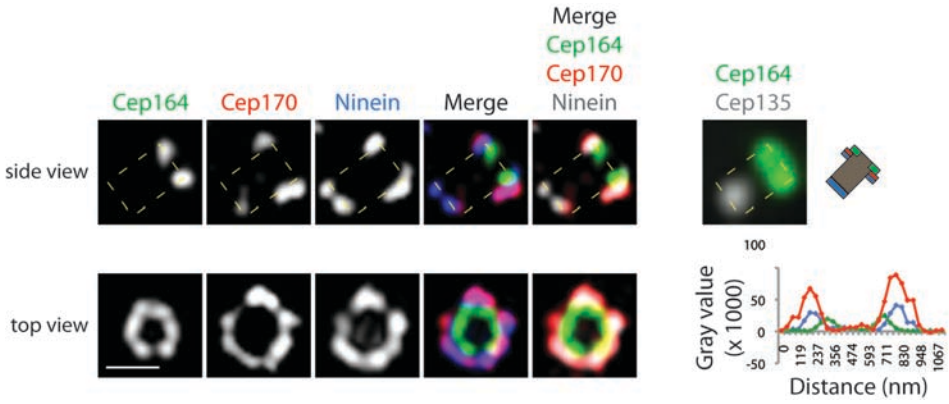

Figure 83 The subdistal appendage proteins Cep170 and Ninein co-localize with each other, but not with the distal appendage protein Cep164. U2OS cells were fixed and stained with the indicated antibodies for 3D-SIM. Exemplary images for centrioles in side-view (upper panel) and top-view (lower panel) are shown. For the side-view a widefield image of Cep135 and Cep164 of the same cell is depicted to illustrate the centriole orientation. For the top-view density plots of ring cross-sections of each channel are given.

5.2.1.1 Number of Cep164-Positive Appendages Varies During the Cell Cycle

In top views of Cep164 rings distinct density masses could readily be resolved (**Figure 84** A). In interphase cells, we mostly observed 6 – 8 of these density masses, even though the 9-fold symmetrical centriole provides space for 9 appendages (Paintrand et al., 1992). As visualized by conventional widefield microscopy, centrosomal Cep164 levels are reduced in mitosis compared to interphase (data not shown). Using 3D-SIM to resolve separate appendages, we observed that only 3 – 4 Cep164-positive density masses were detectable in mitotic cells

(**Figure 84** B). These results indicate that Cep164 is not lost from all appendages to a similar extent upon mitotic entry.

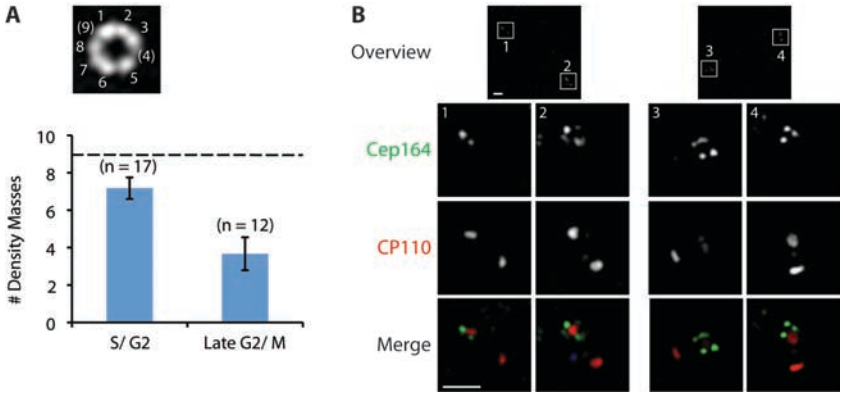

Figure 84 Number of Cep164 density masses decrease from interphase to mitosis. A The number of visible Cep164 density masses within a ring was counted in S/G2 phase cells (before centrosome separation) and in late G2/ M phase cells (after centrosome separation). In the upper panel an example for a centriole in a S/ G2 phase cell and in the lower panel the quantification is shown. In **B** examples for Cep164 staining in late G2/ M phase cells are depicted (scale bars represent 1 µm).

5.2.1.2 CP110 Levels are Reduced at Distal Appendage-Bearing Centrioles

We then correlated the localization of the distal appendage protein Cep164 to the distal centriolar proteins CP110, Cap350 and Centrin. Cep164 surrounds the CP110-stained area of centrioles, whereas Cap350 antibodies label the distal half of centrioles (**Figure 85** A, **Table 5**). Moreover, Centrin localized as a distinct dot more proximally than CP110, thus within the distal lumen of centrioles (**Figure 85** B and Section 5.1.1).

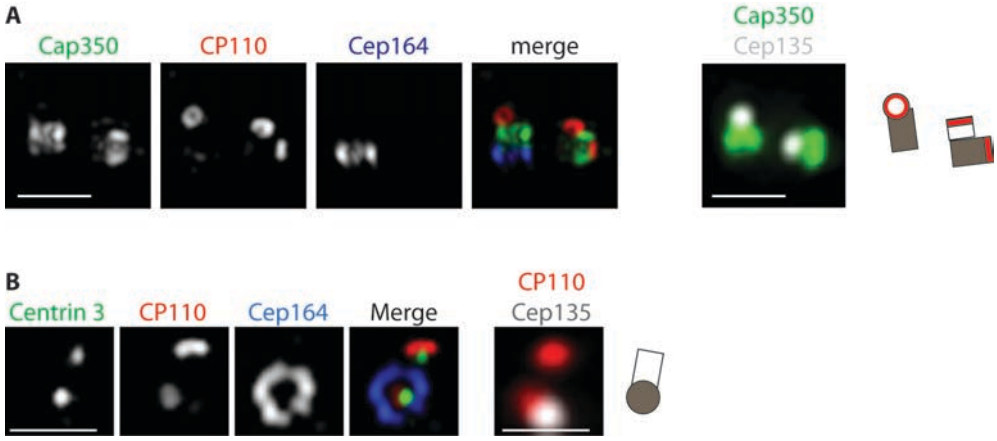

Figure 85 Localization of the distal centriolar proteins Cap350, CP110, Cep164 and Centrin. U2OS cells were fixed and stained with the indicated antibodies (scale bars 1 µm). In the left panel 3D-SIM images are shown. In the right panel widefield images of the same cell are depicted to illustrate the orientation of centrioles. Schematics illustrate orientation. In **A** Cep164 localization was compared with Cap350 and CP110 and in **B** it was compared to Centrin 3 and CP110.

Surprisingly, we noticed that CP110 levels were sometimes reduced at Cep164-bearing centrioles (**Figure 85**). As CP110 caps the distal end of centrioles (Kleylein-Sohn et al., 2007), anti-CP110 antibodies are expected to stain 4 dots in G2 phase cells and such a characteristic 4 dot-staining pattern has indeed been reported (Guderian et al., 2010). The observed level variations are specific for the distal protein CP110, since Centrin levels did not vary in correlation to the presence of Cep164 (**Figure 85** B). Similar CP110 intensity differences were observed in the hTERT-immortalized RPE-1 cell line (**Figure 86**).

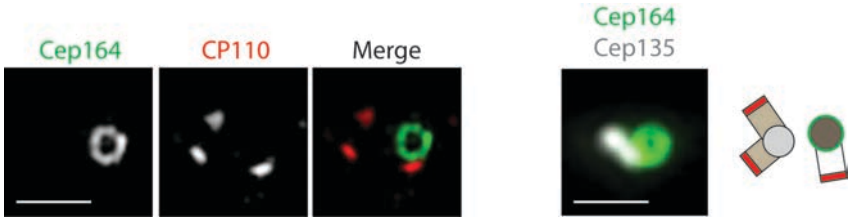

Figure 86 In RPE-1 cells CP110 levels are reduced at Cep164-positive centrioles. RPE-1 cells were fixed and stained with the indicated antibodies (scale bars 1 µm). In the left panel 3D-SIM images of Cep164 and CP110 are shown. In the right panel widefield images of Cep164 and Cep135 of the same cell are depicted. Schematic illustrates centriole orientation.

To examine the correlation between CP110 and Cep164 further, we used conventional widefield fluorescence microscopy. First, we quantified cell cycle-dependent CP110 level changes in relation to Cep164. In interphase S/G2 cells, Cep164-positive centrioles showed

2.5-fold reduced levels of CP110 signal as compared to Cep164-negative centrioles (**Figure 87** A). This reduction cannot be explained by antibody competition, as one centriole showed reduced CP110 staining even when staining for Cep164 was omitted (data not shown). In mitotic cells, near-identical CP110 staining was seen at Cep164-positive and -negative centrioles (**Figure 87** A). In agreement with previous publications CP110 staining was 2-2.5 fold lower in mitotic cells than interphase cells (**Figure 87** A). Similarly, Cep164 staining was reduced in mitosis compared to interphase cells (data not shown and Section 5.2.1.1).

To determine whether there is a causal relationship between the presence of Cep164 and CP110 levels, we depleted Cep164 from U2OS cells and quantified CP110 levels at each centriole. To identify the mature centriole we co-stained cells for the subdistal appendage protein Ninein. Indeed, CP110 levels were comparable at all 4 centrioles, including the appendage-bearing but Cep164-depleted centriole (**Figure 87** B).

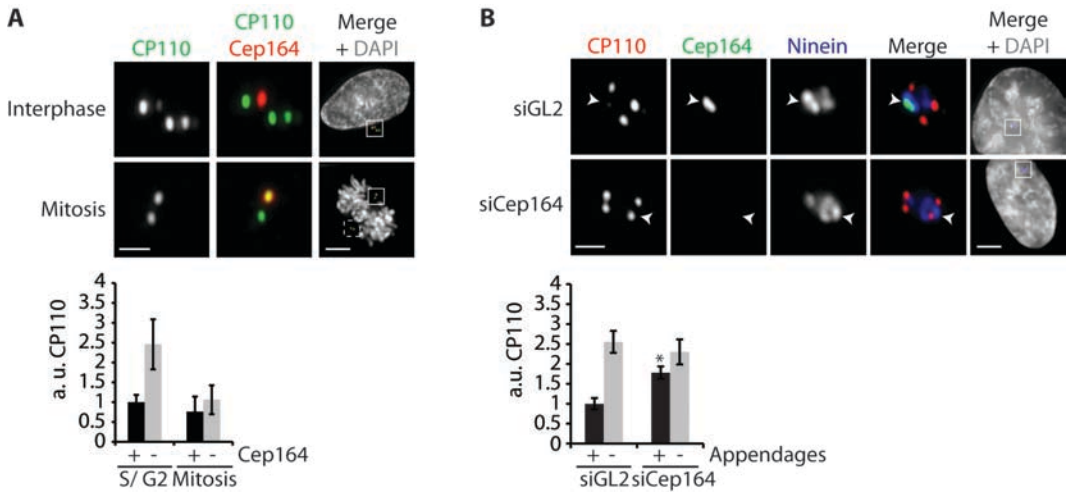

Figure 87 CP110 levels are reduced at appendage-bearing mother centrioles in a Cep164-dependent manner. A U2OS cells were fixed and stained with antibodies against CP110 and Cep164. DNA was visualized by DAPI to differentiate interphase from mitotic cells. In the upper panel representative images are shown (scale bars 1 µm or 5 µm for overview images). In the lower panel quantification of centriolar CP110 levels of Cep164-positive or –negative centrioles is given. **B** U2OS cells were transfected with the indicated siRNA oligonucleotides for 48 h. After fixation the cells were stained with antibodies against CP110, Cep164 and Ninein. DAPI was used to visualize DNA. In the upper panel representative images are shown (scale bars 1 µm or 5 µm for overview images, arrowheads mark appendage-bearing centrioles). In the lower panel quantification of centriolar CP110 levels is depicted.

5.3 Cartwheel Proteins

Next, we investigated factors participating in the initiation of centriole biogenesis, namely Cep135, Sas-6 and STIL. Sas-6 and Cep135 are homologues of the *Tetrahymena* cartwheel proteins Bld10 and Bld12 (Hiraki et al., 2007; Nakazawa et al., 2007). STIL is the predicted human homologue of Sas-5, which complexes with Sas-6 (Stevens et al., 2010; Tang et al., 2011; Arquint et al., 2012; Vulprecht et al., 2012). We identified cells with four centrioles using the coupled widefield system and then examined the localization of STIL, Sas-6 and Cep135 by 3D-SIM. Widefield microscopy has previously revealed that STIL and Sas-6 co-localized (Tang et al., 2011; Arquint et al., 2012). Also with 3D-SIM STIL and Sas-6 were found to co-localize (**Figure 88** A). However, the bulk of Cep135 was seen at considerable distances from Sas-6/STIL (**Figure 88** A upper panel), which was confirmed in RPE-1 cells (**Figure 89**). The localization of Cep135 coincided with that of C-Nap1 (data not shown), a marker for the proximal ends of mother centrioles (Fry et al., 1998).

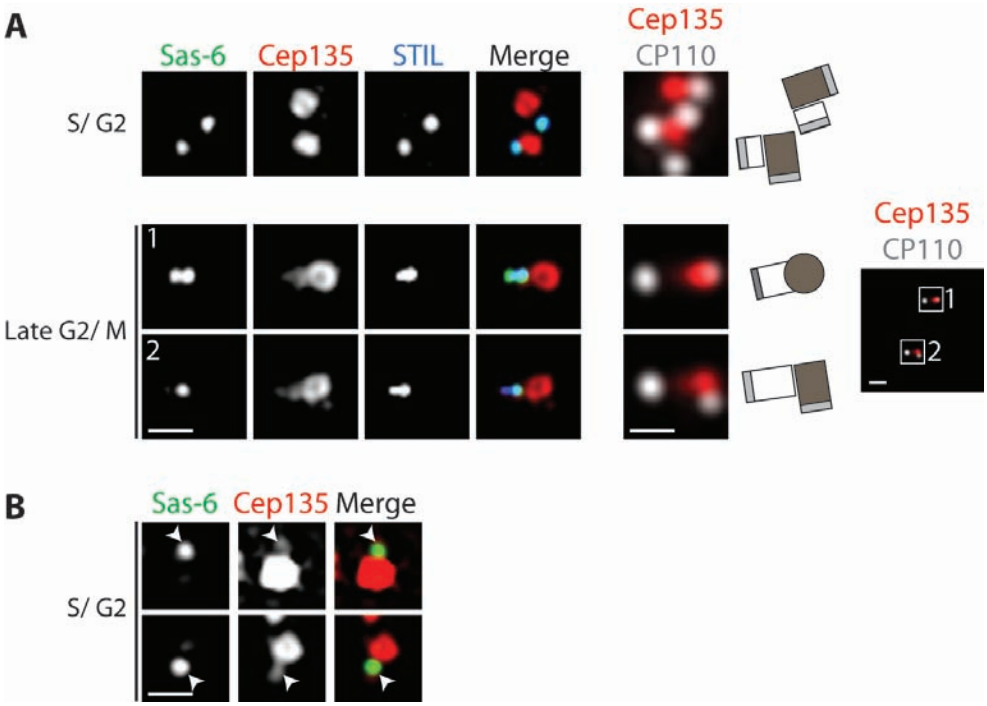

Figure 88 Bulk of Cep135 does not co-localize with Sas-6 and STIL. U2OS cells were fixed and stained with the indicated antibodies for 3D-SIM (scale bars 0.5 µm). **A** In the left panel 3D-SIM images of Sas-6, Cep135 and STIL of either S/ G2 or late G2/ M (after centrosome separation) phase cells are shown. In the right panel widefield images of CP110 and Cep135 of the same cells are depicted. Schematics illustrate centriole orientation. **B** Post-acquisition level enhancement revealed low levels of Cep135 co-localizing with Sas-6 even in S/ G2 phase (indicated by arrowheads).

In late G2 or M phase cells, after centrosome separation, Cep135 staining extended from mother centrioles to the area occupied by Sas-6 and STIL (**Figure 88** A lower panels). This suggests that Cep135 might associate progressively with the proximal ends of daughter centrioles, as these reach more advanced stages of development. In support of this, post-acquisition adjustment of fluorescence intensity of S/G2 phase centrioles allowed the visualization of a faint but reproducible Cep135 signal overlapping with Sas-6 (**Figure 88** B). This co-localization does not reflect bleed-through between channels, as excitation and emission spectra of the utilized fluorophores were clearly distinct and all channels were acquired sequentially (**Figure 94**).

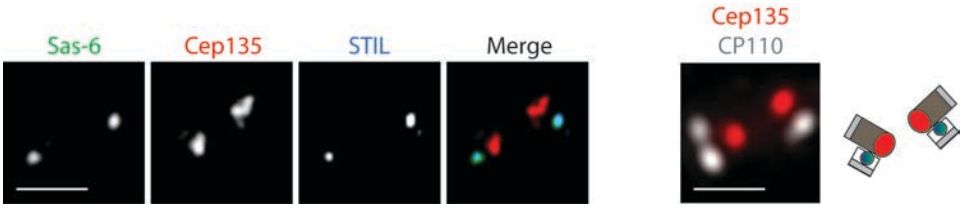

Figure 89 In RPE-1 cells Sas-6 and STIL co-localize, whereas bulk of Cep135 localizes distinctly. RPE-1 cells were fixed and stained with the indicated antibodies (scale bars 1 µm). In the left panel 3D-SIM images of Sas-6, Cep135 and STIL are shown. In the right panel CP110 and Cep135 of the same cell were acquired by widefield microscopy (scale bars 1 µm). Schematic illustrates centriole orientation.

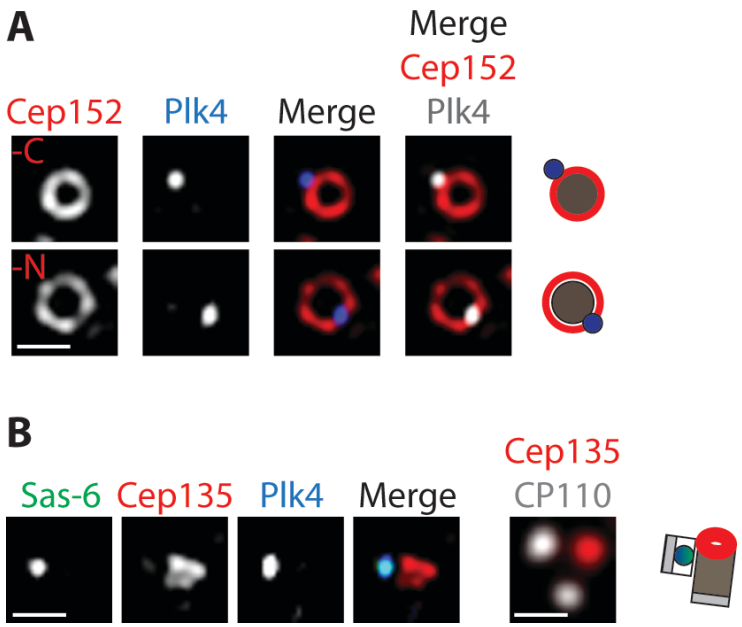

Figure 90 Plk4 is confined to one spot on the ring formed by the N terminus of Cep152 and co-localizes with Sas-6. A, B U2OS cells were fixed and stained with the indicated antibodies. Then 3D-SIM images were acquired (scale bars represent 0.5 µm). For **B** CP110 and Cep135 were visualized by widefield microscopy in addition to determine the centriole orientation (right panel, schematic illustrates orientation).

5.4 Plk4 is an Early Determinant of Centriole Duplication

Because of its key regulatory role in centriole duplication, we then carefully examined the localization of the kinase Plk4 (Bettencourt-Dias et al., 2005; Habedanck et al., 2005). Co-staining for Plk4 and its interaction partner Cep152 revealed that Plk4 localized to a spot that fell onto the ring stained by Cep152-N but outside of the ring defined by Cep152-C (**Figure 90** A). This result is entirely consistent with the identified interaction between Plk4 and the N terminus of Cep152 (Section 4.5.3.1.1). Similarly, Plk4 staining revealed a distinct spot at centrioles using a monoclonal Plk4 antibody (data not shown).

Table 2 Quantification of co-localization.

Channel A	Channel B	Pearson's Coefficient with Costes' Automatic Threshold	Distance between Geometric Centres (nm)
Sas-6	Sas-6	0.62 +- 0.16	60.2 +- 39.3
Sas-6	Cep135 (Interphase)	0.01 +- 0.13	170.2 +- 66.7
Sas-6	Cep135 (Mitosis)	0.53 +- 0.09	45.8 +- 12.4
STIL	Sas-6	0.72 +- 0.11	64.6 +- 26.7
Sas6	Plk4	0.57 +- 0.19	77.4 +- 35.8
			Resolution in x, y, z (nm): 110 ,110, 280

Moreover, Plk4 co-localized with Sas-6 and STIL (**Figure 90** B). To quantify the co-localization of these cartwheel proteins we determined the Pearson's coefficient and the distance between geometric centres (Bolte and Cordelieres, 2006). Due to the sequential acquisition mode of the microscope and the excitation and emission spectra of the applied fluorophores bleedthrough between fluorescence channels did not have to be taken into account (**Figure 94** B, for details see Methods). After Costes' automatic threshold setting the Pearson's coefficient was quantified (**Table 2**), a value ranging from -1 to 1 with mutual exclusiveness at -1, no co-localization at 0 and complete co-localization at 1. In our experiments the value was always below 1, presumably due to the present – even though low – background. To account for 3-dimensionality, we additionally determined the distance between the geometric centers of the channels. We defined proteins to co-localize whenever the distance was lower than the resolution limit of the microscope (130 nm x 130 nm x 300 nm). As positive control we stained cells for Sas-6 in all channels. Using this approach we could show that Sas-6 did indeed co-localize with both STIL and Plk4, but only with Cep135 after centrosome separation (**Table 2**, as discussed in Section 5.3).

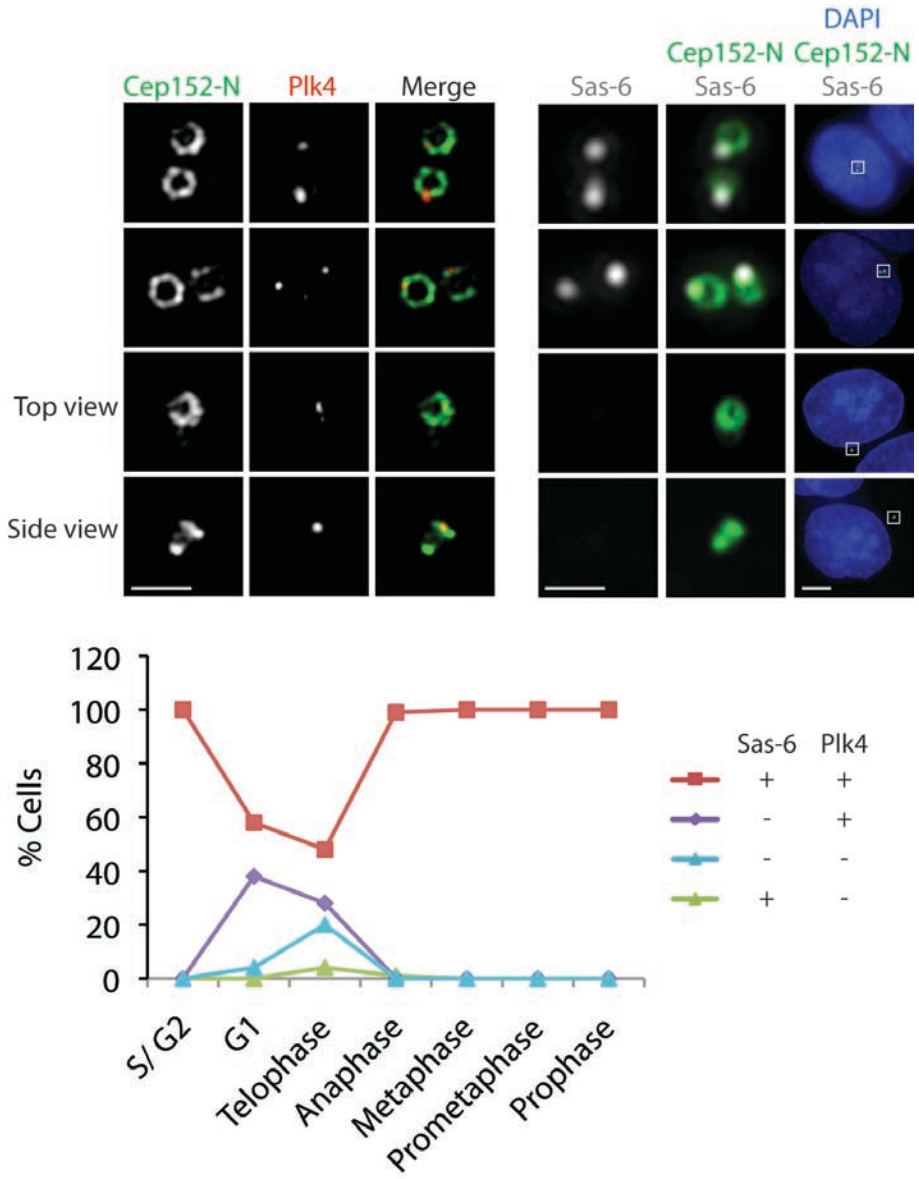

Figure 91 Plk4 is confined to a focussed spot on Cep152 rings also in the absence of Sas-6. U2OS cells were fixed and stained with the indicated antibodies. Red and green channels were acquired by 3D-SIM (left panel, scale bar 1 µm). CP110, Sas-6 and DAPI were additionally acquired using a widefield microscope (right panel, scale bars 1 µm or 5 µm for overview images). Using a widefield microscope the centriolar localization of Plk4 was quantified relative to Sas-6 throughout the cell cycle. Cells were subdivided into four categories based on the presence or absence of centriolar Sas-6 and Plk4: Sas-6+/Plk4+, Sas-6-/Plk4+, Sas-6-/Plk4- and Sas-6+/Plk4-.

The co-localization of Plk4 with Sas-6 in addition to the fact that Sas-6 recruitment is one of the earliest steps of centriole duplication (Strnad et al., 2007) raised the intriguing question of which factor constituted the earlier marker of the centriole duplication site in G1 phase. At the end of mitosis mother and daughter centrioles disengage, i.e. the two tightly oriented

centrioles within a centriole pair lose their close connection. This is concomitant with the loss of Sas-6 and STIL from centrioles, both of which are re-acquired in the following G1 phase (Strnad et al., 2007; Tang et al., 2011; Arquint et al., 2012). Additionally, Sas-6 has been shown to be required for centrosomal STIL localization (Arquint et al., 2012). In contrast to Sas-6 and STIL, Plk4 is found at centrioles at all stages of the cell cycle, albeit at varying levels with a peak in mitosis (**Figure 76** and Sillibourne et al. (2010)). Thus, one can envision two possible Plk4 localizations in G1 phase: either the kinase spreads around the centriolar cylinder or it maintains its defined spot-like localization. To differentiate between both possibilities, we analyzed centriolar Plk4 disposition in relation to Sas-6 at different cell cycle stages (**Figure 91**). Using the coupled conventional widefield system we initially identified cells with Sas-6 either present or absent from centrioles and then examined the localization of Plk4 using 3D-SIM. Regardless of the presence of Sas-6, Plk4 was not distributed equally around mother centriole (visualized by Cep152 staining), but was rather concentrated at one particular spot (representative images by 3D-SIM in **Figure 91**). Quantitative analyses using conventional widefield microscopy revealed that Plk4 localized to 38 % of G1 cells that lacked detectable Sas-6 (graph in **Figure 91**). Similar results were obtained using RPE-1 cells (**Figure 92**).

These data suggest that the site of centriole duplication is determined before the recruitment of Sas-6 to nascent centrioles and that Plk4 represents an early marker for this site on the mother centriole.

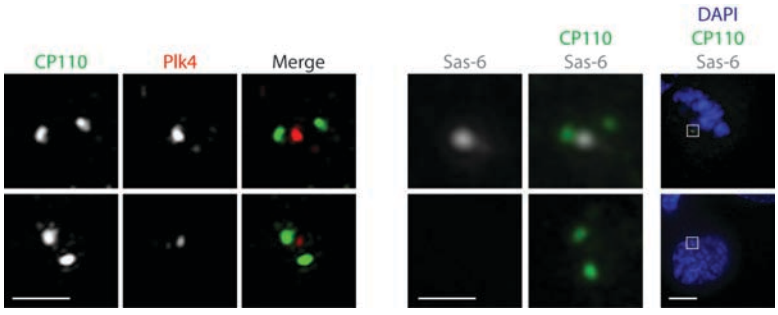

Figure 92 In RPE-1 cells Plk4 is confined to a focussed spot at centrioles in mitosis and G1 phase. RPE-1 cells were fixed and stained with the indicated antibodies. Red and green channel were acquired by 3D-SIM (left panel, scale bar 1 µm). CP110, Sas-6 and DAPI were additionally acquired using a widefield microscope (right panel, scale bars 1 µm or 5 µm for overview images).

6 Discussion

Here, we have studied the centrosome by firstly characterizing the function of both Cep152 and Cep192 in centriole duplication and secondly by investigating the localization of key centriolar proteins at sub-Abbe resolution by structured-illumination microscopy.

6.1 Function of Cep152 and Cep192

Homologues of Cep152 and Cep192 have been implicated in PCM recruitment and/ or centriole duplication (O'Connell et al., 2000; Kemp et al., 2004; Pelletier et al., 2004; Dix and Raff, 2007; Varmark et al., 2007; Blachon et al., 2008). However, the function of Cep152 in humans had not been addressed at all and initial investigations of Cep192 had revealed inconclusive results (Gomez-Ferreria et al., 2007; Zhu et al., 2008). Thus, this project aimed at characterizing the functions of Cep152 and Cep192 at human centrosomes in detail.

6.1.1 Expression and Localization of Cep152 and Cep192

Expression of Cep152 and Cep192

In proteomic or genomic databases 5 isoforms each are predicted for both Cep152 and Cep192. For simplicity, we termed these isoforms Cep152-1 – Cep152-5 and Cep192-1 – Cep192-5, respectively (**Figure 11** and **Figure 17**).

So far, studies of human Cep192 have only considered a short isoform of Cep192, which corresponds to Cep192-2 in our nomenclature. Here, we have shown that predominantly the longest Cep192 isoform (Cep192-1) with a predicted molecular weight of 279 kDa is expressed in HeLa S3 and U2OS cells. Moreover, we confirmed the expression of the N-terminal region, which is specific for this isoform, by RT-PCR in HeLa S3, U2OS, HEK293T and RPE-1 cells. We also found shorter isoforms to be expressed, which were, however, much less abundant in U2OS and HeLa S3 cells than the longest isoform.

In contrast, Cep152 isoforms mainly differ from each other by the presence of an extended C terminus in the long isoforms, which is missing in the short ones. We determined by both Western Blot analysis and RT-PCR that at least one long and one short isoform of Cep152 are expressed in the tested human cell lines. In databases, we found mRNA sequences of isoforms 1, 2 and 4. In addition, we isolated cDNA of isoforms 2 and 4 from a HeLa cDNA library. This is why we used these isoforms for all further experiments. Similarly, all groups who recently published studies on Cep152 used this Cep152-2 (Cizmecioglu et al., 2010; Dzhindzhev et al., 2010; Guernsey et al., 2010; Hatch et al., 2010; Kalay et al., 2010; Sir et al., 2011). However, none of these studies dealt with the expression of a shorter isoform at all, although their antibodies were generated against Cep152 regions, which are common to all isoforms. This discrepancy might be explained by the differing expression levels of long and short isoforms, which is why the less expressed short isoform might have been missed by others.

Localization of Cep152 and Cep192

An antibody targeting Cep192 was available, whereas antibodies directed against Cep152 had to be generated. We then applied these antibodies to determine the localization of Cep192 and Cep152. We found Cep192 to localize along the whole centriolar walls and to the proximal ends of both mother and daughter centrioles in interphase. When cells approached mitosis more Cep192 was recruited to centrosomes and it then also re-localized to the amorphous PCM matrix surrounding centrioles. The employed antibody recognizes all potential isoforms. Therefore, isoform-specific differences in localization cannot be ruled out. However, both overexpressed Cep192-1 and Cep192-2 localized within the extended PCM cloud surrounding centrioles during mitosis. In contrast, Cep152 was localized and restricted to the proximal half of the mature centriole throughout the cell cycle. After mitosis, Cep152 was recruited to the previous daughter centriole before the emergence of a new daughter centriole as visualized by CP110 staining. Similar localization patterns were detected with Cep152 antibodies against both the N and the C terminus. Thus, we did not identify differences in localization between the long and the short isoforms of Cep152.

The differential localization of Cep192 and Cep152 in both interphase and mitosis is reflected by the differing roles of both proteins in PCM recruitment. On the one hand, Cep192 localizes

along the whole centriolar walls in interphase and to the PCM throughout mitosis. Concomitantly, it is involved in efficient recruitment of γ-Tubulin and in MT nucleation. On the other hand, Cep152 remains confined to the proximal half of the mother centriole. In addition, levels peak in prophase, but then rapidly drop towards metaphase when the centrosomal PCM amount is still high. Consistently, we did not observe an effect of Cep152 depletion on γ-Tubulin recruitment or MT nucleation.

Cep192 stabilizes the centrosomal localization of Cep152

When analyzing the dependence of Cep152 and Cep192 on each other, Cep192 was found to localize to centrioles independently of Cep152. In contrast, Cep152 was significantly diminished at centrosomes upon Cep192 depletion, albeit not completely lost. Consistently, Cep63 and CPAP levels were also reduced, both of which have been reported to require Cep152 for centrosomal localization (Cizmecioglu et al., 2010; Dzhindzhev et al., 2010; Sir et al., 2011). Cytoplasmic levels of either of these proteins were confirmed to be unchanged in Cep192-depleted cells, which suggests that Cep192 influences the localization and not the stability of Cep152.

Interestingly, Cep152 interacted with Cep192 in co-immunoprecipitation experiments. Additionally, an interaction at endogenous levels was detected, if immunoprecipitations were performed from purified centrosomes. On the one hand, we potentially only detected an interaction after centrosome purification because of the differing cellular levels of Cep152 and Cep192 in human cells (personal communication, M. Bauer). On the other hand, our results might hint at a centrosome-specific interaction that could be regulated by post-translational modifications. Moreover, in complementation assays the central coiled-coil domain of Cep152 was sufficient for centrosomal localization. The same fragment was sufficient to interact with Cep192, which indicates that Cep192 might be the genuine recruiting factor. However, in this case one would predict a complete loss of Cep152 from centrosomes, if Cep192 was lost. With regard to the subcellular localizations of Cep152 and Cep192 it is obvious that Cep152 cannot simply be recruited to centrosomes solely by Cep192, as Cep192 localizes along both centrioles, whereas Cep152 is restricted to the proximal half of mother centrioles. Thus, the site-specific recruitment of Cep152 either

depends on another locally restricted recruiting factor or this still-to-be-identified recruiting factor is modified locally to allow the interaction with Cep152.

6.1.2 Function of Cep152 and Cep192 in PCM Recruitment

It has been shown previously that human Cep192 is required for efficient PCM recruitment (Gomez-Ferreria et al., 2007; Zhu et al., 2008). We also investigated the role of human Cep152 in PCM recruitment, as Asterless, the fly homologue of Cep152, had been implicated in γ-Tubulin recruitment,.

Interaction of Cep152 with the γTuRC

In immunoprecipitation experiments we identified several γTuRC components as interaction partners of Cep152 by both mass spectrometry and Western Blotting. In contrast to the mass spectrometry results, we also detected the known recruiting factor NEDD1 (GCP-WD) in Cep152 immunoprecipitations by Western Blotting. This discrepancy between the obtained results might be due to difficulties in detecting NEDD1 peptides by mass spectrometry. When we co-expressed NEDD1 with Cep152 in human cells, we detected an interaction that could never be shown, if both proteins were translated *in vitro*. These results indicate, on the one hand, that additional proteins might be required which are missing in the *in vitro* system, i.e. that NEDD1 might not directly interact with Cep152. On the other hand, post-translational modifications might be missing that are prerequisites for this interaction, especially because the subcellular localization of the γTuRC has previously been published to be regulated by phosphorylation (Luders et al., 2006; Haren et al., 2009).

Endogenous immunoprecipitations of Cep152

Apart from that, the fact that none of the proteins, published so far to interact with Cep152, was detected in the endogenous immunoprecipitations indicates that this approach might not be ideal to identify novel interaction partners of Cep152 or centrosomal proteins in general. A project conducted in our laboratory to quantify absolute amounts of centrosomal proteins has

revealed two main aspects: First, centrosomal proteins are generally low abundant with copy numbers as low as 2000 for some proteins. Second, despite the low abundance protein copy numbers generally range from about 2000 to 20,000 depending on protein, cell cycle stage and cell line. γ-Tubulin constitutes an exception among the analyzed proteins, as it is more abundant with about 500,000 copies per cell (personal communication M. Bauer). In addition, one has to consider that the interaction one seeks to detect might be locally restricted to the centrosome and thus engage only a small percentage of proteins. Therefore, it is very likely that physiological interaction partners might not be detected, if endogenous, i.e. predominantly cytoplasmic, proteins are immunoprecipitated. This was for instance the case for the interaction between Cep152 and Cep192, which we only detected after centrosome purification. The higher amount of cellular γ-Tubulin compared to other centriolar proteins might explain why only the γTuRC was identified by mass spectrometric analysis of endogenous Cep152 precipitations, even though the interaction was qualified as very low by label-free quantification. In particular, we did not find e.g. Plk4 or Cep63 by mass spectrometry either, known interaction partners of Cep152 (this study and Cizmecioglu et al., 2010; Dzhindzhev et al., 2010; Hatch et al., 2010; Sir et al., 2011). However, these proteins could be detected by Western Blot analysis. Similarly, Western Blotting confirmed an interaction between Cep152 and the γTuRC, which suggests that this might indeed be an *in vivo* interaction partner of Cep152.

In contrast to Cep192 depletion, Cep152 depletion does not impair centrosomal γ-Tubulin recruitment or MT nucleation

When analyzing the effect of Cep152 on the recruitment of γ-Tubulin to centrosomes and its impact on MT nucleation by the centrosome, we could not detect any eminent impact. Nevertheless, γ-Tubulin has also been implicated in centriole duplication (Kleylein-Sohn et al., 2007). Furthermore, by 3D-SIM we could detect both γ-Tubulin and NEDD1 not only surrounding mother and daughter centrioles, but also localizing within the lumen of mother centrioles. Similar localization patterns have been reported for γ-Tubulin and GCP6 by two other groups (Fuller et al., 1995; Bahtz et al., 2012). Therefore, it is possible that the pool of γTuRC proteins which interacts with Cep152 rather participates in centrosome functions other than MT nucleation into the cytoplasm, such as centriole duplication.

Furthermore, depletion of Cep192 did not substantially affect MT regrowth and γ-Tubulin recruitment in interphase cells. This indicates that Cep192 is dispensable for establishment of the MT network in interphase cells, but becomes essential for the local accumulation of γ-Tubulin within the pericentriolar amorphous protein matrix, when cells approach mitosis to allow the formation of a mitotic spindle.

6.1.3 Function of Cep192 and Cep152 in Centriole Duplication

The localization of Cep152 implied a possible function in centriole duplication. In addition, a number of recent publications dealt with Cep152 mutations implicated in human diseases, such as Seckel syndrome or microcephaly (Guernsey et al., 2010; Kalay et al., 2010). In general, mutations inducing such diseases have been linked to proteins involved in centrosome biology, either for their duplication or the recruitment of PCM. Moreover, Spd-2, the worm homologue of Cep192, is a known centriole duplication factor (Pelletier et al., 2004; Delattre et al., 2006). Therefore, we investigated the involvement of both Cep152 and Cep192 in centriole duplication.

Cep152 and Cep192 are required for faithful centriole duplication

In Cep152-depleted human cells centriole duplication was clearly impaired. This is consistent with three other studies published during the course of this project (Cizmecioglu et al., 2010; Dzhindzhev et al., 2010; Hatch et al., 2010). Importantly, we noticed that Cep152 depletion did not induce a duplication defect as strong as depletion of e.g. Sas-6 or Plk4. Furthermore, the depletion phenotype in Plk4-overexpressing cells could be rescued by co-expressing Cep152 isoforms 2 and 4. Other studies dealing with Cep152 generally used isoform Cep152-2 as Cep152 construct. Here, we show that Cep152-2 on its own is not sufficient to function in centriole duplication. On the one hand, this might hint at a requirement of both long and short Cep152 isoforms in centriole duplication. Both overexpressed long and short isoform localize similarly to the proximal half of mother centrioles and can dimerize with each other. This way, they might possibly form complexes to function together as recruiting platform in

centriole duplication. On the other hand, it is important to consider that Cep152-2 lacks exon 20 that is present in all other isoforms. Thus, Cep152-4 might complement Cep152-2 by providing this missing exon. Even though cDNA of Cep152-2 had been purified from a HeLa cDNA library, one should re-evaluate the expression of the other Cep152 isoforms.

In the literature, contradicting data are available concerning the role of Cep192 in centriole duplication (Gomez-Ferreria et al., 2007; Zhu et al., 2008). The published differences might be explained by the inefficient protein depletion by RNAi found for Cep192 with various siRNA oligonucleotides. When we depleted Cep192, we also observed a centriole duplication defect, which was comparable in extent to Cep152 depletion.

Cep192 and Cep152 co-operate in centrosomal Plk4 recruitment

Next we sought to understand how both proteins participate in centriole duplication and why the depletion effect was not as strong as observed for Sas-6 depletion. Both Cep152 and Cep192 localize around mother centrioles independently of Plk4, which suggests that both proteins lie upstream of Plk4 within the recruitment pathway of centriole duplication. Additionally, in *C. elegans* the Cep192 homologue is required for the recruitment of the kinase Zyg-1 to centrioles. Therefore, we investigated the involvement of both Cep152 and Cep192 in Plk4 recruitment.

Single depletion of Cep152 resulted in a slight increase in Plk4 levels, which is consistent with other studies published during the course of this work (Cizmecioglu et al., 2010; Dzhindzhev et al., 2010; Hatch et al., 2010). Conversely, centrosomal Plk4 levels were reduced upon Cep192 depletion. Interestingly, Plk4 was only unable to localize to centrioles in Cep152-/ Cep192-co-depleted cells. This indicates that Cep152 becomes essential for Plk4 recruitment in the absence of Cep192. Similar results were obtained when analyzing the recruitment of newly formed Plk4. In contrast to Cizmecioglu *et al.* (2010) we did not observe an abolished recruitment of this Plk4 pool. When we depleted either Cep152 or Cep192 before the induction of myc-Plk4 overexpression, myc-Plk4 still localized. Conversely, co-depleting both proteins prevented recruitment of induced myc-Plk4.

In agreement with the effect of double depletion on Plk4 recruitment, only upon depletion of both proteins a similar centriole duplication defect was induced as by depletion of either Plk4

itself or the centriole duplication factor Sas-6. Thus, Cep152 and Cep192 have partly redundant functions in centriole duplication.

Interaction of Cep152 and Cep192 with Plk4

We also investigated the interaction of Plk4 with both Cep152 and Cep192, both of which were found to interact with the kinase.

The interaction of Plk4 with Cep152 was mapped to the N terminal 220 amino acids of Cep152. Consistently, three other studies published similar dependencies, namely amino acids 1 – 512, 1 – 445 or 1 – 217, respectively (Cizmecioglu et al., 2010; Dzhindzhev et al., 2010; Hatch et al., 2010). Within the N terminus there is one stretch of amino acids predicted to form an α-helix, which we show here to be essential for the interaction with Plk4. In contrast, phosphorylation of the conserved SSP site in close proximity to this helix is not required. In agreement, the fragment of Plk4 necessary for the interaction comprises amino acids 265 – 887, which contains the linker and the cryptic polo box, but not the genuine polo box at the very C terminus. The other studies, published during the course of this project, mapped the interaction site to the cryptic polo box alone, i.e. amino acids 581 – 879 (Cizmecioglu et al., 2010), 586 – 887 (Hatch et al., 2010) or 632 – 809 (Dzhindzhev et al., 2010). The discrepancies might result from the usage of other fragments that might fold differently, if expressed alone. The interaction between Plk4 and Cep152 was observed in co-immunoprecipitation experiments of both *in vivo* and *in vitro* translated proteins. During the course of this study Cep152 was published to directly interact with Plk4 (Cizmecioglu et al., 2010; Dzhindzhev et al., 2010; Hatch et al., 2010). However, we did not manage to purify full length Plk4 as a properly folded protein in *E. coli*, which is why we cannot support this conclusion. If Plk4 – and the cryptic polo box in particular – do not adopt the endogenous conformation, it is probable that the aggregated Plk4 unspecifically interacts with Cep152. But we can conclude that Cep152 resides in a complex with Plk4 at least *in vivo*. Despite the fact that Cep63 resides in a complex with Cep152 in human cells (Sir et al., 2011), Cep63 did not interact with Plk4, if both proteins were overexpressed. An interaction between Plk4 and Cep152 was detected when Cep152 and Plk4 were over-expressed or when both proteins were translated *in vitro*. These results indicate that Cep63 is probably not required for the

interaction. However, we cannot rule out a possible involvement of Cep63 on endogenous level.

Consistent with its role in the recruitment of Plk4, Cep192 was also found to interact with the kinase. When both proteins were overexpressed, Plk4 interacted with both full length Cep192-1 and an N-terminal fragment spanning amino acids 1 – 330. Importantly, these amino acids are specific for the longest Cep192 isoform. When this N-terminal fragment was overexpressed, it did not localize to centrioles, but had a dominant-negative effect on centrosomal Plk4 localization. However, we did not detect an interaction between Cep192 and Plk4 on endogenous level. This is likely due to the differences in expression levels between Plk4 and Cep192, as Plk4 is a very low abundant protein, whereas Cep192 is expressed at 10 times higher levels (personal communication M. Bauer).

The interaction of Plk4 with the N terminus of Cep152 nicely fits with data on its orientational disposition at centrioles by 3D-SIM. We could show that the C terminus faces inwards, whereas the N terminus faces outwards from centrioles, where it lies in close proximity to Plk4 being locally concentrated at one position. Interestingly, the C terminus of Cep192 was found to localize in a similar diameter around centrioles as the C terminus of Cep152. The interaction of its N terminus with Plk4 implies that Cep192 might be similarly oriented as Cep152, which has to be tested in the future.

Both Cep152 and Cep192 differ in their localization patterns from that of Plk4. Cep192 localizes along both mother and daughter centrioles, Cep152 localizes to the proximal half of mother centrioles and Plk4 is confined to one local spot on the Cep152 ring. If Cep192 and/ or Cep152 were indeed direct recruiting factors of Plk4, the interaction would have to be locally restricted, as will be discussed later (Section 6.2.4). When Plk4 is overexpressed, it re-localizes around the whole proximal end of the mother centriole, but does not spread over the entire mother centriole or the daughter centriole (Bettencourt-Dias et al., 2005; Habedanck et al., 2005; Kleylein-Sohn et al., 2007). This result indicates that the Cep192-Plk4 interaction has to be restricted to the proximal half of mother centrioles, even if excess amounts of Plk4 are present. Importantly, our results reveal that both the longest Cep192 isoform and to a lesser extent at least one other isoform is expressed. However, the applied Cep192 antibody has been generated against the C terminus of the protein, which is common to all isoforms. By conventional widefield microscopy we could not detect a difference in the localization of

overexpressed Cep192-1 and Cep192-2. Yet, one has to investigate the localization of the individual isoforms and particularly the longest isoform in interphase cells with super-resolution microscopy to rule out potential differential localizations.

Proper centriolar recruitment of CPAP and Sas-6 depends on Cep152 and Cep192

Furthermore, we investigated the impact of Cep152 and Cep192 on other centriole duplication factors besides Plk4. Depletion of either Cep192 or Cep152 resulted in the loss or reduction of certain centriolar proteins: If Cep192 was missing, levels of centrosomal Cep152, Cep63 and CPAP in addition to Plk4 were reduced. In agreement, we could detect an interaction of Cep192 with Cep152. The general reduction in centrosomal protein levels might hint at a stabilizing function of Cep192 at centriolar walls. However, all of the affected proteins are still present at centrioles and might thus be sufficient to allow centriole duplication. In contrast, upon depletion of Cep152 its interaction partners CPAP and Cep63 were absent, whereas Sas-6, Cep192 and Plk4 still localized. Cizmecioglu *et al.* (2010) and Dzhindzhev *et al.* (2010) reported a similar effect of Cep152 depletion on CPAP. However, Hatch *et al.* (2010) claimed that Sas-6 was absent from centrioles in Cep152-depleted cells, which we could not reproduce, even though we used the same siRNA oligonucleotides as they did. In spite of the absence of CPAP and Cep63 upon Cep152 depletion the presence of other duplication factors might favour the generation of new centrioles by locally concentrating the necessary components. Hence, depletion of either Cep192 or Cep152 leads to a less efficient duplication of centrioles, although centriole duplication still occurs to a certain extent.

So far, it has not been resolved how Sas-6 is recruited to centrioles in G1 phase and which proteins are required for this recruitment. Here, we have identified Cep192 and Cep152 to be essential for efficient recruitment of Sas-6 to centrioles. When we depleted either Cep192 or Cep152, Sas-6 was still present at centrioles. However, when we co-depleted both proteins, centriolar Sas-6 levels were reduced. Importantly, when there were still two centrosomes present per cell, one of them consistently accumulated less Sas-6 than the other one. On the one hand, this could result from undetectable residual Cep192 or Cep152 at centrioles, which is sufficient for Sas-6 recruitment. However, we often observed wildtype levels of Sas-6 at one centriole and complete absence from the other one. On the other hand, this could imply that one centriole remains Sas-6-binding-competent throughout the cell cycle despite the

absence of Cep152 or Cep192, whereas the other one does not acquire this competency. This would also indicate that neither Cep152 nor Cep192 were direct recruiting factors of Sas-6, but rather indirectly participated in efficient Sas-6 recruitment. Recently, Wang *et al.* (2011) reported that previous daughter centrioles become duplication competent at the end of mitosis in a Plk1-dependent manner. In Plk1-inhibited cells this centriole does not become duplication competent, whereas the previous mother maintains its competency. Interestingly, the authors used Sas-6 as marker for competency. Cep152 and/ or Cep192 might be involved in such a mechanism by e.g. enabling the phosphorylation of a so-far-unknown Plk1 substrate. However, the mitotic accumulation of Plk1 within the PCM cannot account for this, since depletion of Pericentrin did impair PCM formation and thus Plk1 recruitment, but did not affect centriolar Sas-6 levels. Yet, we cannot rule out that Plk1 recruitment to centriolar walls is impaired in Cep152/ Cep192-depleted cells, especially because both Cep152 and Cep192 contain conserved SSP sites, potential binding sites for Plk1. In addition to Plk1, a possible involvement of Plk4 in the acquisition of duplication competence at the end of mitosis has not been addressed so far. But our results clearly demonstrate that co-depletion of Cep152 and Cep192 prevents centriolar Plk4 recruitment. Thus, impaired Sas-6 recruitment to the previous daughter centriole might be a consequence of the lack of Plk4. When we depleted Plk4 and searched for cells with two centrosomes present, we sometimes detected differing levels of Sas-6 at each centrosome.

To conclude, it is tempting to speculate that centriole duplication can still occur in Cep152- or Cep192-depleted cells, because Plk4 and Sas-6 still bind to centrioles. Only if Plk4 is completely lost from centrioles and Sas-6 is not recruited to newly formed mother centrioles, centriole duplication is impaired similarly to the depletion of Plk4 or Sas-6. A model of how Cep152 and Cep192 are involved in the initiation of centriole duplication is shown in **Figure 93**.

Conservation of Plk4 recruitment function of Cep152 and Cep192

During evolution different organisms seem to have evolved different ways of recruiting the centriole duplication-initiating kinase to centrioles. Whereas Spd-2/Cep192 is essential for Zyg-1 recruitment in *C. elegans* (Delattre et al., 2006; Pelletier et al., 2006), it is dispensable for Sak/Plk4 recruitment in *D. melanogaster* (Dix and Raff, 2007). In contrast, Asterless/Cep152 recruits the kinase to centrioles in flies (Dzhindzhev et al., 2010), but is not

present in worms (Carvalho-Santos et al., 2010). Finally, in humans both Cep152 and Cep192 participate in Plk4 recruitment. Thus, during evolution the two proteins seem to have evolved a partly redundant function to ensure faithful centriole duplication in humans.

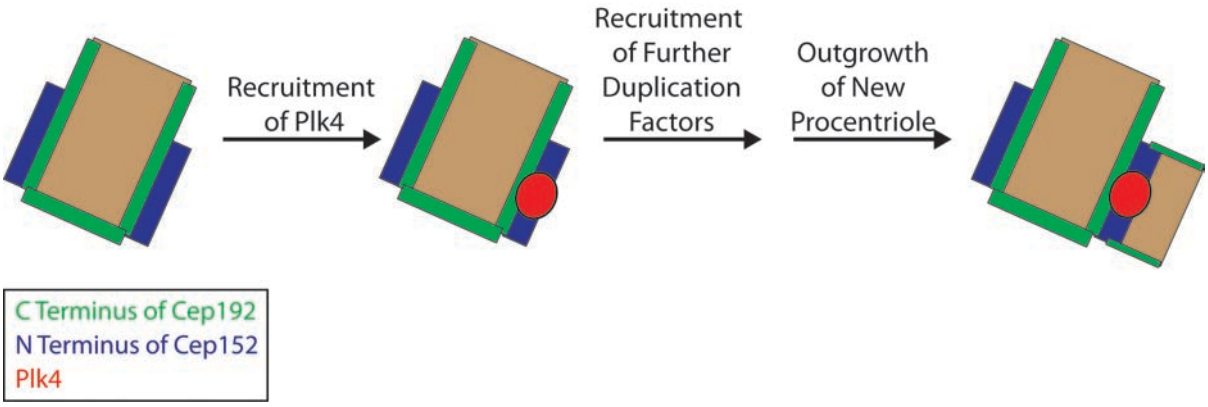

Figure 93 Cep152 and Cep192 participate in the initiation of centriole duplication in human cells. Schematic representation of the early stages of centriole duplication. In G1 phase, Cep192 localizes with its C terminus close to centriolar walls and to proximal ends. In contrast, Cep152 resides around the proximal half of the centriole with the N terminus facing outwards. Both proteins co-operate in the recruitment of the kinase Plk4. Subsequently, further centriole duplication factors are recruited (for details see **Figure 7**) and ultimately, procentriole formation can occur.

Cellular Plk4 levels are elevated in Cep152-depleted cells

When we checked the recruitment of Plk4 in cycling cells in the absence of Cep152, we noticed that centrosomal Plk4 levels were not diminished, but rather increased. Consistently, we also found cytoplasmic levels to be elevated by Western Blot analysis. In accordance, we often found Plk4 to localize as a ring around centrioles in Cep152-depleted cells, presumably around mother centrioles. Despite this disposition we never observed the formation of multiple procentrioles around one mother centriole, which fits to the observed effect of Cep152 depletion on centriole over-duplication in Plk4-overexpressing cells.

This cannot be attributed to impaired centriolar localization of Plk4, as single depletion of Cep192 does not affect cytoplasmic Plk4 levels. In contrast, this Plk4 level increase could be explained by a mechanism in which Cep152 is required for the degradation of Plk4, potentially via their interaction. However, we did not observe an increase in overexpressed myc-Plk4 levels, when we depleted Cep152 in S phase-arrested cells and then induced the overexpression of myc-Plk4 in U2OS:myc-Plk4 cells (L. Cajanek, personal communication).

This implies that Cep152 depletion might not have an impact on Plk4 degradation, but rather on Plk4 expression, as overexpressed myc-Plk4 is not under the control of the endogenous promoter. It has been reported previously that there might be a checkpoint that senses the presence of centrosomes and prevents the cell cycle from progressing in their absence (Hinchcliffe et al., 2001). Furthermore, it was claimed that this pathway depends on p53 (Mikule et al., 2007). Even though this model and the whole concept is still under debate, the obtained results concerning Plk4 levels in Cep152-depleted cells could be explained by a feedback mechanism that elevates the key regulatory kinase, if certain centriolar components are missing.

With regard to the relevance of such a potential feedback mechanism, it has been published that Plk4 overexpression can induce *de novo* centriole formation in addition to regulating the canonical pathway in *Xenopus* and flies (Rodrigues-Martins et al., 2007; Eckerdt et al., 2011). Increase of cellular Plk4 levels might thus constitute a mechansim of how Cep152-depleted cells compensate the lack of Cep152.

Finally, Plk4 levels were also increased at centrosomes, when Sas-6 was depleted. Whether Plk4 level elevations by either Sas-6 or Cep152 depletion have a similar mechanistic origin and whether this is a common effect of depletion of centriole duplication factors, has to be addressed in future experiments.

Plk4-dependent phosphorylation of Cep152 and Cep192

In addition to the role of Cep152 and Cep192 in efficient recruitment of certain centriole duplication factors, it has not been resolved to date how a potential phosphorylation of either protein by Plk4 is involved in centriole duplication. But one can envision a mechanism in which Plk4 phosphorylates either Cep152 or Cep192 to allow the recruitment of downstream duplication factors. So far, it has not been addressed at all, whether Cep192 is a Plk4 substrate.

Here, we have demonstrated that Cep152 is phosphorylated by Plk4 *in vitro*. When we performed kinase assays on Cep152 purified from human cells, we detected three phosphorylation sites within the C terminus that were upregulated compared to the kinase dead control. Consistently, we only observed an upshift of recombinant Cep152-2, but not of

Cep152-4, which lacks the C terminus. However, we used a recombinant protein consisting of amino acids 1 – 430 of Plk4 as active kinase, because no purification conditions have been established to date to express full length Plk4 in a properly folded state. This of course raises the possibility that the observed phosphorylation is not specific, but rather constitutes a nonspecific phosphorylation of protein residues accessible on the protein surface. Hatch *et al.* (2010) performed similar kinase assays, in which either the N terminus or full length Cep152 was purified and used as substrate with recombinant full length Plk4. They report that both full length and the N-terminal fragment of Cep152 are phosphorylated by Plk4. But it is also questionable whether their purified Plk4 is indeed properly folded and thus whether their phosphorylation constitutes a physiological condition. Regarding the domain composition of Plk4 it is possible that the kinase domain is properly folded to allow the phosphorylation event to occur, whereas the C-terminal polo box domain is not, but is sufficiently separated from the kinase domain by the linker (**Figure 46**). The issues about the purification of recombinant Plk4 in an active and properly folded conformation have to be resolved before obtaining conclusive information about Plk4 phosphorylation sites by *in vitro* kinase assays.

6.1.4 Regulation of Cep192 and Cep152

Here, we have reported that Cep152 and Cep192 are required for faithful centriole duplication. If depleted, centriole duplication is impaired. If Cep152 is overexpressed, centriole duplication is also prevented, presumably by the sequestration of Plk4 from centrioles. Similarly, Cep192 overexpression also results in a less efficient centrosomal recruitment of Plk4. This implies that levels of Cep152 and Cep192 have to be regulated during the cell cycle to avoid centriole duplication errors from occurring.

Cell cycle-specific regulation of Cep192

We could show that cellular Cep192 levels remain stable during the cell cycle, whereas centrosomal levels increase in cells approaching mitosis in a similar fashion as other PCM proteins. This is consistent with a previous study, where the centrosomal localization was

analysed by immunostaining (Gomez-Ferreria et al., 2007). Moreover, we detected an upshift of the Cep192 band by Western Blotting in mitotic samples, which might reflect a post-translational modification. In agreement, two studies have recently published that the centrosomal recruitment of Cep192 in mitosis depends on its phosphorylation by Plk1 (Haren et al., 2009; Santamaria et al., 2011).

Cell cycle-specific regulation of Cep152

In contrast to the constant levels of Cep192, cellular Cep152 levels of both long and short isoforms increased during interphase and peaked just before both Plk1 and Cyclin B levels were maximal, which indicates a timepoint in late G2 phase. Concomitantly, centrosomal levels increased until prophase and then rapidly declined. Despite the changes in centrosomal and cytoplasmic Cep152 levels, the protein was never completely lost or degraded. During the course of this study similar results were obtained by another group (Cizmecioglu et al., 2010).

Involvement of βTrCP, Plk1 and Plk4 in Cep152 regulation

When searching for conserved sequences that might hint at a possible mechanism of Cep152 degradation, we found an SSP site within the N terminus and a DSGXXS site within the C terminus. Polo box-containing proteins are known to bind phosphorylated SSP sites, whereas phosphorylated DSG motives are binding sites for the F box protein βTrCP. Due to its location, the DSG motif is only present in long Cep152 isoforms, but neither in the short isoforms nor in *Drosophila* Asterless. Moreover, the SSP site is not conserved in flies either, even though Asterless contains an SSP site at another position. When depleting either βTrCP or the polo box-containing kinase Plk1, cellular as well as centrosomal levels of Cep152 were indeed elevated. In agreement, an effect of Plk1 inhibition on centrosomal Cep152 was published during the course of this study (Sir et al., 2011). Surprisingly, depletion of Plk4 resulted in a similar increase.

In addition to the interaction of Cep152 with Plk4, discussed above, we also detected an interaction with the kinase Plk1. The interaction with both kinases increased after release from S phase. These changes might simply result from the increase in protein levels of

Cep152, Plk1 and/ or Plk4. However, the interaction with Plk1 was also elevated, if cells were arrested in G2 phase compared to S phase, even though Cep152 levels were decreased.

Moreover, we detected an interaction of Cep152 with βTrCP, if both proteins were overexpressed. Yet, mutating the conserved DSG motif alone or in combination with another potential binding site did not abolish the interaction. In addition, co-expression of Plk4 did not induce a difference between wildtype and mutant Cep152. Similarly, the interaction of Cep152 with Plk1 was not lost, if the SSP site was mutated to SAP. Thus, the observed interactions might either be nonspecific or they might be mediated by dimerization with endogenous Cep152. But when we co-expressed Plk4 with Cep152 lacking the N-terminal 46 amino acids under similar conditions, this deletion prevented an interaction with Plk4, indicating that endogenous Cep152 is probably not sufficient to mediate the interaction between the two overexpressed proteins. Thus, the detected interaction is potentially unspecific. The interaction of βTrCP and Cep152 might be temporally or spatially restricted or βTrCP depletion might indirectly affect Cep152 levels by an unknown mechanism. But this potential mechanism cannot include an elevation of Plk4 by βTrCP depletion, as increased Plk4 levels also negatively regulate Cep152.

Even though we could not detect short Cep152 isoforms reproducibly by Western Blotting after depletion of β TrCP, Plk1 and Plk4, we occasionally saw an increase of the lower Cep152 band as well. If this is true, it indicates that βTrCP, Plk1 and Plk4 affect both long and short isoforms despite the absence of a DSG motif from the short isoforms. This suggests that βTrCP either does not act directly on Cep152 or that the short isoforms are passively co-regulated. In agreement with the latter possibility, we found the short isoform Cep152-4 to be very unstable when overexpressed in the presence of cycloheximide. In contrast, the long isoform Cep152-2 was stable under these conditions. Also co-expression of Plk4 did not induce a destabilization of Cep152-2 in CHX assays. However, Plk4 was stable under similar conditions, too, even though it has been published to be constantly degraded (Cunha-Ferreira et al., 2009; Guderian et al., 2010; Sillibourne et al., 2010). Interestingly, Cep152-4 was partially stabilized, if co-expressed with Cep152-2. This can only be explained by the presence of a potential destabilizing sequence within exon 20 in Cep152-4, even though we did not identify such a sequence. Conversely, exon 5 or the extended C terminus in Cep152-2 might provide stability to the otherwise predicted coiled coil-folded structure.

If βTrCP, Plk1 and Plk4 are indeed involved in the regulation of Cep152 and participate in a common pathway, a mechanism could be envisioned, in which Plk4 phosphorylates the SSP site to allow binding of Plk1. Plk1 in turn could phosphorylate both serines of the DSG motif. A similar pathway including Cdk1 and Plk1 has been published for e.g. Bora (Chan et al., 2008; Seki et al., 2008). Alternatively, Cep152 might be primed by a kinase other than Plk4, which allows binding of Plk1. Then Plk1 and Plk4 might phosphorylate one serine each of the Cep152 DSG motif. Similarly, Wee1 is phosphorylated by both Cdk1 and Plk1 at its DSG motif and is then degraded as a consequence (Watanabe et al., 2004). Using *in vitro* kinase assays Cep152-2 and Cep152-4 could be phosphorylated by CDK2 and Aurora A in addition to Plk4. Since substrate specificity of various CDKs in *in vitro* kinase assays is not absolute, it is more likely that CDK1 participates in the degradation of Cep152 in late G2/ M phase. However, in immunoprecipitations of Cep152 from either S phase- or G2 phase-arrested cells more Plk1 was co-purified in G2 phase-arrested cells despite the inhibition of CDK1 by RO3306, which indicates that CDK1 is not the priming kinase. Nevertheless, it is possible that Cep152 might be primed for Plk1 binding by Aurora A in addition to Plk4. To unravel which kinase might phosphorylate Cep152 to allow Plk1 binding Far Western Blots with the PBD of Plk1 as well as consecutive kinase assays have to be performed. Initial experiments using Plk4 as priming kinase did not reveal a binding of the PBD of Plk1 to Cep152 (personal communication, E. Anselm), which argues against a role of Plk4 as priming kinase. Furthermore, a potential interaction with βTrCP can then be tested after in vitro phosphorylation of either wildtype or DSG-mutant Cep152.

Potential involvement of other F-box proteins in Cep152 degradation

Despite the high conservation of the DSG motif in all long Cep152 isoforms, it is still possible that other E3 ligases participate in its degradation. Recently, the F-box proteins Cyclin F and FBXW5 have been implicated in the degradation of other centriole duplication factors, namely CP110 and Sas-6, respectively (D'Angiolella et al., 2010; Puklowski et al., 2011). However, depletion of Cyclin F followed by a release from S phase did not result in the stabilization of Cep152 in contrast to the stabilization of CP110 (data not shown). Moreover, depletion of FBXW5 in asynchronous cells (controlled by depletion of a co-expressed FBXW5 construct) did neither lead to a stabilization of Sas-6 nor of Cep152 (data

not shown). These results argue against an involvement of Cyclin F and FBXW5 in Cep152 degradation.

Levels of several proteins involved in centriole duplication peak in early mitosis

In addition to Cep152, several proteins involved in centriole duplication are by now known to increase during interphase and peak in mitosis, particularly in prophase, such as Sas-6 (Strnad et al., 2007), STIL (Arquint et al., 2012), CP110 (D'Angiolella et al., 2010) or Plk4 (Sillibourne et al., 2010, and this study). This is an intriguing observation, since centriole duplication is initiated at the G1-S transition and should have taken place, until mitosis commences. Nevertheless, the levels are highest at the onset of mitosis. On the one hand, this could simply be a consequence of the regulatory mechanism of centriolar proteins that might be coupled to cell cycle progression. This would imply that levels only drop when cells have passed into a mitotic cell cycle stage. On the other hand, it could indicate that these proteins actually function until or in mitosis e.g. to stabilize the previously formed centriole or already set the framework for centriole duplication in the next cell cycle. Interestingly, we could show that the predicted cartwheel protein Cep135 only becomes detectable at newly formed centrioles at the onset of mitosis (discussed below, Section 6.2.3), which coincides with the drop of other duplication factors and precedes complete loss of the other cartwheel proteins Sas-6 and STIL in late mitosis. In *Chlamydomonas*, the Cep135 homologue Bld10 has been implicated in stabilizing the centriolar structure (Hiraki et al., 2007). This raises the attractive model that centriole composition is kept constant, until Cep135 has been recruited to maintain centriole stability.

6.1.5 Summary

Here, we have investigated the function of human Cep152 and Cep192 in PCM recruitment and centriole duplication. Whereas Cep192 is essential for PCM recruitment and MT nucleation in mitosis, Cep152 is not required for these processes. This difference between Cep152 and Cep192 is in agreement with their differential localization in mitosis: Cep192

spreads out into the amorphous PCM, but Cep152 remains confined to the centriolar wall. Furthremore, we have identified human Cep152 as novel centriole duplication factor and could confirm a requirement of Cep192 for proper centriole duplication. Both Cep152 and Cep192 co-operate in Plk4 recruitment and centriole duplication, as co-depletion had an additive effect on Plk4 recruitment and centriole duplication compared to single depletions.

Thus, Cep192 and Cep152 appear to have evolved redundant functions in humans to at least partly compensate the lack of the other one. To date, only mutations in the *cep152* gene have been identified in centrosome-linked diseases such as microcephaly or Seckel syndrome (Guernsey et al., 2010; Kalay et al., 2010). Based on the close functional inter-relations of Cep152 and Cep192 in centriole duplication, one could speculate that mutations in Cep192 also affect human development.

6.2 Super-Resolution Analysis of Human Centrosomes

As a second approach to further understand the function and relations of centriolar proteins, we used the super-resolution fluorescence microscopy technique 3D-SIM to investigate the disposition of key centriolar and centrosomal proteins. In particular, we have examined the localization of pericentriolar material, appendage and cartwheel proteins and finally of the key regulatory kinase Plk4.

6.2.1 Pericentriolar Material

Initially, we closely examined the localization of proteins surrounding the centriolar cylinders.

Localization of the γTuRC relative to other PCM proteins

In interphase, both γ-Tubulin and the γTuRC-recruiting factor NEDD1 localized around mother and weakly around daughter centrioles. As discussed earlier (Section 6.1.2), staining was also detected within the lumen of mother centrioles. This is consistent with immuno-EM

data on the localization of γ-Tubulin and GCP6 (Fuller et al., 1995; Bahtz et al., 2012). A luminal localization within daughter centrioles is potentially not resolved by 3D-SIM and can therefore not be ruled out. In contrast to these γTuRC components, the prominent PCM proteins Pericentrin, Cep215 and Cep192 were only detected around centrioles, but not within centrioles.

The localization of the γTuRC, exemplified by γ-tubulin and NEDD1, in the lumen of the mature centriole raises an intriguing question of its function at this location. On the one hand, this luminal protein pool might participate in the stabilization of the centriole. On the other hand, the presence within the mother centriole might indicate a potential role of this protein pool in ciliogenesis, when the mature centriole serves as basal body for the outgrowth of a cilium in differentiated cells.

In cells approaching mitosis we were able to visualize the amorphous meshwork of the extended PCM surrounding centrioles. Its amorphous nature has been suggested previously (Dictenberg et al., 1998); however, it cannot be resolved by conventional widefield microscopy. In comparison with other PCM proteins, γ-Tubulin staining extensively overlapped with NEDD1. Conversely, areas of alternating localization were observed when co-staining cells for γ-Tubulin with either Pericentrin, Cep215 or Cep192. This implies that both groups of proteins, i.e. γTuRC components and the proteins essential for their centrosomal recruitment or the stability of the PCM, are mutually exclusive and reside in an alternating fashion within the meshwork of the PCM.

Organization of centriolar and centrosomal proteins around centrioles

We then compared the localization of 18 centriolar and centrosomal proteins in interphase centrioles. The localization patterns could be subdivided into three groups: either dot-like or ring-like or a combination of the two. Proteins that appeared as dots of approximately 80 – 100 nm were Centrin within the distal lumen of centrioles as well as STIL, Sas-6 and Plk4 in-between mother and growing daughter centriole. Interestingly, the latter three proteins are known to be essential in the early stage of the initiation of centriole duplication (Bettencourt-Dias et al., 2005; Habedanck et al., 2005; Leidel et al., 2005; Strnad et al., 2007; Tang et al., 2011; Arquint et al., 2012; Vulprecht et al., 2012).

In addition to γ-Tubulin and NEDD1 the proximal protein CPAP also localized around and within the lumen of centrioles. CPAP allows the outgrowth of centriolar MTs during centriole duplication and its levels determine the length of the nucleated MTs (Kohlmaier et al., 2009; Schmidt et al., 2009; Tang et al., 2009). So far, this ring-/dot-like localization pattern of CPAP has only been observed by immuno-EM in Plk4-overexpressing cells (Kleylein-Sohn et al., 2007). Here, we show that CPAP localizes similarly under physiological conditions. But the differential functions of either pool of CPAP remain elusive to date. Moreover, it is unknown when the luminal localization of CPAP is established, as CPAP is not detectable within the lumen of daughter centrioles in our hands. However, we cannot rule out that low levels are present within daughter centrioles early during the cell cycle, which are either not resolved or not detected due to low antibody sensitivity.

For all proteins that localize in a ring-like fashion to centrioles in top-views of centrioles we determined the ring diameters. Interestingly, the distal protein CP110 and the proximal protein Cep135 stained rings of similar size as the centriolar wall itself (visualized with antibodies against glutamylated tubulin). This implies that these proteins might cap the centriole at proximal and distal ends, respectively. The capping function for CP110 has already been reported (Kleylein-Sohn et al., 2007; Kohlmaier et al., 2009; Schmidt et al., 2009; Tang et al., 2009). In addition, our current observation is consistent with the previous suggestion that Cep135 might serve a microtubule-stabilizing role at proximal ends (Hiraki et al., 2007).

The detected localization of CP110 and Cep135 is in agreement with immunoelectron microscopy data indicating that Cep135 and CP110 associate with the centriolar cylinder at the proximal and distal centriolar ends, respectively (Kleylein-Sohn et al., 2007; Schmidt et al., 2009). However, in those studies we had never detected a central hollow region, i.e. a ring-like localization of CP110 and Cep135. This discrepancy can readily be explained by the examination of centrioles in side-view in the immuno-EM studies. The sample thickness of about 70 nm used for immuno-EM might not allow the lateral resolution of a ring as small as 170 nm.

All other examined proteins formed rings of larger diameter around centrioles. According to the measured diameter, we were able to subdivide the PCM into inner, intermediate and outer PCM. Even though the application of site-specific antibodies only allowed us to draw

conclusions on the localization of the detected protein regions, it still became apparent that the PCM in interphase cells is organized in a highly ordered fashion around centrioles with particular proteins localizing at specific distances from centrioles – thus presumably in specific orientations.

Moreover, proteins that were also detected at daughter centrioles reproducibly stained a ring of smaller diameter than at mother centrioles. This observation supports the notion that PCM is more developed around mother than daughter centrioles (Piel et al., 2000; Wang et al., 2011).

Investigation of Protein orientation

To further illustrate the benefits of using super-resolution microscopy, we stained the protein Cep152 with antibodies targeting either the N or the C terminus. We found that the C-terminal antibody consistently stained a smaller ring than the N-terminal one (also mentioned earlier, Section 6.1.3). Thus, this staining revealed the orientation of Cep152 with the C terminus localizing close to the centriolar wall and the N terminus facing outwards. In general, these results clearly demonstrate that the combination of site-specific antibodies with 3D-SIM represents a powerful approach for determining protein orientation and disposition.

6.2.2 Appendage Proteins

Consistent with immuno-EM data, we observed that subdistal appendage proteins Ninein and Cep170 localized more proximally than the distal appendage protein Cep164 (Paintrand et al., 1992). Additionally, we also measured a bigger ring diameter for the subdistal than for the distal appendage proteins. However, we measured a smaller absolute ring size for the protein Cep164 than it had been reported previously. This discrepancy could be due to different purification/fixation techniques applied, as those authors had already noticed differences in the structure of the appendages depending on the presence of divalent cations during centrosome purification. Furthermore, in a recent study the authors took the external diameter

– instead of the distance between intensity maxima – of the Cep164 ring into account and determined it to be around 500 nm instead of 400 nm by PALM (photoactivated localization microscopy) and STORM (stochastic optical reconstruction microscopy), two other super-resolution microscopy techniques (Sillibourne et al., 2011).

The 9 microtubule blades of a centriole do not carry equal amounts of appendage proteins

Additionally, we noticed the number of discernible density masses within the rings, stained by antibodies against appendage proteins, was consistently below that expected from the 9-fold symmetry of centrioles. At an idealized centriole, that is reconstructed by nine 40° rotations around the center followed by averaging, appendages are detected at each centriolar tube (Paintrand et al., 1992). There are two different possible explanations for this discrepancy: It is conceivable that antibody accessibility is limited for some of the 9 appendages, perhaps due to steric hindrance caused by anchoring of MTs to subdistal appendages. Alternatively, it is possible that not all centrioles carry the full complement of 9 appendages or that appendage proteins do not accumulate to the same extent at all appendages. Interestingly, our data clearly indicate that mitotic centrosomes carry a reduced number of distal appendages as visualized by Cep164 staining and/or that the protein content between different appendages is altered.

Cep164-positive centrioles have reduced CP110 levels

During the course of this study we noticed that the Cep164-bearing, mature centriole often had redued CP110 levels in interphase cells. At all other centrioles levels were increased in interphase and then reduced during mitosis. It is very appealing in view of the role of those mature centrioles as basal bodies in ciliogenesis that Cep164-positive centrioles have decreased CP110 levels. Whereas Cep164 serves as anchor for the basal body at the plasma membrane (Graser et al., 2007), CP110 is a distal cap and has to be removed from the basal body to allow the outgrowth of the ciliary axoneme (Spektor et al., 2007; Kohlmaier et al., 2009; Schmidt et al., 2009; Tang et al., 2009). The fact that CP110 levels at the Cep164-positive centriole remain low throughout the cell cycle might be a mechanistic element of the site-specific regulation of CP110 at the future basal body.

Interestingly, upon Cep164 depletion CP110 levels at the mature centriole became similar to the level at the other centrioles. This restoration of CP110 staining upon Cep164 depletion strongly argues that the presence of Cep164 antagonizes CP110 association with distal ends of fully mature centrioles.

6.2.3 Cartwheel Proteins

Three proteins have been predicted to form the centriolar cartwheel, which templates the 9-fold symmetry during centriole biogenesis, namely Cep135, Sas-6 and Sas-5. Immuno-EM studies in *Tetrahymena* and structural investigations have provided data that Bld12/Sas-6 localizes to and potentially forms the cartwheel hub, whereas Bld10/Cep135 localizes to cartwheel spoke tips (Hiraki et al., 2007; Nakazawa et al., 2007; Kitagawa et al., 2011; van Breugel et al., 2011). Additionally, Sas-5/STIL forms a complex with Sas-6 in *C. elegans* (Delattre et al., 2006; Pelletier et al., 2006) and is an early factor in the centriole duplication pathway in humans (Tang et al., 2011; Arquint et al., 2012; Vulprecht et al., 2012). Using 3D-SIM we could in principle confirm these localizations: Sas-5 and Sas-6 indeed co-localize and stain a distinct spot in-between mother and daughter centrioles, whereas Cep135 forms a ring at proximal ends of centrioles.

However, the ring-like localization of Cep135 was only apparent at mother centrioles, but not at the proximal end of growing centrioles, even though weak Cep135 staining was also detected in co-localization with Sas-6. Because Cep135 is considered a likely homologue of *Tetrahymena* Bld10, the strikingly distinct disposition of Cep135 and Sas-6 came as a surprise. If Cep135 were to localize prominently to the tips of cartwheel spokes during early biogenesis of human centrioles, we would have expected to see this protein in close proximity to Sas-6 at the cartwheel hub. This cannot be attributed to a too low resolution of 3D-SIM, as the expected distance from the ring at mother centrioles to the one at daughter centrioles is high enough to be resolved. Our data do not exclude that Cep135 is a genuine cartwheel component in human cells, but they suggest that the number of Cep135 proteins at these structures might be low in comparison to the amount of Cep135 that 3D-SIM reveals at mother centrioles. This result might therefore serve to exemplify the limits of 3D-SIM, which

depends on a high signal-to-noise-ratio.

The location of Cep135 at proximal ends of mother centrioles in close proximity to C-Nap1 and the proximal pool of Ninein is in agreement with the published interaction of Cep135 with C-Nap1 and its relevance for centrosome cohesion (Kim et al., 2008). Cep135 was described to be required for the localization of C-Nap1 to centrosomes. Our present data might support such a role of Cep135 in centrosome cohesion at mother centrioles.

6.2.4 Plk4

Finally, we examined the localization of the regulatory kinase Plk4 during the cell cycle. So far, its localization on endogenous level had not been investigated at high resolution, even though analysis of Plk4 overexpression had revealed a disposition surrounding the proximal part of mother centrioles (Bettencourt-Dias et al., 2005; Habedanck et al., 2005; Kleylein-Sohn et al., 2007). Here, we show that endogenous Plk4 forms a distinct spot and co-localizes with Sas-6 at the interphase between mother and daughter centriole throughout the cell cycle.

The fact that overexpression of Plk4 results in the re-localization around the whole centriole, whereas it is concentrated at one particular spot at endogenous levels implies that there is an autoregulatory mechanism for Plk4 localization. A positive feedback might comprise either the stabilization of a so far unknown recruiting factor or the generation of binding sites by phosphorylation of a stable recruiting factor by Plk4 itself. Conversely, it is possible that a negative regulator prevents binding of Plk4 and restricts it to one confined location at mother centrioles. Plk4 overexpression could then generate additional binding sites by degrading this negative regulator. Whether such a regulatory mechanism does indeed exist and whether the kinase activity of Plk4 is required, has to be shown in future experiments. In any case, with regard to the co-operation of Cep152 and Cep192 in Plk4 recruitment, as discussed earlier (Section 6.1.3), it is obvious that the interaction would have to be regulated to restrict Plk4 to one particular spot at the proximal half of centrioles. Additionally, based on the results that Plk4 is involved in Cep152 degradation and that Cep152 depletion increases Plk4 levels, whereas Cep152 overexpression prevents binding of Plk4 to centrioles, it is conceivable that

Cep152 constitutes a negative regulator of Plk4 at centrioles. However, we could also show that only co-depletion of Cep152 and Cep192 completely prevented centriolar Plk4 recruitment, thus arguing against such a role of Cep152 at centrioles.

Among known centriole duplication factors identified so far, Cep152 (in complex with Cep63), Cep192 and CPAP surrounded mother centrioles independently of Plk4 levels (this study and Sir et al., 2011). Other factors such as Sas-6 only form a ring around centrioles in Plk4-overexpressing cells (Kleylein-Sohn et al., 2007). The ring-like localization of Cep152 and Cep192 is not surprising, as we could show that they function in the recruitment of Plk4 to centrioles. However, the localization of endogenous CPAP at high resolution without Plk4 overexpression implies that CPAP might also localize and serve as building platform around the complete mother centriole independently of Plk4 levels.

Remarkably, Plk4 remained confined at one particular spot on the circumference of mother centrioles at different cell cycle stages independently of the presence of Sas-6. These data suggest that the site of centriole duplication is determined before the recruitment of Sas-6 to nascent centrioles and that Plk4 represents an early marker for this site on the mother centriole. Finally, the confined Plk4 localization inbetween mother and daughter centrioles throughout the cell cycle could also explain why mother centrioles can only re-duplicate after centriole disengagement at the M-G1 transition, when Plk4 becomes accessible for another round of duplication.

6.2.5 Summary

Here, we have used super-resolution microscopy to get a better understanding of the architecture of human centrosomes. Our study illustrates the power of 3D-SIM for investigating protein localization within an organelle whose small dimensions - barely above the Abbe diffraction limit - restrict the applicability of conventional light microscopy.

In total, we have investigated the disposition of 18 different proteins within substructures of centrosomes, i.e. centrioles, appendages and surrounding PCM. On the one hand, we strengthen several conclusions that had previously been inferred from immuno-EM studies.

On the other hand, we report several novel observations. In particular, we show that in mitotic cells individual PCM components form a meshwork into which γTuRCs are inserted and thus confirm previous suggestions on the amorphous nature of the PCM. Conversely, in interphase cells the PCM is highly ordered with defined diameters surrounding the centrioles. In addition, we show that Cep135, a suspected cartwheel protein, does not extensively co-localize with Sas-6, a documented cartwheel protein. Most interestingly, we show that the regulatory kinase Plk4 marks the site of daugther centriole formation on the circumference of the mother centriole, before Sas-6 can be detected on the site of procentriole assembly.

7 Appendix

Table 3 Potentially centrosome-relevant proteins identified by immunoprecipitation with antibody Cep152-C analyzed by SDS PAGE, gel excision and mass spectrometry.

Accession	Description	Peptide count	Count PI	Count Cep152	Max fold change	Confidence score
O94986	Centrosomal protein of 152 kDa (Cep152)	37	0	34	6.273046289	1592.67
O94986_ISOFORM_2	Centrosomal protein of 152 kDa (Cep152) [ISOFORM 2]	26	0	22	3.629304791	1050.65
Q9UGJ1	Gamma-tubulin complex component 4 (GCP-4) (hGCP4) (h76p)	7	0	6	4.688194294	237.48
Q9BSJ2	Gamma-tubulin complex component 2 (GCP-2) (hGCP2) (hSpc97) (h103p)	7	0	5	1.663319	227.8
Q96RT7	Gamma-tubulin complex component 6 (GCP-6)	9	1	5	1.294291431	276.79
Q96CW5	Gamma-tubulin complex component 3 (GCP-3) (hGCP3) (hSpc98) (h104p)	9	0	6	2.025075475	203.2
Q96RT8	Gamma-tubulin complex component 5 (GCP-5)	7	0	5	2.823972908	259.83
P23258	Tubulin gamma-1 chain (GCP-1)	4	0	4	1.366956026	225.21
O15078	Centrosomal protein of 290 kDa (Cep290) (CT87)	8	1	3	1.443394926	114.31
Q6PGQ7	Protein aurora borealis (HsBora)	16	0	16	6.595785598	987.7
P53350	Serine/threonine-protein kinase PLK1 (PLK-1) (STPK13)	6	0	4	6.897816067	227.69
P30153	Serine/threonine-protein phosphatase 2A 65 kDa regulatory subunit A alpha isoform	5	0	4	5.984782068	196.29
Q12888	Tumor suppressor p53-binding protein 1 (p53-binding protein 1) (p53BP1) (53BP1)	18	0	11	3.265489594	749.81
P04637	Cellular tumor antigen p53	10	0	8	12.84061011	322.81
Q13416	Origin recognition complex subunit 2	7	0	6	4.087643685	259.42
Q7L5D6	UPF0363 protein C7orf20	7	0	8	31.18390693	490.85
Q9BTL3	Protein FAM103A1	6	1	6	2.519518464	220.25

Table 4 Potentially centrosome-relevant proteins identified by immunoprecipitation with Cep152 antibody analyzed by mass spectrometry.

Accession	Description	Peptide count	Confidence score	Max fold change	Mean Scaled to Baseline, ratio 207 (Median)	934 (Median)
O94986	Centrosomal protein of 152 kDa (Cep152)	34	1989.25	3.905211627	4.369573318	2.313467995
O94986_ISOFORM_2	Centrosomal protein of 152 kDa (Cep152) [ISOFORM 2]	24	1523.73	2.754055707	4.824239377	1.653907244
Q9BSJ2	Gamma-tubulin complex component 2 (GCP-2) (hGCP2) (hSpc97) (h103p)	4	155.66	29.96963508	1.413725763	15.05470881
Q96CW5	Gamma-tubulin complex component 3 (GCP-3) (hGCP3) (hSpc98) (h104p)	3	95.65	34.23089002	5.798321896	16.34696824
Q9UGJ1	Gamma-tubulin complex component 4 (GCP-4) (hGCP4) (h76p)	3	122.91	5.474743255	3.834215267	3.256565556
Q96RT8	Gamma-tubulin complex component 5 (GCP-5)	1	74.49	61.00894052	1.372810111	18.43250286
Q96RT7	Gamma-tubulin complex component 6 (GCP-6)	2	58.56	16.92746741	0.173204296	0.184651642
P23258	Tubulin gamma-1 chain (GCP-1)	6	241.85	9.702167306	4.154961782	6.28928658
Q7Z7A1	Centriolin	2	57.03	701.1574159	6161435.867	2248677.322
P06748	Nucleophosmin (NPM)	2	115.08	3.963051743	2.820084137	2.054416973
Q13416	Origin recognition complex subunit 2	1	62.62	26.49115865	3.487420294	19.71147416
Q9UBD5	Origin recognition complex subunit 3	1	42.07	5.843151139	6.218805791	5.367252098
P53350	Serine/threonine-protein kinase PLK1 (PLK-1) (STPK13)	1	47.05	6.312413127	4.315509617	3.705108057
P30153	Serine/threonine-protein phosphatase 2A 65 kDa regulatory subunit A alpha isoform	1	44.25	19.21978434	24.83262239	36.23038323
P36873	Serine/threonine-protein phosphatase PP1-gamma catalytic subunit (PP-1G)	2	97.53	3.140087745	3.149793698	1.929078029

Table 5 Measurement of distances between intensity maxima of centriolar proteins that localize in ring-like patterns around centrioles.

Protein	Localization	Diameter (nm)	# Analyzed Centrioles	M (kDa)	Antigen
glut. Tubulin	Centriole Wall	166.3 +- 20.5	40	55 (Tubulin)	C-Terminus (AA 441-448)
Cep135	Centriole Wall	170.0 +- 9.7	40	135	C-Terminus (AA 745-1218)
CP110	Centriole Wall	165.0 +- 6.6	18	110	N-Terminus (AA 1-149)
Cep192 mother	Inner PCM	281.3 +- 0.5	37	279	C-Terminus (AA 1441-1938)
Cep192 daughter	Inner PCM	217.8 +- 6.6	15	279	C-Terminus (AA 1441-1938)
NEDD1 mother	Inner PCM	300.1 +- 3.5	22	72	C-Terminus (AA 561-661)
NEDD1 daughter	Inner PCM	217.8 +- 17.8	8	72	C-Terminus (AA 561-661)
Cep152-C	Inner PCM	309.6 +- 3.5	64	189	C-Terminus (AA 1378-1654)
Cap350 mother	Inner PCM	313.3 +- 31.5	17	351	Middle (AA 2115-2643)
Cap350 daughter	Inner PCM	279.5 +- 14.0	2	351	Middle (AA 2115-2643)
Cep152-N	Intermediate PCM	414.4 +- 2.9	54	189	N-Terminus (AA 1-87)
Cep215	Intermediate PCM	429.4 +- 9.3	21	215	Middle (AA 503-1010)
γ-Tubulin mother	Intermediate PCM	433.3 +- 16.6	39	51	N-Terminus (AA 38-53)
γ-Tubulin daughter	Intermediate PCM	262.4 +- 49.5	4	51	N-Terminus (AA 38-53)
CPAP	Outer PCM	498.7 +- 19.1	23	153	C-Terminus (AA 1070-1337)
Pericentrin	Outer PCM	499.0 +- 46.5	10	378	N-Terminus (AA 100-600 of mouse Pericentrin 1)
Cep164	Distal appendages	394.1 +- 4.1	30	164	N-Terminus (AA 1-298)
Cep170	Subdistal appendages	540.3 +- 56.8	7	170	N-Terminus (AA 15–754)
Ninein	Subdistal appendages	552.7 +- 10.2	24	244	N-Terminus (AA 1110–2662)

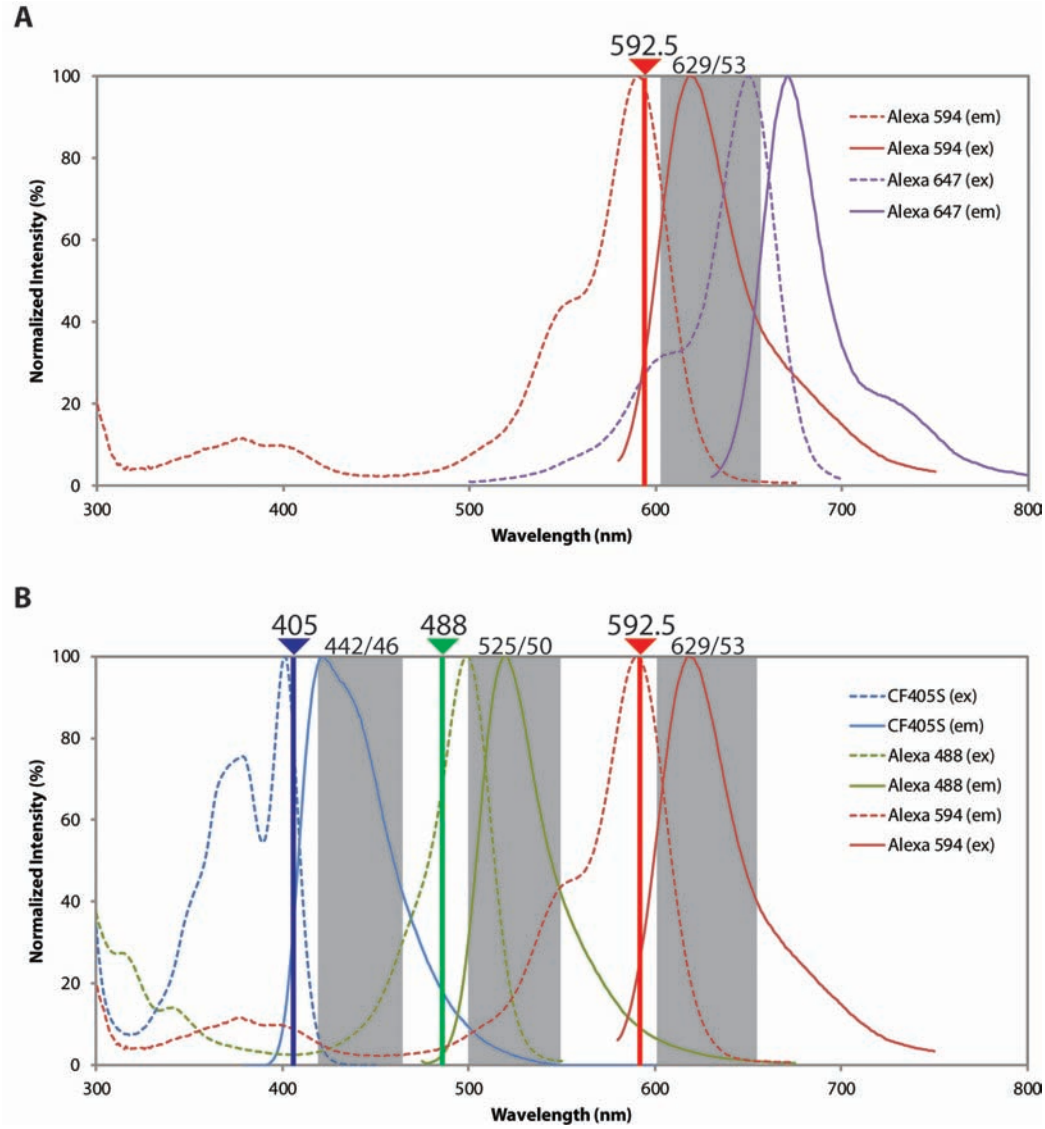

Figure 94 Excitation and emission spectra of the applied fluorophores. Excitation and emission spectra of the applied fluorophores were plotted with the used laser lines and band-pass filters. **A** The 592.5 nm laser only weakly excites Alexa 647 fluorophores, of which only a small fraction of its emission is detected by the 629/53 filter. **B** In consecutive acquisition mode no bleedthrough between blue, green and red channel is possible.

8 Materials and Methods

Sequence Analysis

Cep152 and Cep192 protein sequences were analyzed by the PsiPred server for secondary structure predictions (http://bioinf.cs.ucl.ac.uk/psipred). For identifying motifs and domains, sequences were analysed using ScanProsite (http://prosite.expasy.org/scanprosite), whereas coiled-coil domains were scored using the COILS program (http://www.ch.embnet.org/software/COILS_form.html). Protein alignments were performed using ClustalW2 (www.ebi.as.uk/Tools/mca/clustalw2) and visualized with Espript (espript.ibcp.fr).

Chemicals and Materials

All chemicals were purchased from Merck, Sigma-Aldrich Chemical Company (Sigma, St. Louis, MO), Fluka-Biochemika (Buchs, Switzerland) or Roth (Karlsruhe, Germany) unless otherwise stated. Components for growth media for *E. coli* were from Difco Laboratories (Lawrence, KS) or Merck (Darmstadt, Germany). The Minigel system was purchased from Bio-Rad., tabletop centrifuges were from Eppendorf.

Plasmids and Cloning

Cloning of Plk4, NEDD1, CPAP, STIL, Sas-6, Cep135, Plk1, Cep63, CP110, Cep192 isoform 2 (**Figure 17**), Cep152 clone KIAA0912 and βTrCP1 cDNA has been described previously (Golsteyn et al., 1994; Andersen et al., 2003; Habedanck et al., 2005; Cho et al., 2006; Luders et al., 2006; Gomez-Ferreria et al., 2007; Kleylein-Sohn et al., 2007; Chan et al., 2008; Kim et al., 2008; Schmidt et al., 2009; Sir et al., 2011; Arquint et al., 2012).

cDNA of Cep152 isoform 2 was amplified from a HeLa cDNA library. To this end, RNA was isolated from HeLa cells using the RNeasy Mini kit (QIAGEN) according to the manufacturer's instructions. RT-PCR was performed using Superscript III Reverse Transcriptase (Invitrogen) with oligo-dT primers (Invitrogen). Using the Polymerase Pfu Ultra II kit (Agilent Technologies) Cep152 cDNA was amplified with sequence-specific

primers (for details see **Table 6**). Similarly, cDNA of Cep192 isoform 1 was obtained by amplifying the N-terminus of Cep192 isoform 1 (1 – 3986 bp) from a U2OS cDNA library and ligating this into a construct containing Cep192 isoform 2 after restriction with KpnI (for details see **Table 6** and **Table 7**).

Table 6 Primers used in this study.

Name	Sequence	Purpose
Cep152 nest f	CGCGGTAACAGCCTCCGTGGC	Cloning of Cep152 from cDNA library
Cep152 nest r	GAGGTCTTCCCTTCCATTTTTG	Cloning of Cep152long from cDNA library
Cep152 nest ru	CTATCATTTCGAGGGATGGAAGC	Cloning of Cep152long from cDNA library
Cep152 f1 Kpn1	GCGGGTACCCATGTCATTAGACTTTGGCAGTGTGG	Cloning of Cep152 into COM210 and COM229
Cep152 r1 Xho1	GCGCTCGAGTTAGTCTAGATTAACAAATGGGCTATC	Cloning of Cep152long into COM210 and COM229
Cep152 ru1 Xho1	GCGCTCGAGTCACTTTGACATACCTGACTGTGTAG	Cloning of Cep152short into COM210 and COM229
Cep152 f5 Fse1	GCGGGCCGGCCCCATGTCATTAGACTTTGGCAGTGTGG	Cloning of Cep152 into COM235
Cep152 f3 Sma1	GCGCCCGGGATGTCATTAGACTTTGGCAGTGTGG	Cloning of Cep152 into COM56
Cep152 r3 Not1	GCGGCGGCCGCTTAGTCTAGATTAACAAATGGGCTATC	Cloning of Cep152long into COM235 and COM56
Cep152 ru3 Not1	GCGGCGGCCGCTCACTTTGACATACCTGACTGTGTAG	Cloning of Cep152short into COM235 and COM56
Cep152 Nfw NotI	GCGGCGGCCGCCATGTCATTAGACTTTGGCAGTGTGG	Cloning of Cep152-2 AA 1 – 87 into COM238 for AB production
Cep152 Nrv3 XhoI	GCGCTCGAGTTAATTTACACTTTGAGATTTGGGCAGC	Cloning of Cep152-2 AA 1 – 87 into COM238 for AB production
Cep152 Cfw NotI	GCGGCGGCCGCCATGGTGGGATCCAAAGAGACACATTTG	Cloning of Cep152-2 AA 1378 - 1654 into COM238 for AB

		production
Cep152 Crv XhoI	GCGCTCGAGTTAGTCTAGATT AACAAATGGGCTATC	Cloning of Cep152-2 AA 1378 - 1654 into COM238 for AB production
Cep152-fw	ATGTCATTAGACTTTGGCAGT GTGGCAC	Amplification primer for RT-PCR
Cep152-long-rv	TTAGTCTAGATTAACAAATGG GCTATCAAAGCCACTATC	Amplification primer for RT-PCR
Cep152-short-rv	TCACTTTGACATACCTGACTG TGTAGTTTTGCTTTG	Amplification primer for RT-PCR
Cep152_2C_fw_KpnI	GCGGGTACCCTCAGCACTGCC CCTAACTTC	Cloning of Cep152-2 AA 1380 – 1654 into COM210
Cep152_M_fw_KpnI	GCGGGTACCCCTGCAACAAC AATTTTTAGGAGCTAATG	Cloning of Cep152-2 AA 221 – 1380 into COM210
Cep152_2M_rv_XhoI	GCGCTCGAGTCATGACTGTGT AGTTTTGCTTTGGGAC	Cloning of Cep152-2 AA 221 – 1380 into COM210
Cep152_N_rv_XhoI	GCGCTCGAGTCAGCCTTCGAA TGTGTCACTTCC	Cloning of Cep152-2 AA 1 – 220 into COM210
Cep152_2C_fw2_FseI	GCGGGCCGGCCCCTCAGCACT GCCCCTAACTTC	Cloning of Cep152-2 AA 1380 – 1654 into COM235
Cep152_M_fw2_FseI	GCGGGCCGGCCCCCTGCAAC AACAATTTTTAGGAGCTAATG	Cloning of Cep152-2 AA 221 – 1380 into COM235
Cep152_2M_rv2_NotI	GCGGCGGCCGCTCATGACTGT GTAGTTTTGCTTTGGGAC	Cloning of Cep152-2 AA 221 – 1380 into COM235
Cep152_N_rv2_NotI	GCGGCGGCCGCTCAGCCTTCG AATGTGTCACTTCC	Cloning of Cep152-2 AA 1 – 220 into COM235
Cep152_SSPA2_fw2	GGATGACGACCTCGCCGCTCC AGAGCTCCAG	Mutagenesis primer Cep152 S47A/S48A
Cep152_SSPA2_rv2	CTGGAGCTCTGGAGCGGCGA GGTCGTCATCC	Mutagenesis primer Cep152 S47A/S48A
Cep152_SSPA_fw1x	CTGGATGACGACCTCTCCGCT CCAGAGCTCCAGTATTCG	Mutagenesis primer Cep152 S47A
Cep152_SSPA_rv1x	CGAATACTGGAGCTCTGGAGC GGAGAGGTCGTCATCCAG	Mutagenesis primer Cep152 S47A
Cep152_DSGA_fw1x	GCTATCTAGCCAACAAGATGC	Mutagenesis primer Cep152long

	TGGCTTTGATGCCCCATTTGT TAATCTAGAC	S1644A/S1648A
Cep152_DSGA_rv1x	GTCTAGATTAACAAATGGGGC ATCAAAGCCAGCATCTTGTTG GCTAGATAGC	Mutagenesis primer Cep152long S1644A/S1648A
Cep152-277mut-fw	GACTATGCAGGAAGCCAAAA GAATTCAGTTAGAGATTTATC AGTATGAGGAAGAC	Mutagenesis Primer Cep152 for 277 Oligoresistance
Cep152-277mut-rv	GTCTTCCTCATACTGATAAAT CTCTAACTGAATTCTTTTGGC TTCCTGCATAGTC	Mutagenesis Primer Cep152 for 277 Oligoresistance
Cep152-747mut-fw	GTGAAGAAGGATGAAAAATC AATAGAAGTAGAAACAAAAA CAGATACCTCAGAAAAAC	Mutagenesis Primer Cep152 for 747 Oligoresistance
Cep152-747mut-rv	GTTTTTCTGAGGTATCTGTTTT TGTTTCTACTTCTATTGATTTT TCATCCTTCTTCAC	Mutagenesis Primer for 747 Oligoresistance
Cep152_dpbd_fw1_KpnI	GCGGGTACCCATGCTGGATGA CGACCTCTC	Cloning of Cep152-2 AA 46 – 1654 into COM210 and COM229
NEDD1-fw-KpnI	TTTGGTACCCATGCATTTTAC AGGCGCAG	Cloning of NEDD1 into COM210 and COM229
NEDD1_rv_XhoI	TTTCTCGAGTCAAAAGTGGGC CCGTAATC	Cloning of NEDD1 into COM210 and COM229
Cep63-fw-BamHI	TTTTGGATCCATGGAGGCTTT GTTAGAAGGAATACAAAATC	Cloning of Cep63 into COM210 and COM229
Cep63-rv-XhoI	TTTTCTCGAGCTACTTTAAGG CTGTGAATTGTCTCACTG	Cloning of Cep63 into COM210 and COM229
Cep192-001-fw2-FseI	TTTTGGCCGGCCAAATGGAAG ATTTTCGAGGTATAGCAGAAG AATC	Cloning of Cep192 isoform 1 into COM235
Cep192-001-rv2-NotI	TTTTGCGGCCGCTTAATTTTTT CCAAGAGCTTCACCAATTAGT CG	Cloning of Cep192 isoform 1 into COM235
Cep192-001-M-KpnI-rv	CAGAGGGAAGAGGTACCCAT CCATC	Cloning of Cep192-1 bp 1 - 3986 into Cep192-2

Cep192-N-rv1_NotI	TTTTGCGGCCGCTTAACCAGAGGAAAATGGTAACATACCATC	Cloning of Cep192-1 AA 1 - 330 into COM235
Cep192-N-rv2_NotI	TTTTGCGGCCGCTTACAGATCAAAACCACCTCTATTGGC	Cloning of Cep192-1 AA 1 - 386 into COM235
Cep192-2-fw_FseI	AAAGGCCGGCCAAATGGAAGATTTTCGAGGTATAGCAG	Cloning of Cep192 isoform 2 into COM235
Cep192-2-rv_NotI	AAAGCGGCCGCTTAATTTTTTCCAAGAGCTTCACCAA	Cloning of Cep192 isoform 2 into COM235

All cloning procedures were performed according to standard techniques as described in "Molecular Cloning: A Laboratory Manual" (Sambrook, 1989; 2nd edition) and "Current Protocols in Molecular Biology" (Wiley, 1999). Restriction enzymes were purchased from Fermentas (Burlington, Ontario, Canada) and ligation reactions were performed using T4 DNA ligase (NEB, Ipswich, MA). Plasmid purifications and DNA extractions from agarose gels were done as specified by the supplier (QIAGEN). Sequence mutations in Cep152 were inserted by using the QuickChange site-directed mutagenesis kit (Stratagene) according to the manufacturer's instructions using specific primers. For a complete list of primers used in this study see **Table 6**. All initial plasmids were checked by DNA sequencing at Medigenomix (Martinsried, Germany) or Microsynth (Basel, Switzerland). For a list of plasmids used in this study see **Table 7**.

Table 7 Plasmids used in this study.

Name	cDNA	Tag	Vector	Cloning Strategy
KFM26	Cep152 C	His	pET28b mod	PCR from KFM61, 834 bp, into COM238, 5'NotI, 3'XhoI
KFM29	Cep152 N3	His	pET28b mod	PCR from KFM61, AS 1-87, 1 – 261 bp, into COM238, 5'NotI, 3'XhoI
KFM56	Cep152 4	N3xmyc	pcDNA3.1	PCR from JW380, into COM210, 5'KpnI, 3'XhoI
KFM57	Cep152 4	NFLAG	pcDNA3.1	PCR from KFM56, into COM235, 5'FseI, 3'NotI

KFM61	Cep152 2	/	pCR-XL-TOPO	clone IRCMp5012G0825D from Imagenes
KFM62	Cep152 2	N3xmyc	pcDNA3.1	PCR from KFM 61, into COM210, 5'KpnI, 3'XhoI
KFM63	Cep152 2	NFLAG	pcDNA3.1	cut from KFM62, into COM229, 5'KpnI, 3'XhoI
KFM64	Cep152 2 N	N3xmyc	pcDNA3.1	PCR from KFM62, AS 1 - 220, into COM210, 5'KpnI, 3'XhoI
KFM65	Cep152 2 M	N3xmyc	pcDNA3.1	PCR from KFM62, AS 221 - 1308, into COM210, 5'KpnI, 3'XhoI
KFM66	Cep152 2 C	N3xmyc	pcDNA3.1	PCR from KFM62, AS 1308 - 1654, into COM210, 5'KpnI, 3'XhoI
KFM67	Cep152 2 NM	N3xmyc	pcDNA3.1	PCR from KFM62, AS 1 - 1308, into COM210, 5'KpnI, 3'XhoI
KFM68	Cep152 2 MC	N3xmyc	pcDNA3.1	PCR from KFM62, AS 1308 - 1654, into COM210, 5'KpnI, 3'XhoI
KFM69	Cep152 2 N	NFLAG	pcDNA3.1	PCR from KFM62, AS 1 - 220, into COM235, 5'FseI, 3'NotI
KFM70	Cep152 2 M	NFLAG	pcDNA3.1	PCR from KFM62, AS 221 - 1308, into COM235, 5'FseI, 3'NotI
KFM71	Cep152 2 C	NFLAG	pcDNA3.1	PCR from KFM62, AS 1308 -1654, into COM235, 5'FseI, 3'NotI
KFM72	Cep152 2 NM	NFLAG	pcDNA3.1	PCR from KFM62, AS 1 - 1308, into COM235, 5'FseI, 3'NotI
KFM73	Cep152 2 MC	NFLAG	pcDNA3.1	PCR from KFM62, AS 1308 - 1654, into COM235, 5'FseI, 3'NotI
KFM74	NEDD1	N3xmyc	pcDNA3.1	PCR from JK78, into Com210, 5'KpnI, 3'XhoI
KFM75	Cep152 2 SSPA2	N3xmyc	pcDNA3.1	Mutagenesis PCR from KFM62, SSP -> AAP, COM210, 5'KpnI, 3'XhoI
KFM78	NEDD1	NFLAG	pcDNA3.1	cut from KFM74, into COM229, 5'KpnI, 3'XhoI
KFM91	Cep152 2 C DSGA	N3xmyc	pcDNA3.1	mutagenesis from KFM66, AS 1308 - 1654, S1644A, S1648A
KFM98	Cep152 2	N3xmyc	pcDNA3.1	cut EcoRI-XhoI from KFM91 into

	DSGAA			KFM62
KFM99	beta-TrCP	NFLAG	pcDNA3.1	PCR from GU174 into COM229, BamHI and XhoI
KFM100	Cep152 2	N-GST	pGEX-5X-2	PCR from KFM61 into COM56, fSmaI, rNotI
KFM101	Cep152 4	N-GST	pGEX-5X-2	PCR from CW381 into COM56, fSmaI, rNotI
KFM102	Cep152 l 747 resist.	NFLAG	pcDNA3.1	mutagenesis from KFM63
KFM103	Cep152 l 277 resist.	NFLAG	pcDNA3.1	mutagenesis from KFM63
KFM106	Cep152 s 747 resist.	NFLAG	pcDNA3.1	mutagenesis from KFM57
KFM107	Cep152 s 277 resist.	NFLAG	pcDNA3.1	mutagenesis from KFM57
KFM110	Cep63	Flag	Tag2b	Sir et al. (2011)
KFM111	Cep63	NFLAG	pcDNA3.1	PCR from KFM110
KFM112	Cep192-2	GFP	pEGFP	Gomez-Ferreria et al. (2007)
KFM113	Cep192-2	NFLAG	pcDNA3.1	PCR from KFM112
KFM114	Cep192-1	NFLAG	pcDNA3.1	PCR of bp 1 - 3986 ligated into KFM113
KFM115	Cep192-1 AA 1 - 519	NFLAG	pcDNA3.1	PCR from KFM114
KFM116	Cep192-1 AA 1 - 386	NFLAG	pcDNA3.1	PCR from KFM114
KFM117	Cep192-1 AA 1 - 330	NFLAG	pcDNA3.1	PCR from KFM114
KFM118	Cep192-1	N3xmyc	pcDNA3.1	PCR from KFM114
CA01	STIL	NFLAG	pcDNA3.1	Arquint et al. (2012)
CA02	STIL	N3xmyc	pcDNA3.1	Arquint et al. (2012)
GU104	Sas-6	NFLAG	pcDNA3.1	Kindly provided by G. Guderian
AG04	Cep135	N3xmyc	pcDNA3.1	Kindly provided by A. Gabryjonczyk
AG05	Cep135	NFLAG	pcDNA3.1	Kindly provided by A. Gabryjonczyk
AH30	Plk1	NFLAG	pcDNA3.1	Hanisch et al. (2006)
TS24	CP110	NFLAG	pcDNA3.1	Schmidt et al. (2009)
TS36	CPAP	N3xmyc	pcDNA3.1	Schmidt et al. (2009)

TS34	CPAP	NFLAG	pcDNA3.1	Schmidt et al. (2009)
JW127	Plk4	NFLAG -TO	pcDNA3.1	Guderian et al. (2010)
JW153	Plk4	N3xmyc -TO	pcDNA3.1	Guderian et al. (2010)
HR9	Plk4	N3xmyc	pcDNA3.1	Habedanck et al. (2005)

Antibodies

Polyclonal rabbit antibodies against His-tagged Cep152 (aa1-87 and aa1378-1654) were raised at Charles River Laboratories (Elevages Scientifique des Dombes, Charles River Laboratories, Romans, France) and then purified according to standard protocols. Anti-CPAP, anti-Sas-6, polyclonal anti-Plk4 and anti-Cep135 (Kleylein-Sohn et al., 2007), anti-CP110 and anti-Cep192 (Schmidt et al., 2009), anti-centrin-3 (Thein et al., 2007), anti-Cep164 and anti-Ninein (Graser et al., 2007), anti-Cep215 (Graser et al., 2007), anti-Cap350 (Yan et al., 2006), anti-Cep170 (Guarguaglini et al., 2005), anti-STIL (Arquint et al., 2012) and monoclonal anti-Plk4 (Guderian et al., 2010) have been described previously. A polyclonal antibody against Cep63 was kindly provided by F. Gergely (Cambridge, UK; Sir et al. (2011)) and a monoclonal antibody against Plk4, which was used Western Blotting of endogenous Plk4 in this study, was kindly provided by I. Hoffmann (Heidelberg, Germany; Cizmecioglu et al. (2010)). NEDD1, α-Tubulin, γ-Tubulin, Pericentrin, GT335 and Flag antibodies were purchased from Sigma (Taufkirchen, Germany). AlexaRed-594-, Alexa-555-, AlexaGreen-488-, AlexaCy5-647-labelled secondary anti-mouse and anti-rabbit antibodies were purchased from Invitrogen (Carlsbad, CA, USA) and CF405S-labelled secondary anti-mouse and anti-rabbit antibodies were purchased from Biotium. To simultaneously visualise different polyclonal rabbit antibodies, these were directly labelled by AlexaRed-594, AlexaRed-555, AlexaGreen-488 and AlexaCy5-647 fluorophores, using the corresponding Antibody Labeling Kits (Invitrogen). Whenever required, secondary antibodies were blocked using anti-Flag antibodies prior to the incubation with directly coupled antibodies of the same species.

Cell Culture and Transfections

All cells were grown at 37°C in a 5% CO_2 atmosphere. HeLa, U2OS or HEK 293T cells were cultured in Dulbecco's modified Eagle's medium (DMEM), supplemented with 10% heat-inactivated fetal calf serum (FCS, PAN Biotech, Aidenbach, Germany) and penicillin-streptomycin (100 µg/ml, Gibco-BRL, Karlsruhe, Germany). Cells adherent on acid treated glass coverslips were transiently transfected using TransIT (Mirus Bio, Madison, WI) according to the manufacturer's protocol. Transient transfections of HEK 293T or U2OS cells were performed using TransIT-LT1 transfection reagent (Mirus Bio, Madison, WI) according to the manufacturer's protocol. hTERT-RPE1 cells were cultured in DMEM Nutrient Mixture F-12 Ham (Sigma, Munich, Germany) supplemented with 10 % FCS (as above), penicillin/streptomycin (as above), 1 % glutamine (PAN Biotech, Aidenbach, Germany; 200 mM), and 0.35 % sodium bicarbonate (Sigma, Munich, Germany).

The tetracycline-inducible U2OS myc-Plk4-WT cell line (U2OS:myc-Plk4-WT) has been described previously (Kleylein-Sohn et al., 2007). A tetracyclin-inducible cell-line expressing myc-tagged kinase-dead Plk4 (U2OS:myc-Plk4-KD) was generated by transfection of U2OS T-REx cells (Invitrogen). Stable transformants were established by selection for 2 weeks with 1 mg/ml G418 (Invitrogen) and 50 µg/ml hygromycin (Merck). U2OS cells were cultured as described previously (Habedanck et al., 2005) and myc-Plk4 expression was induced by the addition of 1 µg/ml of tetracyclin.

To induce S-phase arrests, cells were either incubated with 1.6 µg/ml aphidicolin or 2 mM thymidine. Cell cycle synchronizations in mitosis were performed by a single thymidine (2 mM) block followed by a release from thymidine for 12 h. Mitotic cell cycle arrest in prometaphase was induced by nocodazol (0.2 µg/ml) or monastrol (0.14 mM) treatment for 16 h and mitotic cells were isolated by mitotic shake-off. To inhibit Plk1 1 µM TAL was added (ZK-Thiazolidinone). Cdk was inhibited by adding 25 µM roscovitin (RO).

siRNA-Mediated Protein Depletion

Transfections were performed using Oligofectamin (Invitrogen) according to manufacturer's protocol. All siRNA duplex oligonucleotides were ordered from Qiagen, Hilden, Germany. For a complete list of siRNA duplex oligonucleotides used in this study see **Table 8**.

Table 8 siRNA oligonucleotides used in this study.

Target Gene	Target Sequence	#	Reference
GL2	CGTACGCGGAATACTTCGA	245	Elbashir et al. (2001)
Cep152	GCGGATCCAACTGGAAATCTA	277 (oligo Cep152-1)	Graser et al. (2007)
Cep152	GCATTGAGGTTGAGACTAA	747 (oligo Cep152-2)	this work
Cep192	AAGGAAGACATTTTCATCTCT	909 (oligo Cep192-1)	Zhu et al. (2008)
Cep192	CAGAGGAATCAATAATAAA	912 (oligo Cep192-2)	Gomez-Ferreria et al. (2007)
Plk4	CTGGTAGTACTAGTTCACCTA	302	Habedanck et al. (2005)
Sas-6	CTAGATGATGCTACTAAGCAA	295	Graser et al. (2007)
βTrCP	GTGGAATTTGTGGAACATC	488	Guardavaccaro et al. (2003)
Pericentrin	GCAGCTGAGCTGAAGGAGA	236	Dammermann and Merdes (2002)
Cep164	CAGGTGACATTTACTATTTCA	278	Graser et al. (2007)

MT Regrowth Assay

MT regrowth assays in asynchronously growing U2OS cells were performed by placing tissue culture plates on ice for 45 min, before MT regrowth was induced by the addition of prewarmed growth medium for the indicated time. Cells were then immediately fixed in -20° methanol and prepared for immunofluorescence.

Flow Cytometric Analysis

After transfection with siRNA duplexes, HeLa cells were detached by trypsinization and washed with ice-cold PBS. Cells were fixed in 70% ethanol, followed by an incubation for 30 minutes in PBS, 10µg/ml RNase A (Sigma-Aldrich) and 5µg/ml propidium iodide (Sigma-Aldrich). Analysis of the fixed cells was performed with a FACScan (Becton Dickinson) and the WinMDI software, according to the manufacturer's instructions.

Cell Extract Preparation

24 hours post transfection, HEK 293T cells were collected and washed in PBS and lysed on ice for 30 minutes in lysis buffer (50 mM Tris-HCl pH 7.4, 0.5% IgePal, 150 mM NaCl, 1 mM DTT, 50 mM NaF, 1 mM PMSF, 25 mM β-glycerophosphate, 1 mM vanadate, Complete Mini Protease Inhibitor Cocktail (Roche Diagnostics)). Lysates were cleared by centrifugation for 15 minutes at 13,000 g, 4°C.

Centrosome Purification

Human centrosomes were purified from the T-lymphocyte KE-37 cell line according to the protocols reported in Moudjou and Bornens (1994) and Andersen et al. (2003).

Recombinant Protein Purification

Poly-histidine tagged Cep152 fragments spanning either residues 1 – 87 or 1380 – 1654 were expressed in *E. coli* BL21 DE3and purified under denaturing conditions with Ni^{2+} NTA resin (QIAGEN) for antibody generation. Standard protocols were used.

GST-tagged Cep152-2 and Cep152-4 were expressed in *E. coli* BL21 DE3 and purified using N-Lauroylsarkosyl as detergent and Glutathione agarose beads (Amersham) as described previously (Frangioni and Neel, 1993).

Biochemical Assays

To assay protein degradation kinetics, translation was inhibited by the addition of 10 µg/ml cycloheximide for the indicated time and protein samples were analyzed by SDS-PAGE and Western Blotting after cell extract preparation.

For immunoprecipitations, the extracts were incubated with proteinG beads (GE Healthcare) and 5 µ g of the appropriate antibodies for 1.5 hours at 4°C. Immunocomplexes bound to beads were washed three times with wash buffer (50 mM Tris-HCl pH 7.4, 1 % IgePal, 300

mM NaCl). Bound proteins were eluted by boiling in 2x SDS sample buffer, resolved by SDS-PAGE and analyzed by immunoblotting.

For *in vitro* binding assays, proteins were *in vitro* translated using the TNT-T7 quick coupled transcription/translation system (Promega) according to the manufacturer's protocol. For interaction studies immunoprecipitations were then performed as described above.

In vitro kinase assays using immunoprecipitated Cep152 or recombinant Cep152 were carried out at 30°C in kinase buffer (50 mM HEPES pH 7.0, 100 mM NaCl, 10 mM $MgCl_2$, 5% glycerol, 1 mM DTT). Kinases were kindly provided by G. Guderian (Plk4 kinase domain AA 1 – 430), E. Nigg (Plk1) and A. Wehner and A. Santamaria (CDK1 and Aurora A). Reactions were stopped after 30 minutes by addition of sample buffer. Samples were then analyzed by SDS-PAGE or immunoblotting and autoradiography.

Mass Spectrometry

Proteins were either analyzed by mass spectrometry after SDS-PAGE (1) or directly after elution from beads (2).

First, proteins isolated by co-immunoprecipitation with Cep152 antibodies were kindly analysed by K. Dulla and R. Körner (Max-Planck Institute of Biochemistry, Martinsried, Germany) as described previously (Sauer et al., 2005). Briefly, Coomassie Blue stained protein bands were in-gel digested by trypsin (Promega, sequencing grade). Peptides were desalted and concentrated using C18 extraction tips and analyzed according to standard protocols.

Second, after co-immunoprecipitation with Cep152 antibodies proteins were directly eluted and kindly analysed by M. Bauer and A. Schmidt of the Mass Spectrometry Core Facility (Biozentrum Basel, Switzerland). Standard protocols were employed.

Fluorescence Microscopy Techniques

Cells were fixed in methanol for 5 minutes at −20°C. Antibody incubations and washings were performed as described previously (Meraldi et al., 1999). Super-resolution 3D-SIM

imaging was performed with a DeltaVision OMX V3 system (Applied Precision) equipped with a 100x/1.40 NA PlanApo oil immersion objective (Olympus), Cascade II:512 EMCCD cameras (Photometrics) and 405, 488 and 592 nm diode lasers and appropriate emission filters. SI reconstruction and image processing was performed with the SoftWoRx 3.7 imaging software package (Applied Precision). For analyses of co-localizations we aligned the acquired channels using fluorescent beads (Invitrogen) fixed on the same slides as references. To rule out bleedthrough between channels, each channel was acquired sequentially. This way, the applied 3D-SIM with the three laser lines 405 nm, 488 nm and 592.5 nm in combination with the used bandpass filters allowed us to detect each channel separately without any bleedthrough (**Figure 94**).

Wide-field imaging was performed on a PersonalDV microscope system (Applied Precision) equipped with a 60x/1.42 PlanApo oil objective (Olympus), CoolSNAP ES2 interline CCD camera (Photometrics), Xenon illumination and appropriate filter sets for DAPI, FITC, TRITC and Cy5. Image stacks were recorded with a z-distance of 200 nm and subjected to a constrained iterative deconvolution (conservative ratio, 4 cycles, medium noise filtering, SoftWoRX, 3.7. imaging software package, Applied Precision). Motorized stage positions could be mapped between the two systems, allowing to re-locate cells for consecutive imaging on both systems. This coupled setup allowed us to image cells with conventional wide-field deconvolution microscopy prior to super-resolution imaging to visualize Alexa-647-stained centrioles with the far-red reference channel to determine their orientation and age within a centriole pair whenever required. By this approach one could e.g. distinguish between the mature “mother centriole” and the orthogonally growing “daughter centriole”. Of note, the 592 nm laser line of the 3D-SI microscope excites Alexa-647 with only about 25 % efficiency of which only a minor fraction of the emitted signal transmits through the 629/53 bandpass filter. Accordingly, bleed-trough of the 647 nm signal can be neglected when detecting the Alexa-594 fluorophore signal with 3D-SIM (**Figure 94**).

For alignment we used fluorescent beads fixed on the same slides as the stained cells to adjust the alignment of the three detected channels. Moreover, we acquired each channel sequentially. Furthermore, the applied 3D-SIM with the three laser lines 405 nm, 488 nm and 592.5 nm in combination with the used bandpass filters allowed us to detect each channel separately without any bleedthrough (**Figure 94**). Based on this, we used Costes’ automatic threshold setting to determine Pearson’s coefficient, a value ranging from -1 to 1 with mutual

exclusiveness at -1, no co-localization at 0 and complete co-localization at 1 (Bolte and Cordelieres, 2006). In our experiments the value was always below 1, presumably due to the present – even though low – background. To account for three dimensionality, we additionally determined the distance between the geometric centers of the channels in addition (Bolte and Cordelieres, 2006). We defined proteins to co-localize whenever the distance was lower than the resolution limit of the microscope (130 nm x 130 nm x 300 nm).

For fluorescence intensity quantifications stainings were analyzed using a DeltaVision microscope on a Nikon TE200 base (Applied Precision), equipped with an APOPLAN 100×/1.4 N.A. oil-immersion objective. Serial optical sections obtained 0.2-µm apart along the *z*-axis were processed using a deconvolution algorithm and projected into one picture using Softworx. For quantitation of centrosomal protein levels with ImageJ, *z*-stacks were acquired with the same exposure and maximum-intensity projections were carried out. Background signal intensity was subtracted from CP110 and Plk4 signal intensity.

Electron Microscopy and Immunogold Labelling

Electron microscopy was kindly performed by Y.-D. Stierhof (ZMBP, University of Tübingen, Germany). For electron microscopy, cells were fixed with 2.5% glutaraldehyde (Sigma-Aldrich, Steinheim, Germany) in PBS for 60 min, stained with the indicated primary antibodies and nano-gold-labelled secondary antibodies, embedded in 2% low melting agarose (SeaPlaque Agarose; Marine Colloids, Rockland, USA) and post-fixed with 1% osmium tetroxide (Plano, Wetzlar, Germany) in PBS for another 60 min followed by staining with 1 % uranyl acetate (Science Services, München, Germany) in distilled water for 45 min. After dehydration with ethanol, cells were embedded for ultrathin sectioning in epoxy resin (Epon; Roth, Karlsruhe, Germany). Sections were stained with 1% uranyl acetate and lead citrate (Science Services, München, Germany) and viewed in a LEO 906 transmission electron microscope.

9 Abbreviations

All units are abbreviated according to the International Unit System.

AA: amino acid(s)

Ab: antibody

ATP: adenosine 5´-triphosphate

βTrCP: β-transducin repeat containing protein

bp: base pair(s)

BSA: bovine serum albumin

cDNA: complementary DNA

Cdk: Cyclin-dependent kinase

Cep: centrosomal protein

C. elegans: *Caenorhabditis elegans*

CHX: cycloheximide

CP110: centrosomal protein of 110 kDa

CPAP: centrosomal P4.1-associated protein

DAPI: 4´,6-diamidino-2-phenylindole

D. melanogaster: *Drosophila melanogaster*

DNA: deoxyribonucleic acid

DTT: dithiothreitol

DV: Deltavision

ECL: enhanced chemiluminescence

E. coli: *Escherichia coli*

EDTA: ethylenedinitrilotetraacetic acid

FCS: fetal calf serum

HCl: hydrochloric acid

HEPES: N-2-hydroxyethylpiperazine-N`-2-ethane sulfonic acid

IgG: immunoglobulin G

IF: immunofluorescence

IP: immunoprecipitation

IPTG: isopropyl-beta-D-thiogalactopyranoside

kDa: kilodalton

kd: kinase-dead

min: minute(s)

MT: microtubule

MTOC: microtubule-organizing centre

pAb: polyclonal antibody

PBD: polo-box domain

PBS: phosphate-buffered saline

PCM: pericentriolar material

PCR: polymerase chain reaction

Plk1: Polo-like kinase 1

Plk4: Polo-like kinase 4

PMSF: phenylmethylsulfonyl fluoride

RNA: ribonucleic acid

RT: room temperature; reverse transcription

Sak: Snk/Fnk akin kinase

SDS-PAGE: sodium dodecylsulfate polyacrylamid gelelectrophoresis

3D-SIM: Three-dimensional structured illumination microscopy

siRNA: small interference ribonucleic acid

TAL: ZK-Thiazolidinone

UTR: untranslated region (of mRNA)

WB: Western Blot

WT: wildtype

10 References

.

Andersen, J. S., C. J. Wilkinson, T. Mayor, P. Mortensen, E. A. Nigg and M. Mann (2003). "Proteomic characterization of the human centrosome by protein correlation profiling." Nature **426**(6966): 570-4.

Arquint, C., K. F. Sonnen, Y. D. Stierhof and E. A. Nigg (2012). "Cell-cycle-regulated expression of STIL controls centriole number in human cells." J Cell Sci Suppl.

Bahtz, R., J. Seidler, M. Arnold, U. Haselmann-Weiss, C. Antony, W. D. Lehmann and I. Hoffmann (2012). "GCP6 is a substrate of Plk4 and required for centriole duplication." J Cell Sci Suppl **125**(Pt 2): 486-96.

Blachon, S., J. Gopalakrishnan, Y. Omori, A. Polyanovsky, A. Church, D. Nicastro, J. Malicki and T. Avidor-Reiss (2008). "Drosophila asterless and vertebrate Cep152 Are orthologs essential for centriole duplication." Genetics **180**(4): 2081-94.

Blangy, A., H. A. Lane, P. d'Herin, M. Harper, M. Kress and E. A. Nigg (1995). "Phosphorylation by p34cdc2 regulates spindle association of human Eg5, a kinesin-related motor essential for bipolar spindle formation in vivo." Cell **83**(7): 1159-69.

Bobinnec, Y., M. Moudjou, J. P. Fouquet, E. Desbruyeres, B. Edde and M. Bornens (1998). "Glutamylation of centriole and cytoplasmic tubulin in proliferating non-neuronal cells." Cell Motil Cytoskeleton **39**(3): 223-32.

Bolte, S. and F. P. Cordelieres (2006). "A guided tour into subcellular colocalization analysis in light microscopy." J Microsc **224**(Pt 3): 213-32.

Bonaccorsi, S., M. G. Giansanti and M. Gatti (1998). "Spindle self-organization and cytokinesis during male meiosis in asterless mutants of Drosophila melanogaster." J Cell Biol **142**(3): 751-61.

Bond, J., E. Roberts, K. Springell, S. B. Lizarraga, S. Scott, J. Higgins, D. J. Hampshire, E. E. Morrison, G. F. Leal, E. O. Silva, S. M. Costa, D. Baralle, M. Raponi, G. Karbani, Y. Rashid, H. Jafri, C. Bennett, P. Corry, C. A. Walsh and C. G. Woods (2005). "A centrosomal mechanism involving CDK5RAP2 and CENPJ controls brain size." Nat Genet **37**(4): 353-5.

Boveri, T. (1888). "Zellenstudien I-VI." Jenaische Zeitschr. Naturwissen.

Boveri, T. (1914). "Zur Frage der Entstehung maligner Tumoren."

Carvalho-Santos, Z., P. Machado, P. Branco, F. Tavares-Cadete, A. Rodrigues-Martins, J. B. Pereira-Leal and M. Bettencourt-Dias (2010). "Stepwise evolution of the centriole-assembly pathway." J Cell Sci **123**(Pt 9): 1414-26.

Chan, E. H., A. Santamaria, H. H. Sillje and E. A. Nigg (2008). "Plk1 regulates mitotic Aurora A function through betaTrCP-dependent degradation of hBora." Chromosoma **117**(5): 457-69.

Cizmecioglu, O., M. Arnold, R. Bahtz, F. Settele, L. Ehret, U. Haselmann-Weiss, C. Antony and I. Hoffmann (2010). "Cep152 acts as a scaffold for recruitment of Plk4 and CPAP to the centrosome." J Cell Biol **191**(4): 731-9.

D'Angiolella, V., V. Donato, S. Vijayakumar, A. Saraf, L. Florens, M. P. Washburn, B. Dynlacht and M. Pagano (2010). "SCF(Cyclin F) controls centrosome homeostasis and mitotic fidelity through CP110 degradation." Nature **466**(7302): 138-42.

Dammermann, A. and A. Merdes (2002). "Assembly of centrosomal proteins and microtubule organization depends on PCM-1." J Cell Biol **159**(2): 255-66.

Delattre, M., C. Canard and P. Gonczy (2006). "Sequential protein recruitment in C. elegans centriole formation." Curr Biol **16**(18): 1844-9.

Dix, C. I. and J. W. Raff (2007). "Drosophila Spd-2 recruits PCM to the sperm centriole, but is dispensable for centriole duplication." Curr Biol **17**(20): 1759-64.

Eckerdt, F., T. M. Yamamoto, A. L. Lewellyn and J. L. Maller (2011). "Identification of a polo-like kinase 4-dependent pathway for de novo centriole formation." Current biology : CB **21**(5): 428-32.

Fliegauf, M., T. Benzing and H. Omran (2007). "When cilia go bad: cilia defects and ciliopathies." Nat Rev Mol Cell Biol **8**(11): 880-93.

Frangioni, J. V. and B. G. Neel (1993). "Solubilization and purification of enzymatically active glutathione S-transferase (pGEX) fusion proteins." Anal Biochem **210**(1): 179-87.

Fry, A. M., T. Mayor, P. Meraldi, Y. D. Stierhof, K. Tanaka and E. A. Nigg (1998). "C-Nap1, a novel centrosomal coiled-coil protein and candidate substrate of the cell cycle-regulated protein kinase Nek2." J Cell Biol **141**(7): 1563-74.

Fuller, S. D., B. E. Gowen, S. Reinsch, A. Sawyer, B. Buendia, R. Wepf and E. Karsenti (1995). "The core of the mammalian centriole contains gamma-tubulin." Current biology : CB **5**(12): 1384-93.

Goetz, S. C. and K. V. Anderson (2010). "The primary cilium: a signalling centre during vertebrate development." Nature reviews. Genetics **11**(5): 331-44.

Gomez-Ferreria, M. A., U. Rath, D. W. Buster, S. K. Chanda, J. S. Caldwell, D. R. Rines and D. J. Sharp (2007). "Human Cep192 is required for mitotic centrosome and spindle assembly." Curr Biol **17**(22): 1960-6.

Graser, S., Y. D. Stierhof, S. B. Lavoie, O. S. Gassner, S. Lamla, M. Le Clech and E. A. Nigg (2007). "Cep164, a novel centriole appendage protein required for primary cilium formation." J Cell Biol **179**(2): 321-30.

Graser, S., Y. D. Stierhof and E. A. Nigg (2007). "Cep68 and Cep215 (Cdk5rap2) are required for centrosome cohesion." J Cell Sci **120**(Pt 24): 4321-31.

Griffith, E., S. Walker, C.-A. Martin, P. Vagnarelli, T. Stiff, B. Vernay, N. A. Sanna, A. Saggar, B. Hamel, W. C. Earnshaw, P. A. Jeggo, A. P. Jackson and M. O'Driscoll (2007). "Mutations in pericentrin cause Seckel syndrome with defective ATR-dependent DNA damage signaling." Nat Gen.

Gul, A., M. J. Hassan, S. Hussain, S. I. Raza, M. S. Chishti and W. Ahmad (2006). "A novel deletion mutation in CENPJ gene in a Pakistani family with autosomal recessive primary microcephaly." J Human Genet **51**(9): 760-4.

Habedanck, R., Y. D. Stierhof, C. J. Wilkinson and E. A. Nigg (2005). "The Polo kinase Plk4 functions in centriole duplication." Nat Cell Biol **7**(11): 1140-6.

Haren, L., T. Stearns and J. Luders (2009). "Plk1-dependent recruitment of gamma-tubulin complexes to mitotic centrosomes involves multiple PCM components." PLoS ONE **4**(6): e5976.

Hatch, E. M., A. Kulukian, A. J. Holland, D. W. Cleveland and T. Stearns (2010). "Cep152 interacts with Plk4 and is required for centriole duplication." J Cell Biol **191**(4): 721-9.

Hinchcliffe, E. H., F. J. Miller, M. Cham, A. Khodjakov and G. Sluder (2001). "Requirement of a centrosomal activity for cell cycle progression through G1 into S phase." Science **291**(5508): 1547-50.

Hiraki, M., Y. Nakazawa, R. Kamiya and M. Hirono (2007). "Bld10p constitutes the cartwheel-spoke tip and stabilizes the 9-fold symmetry of the centriole." Curr Biol **17**(20): 1778-83.

Kim, K., S. Lee, J. Chang and K. Rhee (2008). "A novel function of CEP135 as a platform protein of C-NAP1 for its centriolar localization." Exp Cell Res **314**(20): 3692-700.

Kleylein-Sohn, J., J. Westendorf, M. Le Clech, R. Habedanck, Y.-D. Stierhof and E. A. Nigg (2007). "Plk4-Induced Centriole Biogenesis in Human Cells." Developmental Cell **13**(2): 190-202.

La Terra, S., C. N. English, P. Hergert, B. F. McEwen, G. Sluder and A. Khodjakov (2005). "The de novo centriole assembly pathway in HeLa cells: cell cycle progression and centriole assembly/maturation." J Cell Biol **168**(5): 713-22.

Luders, J. and T. Stearns (2007). "Microtubule-organizing centres: a re-evaluation." Nat Rev Mol Cell Biol **8**(2): 161-7.

Lupas, A., M. Van Dyke and J. Stock (1991). "Predicting coiled coils from protein sequences." Science **252**(5009): 1162-4.

Mikule, K., B. Delaval, P. Kaldis, A. Jurcyzk, P. Hergert and S. Doxsey (2007). "Loss of centrosome integrity induces p38-p53-p21-dependent G1-S arrest." Nat Cell Biol **9**(2): 160-70.

Moritz, M., M. B. Braunfeld, J. W. Sedat, B. Alberts and D. A. Agard (1995). "Microtubule nucleation by gamma-tubulin-containing rings in the centrosome." Nature **378**(6557): 638-40.

Moudjou, M. and M. Bornens (1994). Isolation of centrosomes from cultured animal cells. Cell Biology: A Laboratory Handbook. J. E. Celix. London, Academic Press**:** 595-604.

Nigg, E. A. (2007). "Centrosome duplication: of rules and licenses." Trends Cell Biol **17**(5): 215-21.

Nigg, E. A. and J. W. Raff (2009). "Centrioles, centrosomes, and cilia in health and disease." Cell **139**(4): 663-78.

Nigg, E. A. and T. Stearns (2011). "The centrosome cycle: Centriole biogenesis, duplication and inherent asymmetries." Nat Cell Biol **13**(10): 1154-60.

Paintrand, M., M. Moudjou, H. Delacroix and M. Bornens (1992). "Centrosome organization and centriole architecture: their sensitivity to divalent cations." J Struct Biol **108**(2): 107-28.

Palazzo, R. E., J. M. Vogel, B. J. Schnackenberg, D. R. Hull and X. Wu (2000). "Centrosome maturation." Curr Top Dev Biol **49**: 449-70.

Pan, J. and W. Snell (2007). "The primary cilium: keeper of the key to cell division." Cell **129**(7): 1255-7.

Pelletier, L., E. O'Toole, A. Schwager, A. A. Hyman and T. Muller-Reichert (2006). "Centriole assembly in Caenorhabditis elegans." Nature **444**(7119): 619-23.

Puklowski, A., Y. Homsi, D. Keller, M. May, S. Chauhan, U. Kossatz, V. Grunwald, S. Kubicka, A. Pich, M. P. Manns, I. Hoffmann, P. Gonczy and N. P. Malek (2011). "The SCF-FBXW5 E3-ubiquitin ligase is regulated by PLK4 and targets HsSAS-6 to control centrosome duplication." Nat Cell Biol **13**(8): 1004-9.

Reichert, W. M. and G. A. Truskey (1990). "Total internal reflection fluorescence (TIRF) microscopy. I. Modelling cell contact region fluorescence." J Cell Sci **96 (Pt 2)**: 219-30.

Rodrigues-Martins, A., M. Riparbelli, G. Callaini, D. M. Glover and M. Bettencourt-Dias (2007). "Revisiting the role of the mother centriole in centriole biogenesis." Science **316**(5827): 1046-50.

Rogers, S., R. Wells and M. Rechsteiner (1986). "Amino acid sequences common to rapidly degraded proteins: the PEST hypothesis." Science **234**(4774): 364-8.

Santamaria, A., B. Wang, S. Elowe, R. Malik, F. Zhang, M. Bauer, A. Schmidt, H. H. Sillje, R. Korner and E. A. Nigg (2011). "The Plk1-dependent phosphoproteome of the early mitotic spindle." Molecular & cellular proteomics : MCP **10**(1): M110 004457.

Sauer, G., R. Korner, A. Hanisch, A. Ries, E. A. Nigg and H. H. Sillje (2005). "Proteome analysis of the human mitotic spindle." Mol Cell Proteomics **4**(1): 35-43.

Schmidt, T. I., J. Kleylein-Sohn, J. Westendorf, M. Le Clech, S. B. Lavoie, Y. D. Stierhof and E. A. Nigg (2009). "Control of Centriole Length by CPAP and CP110." Curr Biol.

Seki, A., J. A. Coppinger, H. Du, C. Y. Jang, J. R. Yates, 3rd and G. Fang (2008). "Plk1- and beta-TrCP-dependent degradation of Bora controls mitotic progression." J Cell Biol **181**(1): 65-78.

Sillibourne, J. E., C. G. Specht, I. Izeddin, I. Hurbain, P. Tran, A. Triller, X. Darzacq, M. Dahan and M. Bornens (2011). "Assessing the localization of centrosomal proteins by PALM/STORM nanoscopy." Cytoskeleton (Hoboken).

Sillibourne, J. E., F. Tack, N. Vloemans, A. Boeckx, S. Thambirajah, P. Bonnet, F. C. Ramaekers, M. Bornens and T. Grand-Perret (2010). "Autophosphorylation of polo-like kinase 4 and its role in centriole duplication." Mol Biol Cell **21**(4): 547-61.

Sir, J. H., A. R. Barr, A. K. Nicholas, O. P. Carvalho, M. Khurshid, A. Sossick, S. Reichelt, C. D'Santos, C. G. Woods and F. Gergely (2011). "A primary microcephaly protein complex forms a ring around parental centrioles." Nat Genet **43**(11): 1147-53.

Strnad, P., S. Leidel, T. Vinogradova, U. Euteneuer, A. Khodjakov and P. Gonczy (2007). "Regulated HsSAS-6 levels ensure formation of a single procentriole per centriole during the centrosome duplication cycle." Dev Cell **13**(2): 203-13.

Thein, K. H., J. Kleylein-Sohn, E. A. Nigg and U. Gruneberg (2007). "Astrin is required for the maintenance of sister chromatid cohesion and centrosome integrity." J Cell Biol **178**(3): 345-54.

Wang, W. J., R. K. Soni, K. Uryu and M. F. Tsou (2011). "The conversion of centrioles to centrosomes: essential coupling of duplication with segregation." J Cell Biol **193**(4): 727-39.

Watanabe, N., H. Arai, Y. Nishihara, M. Taniguchi, T. Hunter and H. Osada (2004). "M-phase kinases induce phospho-dependent ubiquitination of somatic Wee1 by SCFbeta-TrCP." Proc Natl Acad Sci U S A **101**(13): 4419-24.

Wolff, A., B. de Nechaud, D. Chillet, H. Mazarguil, E. Desbruyeres, S. Audebert, B. Edde, F. Gros and P. Denoulet (1992). "Distribution of glutamylated alpha and beta-tubulin in mouse tissues using a specific monoclonal antibody, GT335." Eur J Cell Biol **59**(2): 425-32.

Wong, C. and T. Stearns (2003). "Centrosome number is controlled by a centrosome-intrinsic block to reduplication." Nat Cell Biol **5**(6): 539-44.

Yan, X., R. Habedanck and E. A. Nigg (2006). "A complex of two centrosomal proteins, CAP350 and FOP, cooperates with EB1 in microtubule anchoring." Mol Biol Cell **17**(2): 634-44.

Zhu, F., S. Lawo, A. Bird, D. Pinchev, A. Ralph, C. Richter, T. Muller-Reichert, R. Kittler, A. A. Hyman and L. Pelletier (2008). "The mammalian SPD-2 ortholog Cep192 regulates centrosome biogenesis." Curr Biol **18**(2): 136-41.

11 Curriculum Vitae

Katharina Friederike Sonnen, née Mayer

Born May 7th, 1983 in Dortmund, Germany

Education

09/2007 – 04/2012	PhD studies
	Max-Planck Institute of Biochemistry, Martinsried, Germany and the Biozentrum of the University Basel, Switzerland
09/2006 – 06/2007	Diploma Thesis
	University of Birmingham, UK
10/2002 – 07/2007	Diploma Studies in Biochemistry
	Friedrich Schiller University Jena, Germany
06/2002	Abitur (equivalent to A levels)
	Clara Schumann Gymnasium Holzwickede, Germany

Fellowships

03/2011 – 05/2011	EMBO short-term fellowship
08/2008 – 08/2010	PhD Fellowship of the Boehringer Ingelheim Fonds
09/2007 – 04/2012	Member of the International Max Planck Research School for Molecular and Cellular Life Sciences, Martinsried (Munich), Germany
10/2006 – 06/2007	Erasmus Fellowship to study abroad
08/2004 – 04/2012	e-fellows.net
10/2002 – 09/2004	Fellowship of the Fonds of the Chemical Industry, Germany

Publications

Christian Arquint, Katharina F. Sonnen, York-Dieter Stierhof and Erich A. Nigg: *Cell Cycle-Regulated Expression of STIL Controls Centriole Numbers in Human Cells*. Journal of Cell Science 125 (2012)

Nicholas J. Davies, Rachel E. Hayden, Paul J. Simpson, Jane Birtwistle, Katharina F. Mayer, Jonathan P. Ride and Chris M. Bunce: *AKR1C Isoforms Represent a Novel Cellular Target for Jasmonates alongside Their Mitochondrial-Mediated Effects.* Cancer Research 69 (2009)

12 Acknowledgements

Firstly, I want to thank Erich for giving me the opportunity to work in his laboratory, but more importantly for his constant advice and support, the sometimes troubling discussions about science, experiments and life in general and finally for the possibility to develop some kind of independence in conducting scientific research.

Next, I am grateful to Peter Scheiffele and Zuzana Storchova for their help and advice as members of my These Advisory Committee and my PhD Committee and to Markus Affolter for agreeing to chair my PhD defence.

Moreover, I have to thank EMBO, IMPRS-LS and BIF for the financial support I received during my PhD studies. In addition, I would like to thank Hans Joerg, Maxi and Ingrid from IMPRS for the education outside the lab, also for all the barbecues and friendly atmosphere we experienced in Munich. Similarly, I am thankful to Claudia, Monika and Sandra from BIF for the personal support and particularly the Hirschegg seminar that allowed us to meet and make friends from all over Europe.

Apart from that, I want to thank Lothar Schermelleh, Jürgen Neumann and Heinrich Leonhardt from the LMU in Munich, as they provided the technical knowledge as well as the equipment that allowed me to perform the super-resolution project on human centrosomes. In this regard, I am also grateful to Oliver Biehlmaier from the Microscopy core facility at the Biocenter in Basel for his help with analyzing and interpreting fluorescence microscopy data.

Additionally, I would like to thank Roman Körner and Kalyan Dulla from the MPI of Biochemistry in Munich and Alex Schmidt, Timo Glatter and Manuel from the Mass Spec core facility in Basel for help with performing and analyzing my mass spec data.

Moreover, I am grateful to York-Dieter Stierhof (University of Tübingen) for performing the immunoelectron microscopic analyses and to Fanni Gergely (Cambridge, UK), Lawrence Pelletier (Toronto, Canada) and Ingrid Hoffmann (Heidelberg, Germany) for providing reagents.

Special thanks go to Alison, Zdenka and Nadine as well as Klaus, Alicja, Claudia, Durda, Lidia, Elisabeth, Anja, Albert, Elena and Fabien for providing the infrastructure and

atmosphere that facilitates efficient work in a lab so much. In particular, I would like to thank Elena for being so supportive and helpful in every respect of a PhD student's life.

Next, I am very thankful to Eduard for working together with me on the Cep152 – Cep192 project and sharing all the ups and downs, especially towards the end of my PhD, with me…

Moreover, I want to thank Thorsten, Jens and Gernot, the "ground floor centrosomes" in Munich, for the endless discussions and all the fun we had inside and outside of the lab. Of course, I am also grateful to Manuel, Christian, Anna and Lukas in addition to Eduard, the "Basel centrosomes", for the nice atmosphere in the lab and the discussions we had about these "bloody" centrioles.

I would also like to thank Manuel (K.), Luca and Gary for being there – in both Munich and Basel – whenever necessary, all the support and the beer we had together and, of course, to Gary for being such a cool guy. Additionally, I am extremely grateful to Manuel (B.), Fabien and Anna S. for the in-depth discussions about life, science and research and the morning coffee + *Schoko-Croissant*, to Fabien for being so unbelievably annoying and to Manuel for his friendship. Furthermore, I am thankful to all the others of the Nigg lab, such as Ulf, Conrad and Anna B., but also Anne and Silvia for providing the friendly atmosphere to survive. I already miss all of you!

Particularly, I would like to thank Nadja and Gernot for all the fun, for biking, swimming and skiing, for the triathlon "experiences" and for all those *Kölner Abende*, for their friendship. But of course, I am also very thankful to all my "non-science-related" friends from home.

Last, but not least, I would like to thank my family for their support and faith during the course of my studies. I am especially grateful to my parents and grandparents for enabling all this and always being there. But I also have to thank my brothers for annoying and distracting me as much as they could and also all the others of my extended family for their help, their presence and their love. I love you all!